2nd INTERNATIONAL SYMPOSIUM

FUNDAMENTALS OF TECHNICAL PROGRESS IN MEDICINE

EMISSION TOMOGRAPHY
NUCLEAR MAGNETIC RESONANCE
DIGITIZED RADIOGRAPHY
ULTRASONOGRAPHY
X RAY CT SCANNING

LIEGE·BELGIUM
APRIL 15·16, 1983

2ème SYMPOSIUM INTERNATIONAL

FONDEMENTS DES NOUVEAUTES TECHNIQUES EN MEDECINE

TOMOGRAPHIE PAR EMISSION
RESONANCE MAGNETIQUE NUCLEAIRE
RADIOGRAPHIE DIGITALISEE
ULTRASONOGRAPHIE
TOMODENSITOMETRIE PAR RAYONS X

LIEGE·BELGIQUE
15·16 AVRIL 1983

COMPTES RENDUS

J.C. DEPRESSEUX, J. GARSOU, P. GENARD,
W. GORDENNE, G. MERCHIE, J.P. SCHAAPS
Editeurs

AVANT-PROPOS.

Notre Symposium de 1979 s'adressait à l'ultrasonographie, le planning dosimétrique en radiothérapie et le traitement des informations en médecine nucléaire.

Malgré les difficultés économiques actuelles, la résonance magnétique nucléaire, la tomographie radioisotopique par photons ou positrons, la radiographie digitalisée ont atteint un degré de développement tel qu'il s'impose en 1983 de faire le point sur ces thèmes et de s'interroger sur leur évolution possible.

Si l'équipement médical lourd est resté l'apanage de la radiothérapie jusqu'aux années 70, le diagnostic se raffine depuis, grâce à des techniques diversifiées d'imagerie requérant des investissements de plus en plus lourds.

L'exploitation optimale au bénéfice du patient de systèmes aussi sophistiqués nécessite la collaboration de physiciens médicaux hautement spécialisés, à formation sanctionnée.

Quant aux répercussions sur le plan de la politique de santé publique de l'application de ces nouveaux moyens d'investigation, elles doivent être envisagées en sorte de les rendre les plus accessibles.

Julien GARSOU

TABLE DES MATIERES — TABLE OF CONTENTS

II. 7.1. L. POURCELOT (Tours, France)
Résistance circulatoire placentaire et pathologie foetale

II. 8.1. D. BEYER, R. LORENZ, L. HEUSER (Cologne, FRG)
Ultrasonography of superficial organs - Focussing on scrotal contents

II. 9.1. P.M. BRET (Lyon, France)
Ultrasonographie d'intervention - Données techniques

II.10.1. R.Ch. OTTO (Zürich, Switzerland)
Experience with ultrasound guided fine needle punctures (2100 patients)

II.11.1. M.C. PLAINFOSSE, A. HERNIGOU, S. MERRAN (Paris, France)

III. RADIOGRAPHIE DIGITALISEE/DIGITIZED RADIOGRAPHY

III. 0.1. B.M. MOORES (Manchester, U.K.)
Design and physical performance of digital fluorography systems

III. 1.1. R. NOWOTNY, J. KEMMER (Wien, Austria)
Silicon µstrip-detectors for linear X-ray sensing

III. 2.1. G. HAENDLE (Erlangen, FRG)
Digital subtraction in angiography

III. 3.1. R. KLAUSZ (Paris, France)
Etat actuel de la digitalisation

III. 4.1. D. BLAKESLEY (Wembley, U.K.)
The impact of digital electronics on the radiographic departments

III. 5.1. G. WILMS, J. SMITS, F. DE SOMER (Leuven, Belgium)
D.I.V.S.A. applications to the intracranial vascular system

III. 6.1. G. TROTTEUR, P. MAGOTTEAUX, C. SAIVE, G.F. LEROUX (Liège, Belgique)
Angiopneumographie : technique optimale d'examen en angiographie numérisée

III. 7.1. C. GILATH (Ramat Gan, Israël)
Advances in digital fluoroscopy with special emphasis on cardiologic application

III. 8.1. P.Z. WASOWSKI (Frankfurt/Main, FRG)
Current developments in digital substraction angiography - Temporal, dual energy. Discussion of clinical data and future trends

III. 9.1. E. BREATNACH (Birmingham, Al., U.S.A.)
Digital radiography of the chest : clinical experience with a prototype model

IV. TOMODENSITOMETRIE PAR RAYONS X/X RAY CT

IV. 0.1. L. JEANMART (Bruxelles, Belgique)
Tomographie computée, facteur de luxe ou d'économie ?

IV. 1.1. M. OSTEAUX, C. NICAISE, Ph. PEETRONS, L. COOLS, L. JEANMART (Bruxelles, Belgique)
Calcul T.C. de volumes d'organes. Méthodologie, possibilités et limites.

IV. 2.1. B. KURTZ, G. STOCKLE, K.H. HUBENER, U. REINHARD (Tübingen, FRG)
Computed tomography and lung function analysis in diffuse interstitial lung fibrosis

IV. 3.1. K. LACKNER (Bonn, FRG)
Computerized tomography of the heart

IV. 4.1. G.P. VIJVERBERG (Eindhoven, the Netherlands)
High resolution in CT

IV. 5.1. R. TRIERWEILER (Erlangen, FRG)
Treatment planning based on an array-processor

V. TOMOGRAPHIE D'EMISSION/EMISSION TOMOGRAPHY

V. 0.1. M.M. TER POGOSSIAN (St Louis, Missouri, U.S.A.)
Emission tomography

V. 1.1. R. CAMPAGNOLO, P. GARDERET, J. VACHEZ (Grenoble, France) F. SOUSSALINE (Orsay, France)
Principes de la tomographie positronique à temps de vol

V. 2.1. M.M. TER POGOSSIAN (St Louis, Missouri, U.S.A.)
Time-of-flight positron emission tomography : designs and realisations

V. 3.1. R. ALLEMAND, E. TOURNIER, M. LAVAL, J.L. LECOMTE, A. BOUVIER; P. DARIER, R. GARIOD (Grenoble, France), D. COMAR (Orsay, France), M. BOURDOISEAU, M. BARDY (Saclay, France)
Nouvelles perspectives technologiques offertes par la tomographie positronique à temps de vol

V. 4.1. J.C. DEPRESSEUX (Liège, Belgium)
Biomodelization of kinetic studies with positron emission tomography

V. 5.1. M.M. TER POGOSSIAN (St Louis, Missouri, U.S.A.)
Clinical applications of time-of-flight positron emission tomography

V. 6.1. F. SOUSSALINE (Orsay, France)
Méthodes de reconstruction et facteurs intervenant dans l'exploitation quantitative en tomographie d'émission gamma

V. 7.1. S. LARSSON (Stockholm, Sweden)
SPECT - Current status, limitations and applications

V. 8.1. F. AUBRY, R. DI PAOLA (Villejuif, France)
Etude du bruit statistique en tomographie d'émission gamma

V. 9.1. G. VAN OORTMARSSEN (Uithoorn, the Netherlands)
New technical developments in ECT

V.10.1. F. VERMEULEN (Ghent, Belgium)
An improvement stochastic reconstruction technique for tomographic imaging

V.11.1. P. BLOCKX, F. VAN DE VIJVER (Antwerpen, Belgium)
Comparison of spect results with elliptic rotating camera and rotating slant hole collimator

V.12.1. J.L. MORETTI, S. ASKIENAZY, C. RAYNAUD, P. CESARO, J. RAPIN, A. BARDY (Créteil, France)
Applications tomographiques de l'sopropyl-iodo-amphétamine 123I (AMP 123I) en pathologie cérébro-vasculaire

V.13.1. R. FRACKOWIAK (London, U.K.)
Neurological applications of positron emission tomography

V.14.1. C. DE LANDSHEERE, D. RAETS, M.P. LAROCK, W. BURGUET, D. LAMOTTE, M. CHEVIGNE, R. RIGO (Liège, Belgium)
Cardiological applications of emission computed tomography

V.15.1. C. SCHEIBER, J. CHAMBRON (Strasbourg, France)
Evaluation of the digital gamma camera Elscint APEX 415 ECT in emission tomography : first clinical results

POSTERS

P. MALMBORG, H. LUNDQVIST, C.G. STALNACKE (Uppsala, Sweden)
Experiences from the first year of positron emission tomography with short-lived radionuclides in Uppsala

L. POURCELOT (Tours, France)
Détection des plaques d'athérome carotidiennes et fémorales

R.J. WHITROW (Brighton, U.K.)
Data capture and display of moving heart walls from gamma camera images

I. RESONANCE MAGNETIQUE NUCLEAIRE / NUCLEAR MAGNETIC RESONANCE

NUCLEAR MAGNETIC RESONANCE

R.C. HAWKES (Nottingham, U.K.)

Text not received.

The Aberdeen Proton NMR Imaging Program with Primary Emphasis on Relaxation Time.

J. Mallard
Dept of BioMedical Physics and BioEngineering, University of Aberdeen,
Foresterhill, Aberdeen AB9 2ZD, Scotland.

Introduction.

We now stand on the threshold of a completely new method of imaging, called nuclear magnetic resonance imaging or, in its more common abbreviated form, NMR imaging. In it, the protons of hydrogen in water (mainly) are located and imaged.

The protons of hydrogen behave like very tiny bar magnets of a definite strength, or magnetic moment. If they are placed in a magnetic field they will tend to line up more or less parallel to that field and will precess around it just like the top does around the vertical gravitational field. The rate, or frequency, of this precession is proportional to the magnetic field strength in which they are placed.

By beaming onto them electromagnetic radiation of exactly the same frequency as their precession they absorb energy from the beam which changes their alignment relative to the applied magnetic field. It is possible to turn them through 90° or through 180° at the time the magnetic field and the appropriate radiation are applied simultaneously. The frequency of radiation which has to be used is in the radio-frequency band, normally in the region of MHz or tens of MHz.

When the irradiating frequency is switched off, the excited nuclei have surplus energy which they radiate to their surroundings at the same resonant frequency. From a sample containing a large number of such nuclei, one by one they are then able to fall back, or relax, to their original alignment so that the sample re-emits its resonant frequency as a signal which can be detected and measured. The strength or intensity of the signal is proportional to the number of protons which relax per unit time, which is initially related to the number of protons present in the sample.

Now the signal intensity will fall with time as more and more of the excited protons have relaxed. The length of time needed for this relaxation is associated with the environment of the protons - a measurement known as the relaxation time.

It helps to understand the principle of imaging using NMR by taking the simple example of two tubes of water lying side by side in a uniform magnetic field (Fig. 1). It is not possible to distinguish between the two tubes of water because both have been subject to the same magnetic field and hence have the same resonant frequency; but if one now adds a field gradient to the applied magnetic field so that the field is stronger on one side than the other, one tube will now be in a slightly stronger field than the other and will resonate at a slightly higher frequency. The tube positioned in the higher field will absorb energy, and then re-emit it, at a higher frequency than the other tube.

The use of a magnetic field gradient inside an NMR spectrometer makes it possible to identify position from the frequency of the emitted signal, the amount of water (or proton concentration) from the size of the signal, and relaxation time from the decay of the signal.

In the method which has been developed in Aberdeen since 1972, two images are built up to show the distribution of proton concentration, and of the relaxation time (T_1), from a transverse cross-section of the body. The radiofrequency used is 1.7 MHz and the patient is placed in a magnetic field of 400 gauses (0.4 Ts), which is applied in the posterior-anterior direction of a supine patient.

The imaging principle employed is that of 'selective excitation' (Mansfield et al. 1976: Hutchison, 1976). The particular form used (spin-warp imaging)(Edelstein et al. 1980) tolerates a much larger magnetic non-uniformity than projection reconstruction method (Hutchison et al. 1978: Sutherland and Hutchison 1978) and also the effect of patient movement is less drastic.

A 256 second scan collects data for both a proton density and T_1 image. The T_1 value for each imaging element is calculated and $T_1 = 200/\ln(2 \times S_2)/(S_0 \quad S_2)$; the 128 x 128 element S_0 and T_1 arrays are then interpolated into 256 x 256 arrays and displayed using 16 colour-coded levels, or grey scale.

The tomographic sections have a Gaussian profile with thickness (equivalent rectangular width) 18.5 mm. Each imaging element is 3.75 mm wide, x 3.5 mm high, x 18.5 mm thick, comprising a volume of about 1/4 cm^3. In each imaging element, the uncertainty in proton density for muscle tissue is about + 2.5%, and the uncertainty in T_1 is about ± 3.5 % for T_1 close to 200 ms, with some worsening as T_1 departs from that optimum value.

The apparatus is described in detail in Hutchison et al. 1980 and has resulted from the work of a team of people in my Department (Table 1) all of whom are co-authors of this review which I have been invited to present.

The many human images shown in the lecture have mostly been obtained with the NMR imaging method described above in the MK I machine, a photograph of which is shown in Mallard (1981). A Mk.II machine has been completed at the time of writing using the same basic layout and imaging technique, but having improved signal-to-noise ratio, (more than twice) improved spatial resolving power and improved patient ingress and egress. This machine is the prototype of two models for commercial production with a magnetic field strength of 800 gauss (0.08 Tesla)*.

To date, over 1000 patients and healthy volunteers have been examined using the technique and no short or medium term ill-effects have been experienced by or observed in any of the subjects.

Of the two available proton measurements, T_1 and proton density, each contribute valuable information about the anatomy and pathology seen on each section. Because T_1 values are dependent on the degree of water binding to tissue protein, they are the most valuable in characterising soft tissue. Tissues such as muscle and liver, which have much protein-bound water, have short T_1 values (Table 2) whilst other tissues such as cardiac muscle or spleen have longer values. Body fluids such as urine and cerebro spinal fluid (C.S.F.) have long values. Whilst there is some overlap in the T_1 values of some normal tissues, their anatomical sites make identification simple and precise.

When malignant tissue is present it tends to have T_1 which is longer - from 25% to more than 100% longer - than the normal tissue in which it is situated, making for easy recognition of soft tumours (Smith et al. 1981d). Similarly, inflammatory and oedematous conditions are easily recognised and characterised. Table 3 summarizes T_1 values for normal and diseased states and tissue of the liver, averaged from in;vivo measurements on patients using the Aberdeen MK I NMR Imager using the colour coding and/or the region of interest programme. Table 4 gives data obtained in the same manner for brain pathologies.

The proton density images give a display of the proton concentration, which, in soft tissue, appears not to vary significantly from tissue to tissue, making the differentiation of soft tissue organs difficult on these images. However, there are significant differences in proton density between bone, soft tissue and fluids, and air, this fact enabling the easy recognition of bone and fluids when they are bounded by soft tissue. The proton density images are more akin to X-ray CT images.

The Aberdeen method (spin-warp) is tolerant of small body movements, both volunatary and involuntary, such as respiratory, cardiac and peristaltic motions, from which no imaging artefacts arise. Also there are no artefacts caused by gas-soft tissue interfaces, nor by bone-soft interfaces, both of which can be troublesome on X-ray CT images. Also, the Aberdeen configuration of magnetic fields makes the images far less dependent upon the magnetic environment of the imager, and itself causes much less effect upon that environment. The machine is light compared with others (1.5 tons) and installation and running problems and costs are far less.

This presentation was illustrated with human in-vivo images of 30 patients.

It is clear that proton NMR imaging is a new but very important contribution to medical imaging, not only for diagnostic imaging of lesions and response to therapy, but also for systemic disease. In addition it is a new tool to study physiological and biochemical phenomena in-vivo, which will lead to a better understanding of living processes.

*M & D Technology Ltd., Unit 1, Mastrick Undustrial Estate, Aberdeen, Scotland.
Asahi Chemical Industry Ltd., Tokyo, Japan.

References.

Besson, J.A.C., Glen, A.I.M., Foreman, E.I., MacDonald, A. Smith, F.W., Hutchison, J.M.S., Mallard, J.R., Ashcroft, G.W.; Nuclear magnetic resonance observations in Alcoholic cerebral disorder and the role of Vasopressin. Lancet of Oct. 24th 1981, 923-924.

Edelstein, W.A., Hutchison, J.M.S., Johnson, G., and Redpath, T.; 1980. Spin-warp NMR imaging and applications to whole-body imaging. Phys.Med Biol., 25, 751-756.

Ernst, R.R.; Gyromagnetic resonance Fourier transform Zeugmatography. U.S. Patent,4,070,611,1978.

Hutchison, J.M.S.; 1976, Imaging by nuclear magnetic resonance. Proc.7th L.H. Gray Conf. on Medical Images, Leeds(Bristol) Inst. of Physics; Wiley) 135-141.

Hutchison, J.M.S., Sutherland, R.J., and Mallard, J.R.; 1978, NMR Imaging; image recovery under magnetic fields with large non-uniformities. J.Phys. E.Sci. Instrum 11, 217-221.

Hutchison, J.M.S., Edelstein, W.A., and Johnson, G.; 1980, A whole-body NMR imaging machine. J.Phys. E.; Sci. Instrum. 13, 947-955.

Kumar,A., Welti, D., Ernst, R.R.; NMR Fourier Zeugmatography. J.Mayn. Resonance, 18, 1975, 68.

Mallard, J.R., Hutchison, J.M.S., Foster, M.A., Edelstein, W.A., Ling, C.R., Smith, F.W., Reid, A., Selbie, R., Johnson, G., and Redpath, T; 1981, Medical Imaging by Nuclear Magnetic Resonance; a review of the Aberdeen physical and biological programme. In: Medical Radionuclide Imaging 1980 (IAEA: Vienna) I, 117-144.

Mallard, J.R., 1981, The noes have it, Do they? Silvanus Thompson Memorial Lecture 1981. Brit J. Radiol. 54, 831-849.

Mansfield, P., Maudsley, A.A., and Raines, T.; 1976. Fast scan proton density imaging by NMR. J.Phys.E. Sci. Instrum. 9, 271278.

Smith, F.W., Mallard, J.R., Hutchison, J.M.S., Reid, A., Johnson, G., Redpath, T., Selbie,R.; 1981, (a) Clinical application of nuclear magnetic resonance, Lancet 1, 78-79.

Smith, F.W., Hutchison,J.M.S., Mallard, J.R., Johnson, G., Redpath, T., Selbie, R., Reid, A., Smith, C.C.; 1981, (b) Oesophageal carcinoma demonstrated by whole-body nuclear magnetic imaging. Brit. Med. J. 282, 510-512.

Smith, F.W., Hutchison, J.M.S., Mallard, J.R., Reid, A., Johnson, G., Redpath, T.W., Selbie,R.; 1981, (c) Renal cyst or tumour differentiation by wholebody nuclear magnetic resonance imaging. Diagnostic Imaging 50, 61-65.

Smith, F.W., Mallard, J.R., Reid, A., Hutchison, J.M.S.; 1981, (d Nuclear magnetic resonance tomographic imaging in liver disease. Lancet 1, 963-966.

Smith F.W., Reid, A.,Hutchison, J.M.S.,and Mallard, J.R., 1981, (e) NMR Tomographic imaging - a new look at the pancreas. Radiology, 142, 677-680.

Sutherland, R.J. and Hutchison, J.M.S.; 1978, Three-dimensional NMR imaging using selective excitation. J.Phys. E.;Sci. Instrum. 11, 79-83.

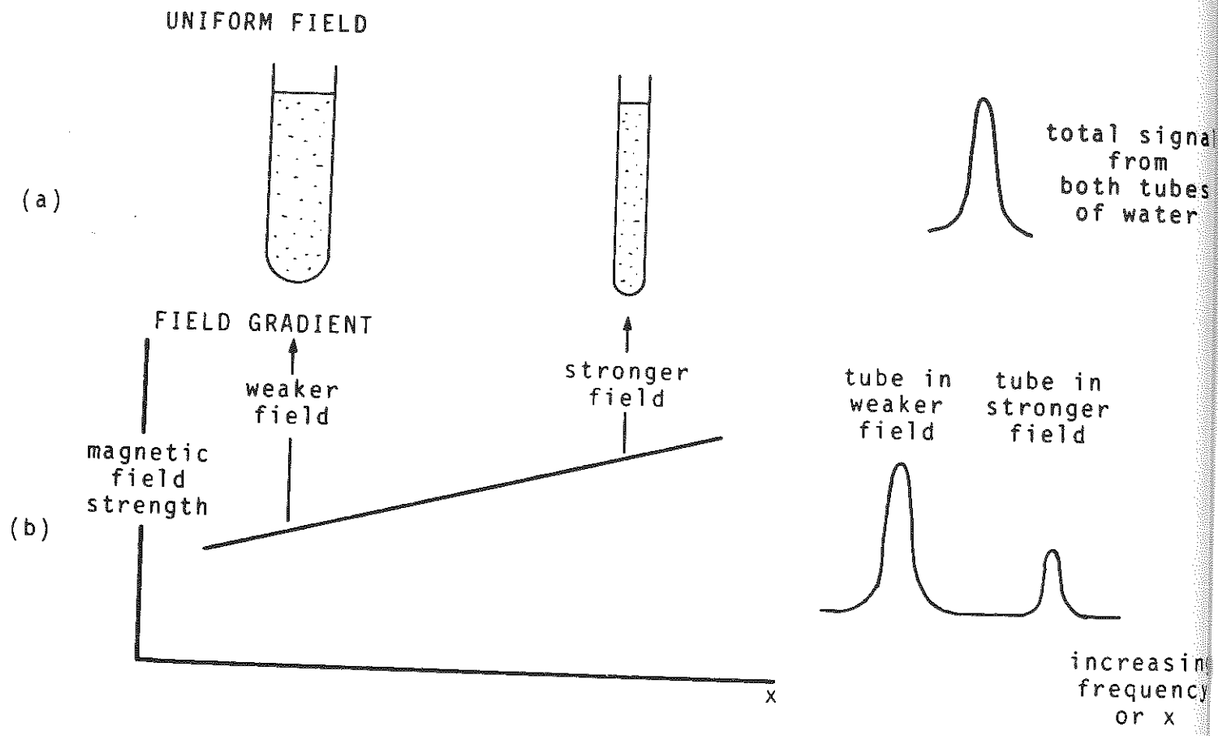

Fig. 1.

TABLE 1
Department of Bio-Medical Physics
and Bio-Engineering, University of Aberdeen.

NUCLEAR MAGNETIC RESONANCE (NMR)
GROUP 1972 ONWARDS.

Physical.

Dr. J.M.S. Hutchison	
Dr. R.E. Gordon	1972-75
Mr. G. Johnson	1978-
Mr. R. Selbie	1980 -
Dr. W.A. Edelstein	1978 - 80
Dr. R. Sutherland	1975 - 78
Mr.T. Redpath	1979 -
Dr. L. Eastwood	1980 -

Biological.

Dr. M.A. Foster	
Mrs. C.R. Ling	1978 - 81

The Group has been assisted since 1980 by Dr. F.W. Smith, Consultant in Nuclear Medicine and Dr. A. Reid, Research Officer, (Medical).

TABLE 2

Some Typical Spin-Lattice Relaxation Times of Human Tissues.

Measured from in-vivo NMR Images at 1.7 MHz.

Normal Tissues.

Skeletal Muscle	150 - 200 ms
Liver	140 - 170 ms
Bone	190 - 220 ms
Eye	240 - 260 ms
Cerebral Cortex	250 - 300 ms
Bile Ducts	250 - 300 ms
Kidney	300 - 320 ms
Blood	350 - 420 ms
C.S.F.	800 - 1000 ms

Pathology.

Cirrhosis	180 - 300 ms.
Liver Tumours	300 - 450 ms
Lung Carcinoma	350 - 400 ms
Renal Carcinoma	400 - 450 ms
Fat	120 - 150 ms
Pancreas	180 - 200 ms
Cardiac Muscle	240 - 260 ms
Spleen	250 - 290 ms
Cerebellar Cortex	250 - 300 ms
Spinal Cord	290 - 300 ms
Bile in Gall Bladder (depending on obstruction or not)	300 - 700 ms
Urine	) 1000 ms

TABLE 3
T_1 Values - Liver.

Normal Liver	140 - 170 ms
Chronic active hepatitis	170 - 180 ms
Cirrhosis	180 - 300 ms
Secondary Liver tumour	280 - 450 ms
Hepatoma	300 - 450 ms
Cholangiocarcinoma	200 - 350 ms
Simple serous cyst	800 - 1000 ms
Haemangioma	350 - 370 ms
Ascitic fluid	700 - 1000 ms

AVENIR MULTIDISCIPLINAIRE DE LA R.M.N. BIOMEDICALE.

Robert N. MULLER
Faculté de Médecine
Université de l'Etat à Mons
7000 Mons - Belgium.

Au cours de la dernière décennie, la Résonance Magnétique Nucléaire (RMN) - jusqu'alors outil du physicien et du chimiste - a étendu son domaine d'applications aux sciences biologiques et médicales.
Deux noms sont associés à cette spectaculaire évolution : celui de Paul C. LAUTERBUR de l'Université de New York à Stony Brook et celui de Raymond DAMADIAN de l'Université de New York à Brooklyn.
Le premier, déjà connu pour ses travaux originaux dans le domaine de la spectrographie de RMN du carbone-13, imagina et expérimenta avec succès une nouvelle méthode de production d'images qu'il nomma *zeugmatographie* ; le second découvrit que le signal de RMN produit par les protons de l'eau cellulaire reflète, dans certains cas, un état pathologique.
Depuis, l'essor de la RMN biomédicale s'est poursuivi dans deux directions parallèles : celle de l'imagerie qui exploite le signal spatialement encodé, et celle de la spectroscopie qui utilise l'information en vue d'une caractérisation biochimique des tissus. Cette dernière approche offre d'intéressantes perspectives dans le cadre des études du métabolisme et de la pathologie.
L'image est généralement obtenue au départ de signaux émis par les atomes d'hydrogène présents - en abondance - dans les graisses et l'eau des tissus tandis que l'application de la spectroscopie se révèle plus fructueuse lorsqu'elle s'adresse à l'examen d'espèces nucléaires (^{31}P, ^{13}C) plus riches en informations métaboliques.

Diverses contraintes technologiques retardent l'apparition d'un appareil mixte qui soit à même de combiner l'examen morphologique à une exploration spectroscopique de zones sélectionnées. L'évaluation clinique de la RMN en tant qu'outil de diagnostic morphologique a commencé ; ses succès sont enthousiasmants. L'absence de radiation ionisante, la possibilité de production d'images tridimensionnelles exemptes d'effets de volumes partiels et visualisées selon des plans d'observation arbitraires, le haut degré de contraste et sa dépendance multi-paramétrique ainsi que la représentation des flux sont au nombre des avantages reconnus à la technique.

Si les premiers résultats morphologiques et spectroscopiques de la RMN biomédicale l'ont déjà imposée comme une technique d'avenir, de nombreuses questions subsistent. Leurs réponses, comme les applications et les développements ultérieurs de la technique dépendent étroitement de recherches relevant de la technologie pure, de l'informatique, de la chimie, de la physique, des sciences mathématiques ou pharmaceutiques autant que des sciences biomédicales. En effet, parallèlement à la poursuite de l'évaluation objective des apports de la méthode sur le plan du diagnostic morphologique, un large éventail de thèmes reste offert :

- étude systématique *in vitro* et *in vivo* des paramètres de relaxation nucléaire T_1 et T_2 et évaluation de leur éventuelle signification physiopathologique ;
- détermination des valeurs optimales des fréquences d'imagerie ;
- amélioration du " software " : acquisition et traitement du signal, procédures de reconstruction et de visualisation des images ;
- affinement des procédures d'extraction des paramètres de relaxation nucléaire à partir des images ;
- nouvelles séquences d'impulsions ;
- problème de l'"image standard " ;
- mise au point d'agents de contrastes spécifiques ;
- amélioration du " hardware " : bobines de surface, aimants, ...
- examens histopathologiques *in vivo* par le biais d'analyses spectrales " hétéronucléaires " (^{31}P, ^{19}F, ^{13}C) combinées à des observations morphologiques par imagerie protonique ou hétéronucléaire.

Les progrès de la RMN biomédicale ne seront pas liés uniquement aux solutions technologiques qui simplifieront l'accès aux divers paramètres nucléaires car la signification exacte de ces derniers et leur utilisation restent des problèmes difficiles dont les solutions reposeront sur les efforts d'équipes pluridisciplinaires.

Remerciements : nous tenons à exprimer notre gratitude envers le Fonds National de la Recherche Scientifique et le département des affaires scientifiques de l'O.T.A.N. qui ont contribué - par le biais de bourses de recherche et de voyage - à notre séjour de perfectionnement à l'Université de New York.

BIBLIOGRAPHIE.

- Nuclear Magnetic Resonance Imaging in Medicine, L. KAUFMAN, L.E. CROOKS et A.R. MARGULIS, Eds. Ikagu Shoin, New York, Tokyo (1981).
- NMR Imaging in Biomedicine, P. MANSFIELD et P.G. MORRIS, Academic Press, New York (1982).
- Nuclear Magnetic Resonance (NMR) imaging, C.L. PARTAIN, A.E. JAMES, F.D. ROLLO et R.R. PRICE, Eds. W.B. Saunders Co, Philadelphia (1983).
- NMR Imaging, Proceedings of the International Symposium on Nuclear Magnetic Resonance Imaging, Browman-Gray School of Medicine of Wake Forrest (1982).
- Proceedings of the First Annual Meeting of the Society of Magnetic Resonance in Medicine - Boston, Août 1982.
- Nuclear Magnetic Resonance and its applications to living systems, D. GADIAN, Oxford UP - New York (1982).
- Topical Magnetic Resonance, R.E. GORDON, P.E. HANLEY et D. SHAW, dans Progress in Nuclear Magnetic Resonance Spectroscopy, Vol. 15 (1), Pergamon Press, New York (1982).

TRENDS IN NMR IMAGING

J. PENNOCK (London, U.K.)

Text not received.

NMR IMAGING

B. ZIMMERMANN (Erlangen, FRG)

Text not received.

BRUKER'S CONTRIBUTION TO N.M.R. TOMOGRAPHY

Paul Jung - (Bruker Spectrospin -Brussels)

SUMMARY

After a review of methods and technology paving the way of N.M.R. in medecine,the specific options of BRUKER's N.M.R. Imaging Systems will be outlined.

The N.M.R. is now a well established method and its spectroscopic applications to biology and medecine in vitro are nearly as old as the N.M.R. itself.

The extraordinary interest shown by the medical world for the N.M.R. is however quite recent. This can be explained by the progress in sensitivity of the N.M.R. method, which has been achieved by the introduction of computer and the :
" FAST FOURIER TRANSFORM "algorithme (FFT) to N.M.R. spectroscopy. (1)

The FFT enables the experimeter to acquire the total N.M.R. information simultaneously instead of successively.The gain (G) in sensitivity by the FFT , when compared to the slow acquisition method used earlier , is given by:

$$G = \left(\frac{B}{\Delta\nu}\right)^{1/2}$$

where B is the bandwidth of the spectrum,
and $\Delta\nu$ is the width of a single line.

A typical gain is 50-500 , depending on the type of spectrum and linewidth.

This has opened the way to N.M.R. ZEUGMATOGRAPHY (N.M.R.IMAGING) introduced by LAUTERBUR (2) in I974.

In SPECTROSCOPY : the N.M.R. absorption is characterized by a frequency ν

$$\nu(\delta) = \frac{B_o}{2\pi}\gamma(1+\delta) = \nu_o(1+\delta)$$

where B_o is the constant magnetic field, the spectroscopic information being the chemical shift δ

In ZEUGMATOGRAPHY : a " pseudo spectroscopy " is introduced by the application of one or several gradients to the magnetic field, but only one spectroscopic species is observed. Simplified to one dimension , this results in :

$$\nu(x) = \frac{\gamma}{2\pi}\left[B_o + \frac{\partial B}{\partial x}x\right](1+\delta)$$

$$\nu(x) = \nu_o\left(1 + \frac{1}{B_o}\frac{\partial B}{\partial x}x\right)$$

The Zeugmatographic information being x ,the frequency of the absorption gives the spatial information.

By the FFT all frequencies (ν) are observed simultaneously and converted into spatial information (x).

The next step would be the combination of spectroscopy and zeugmatography. This implies that the three dimensional information (x,y,z,)and the chemical shift information (δ) are recovered simultaneously. Simplified to one dimension, this results in:

$$\nu(x,\delta) = \nu_o\left(1+\delta+\frac{1}{B}\frac{\partial B}{\partial x}x\right)$$

The feasibility of the so-called 4 DIMENSIONAL IMAGING has been demonstrated on 31 P by BENDEL ,LAI and LAUTERBUR in I980.(3)

The potentialities of N.M.R. (spectroscopy & imaging) are enhanced even more by the existence of relaxation phenomena which deliver supplementary information and which can be recovered by a suitable choice of parameters of the experiment.

Since the advent of real whole body N.M.R. tomography a bright future seems to be promised to N.M.R. in medecine. Also the research and development in universities and industry undergoes a rapid and confusing proliferation.

One of the key issues in this development is the optimisation of sensitivity.
The sensitivity is proportional to the 2/3 power of the frequency or the magnetic field. However,the conductivity of the body attenuates the RF field whenever the wavelenght is comparable to the dimension of the body. At increasing frequency the attenuation finally affects adversely the gain in sensitivity. A broad sensitivity optimum is thought to be in the range of 5-20 MHz for whole body dimensions. For small bodies,the frequency optimum is proportionally higher. This is shown in Fig.1

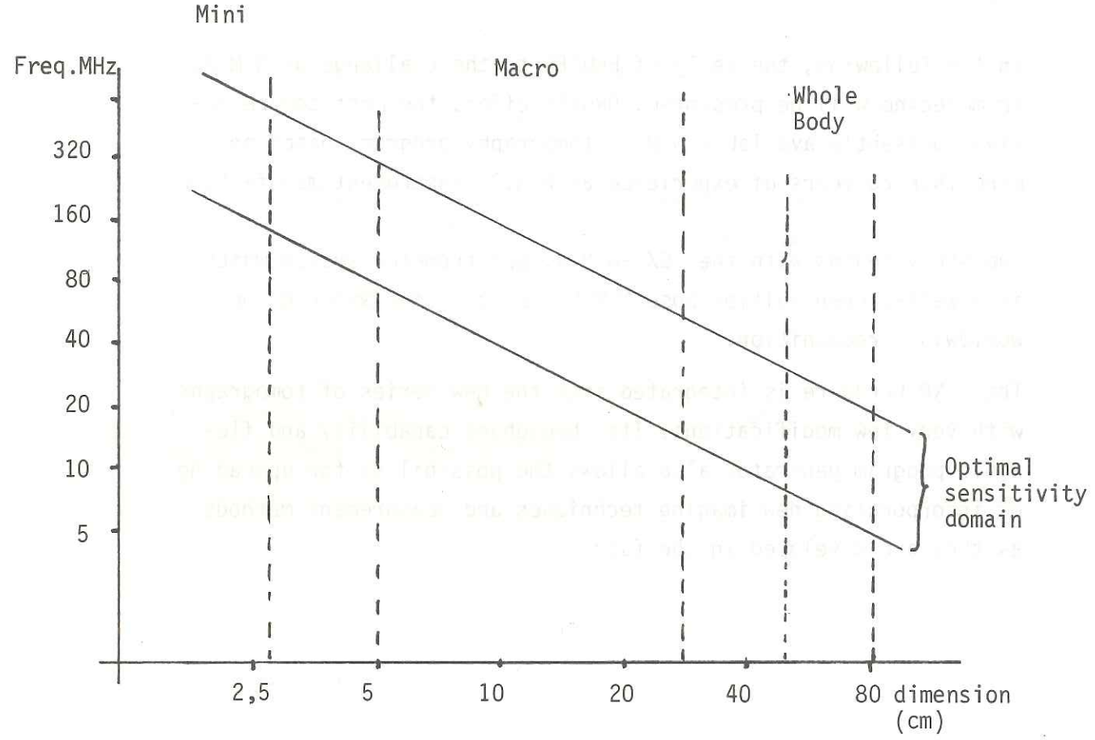

Fig.1-The domain of optimum sensitivity for biological tissues is shown as a function of frequency & dimension of the sample.

The progress in technology and methods is limited by such factors as :

- the low sensitivity of proton N.M.R.
- the very low sensitivity of nuclei other than proton,
- the R.F. loss at higher frequencies,
- the cost of the system.

In addition to improvements in technology , manufacturers of N.M.R. equipment for medecine require collaboration with medical research centers. The medical research centers, on the other hand , have to build up an interdisciplinary team.

Although whole body N.M.R. tomography can be used today in routine clinical applications, the need for fundamental medical research and development of techniques and methods is widely recognized.

In the following, the reply of BRUKER to the challenge of N.M.R. in medecine will be presented. BRUKER offers the most comprehensive, presently available N.M.R. tomography program, based on more than 20 years of experience as N.M.R. instrument manufacturer.

The story begins with the CXP-N.M.R. spectrometer system which is a well-proven multipurpose N.M.R. spectrometer which gained worldwide recognition.

The CXP hardware is integrated into the new series of tomographs with very few modifications. Its broadband capability and flexible program generator also allows the possibility for upgrading or incorporating new imaging techniques and measurement methods as they are developed in the futur.

...../.....

WHOLE BODY SYSTEMS :

The whole body systems of BRUKER are equipped with resistive magnets and dual computer system.
The BRUKER computer ASPECT 3000 is a dedicated computer produced in-house and used in all N.M.R. and I.R. spectrometers. This computer assumes the control of the instrument and the data acquisition . The second computer is a D.E.C. System allowing image reconstruction in virtual real time.

The expertise in magnet building has allowed BRUKER to manufacture its own resistive magnets.

- The B.N.T. 1000 is equipped with an air core resistive magnet working at:

  0,15 Tesla/ 6 MHz / 65 kW

- The B.N.T. 1100 is equipped with a completely new and original design. It comprises a resistive coil system with an integrated iron screen

  0,23 Tesla / 10 MHz / 66 kW

  This design offers the following avantage:

  . Increased field strength at moderate consumption,
  . No influence with critical external instrument ,
  . No influence of environmental iron
  . No Faraday cage required .

A schematic representation of the field configuration of both magnet systems is given in fig. 2

...../.....

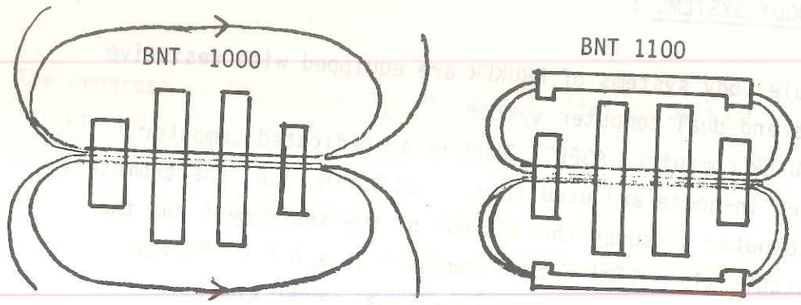

MAGNET SYSTEM	B.N.T. 1000	B.N.T.1100		
Frequency (MHz)	6	6	8	10
Field (Tesla)	0,14	0,14	0,188	0,23
Power (Kw)	60	21	39	66
advantages : . higher fields . lower stray fields . no shielding required				

Fig.2

Field configuration of BNT 1000/1100 Magnets

The stray fields of both magnets is shown in Fig. 3

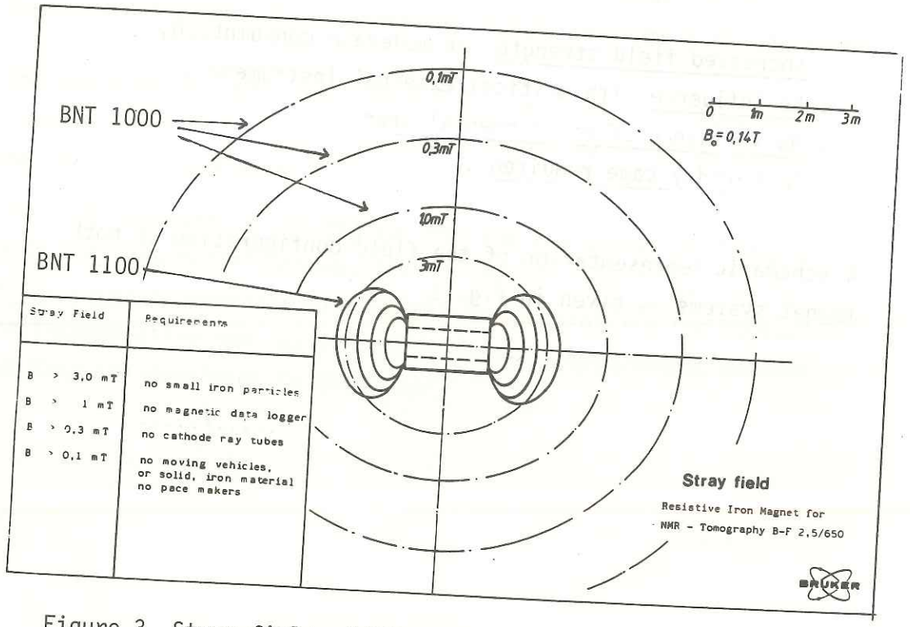

Figure 3 Stray field of BNT 1000 and BNT 1100 magnet system compared

		Magnetic Field (Tesla)	Proton Frequency (MHz)	Free Access (mm)	Resolution Dimension (mm)	Frequency Range (M Hz)	Proton Imaging	Other Nuclei Spectroscopy	Other Nuclei Imaging	In vitro Spectroscopy	IN VIVO SPECTROSCOPY: Organs Tissues	IN VIVO SPECTROSCOPY: Small Animals Limbs	Surface Coil	Localized Magnetic Resonnance
MINI	CPX 200	4,7	200	25	$\frac{1x10^{-9}}{20}$	20 - 200	yes	yes	yes	yes	yes	yes	yes	yes
	CPX 300	7,0	300	25	$\frac{1x10^{-9}}{20}$	30 - 300	yes	yes	yes	yes	yes	yes	yes	yes
MACRO	BNT 80	1,9	80	240	$\frac{1x10^{-5}}{75}$	10 - 90	yes	yes	yes	yes	yes	yes	yes	yes
	BNT 100	2,35	100	240	$\frac{4x10^{-6}}{190}$	10 - 100	yes	yes	yes	yes	yes	yes	yes	yes
WHOLE BODY	BNT 1000	0,14	6	710	$\frac{2x10^{-5}}{350}$	-	yes	-	-	-	-	-	-	-
	BNT 1100	0,23	10	750	$\frac{2x10^{-5}}{350}$	-	yes	-	-	-	-	-	-	-

TABLE 1 - Comparison of potentialities of BRUKER N.M.R. Tomography and Spectroscopic Systems

MACRO -IMAGING SYSTEM B.N.T. 80

This system consists of a CXP-console , which is connected to a superconducting horizontal-bore magnet B-C 19/300 (field stregth I9 kG , 300 mm RT- bore) . It is suited for proton and X- nucleus examinations of test animals and human extremities. Because this combination of imaging technology and HR-NMR on selected areas has been designed with experimental applications to defined areas in mind , it is the universal system for human medical research.

MINI -IMAGING SYSTEM (CXP 200 / 300 T)

This is a combination of standard spectrometers with a superconducting cryomagnet (of either 4,7 or 7,0 T and having an RT -bore of 98 mm). This system allows in-vitro examinations with high spatial resolution of small tissue samples or in-vivo measurements using small test animals (e.g. mice) , or perfused organs.

The principal caracteristics and applications of all N.M.R. tomography system offered by BRUKER are summarized in table 1 and provides a synoptic view of the technological options which include routine whole body systems as well as versatile smaller systems for medical research in imaging and spectroscopy.

References:

1- R.R. ERNST and W.A. ANDERSON ,Rev.Sci.Instr. 37,93 (I966)
2- P.C. LAUTERBUR ,Pure and Appl.Chem. 40,1-2 (I974)
3- P. Bendel, Lai and P.C. LAUTERBUR , J. Mag.Res.38,343 (I980)

APPLICATION DE LA RMN DU ^{23}Na A L'ETUDE DES ECHANGES IONIQUES.

Pierre G.CARLIER*o+, Jean GRANDJEAN+, Michelle GILLES-BAILLIEN°, Jean-Marie KRZESINSKI*o, Georges L.RORIVE*o et Pierre LASZLO+

* Institut de Médecine, Département de Clinique et Pathologie Médicales
o Laboratoire de Biochimie Générale et Comparée
+ Laboratoire de Chimie Organique Physique
UNIVERSITE DE LIEGE, Liège, Belgique.

SUMMARY.
One single line is usually observed in the ^{23}Na NMR spectra of biological systems. Some anionic paramagnetic species interacting with the sodium shift the sodium signal. So long as it does not enter the cell, a shift reagent splits the resonance line into two components : the intra(unshifted) and the extracellular Na (shifted). The method is applied to intestinal epithelium and to erythrocytes. Extracellular medium is enriched with dysprosium tripolyphosphate 2.5 mM. Na-K pump activity is studied in human erythrocytes. Ouabain (10^{-4}M) inhibition can be followed by the increase of the internal Na peak on the successive spectra whereas it does not change in the control. Na efflux out of the Na loaded erythrocytes can be measured as well. After incubation in a recovering medium, intracellular Na, as calculated from the successive spectra, returns progressively to normal. Simultaneously, the external peak shift reduces. This method can successfully demonstrate attenuations of the Na-K pump in pathological circumstances, such as chronic renal failure. The effects of polyether antibiotics on the sodium transport are also studied by this way. For instance, monensin causes a swift Na efflux that transiently broadens the external signal. Using shift reagent, ^{23}Na NMR is an efficient tool for ionic membrane exchange studies.

Correspondance : Dr.Pierre G.CARLIER
Laboratoire de Biochimie
Place Delcour, 17
4020 LIEGE.

Les résultats les plus probants quant aux possibilités de la RMN dans l'exploration des systèmes biologiques ont été apportés par le ^{31}P et le ^{13}C (Gadian, 1982). En dépit d'applications biochimiques de valeur, par exemple, l'étude des interactions cations-protéines cytosoliques (Delville et al., 1980) ou cations-membranes (Urry et al., 1980), la RMN du ^{23}Na ne semblait présenter qu'un intérêt biologique plus limité. La principale raison en était l'absence de déplacement spontané de la résonance du ^{23}Na en fonction des variations de l'environnement moléculaire. Des complexes paramagnétiques à base de sels de lanthanides, ont été récemment proposés pour modifier la fréquence de résonance du ^{23}Na (Gupta et Gupta, 1982; Pike et al., 1982). Dans la mesure où ces complexes ne passent pas la barrière membranaire, ils permettent de dissocier le Na intracellulaire du Na extracellulaire. Ces agents de déplacement ouvrent de nouvelles perspectives à la RMN du ^{23}Na. Nous les avons évalué dans le domaine de l'étude des échanges ioniques au niveau de tissus vivants.

MATERIEL ET METHODES.

Nous avons étudié l'activité de la pompe Na-K dépendant de la Na-K ATPase au niveau de globules rouges humains. Le sang a été prélevé dans des seringues héparinées, puis centrifugé à 1500 g pendant 6 minutes. Le plasma et la couche superficielle de globules ont été écartés. Après lavage dans du NaCl 150 mM, les globules rouges ont été utilisés, soit tels quels, soit après une charge en Na de 20 heures à 4°C (Garay et Meyer, 1979).

Le tripolyphosphate de dysprosium a été utilisé comme agent de déplacement. Pour les expériences en RMN, le milieu d'incubation avait la composition suivante : saccharose 250 mM, NaCl 25 mM, KCl 2 mM, glucose 5 mM, tripolyphosphate de dysprosium 2.5 mM. Le milieu a été ajusté à pH 7.40 et thermostaté à 37°C. L'hématocrite était de 66 %.

La pompe Na-K a été inhibée par l'adjonction d'ouabaïne 10^{-4}M à un milieu sans potassium.

Lorsque des ionophores ont été ajoutés, ils ont été préalablement dissous dans 30 ul d'éthanol. Leur concentration finale était de 0.7 mM.

Les échanges de Na ont également été étudiés au niveau de l'épithélium intestinal de tortue terrestre. L'épithélium a été isolé et préparé comme décrit précédemment (Baillien et Schoffeniels, 1961). Le pouvoir osmotique du milieu d'incubation a été augmenté par l'adjonction d'urée 50 mM. Les expériences ont été réalisées à 20°C. Les spectres correspondant à 300 et 1000 accumulations ont été obtenus à l'aide d'un spectromètre Brüker WP 80 opérant à la fréquence de 21.16 mHz.

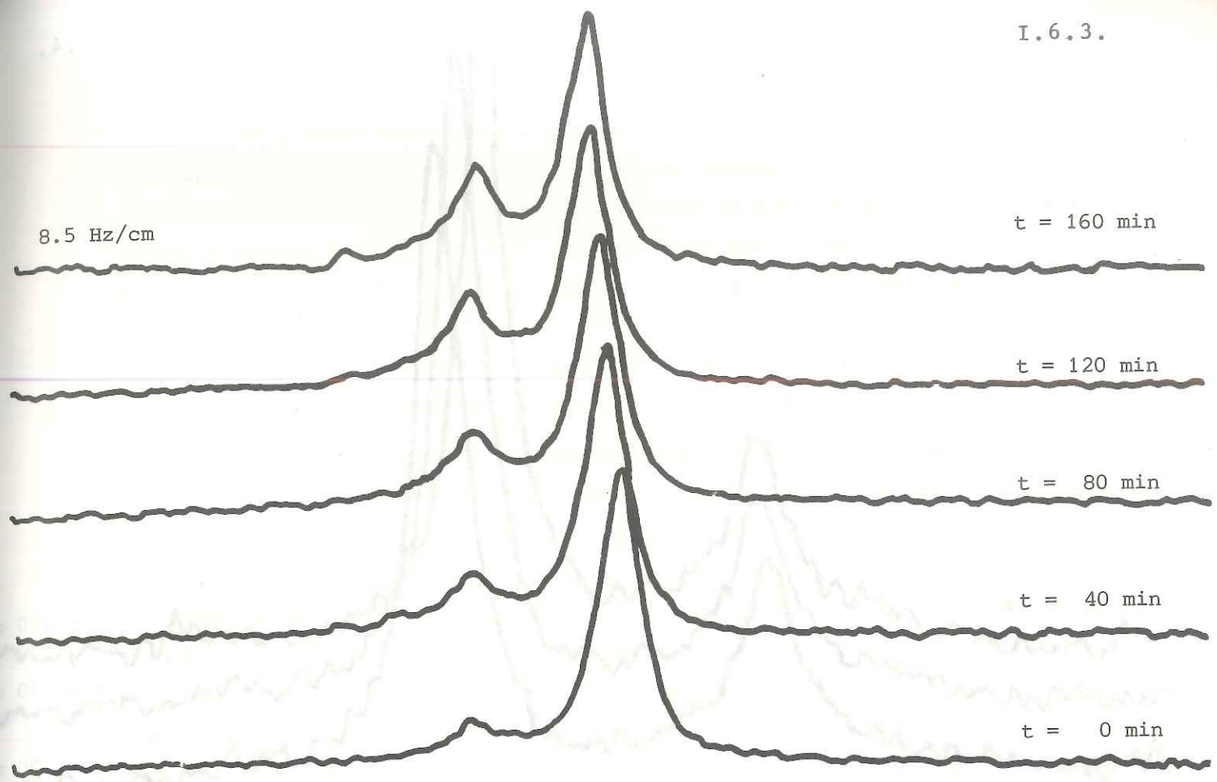

Figure 1. Effet de l'inhibition de la pompe Na-K par l'ouabaïne sur la teneur intracellulaire en Na de globules rouges (pic de gauche : Na intracellulaire; pic de droite : Na extracellulaire).

RESULTATS ET DISCUSSION.

Les conséquences de l'inhibition de la pompe Na-K sont détectées par la RMN du ^{23}Na (figure 1).Le pic de gauche correspond au Na intracellulaire. La surface de ce pic augmente au cours du temps et signe l'entrée de Na consécutive à l'inhibition de la pompe Na-K. Au contraire, dans l'échantillon témoin, le pic de Na intracellulaire reste stable.

Lorsqu'ils sont replacés dans des conditions favorables, les globules rouges préalablement chargés en Na chassent activement le Na excédentaire. Ce point est illustré dans la fibure 2b par la diminution progressive de la surface du pic de Na intracellulaire. En présence d'ouabaïne, les globules rouges sont incapables de mener à bien le rejet de Na, comme le montre la figure 2a. Le pic de Na intracellulaire ne diminue pas.

Les agents de déplacement autorisent bien plus qu'une simple séparation de Na intra- et extracellulaire. Ils permettent à la RMN du ^{23}Na de suivre l'activité de la pompe Na-K.

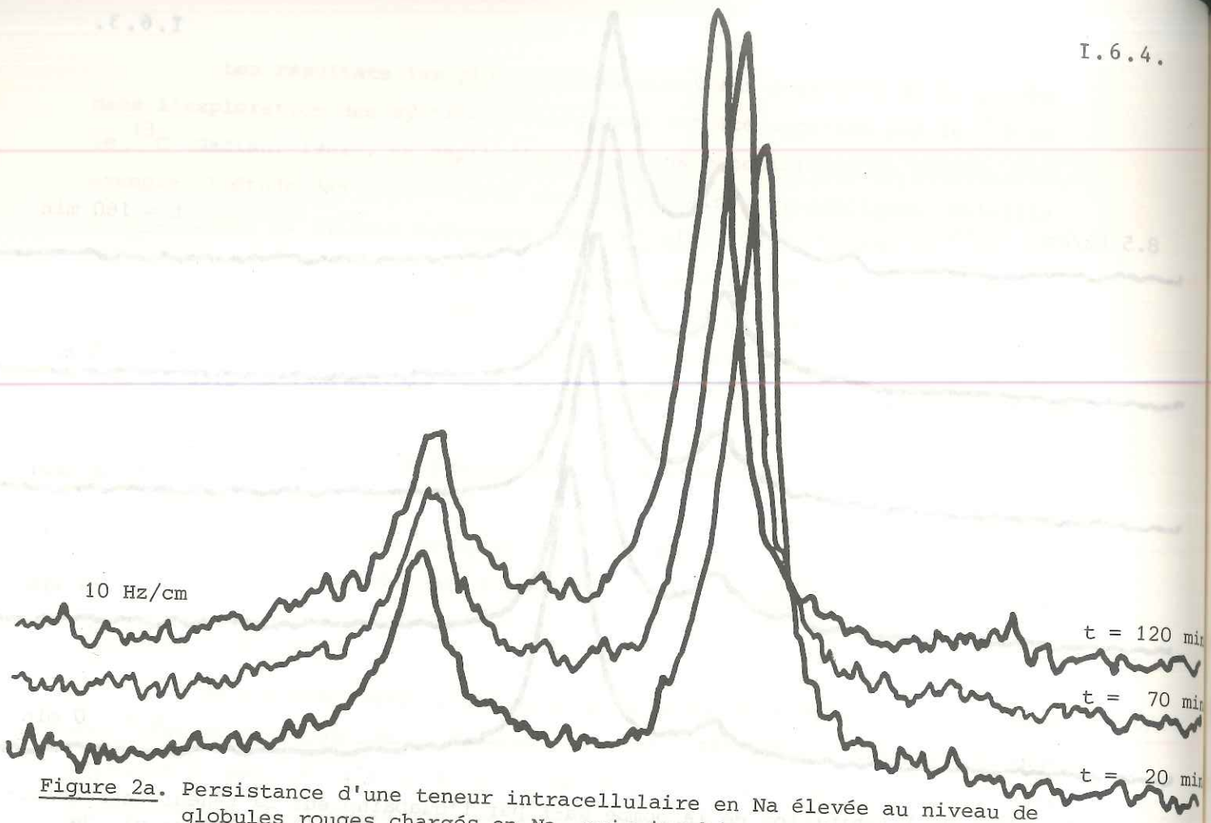

Figure 2a. Persistance d'une teneur intracellulaire en Na élevée au niveau de globules rouges chargés en Na, puis incubés en présence d'ouabaïne (pic de gauche : Na intracellulaire; pic de droite : Na extracellulaire).

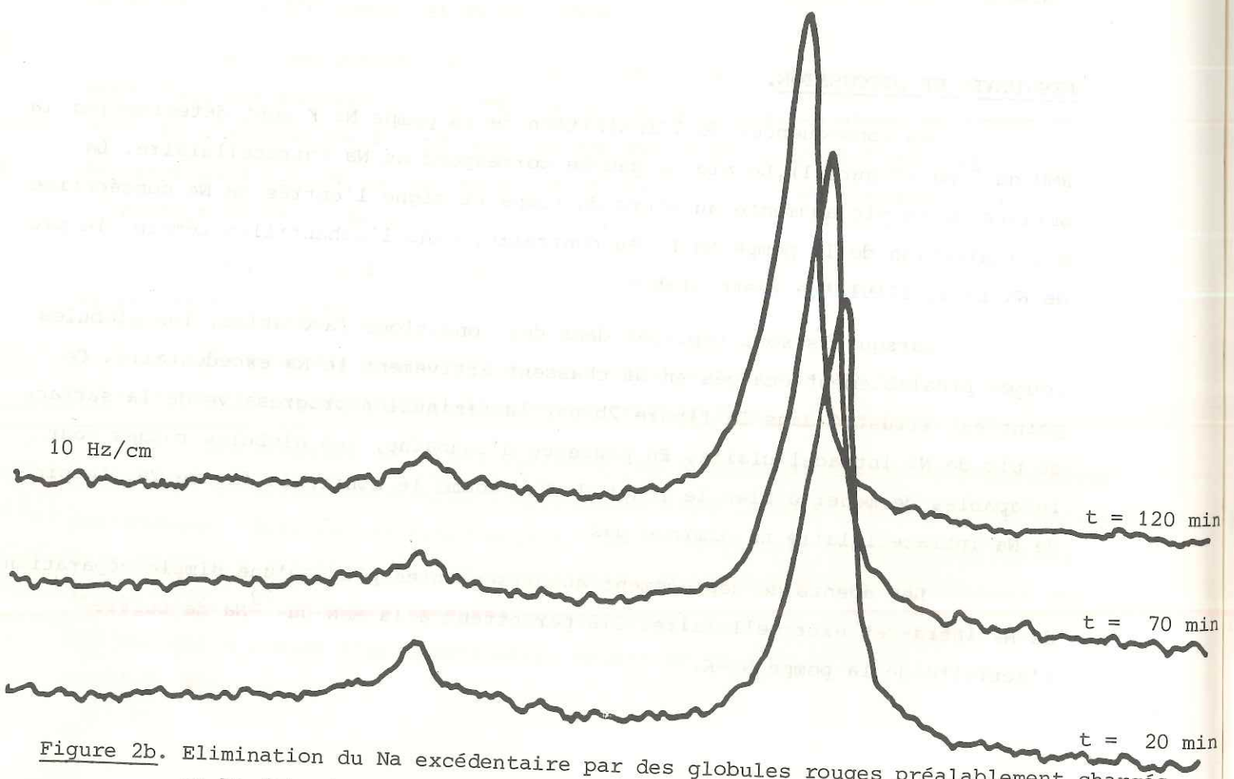

Figure 2b. Elimination du Na excédentaire par des globules rouges préalablement chargés en Na (pic de gauche : Na intracellulaire; pic de droite : Na extracellulaire).

Il existe plusieurs circonstances où l'activité des pompes sodiques membranaires est perturbée. Parmi celles-ci, citons l'hypertension, la grossesse, l'insuffisance rénale. L'activité de la pompe Na-K a été mesurée par RMN sur des globules rouges prélevés chez des insuffisants rénaux avant et après dialyse. Après une charge en Na, ces globules se comportent différemment suivant le moment du prélèvement. Avant dialyse (figure 3a), la pompe Na-K est fonctionnellement muette : le pic de Na interne ne se modifie pas. Après dialyse, elle récupère une certaine activité (figure 3b) : le pic du Na interne diminue.

Ce flux sortant de Na peut également être démontré par les variations de déplacement chimique du pic externe. Le déplacement chimique du Na dépend du rapport entre la concentration du complexe et celle du Na et des autres cations (Grandjean et al., non publié). Lorsqu'on ajoute du Na (ou lorsque des cellules éliminent du Na), le rapport complexe/cations diminue et le déplacement chimique se réduit. C'est ce que l'on observe dans la figure 3b quand la pompe est active. De plus, lorsqu'on incube des globules rouges prélevés après dialyse avec du plasma prélevé avant dialyse, on obtient à nouveau une inhibition de la pompe Na-K. Ces résultats sont compatibles avec l'existence chez l'insuffisant rénal d'un facteur humoral inhibant la pompe Na-K (Krzesinski et Rorive, 1983).

La RMN du ^{23}Na est donc apte à explorer de façon fine et précise des situations pathologiques.

Les échanges de Na ont ensuite été abordés au niveau d'un tissu plus structuré. Le choix s'est porté sur l'intestin de tortue en raison des faibles besoins énergétiques de ce tissu, ce qui dispense de la mise en place d'un circuit d'oxygénation. L'épithélium intestinal de tortue en hibernation est relativement résistant à l'action de l'ouabaïne. Néanmoins, à la concentration de 5.10^{-4}M, on observe une augmentation modérée, mais significative du pic interne (figure 4b), alors que ce pic ne change pas dans l'échantillon témoin (figure 4a). De plus, dans l'échantillon témoin, on détecte un épaulement au niveau du pic externe. Cet épaulement croît pour finalement s'individualiser sous la forme d'un troisième pic. Il pourrait dépendre de la pénétration progressive du complexe dans un compartiment extracellulaire. La présence de deux pics de Na externe pourrait s'expliquer par des échanges lents entre le milieu d'incubation et ce compartiment extracellulaire. En fonction des résultats isotopiques antérieurs (Gilles-Baillien, 1981), ce troisième compartiment pourrait correspondre au mucus.

Pour finir, l'action de plusieurs ionophores a été testée sur des globules rouges. L'effet de la monensine est représenté sur la figure 5. La décroissance rapide du pic interne, la réduction du déplacement chimique,

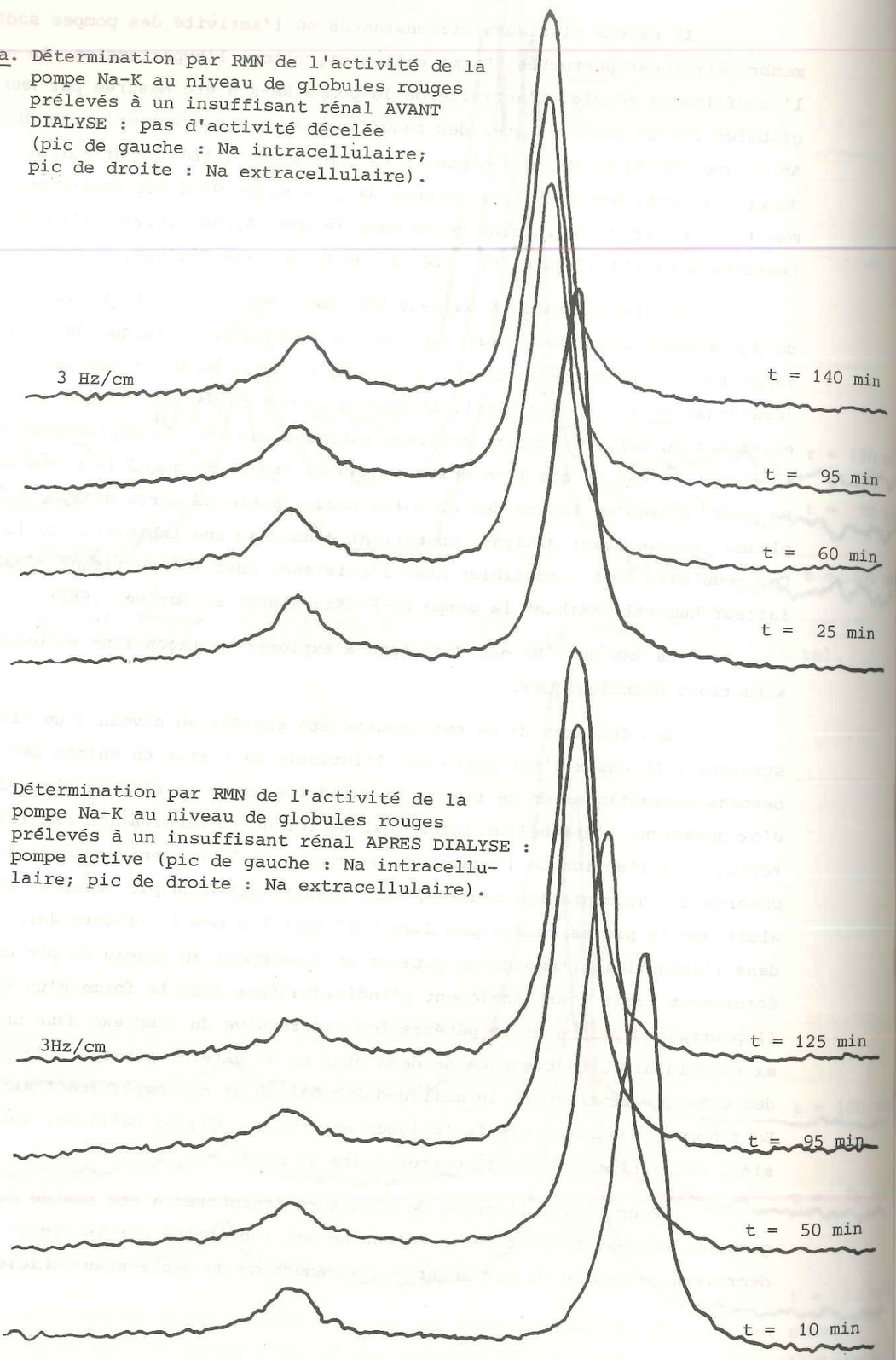

Figure 3a. Détermination par RMN de l'activité de la pompe Na-K au niveau de globules rouges prélevés à un insuffisant rénal AVANT DIALYSE : pas d'activité décelée (pic de gauche : Na intracellulaire; pic de droite : Na extracellulaire).

Figure 3b. Détermination par RMN de l'activité de la pompe Na-K au niveau de globules rouges prélevés à un insuffisant rénal APRES DIALYSE : pompe active (pic de gauche : Na intracellulaire; pic de droite : Na extracellulaire).

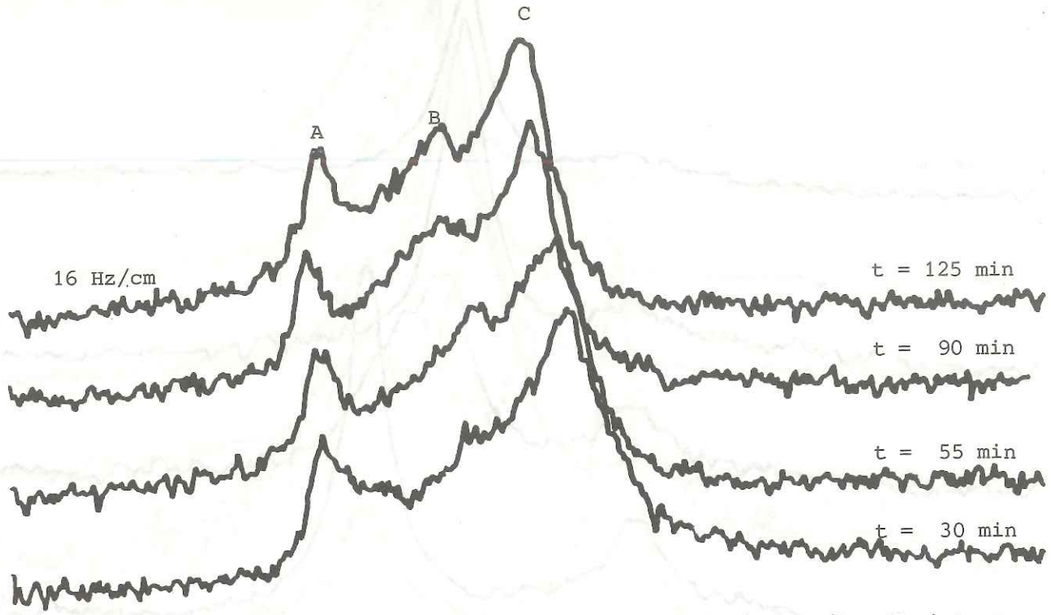

Figure 4a. Incubation d'épithélium de tortue dans un milieu sans ouabaïne (A : Na int.; B : Na ext. ; C : pic à identifier)

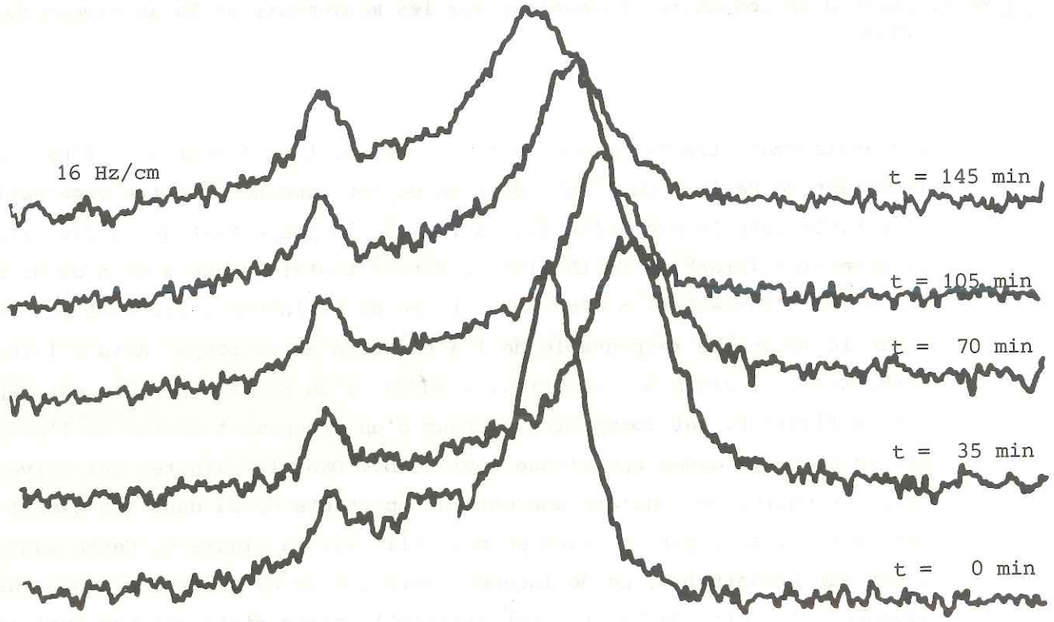

Figure 4b. Incubation d'épithélium de tortue dans un milieu avec ouabaïne.

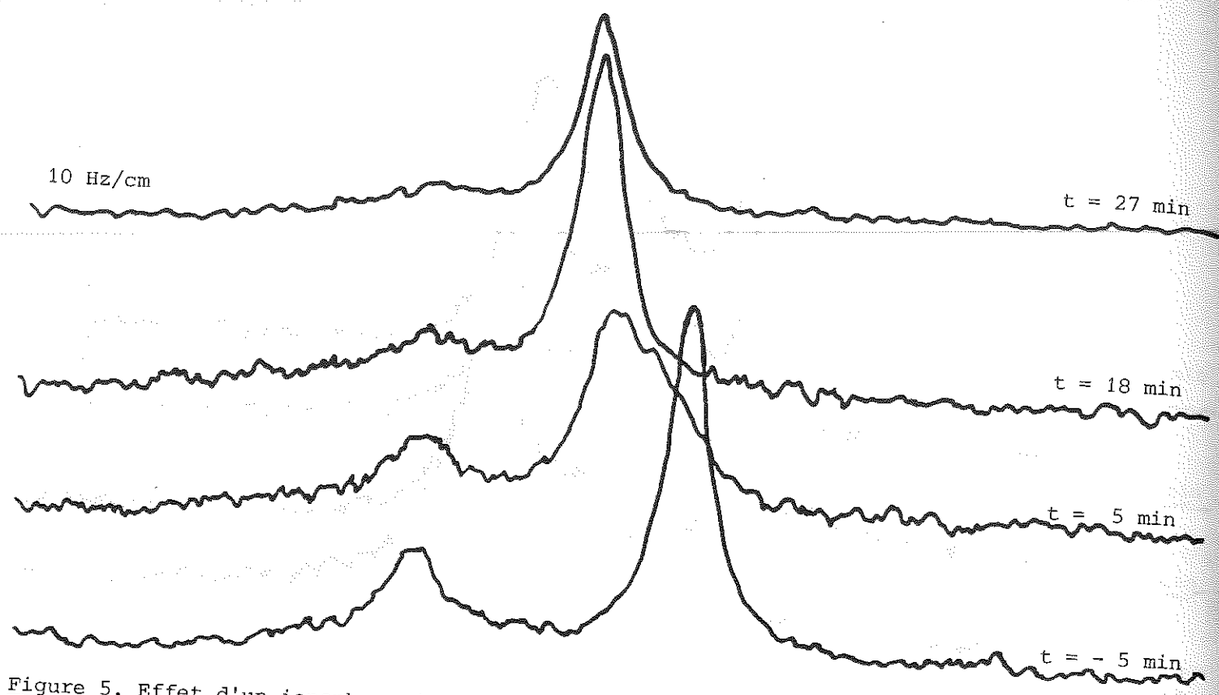

Figure 5. Effet d'un ionophore (monensine) sur les mouvements de Na au niveau du globule rouge.

l'élargissement transitoire du pic externe, sont en faveur d'un flux sortant important de Na lors de l'introduction de cet ionophore. Cette observation est compatible avec la propriété activatrice de la pompe Na-K qui a été attribuée à la monensine (Brock et Smith, 1982). Notons toutefois que nous n'avons pas objectivé d'augmentation même transitoire de Na interne, proposée par ces auteurs comme le mécanisme responsable de l'activation de la pompe. Afin d'illustrer la diversité de leurs modes d'action, l'effet d'un autre ionophore est représenté sur la figure 6. Cet ionophore, porteur d'un groupement dérivé de l'acide tétronique, est en principe assez spécifique pour le Na. Dans les minutes qui suivent l'addition de l'ionophore, on constate une entrée importante de Na dans les globules rouges. Ceci est illustré par le tracé en pointillé sur la figure 6. Cette augmentation n'est que transitoire. Le déplacement chimique de Na externe diminue ensuite progressivement; les pics de Na intra-et extracellulaires finissent par fusionner (figure 6). Cette dernière observation est compatible avec un passage progressif du complexe à l'intérieur des globules. La réduction progressive du déplacement chimique pourrait correspondre à une fixation de complexe au niveau de récepteurs aux phosphates situés à la face interne de la membrane.

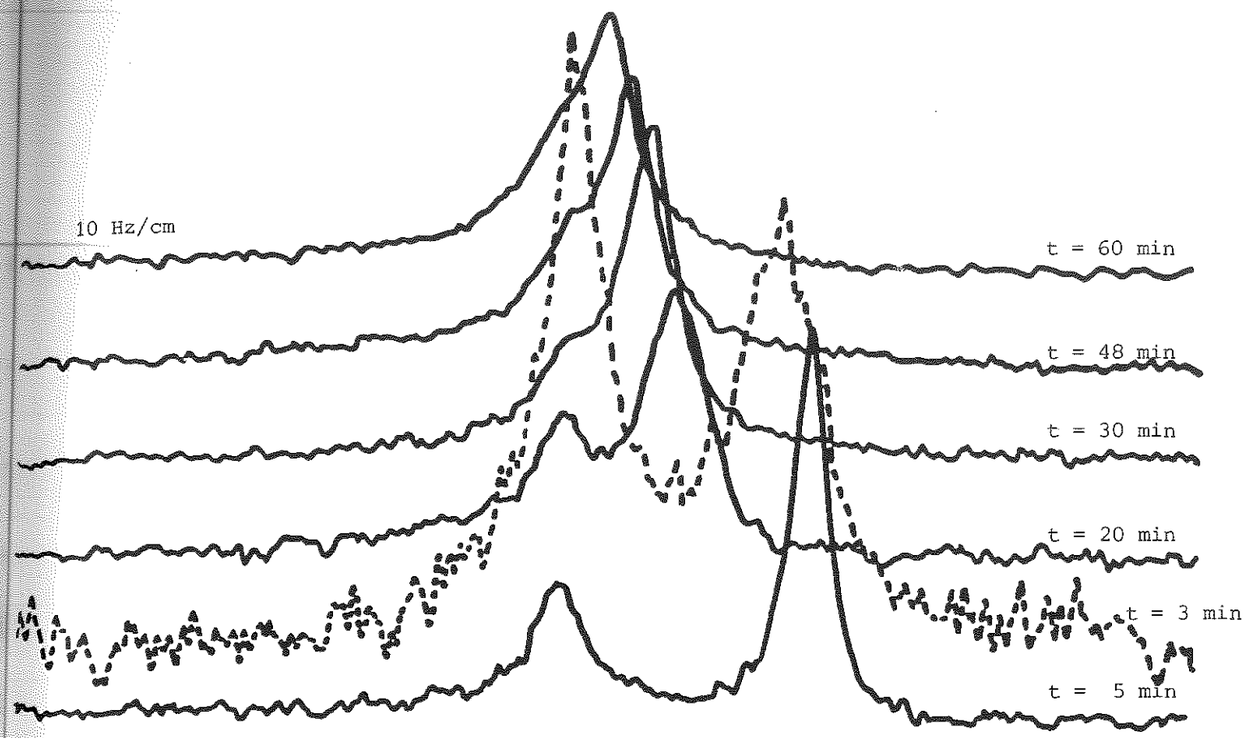

Figure 6. Effet d'un ionophore porteur d'un groupement dérivé de l'acide tétronique sur les mouvements de Na au niveau du globule rouge (à comparer à la figure 5). Le spectre en pointillé a été agrandi 2 fois).

En conclusion, la RMN du ^{23}Na se révèle suffisamment sensible pour apporter des renseignements de valeur sur les échanges membranaires de Na. En outre, cette technique présente plusieurs avantages par rapport aux méthodes classiques d'investigation : absence de traceur radioactif, possibilité de mesures répétées sur un même échantillon, détermination simultanée de Na intra- et extracellulaire. La RMN du ^{23}Na est donc un outil utile dans l'étude des échanges ioniques membranaires.

REFERENCES.

BAILLIEN, M. and SCHOFFENIELS, E.
Transport actif d'acides aminés au niveau de l'épithélium intestinal isolé de la tortue grecque.
Biochim.Biophys.Acta, 1961, 53, 521-536.

BROCK, T.M. and SMITH, J.B.
Reversible stimulation of the Na^+/K^+ pump by monensin in cultures of vascular smooth muscle.
Life Sciences, 1982, 31, 1043-1050.

DELVILLE, A., GRANDJEAN, J., LASZLO, P., GERDAY, C., BRZESKA, H. and DRABIKOWSKI, W.
Sodium-23 nuclear magnetic resonance as an indicator of sodium binding to calmodulin and tryptic fragments in relation to calcium content.
Eur.J.Biochem., 1980, 109, 515-522.

GADIAN, D.G.
Nuclear magnetic resonance and its applications to living systems.
Clarendon Press, Oxford, 1982.

GARAY, R.P. and MEYER, P.
A new test showing abnormal net Na^+ and K^+ fluxes in erythrocytes of essential hypertensive patients.
Lancet, 1979349-353.

GILLES-BAILLIEN, M.
Na, cycloleucine and insulin compartments in tortoise intestinal mucus. Possible role of the mucus in intestinal absorption processes.
Molecular Physiology, 1981, 1, 265-272.

GUPTA, R.K. and GUPTA, P.
Direct observation of resolved resonances from intra- and extracellular sodium-23 in NMR studies of intact cells and tissues using dysprosium(III) tripolyphosphate as paramagnetic shift reagent.
Journal of Magnetic Resonance, 1982, 47, 344-350.

KRZESINSKI, J.M. and RORIVE, G.L.
An additionnal argument for the inhibition of the Na-K pump in hypertension.
Sous presse.

PIKE, M.M., SIMON, S.R., BALSCHI, J.A., and SPRINGER, C.S.Jr.
High-resolution NMR studies of transmembrane cation transport : use of an aqueous shift reagent for ^{23}Na.
Proc.Natl.Acad.Sci., 1982, 79, 810-814.

URRY, D.W., TRAPANE, T.L., ANDREWS, S.K., LONG, M.M., OVERBECK, H.W. and OPARIL, S.
NMR observation of altered sodium interaction with human erythrocyte membranes of essential hypertensives.
Biochem. Biophys.Research Communications,1980, 96(1), 514-521.

NUCLEAR MAGNETIC RESONANCE

A. LUITEN (Eindhoven, the Netherlands)

Text not received.

COST EFFICIENCY OF PRESENT DAY NMR-CT SYSTEMS IN CLINICAL PRACTICE

A.M. Ruis, Dr R. Hauke - TOSHIBA MEDICAL SYSTEMS EUROPE

This lecture attempts to analyze the cost efficiency of the presently available nuclear magnetic resonance imaging systems.

The NMR-CT imaging systems can be divided into 3 classes, which differ from eachother in the way the main magnetic field is created. These classes are :

1. Resistive magnet systems
2. Superconductive magnet systems
3. Permanent magnet systems

In order to use the magnetic fields created by either one of these magnet designs for NMR-CT imaging, it is necessary to overlay the main magnetic field with gradient fields of far less magnetic strength which restrict the NMR phenomena to a limited, well defined, area, generally a slice. The NMR phenomena itself, the toppling over of spinning atoms, is accomplished through short bursts of radio frequency energy. The disallignment thus caused within the main magnetic field disappears gradually under the emission of very weak radiowave signals of the same frequency as the one applied earlier on. The weakness of these signals may be appreciated if one is aware, that special shielding precautions, on walls, floors etc., have to be taken, in order to prevent disturbance of the measurements due to such simple things as processor emitted noise on the same frequency.

The forementioned applies to all classes of NMR-CT designs, and each one has its own specific features, including benefits and disadvantages.

1. The RESISTIVE magnet NMR-CT system, of which figure 1 is an outline, shows you schematically the design of this type of magnet system. It consists generally of 4 fairly simple air-cored copper coils, through which the necessary cooling medium (water) flows. The coil configuration resembles, as closely as the technology involved allows, a sphere, which, theoretically, is the best shape in which to create a uniform magnetic field. The magnetic fields that have to be created for NMR-CT imaging purposes, do require a rather substantial amount of electrical power, which causes the coils to become fairly warm. The cooling facilities required for resistive magnet NMR-CT systems will be high powered professional equipment.
The sphere imitating magnet design, does allow the resistive NMR-CT systems to be very compact (figure 2), which results in an overall decrease of site preparations to be made in order to (RF-)shield the systems.

2. The SUPERCONDUCTIVE magnet NMR-CT systems (figure 3) use a completely different technology to obtain the required main magnetic fields. In fact the technology involved is so specialized that most present day superconductive magnets are made by a small number of companies, out of which OXFORD INSTRUMENTS, INTERMAGNETICS GENERAL and BRUKER are three well known ones. The superconductive magnet is based upon the principle, that certain materials become superconductive at extremely low temperatures. The materials, generally niobium-titanium wires, are kept at these low temperatures (approx. 4° Kelvin) within a cylindrical tank filled with liquid Helium. This tank is insulated by liquid nitrogen which again is insulated by a vacuum. The magnet itself consists therefore of several tanks inside eachother. The magnet shape solenoid is the closest resemblance of the sphere this technology allows. Due to the required cooling the superconductive systems tend to be both larger and heavier than resistive systems, thereby requiring more extensive site preparations. On the other hand, the obtainable magnetic fields can be much higher and can be reached with much lower electrical power consumption.

The Helium for superconductive magnet systems is produced in the USA as a natural gas and is a so called "DEFENSE RESTRICTED USE" product, which in some european and eastern block countries can only be purchased via contracts and approved suppliers. Maintenance wise, the superconductive systems are more vulnerable since both vacuum and temperature leaks could easily lead to down-time, whereby one should bear in mind, that restarting the magnet currently takes more than one week.

3. The PERMANENT magnet NMR-CT systems use magnets which generally consist of soft iron alloys, the parts of which are either magnetized at the production site, or on-site in the hospital. Several permanent magnet designs are nowadays in use, the two commonly used are the Watson design, which is shown in figure 5, which consists of two soft iron poles capped with two thinner soft iron plates and the so-called "C"-magnet which, as the name already suggests, resembles the letter C. Compared with the resistive and the superconductive types, the permanent magnet's main magnetic field does not point in the horizontal plane, but in the vertical plane. The uniformity of the permanent magnet's field depends on other parameters than observed in the case of the resistive and superconductive magnets. Some of these parameters are pole-to-pole distance, pole-surface etc.
The permanent magnets do posses a kind of self-shielding effect, that makes them much less vulnerable for external magnetic interference.
Due to the obvious absence of cooling equipment and main magnetic field power supply (not gradient- and shim(=correction) power supply) the required floorspace is minimal. Maintenance costs should, for the above reasons, be expected to be less than for both other types of magnet designs.
In order to reach adequate magnetic fields for NMR-CT imaging purposes, the permanent magnets are made from special soft-iron alloys. These alloys result in the systems being expensive and heavy. The magnets themselves come as, 1.000 kg maximum, blocks which are magnetized and put together into a total unit weighing some 100.000 kilograms. The on-site magnetization is most often used due to the shock liability of the magnet.

Limited clinical practice has up until now been obtained with permanent magnet NMR-CT systems. An example of a permanent magnet system is shown on figure 6. Depending on their main magnetic field strength, this magnet concept allows the production of very compact NMR-CT systems.

The following tables list some key Resistive, Superconductive and Permanent magnet data.

Applicable to all NMR-CT systems, independent from their design, shall be the current safety regulations. The present-day commonly referred to recommendations are listed in figure 7.
Possibly in the future more stringent regulations could result in cumbersome extra shielding being required. Due to the limited magnetic fields obtainable in the case of the resistive magnet systems, and the self-shielding effect and special geometry in the case of the permanent magnet, these two systems will be less vulnerable for such kind of recommendations. This applies to a less extent for the to be expected phosphorus measuring superconductive systems, for which a new building should probably be constructed anyway.

Coming to the main subject of this lecture, the cost-efficiency of present-day NMR-CT systems in clinical use. The estimations are all based upon a depreciation period of 5 years, a patient throughput of 10 patients per day, and 18 working days per month. The estimations do not take into account the specialist's remuneration.

Summaryzing :

From the present-day NMR-CT systems, the resistive magnet systems seem to be the most cost-efficient ones. I would like to emphasize the prefix : present-day, because a lot of research is going on to improve the performance of the various systems. Examples might be the efforts which are being made to decrease the resistive magnet's power consumption and the efforts now poured into the production of superconductive systems, in which the Helium and Nitrogen boil-off rates are greatly diminished.

In general I would like to point out, that the manufacturers of x-ray CT systems are in an advantageous position in relation to diagnostic imaging presentation, because of their already massive investments in display system technology including specialized software.

This cost-efficiency estimation deliberately did not take into account the "other elements" superconductive NMR-CT systems, due to the limited availability of data. Recent publications indicate, that one of the major drawbacks of these systems, which is the need to wait for a rather long magnetic field stabilization period, in the order of hours, when magnets are switched from phosphorus measuring level (approx. 15.000 Gauss) to the hydrogen imaging level (approx. 3.500 Gauss), has been overcome.

Until the clinical relevance of in vivo registration of chemical shifts has not been unequivocally proven, the use of these expensive, both in initial investment and in required site preparations, systems should be restricted to a certain number of research institutes. An even better situation would evolve, if and when it would be found, that the in vivo chemical shift measurements renders many existing diagnostic methods superfluous, thereby opening the way to the decrease in overall healthcare spending, which many of our national governments advocate.

NUCLEAR MAGNETIC RESONANCE IMAGING MAGNET SYSTEMS

	RESISTIVE MAGNET	SUPERCONDUCTIVE MAGNET	PERMANENT MAGNET
MATERIAL	AIR CORED COPPER WIRES	NIOBIUM-TITANIUM (NbTi) EMBEDDED IN A COPPER MATRIX	SOFT IRON ALLOYS
MAXIMUM MAGNETIC FIELD	1.500 GAUSS	20.000 GAUSS	3.000 GAUSS
POWER CONSUMPTION	120 KVA	30 KVA	NIL (EXCEPT GRADIENT AND SHIM POWER SUPPLY
COOLING MEDIUM	WATER	LIQUID HELIUM LIQUID NITROGEN	NOT REQUIRED
COOLING MEDIUM CONSUMPTION	60 LITERS/MINUTE	HELIUM : 0.5-0.75 L/HR NITROGEN : 2 - 3 L/HR	NIL

NUCLEAR MAGNETIC RESONANCE IMAGING MAGNET SYSTEMS

	RESISTIVE MAGNET	SUPERCONDUCTIVE MAGNET	PERMANENT MAGNET
COOLING MEDIUM PRICE	HFL 0,50/1.000 LITERS	HELIUM : HFL 16,-/LITER NITROGEN : HFL 1,-/LITER	NIL
ESTIMATED RUNNING COSTS PER DAY	HFL 400,--	HFL 800,-- (90 % COOLING)	HFL 100,- (GRADIENT AND SHIM POWER SUPPLY)
HEAT DISSIPATION	250.000 BTU/HR	50.000 BTU/HR	NIL
WEIGHT	APPROX. 3.000 KG	5.000 - 10.000 KG	UP TO 100.000 KG
WARMING-UP TIME	APPROX. 1 HOUR	2 - 4 WEEKS	NIL
ADVANTAGES	LOW PRICE LOW RUNNING COSTS EASY PRODUCABLE	HIGH AND STABLE FIELD HIGH UNIFORMITY LOW POWER CONSUMPTION	NO COOLING REQUIRED NO POWER CONSUMPTION NO RF SHIELDING REQUIRED
DISADVANTAGES	HIGH POWER CONSUMPTION LOW MAGNETIC FIELD	HIGH PRICE HIGH RUNNING COSTS HEAVY	EXTREMELY HEAVY VERY EXPENSIVE SHOCK LIABLE ON-SITE MAGNETIZATION REQUIRED

MAGNETIC FIELD SAFETY RECOMMENDATIONS

PATIENT EXPOSURE (NATIONAL RADIATION PROTECTION BOARD - UNITED KINGDOM)

STATIC FIELD	GRADIENT FIELD	PULSED RF FIELD
LESS THAN 25.000 GAUSS	LESS THAN 200.000 GAUSS FOR PULSE DURATIONS OF 10 MSEC OR MORE	LESS THAN 1^{o} C INCREASE OF AVERAGE BODY TEMPERATURE

STAFF EXPOSURE (UNOFFICIAL STATIC MAGNETIC FIELD EXPOSURE LEVELS AS ARE SET BY THE BROOKHAVEN-U.S.A. AND CERN-CH ACCELERATOR LABORATORIES)

FIELD STRENGTH	EXPOSURE TIME	BODY REGION
200 GAUSS	EXTENDED PERIODS	WHOLE BODY
2.000 GAUSS	SEVERAL MINUTES	WHOLE BODY
2.000 GAUSS	EXTENDED PERIODS	EXTREMITIES
20.000 GAUSS	SEVERAL MINUTES	WHOLE BODY

NUCLEAR MAGNETIC RESONANCE IMAGING SYSTEMS
COST EFFICIENCY ESTIMATIONS

x 1.000 HFL

INVESTMENT	RESISTIVE MAGNET	SUPERCONDUCTIVE MAGNET	PERMANENT MAGNET
PURCHASE PRICE INCLUDING VAT	3.000	4.620	6.000
SITE PREPARATIONS INCLUDING VAT	400	500	200
TOTAL INVESTMENT	3.400	5.120	6.200

NUCLEAR MAGNETIC RESONANCE IMAGING SYSTEMS
COST EFFICIENCY ESTIMATIONS

x 1.000 HFL

ANNUAL FIXED COSTS	RESISTIVE MAGNET	SUPERCONDUCTIVE MAGNET	PERMANENT MAGNET
ANNUITY (SYSTEM+SITE)	898	1.352	1.637
PERSONNEL	240	260	240
RENTAL,COOLING,POWER	122,5	216	53
INSURANCE 1 %	34	51,2	62
FIXED COSTS YEAR 1	1.294,5	1.879,2	1.992
SERVICE CONTRACT	210	324,4	210
FIXED COSTS YEARS 2-5	1.504,5	2.202,6	2.202

NUCLEAR MAGNETIC RESONANCE IMAGING SYSTEMS
COST EFFICIENCY ESTIMATIONS

HFL

PATIENT REMUNERATION	RESISTIVE MAGNET	SUPERCONDUCTIVE MAGNET	PERMANENT MAGNET
REMUNERATION	680,-	990,-	1.000,-
ACTUAL PATIENT COSTS	40,-	40,-	40,-
PATIENT REMUNERATION	720,-	1.030,-	1.040,-

ASSUMPTION : 10 PATIENTS PER DAY, 18 WORKING DAYS PER MONTH

Parametric Imaging in NMR Tomography

R. Knopp, H.J. Biersack, C. Winkler

Institut für klin. und exp. Nuklearmedizin der Universität, Bonn, FRG

Unlike conventional imaging techniques like radionuclide scintigraphy or X ray CTscans, in which the information portrayed is a reflection of essentially only a single physical parameter (distribution of radioactivity, X ray beam attenuation), Nuclear Magnetic Resonance (NMR) tomography may be performed by a number of techniques. NMR scanners produce images which depict the location and behavior of atomic nuclei emitting NMR signals. The extend to which the nuclei's spin density and relaxation times T1 and T2 contribute to image contrast depends upon the specific radiofrequency pulse sequence used. The pulse program can be chosen to enhance image contrast by emphasizing T1 or T2 contributions respectively, to signal intensity. This is demonstrated in fig. 1 displaying 4 selected pictures of a Carr-Purcell-sequence in a patient with glioblastoma.

The time intervals between the first RF pulse and image acquisition are 27, 81, 135, and 216 ms. The area of tumor surrounded by edema contrasts very well in the two last images. However, since the proton density in the tumor-edema region does obviously not differ from that within normal brain tissue the pathological process is not to be noticed in the first echo image emphasizing preferently spin density. The transverse magnetization of the tumor tissue decays more slowly when compared to the unaffected tissue (3) so that in the latest picture of the sequence the tumor-edema area is clearly difened.

In principle, similar conditions have to be taken into consideration when spin-lattice relaxation (T1) is used for NMR imaging. In spite of the fact that T1 may be extremely useful for diagnostic

purposes it has turned out to be disadvantageous that in the techniques used up to present the so called T1 and also T2 images represent a mixture of parameters. Thus the resulting tomograms depend at an undefined extend to spin density in addition to relaxation time (1).

In view of this fact it cannot be excluded that standardization problems have to be faced by the clinician because the result of the examination might vary for the same patients if examined at different times, from one patient to another and from one facility to the next.

In order to overcome this considerable disadvantage we developed a method of parametric imaging which renders possible a clearcut separating the different parameters on which the NMR tomogram is based (2). When the exponential function of relaxation is assessed the true value of relaxation time and also of spin density can easily be calculated from the respective curve and protrayed as an image. Fig. 2 shows the decay of transverse magnetization in a tumor-edema area in comparison to the decay in a normal brain region representing exponential least square fits. The constant coefficients of the exponential function serve for generating parametric frames (fig. 3) which are unaffected by undefined mixtures of NMR parameters.

In our opinion it is indispensable to use parametric imaging techniques for standardized application of NMR tomography in clinical practise.

Our experiments were performed on hand of the BRUKER BNT 1000 tomography system (0, 15 T, 6 MHz), and we would like to particularly thank Dr. P.Brunner and Mr. Ratzel for their continued support during the measurements.

References:

1. Bydder, G.M., R.E.Steiner et al.: Clinical NMR Imaging of the Brain - 140 Cases. Amer.J.Radiol. 139 (1983) 215-236
2. Knopp, R., H.Schmidt, H.J.Biersack, C.Winkler: Untersuchungen zur Technik der Kernmagnetresonanz Tomographie - Parametrische T_2-Darstellung. NucCompact 13 (1982) 289-290
3. Pykett, I.L., J.H.Newhouse et al.: Principles of Nuclear Magnetic Resonance Imaging. Radiology 143 (1982) 157-168

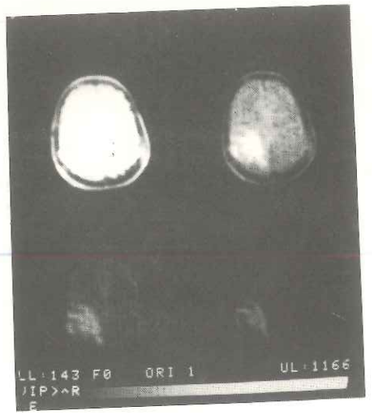

Fig. 1: 4 selected images out of a Carr-Purcell sequence comprising a total of 8 images in a patient with a glioblastoma (tumor surrounded by edema). The time intervals between the first RF pulse and image acquisition are 27, 81, 136 and 216 ms.

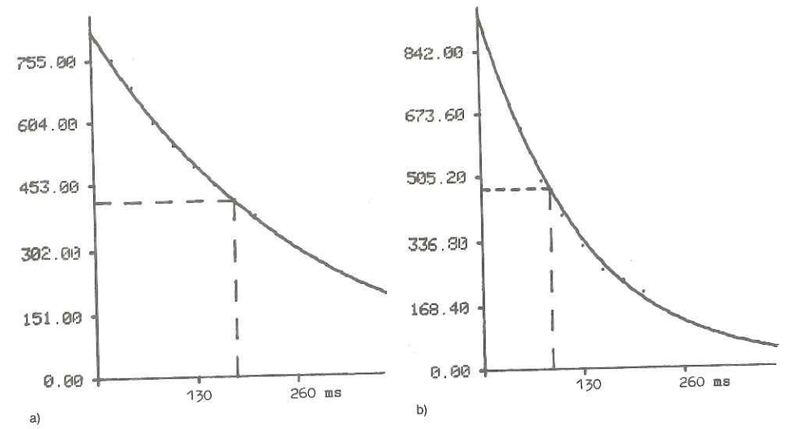

Fig. 2: Monoexponential fit of the proton spin relaxation in two regions of interest: a) the tumor area and b) a contralateral unaffected area.

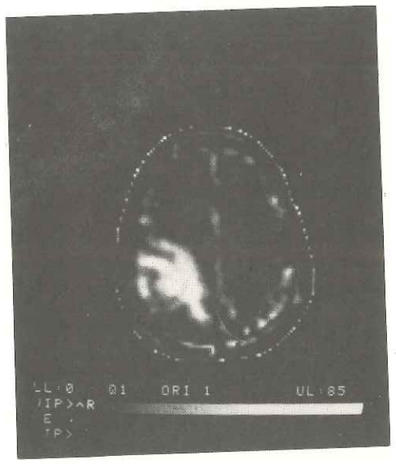

Fig. 3: Parametric T2 presentation obtained after monoexponential fitting of the spin-echo-sequence.

ETUDE COMPARATIVE DES ACQUISITIONS BI- ET TRI-DIMENSIONNELLES EN RMN

M. COLLARD (Montignies-le-Tilleul, Belgique)

Texte non parvenu.

AN OVERVIEW OF NMR IN CANCER

R. MATHUR-DE VRE

INSTITUT D'HYGIENE ET D'EPIDEMIOLOGIE

BRUSSELS

The vast scope for the applications of NMR Spectroscopy in cancer for diagnosis and research was revealed by two important events : (i) The publication of a report by Damadian (1) showing that NMR parameters (T_1 and T_2) of tissue water are different for normal and cancerous cells, and (ii) the description of an experiment by Lauterbur (2) designed to illustrate the resolution of different NMR terms in the heterogeneous biological space.

The NMR spectroscopy can be profitably applied in the field of cancer both by imaging techniques, and non-imaging methods such as tissue characterization using high resolution NMR. Imaging localizes in the biological space those tissues that exhibit an abnormal behaviour of water, whereas tissue characterization leads to precise and meaningful identification of pathological and physiological details of tissues.

In the NMR studies of cancer cells, the commonly employed index parameters are the relaxation times and signal intensity. T_1 and T_2 provide complementary information about the molecular states of water in cells and tissues. As a result, certain types of lesions are better seen either in T_1 or in T_2 images, but most are detectable when T_1 and T_2 are used in conjunction with each other. A very important and unique feature of NMR is its multiparameter nature that renders it useful as a means for research but highly complex for medical diagnosis.

Most of the work on cancer detection by NMR reported so far is based on the proton signal from tissue water. Recent studies on ^{31}P have also revealed some interesting applications (3). The initial studies by ^{1}H NMR were performed on tumours of diverse histological types, with tumours of animal and human origin, excised tumours and for tumours transplanted in live animals.

./...

A striking observation from these and more recent studies by imaging is, that the cancerous tissues generally exhibit longer relaxation times T_1 and T_2 values as compared with the corresponding or the surrounding normal tissues.

The state of "water balance" of cells and tissues, i.e., the water content and multiple intrinsic structures of water are sensitive to many essential biological processes. This gives rise to high sensitivity of NMR relaxation times to detect abnormal states of tissues, lesions and tumours that are associated with changes in the state of water. However, the dependence of "water balance" on a number of pathological conditions (some of which may be cancerous) and other physiological processes, as well as the effects of extrinsic physical parameters on T_1 and T_2, strongly limit the unique diagnostic capabilities of NMR for malignant tissues, resulting in a lack of specificity.

Figure 1 and Table 1 summarize some relaxation times of various tissues in live rats and human patients. In certain cases overlapping between relaxation times of normal and cancerous tissues has been reported. Ever since the discovery of the usefulness of NMR in cancer, research activities developed along two main lines: (i) Checking the specificity and sensitivity for diagnostic purpose. (ii) Seeking a satisfactory explanation for the increase in relaxation times.

COMPARISON OF T_1 AND T_2 TIMES FOR VARIOUS NORMAL AND ABNORMAL TISSUES IN LIVE RATS. P, PYOGENIC ABSCESS; S, STERILE ABSCESS (11)

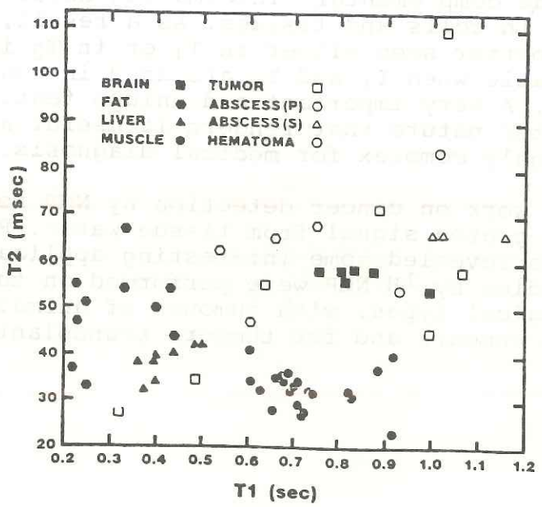

Figure 1.

./...

RELAXATION TIMES+ FOR NORMAL AND PATHOLOGICAL TISSUES FROM PATIENTS (12)

TISSUES	T_1	TISSUES	T_1
CEREBRUM GREY MATTER	275	METASTASES (LIVER)	300-450
WHITE MATTER	225	PANCREATITIS	200-275
CEREBRO-SPINAL FLUID	350-1000	CARCINOMA PANCREAS	275-400
BLOOD	340-370	KIDNEY	300-340
EDEMA	360-420	URINE	600-1000
INFARCT	320-375	ACUTE TUBULAR NECROSIS	400-420
GLIOMA	250-350	CARCINOMA	400-450
METASTASES (CEREBRRUM)	250-350	METASTASES (KIDNEY)	400-450
MENINGIOMA	200-300	SIMPLE CYST	600-1000
LIVER	140-170	ABSCESS	390-420
SPLEEN	250-290	BLADDER CARCINOMA	200-240
PANCREAS	180-200	PROSTATE	250-325
BILE	250-300	CARCINOMA PROSTATE	350-450
CIRRHOSIS	180-300		

+VALUES AT 1.7 MHz (MS)

Table 1

From the point of view of detecting cancerous state by NMR, it is important to indicate that two types of discriminating effects are encountered : (i) Those in which T_1 and T_2 of the affected tissues are generally found to be longer than other normal tissues. (ii) Those in which relaxation times of uninvolved and distant organs and serum are enhanced in the presence of fast growing tumours. This was defined as "systemic effect".(4)

The earlier studies on experimental tumours in animals raised several questions :

(1) Would it be possible to distinguish malignant tissues from begign lesions, necrotic tissues and other abnormal but non malignant states ?

(2) Would the same sensitivity for elevated T_1 and T_2 values reported for animal tissues be observed for human tumours also ?

(3) What is the basis underlying elevated T_1 and T_2 values in tumours as compared with normal tissues ?

The answers to these questions are still controversial. There are reports indicating that NMR can be very sensitive but not specific for unequivocal identification of malignant tissues. Other diseases perturbing the state of water also enhance the relaxation times. Several examples are reported in the literature of non-malignant processes such as inflammation (5), sickle cell disease (6), and post-mortem changes in muscle (7) which produce a similar change in the NMR parameters. In thyroïd gland tissue, anti-thyroïd drug treatment and malignant transformation of the gland were found to produce the same extent of increase in T_1 (8,9).

./...

It has been suggested that the enhancement of T_1 and T_2 of water protons in cancerous cells with respect to the normal state is due to :

(1) Increase in the toal water content.

(2) Increase in the ratio of free to bound water.

(3) Change in the structure of intracellular water : tumours exhibiting a higher degree of rotational freedom.

(4) Growth rate of tumours.

(5) Change in the concentration of paramagnetic ions.

Most probably, the true explanation comprises a relative contribution from all these factors rather than exclusively from one single term as is often errorneously considered. Ling (10) has shown that only 10% of the difference in T_1 between normal and cancerous tissues can be attributed to the change in water content, other factors specific to each tissue also make important contributions.

According to Koutcher et al (3), ^{31}P NMR indicates a more clear cut distinction between normal and cancerous cells than the difference observed for ^{1}H NMR. Probably a more reliable discrimination may be obtained by combining ^{1}H and ^{31}P NMR than by applying one technique alone. It has been proposed that ^{31}P might serve as a useful probe for studying the mechanism of carcinogenesis. Griffiths et al (3a, 3b) suggested from studies on living rats that ^{31}P NMR will be an important tool for studying tumours with a possibility of providing information on the tumour type and its degree of differentiation.

THE BIOPHYSICAL BASIS OF PROTON NMR

In biological systems, water represents a very complex, organized and heterogeneous network that plays a crucial role in maintaining the structural and conformational integrity of all biostructures. As a matter of fact, the biological tissues are marked with microscopic and macroscopic heterogeneity. The modified properties of water near the macromolecular surfaces influence the relaxation times in a characteristic manner by the coupling of relaxation mechanisms with local fluctuating fields produced by the intrinsic dynamic structure of water. With the result, that T_1 and T_2 provide a lot of useful and complementary information about the state of tissue water. This is because T_1 is sensitive to rapidly fluctuating local fields such as those generated by fast rotational motion. Whereas, T_2 senses both the fast and relatively slower fluctuations due to molecular exchange, diffusion of water molecules and proton transfer.

RESULTS FORM WHOLE BODY IMAGING

Over the past few years, interest in medical applications of NMR has continued to grow at a very fast pace. Considerable efforts have been devoted to checking the diagnostic proficiency and exploring new domains.

From the vast literature available on this subject, I have selected three specific examples from the point of view of illustrating the diversity of practical information available from this technique rather than reviewing extensively different biological systems investigated so far.

(1) Davies et al (11) employed the results of imaging of experimentally induced tumours in live rats to obtain relaxation times T_1 and T_2, and correlated them with water content, extracellular fluid volume and plasma concentration in an effort to delineate the importance of determining physical causes of the information available from imaging. They concluded that it is the water content rather than its distribution that affects T_1 and T_2. From a review of several images obtained from : (i) liver injected with 3924A hepatoma (ii) hind legs injected with adenocarcinoma R3230AC mammary, they showed that some lesions could be discriminated either in T_1 or T_2, some in both but all were detactable when T_1 and T_2 were used together for constructing the images. They emphasized on the need of using both T_1 and T_2 for diagnostic purposes.

(2) Images of liver have shown (12) that cirrhosis and hepatocellular diseases have characteristic features. Cirrhosis is not a cancer but a pathological state for which in certain cases a cancer (Hepatoma) may develop, as in the case of cirrhosis by hypoproteinemia. Gore et al (13) reported that whilst cirrhosis increased T_1 of liver, primary biliary cirrhosis and hemachromatosis gave shorter T_1 for liver because they are associated with accumulation of paramagnetic materials.

(3) Hazlewood et al (14) obtained T_1 values from images of human brains. For a patient with neurological symptoms, they observed a higher T_1 value in the region of a mass detected by CAT scan prior to NMR imaging. Their proposal that the mass might be a tumour was confirmed when the lesion removed at surgery was reported to be a glioma.

HIGHLIGHTS AND SHORTCOMINGS OF NMR IN CANCER

The following section outlines certain highlights and shortcomings of NMR.

Highlights

(1) NMR is non-invasive and does not employ ionizing radiations.

(2) As a result, NMR can be safely employed for repeated observations of patients.

(3) In soft tissues one observes high sensitivity and very good resolution.

(4) NMR provides molecular and biochemical information, and reflect the pathological and physiological details that are not accesible by any other technique applicable to living systems.

Shortcomings

(1) Lack of specificity for unequivocal identification of malignant tissues. In other words, NMR is highly sensitive for detecting certain types of lesions but not specific for cancer.

(2) In certain cases there is overlapping of relaxation times that precludes clear cut discrimination between normal and cancerous tissues. This is a serious setbacks for the use of NMR in early detection of cancer.

(3) Multiparameter dependence of NMR often gives rise to complex and ambiguous results, and introduce a number of variable parameters that need to be carefully controlled in experiments.

CURRENT TRENDS AND FUTURE PERSPECTIVES

(1) The variations in T_1 and T_2 are generally considered as effective index parameters for discriminating between the normal and cancerous tissues, eventhough some overlapping is known to occur.

(2) The earlier prognostic views on the unique diagnostic capabilities of NMR in cancer are now being looked upon with great caution and reserve by several groups. It has been suggested to use NMR as a diagnostic tool in cancer in the actual situation as a complement to other imaging methods.

(3) Attention has been drawn to the fact that "NMR Imaging" may be profitably employed as a screening device.

(4) Since repeated observations by NMR are possible without apparent risk to the patient, in-vivo imaging may be invaluable for following the treatment of tumours and study the effects of radiotherapy.

(5) The need for effective clinical evaluation of NMR is likely to promote active research in tissue characterization by high resolution techniques for precise and meaningful identification of tissues.

There is no doubt that NMR applications in the field of cancer, by imaging and non-imaging methods hold a great promise for future. The continued interest and progress in NMR techniques and clinical evaluation studies may yet unfold new and enlightening results and stimulate activities in many unexplored fields.

./...

REFERENCES

(1) R. Damadian, Tumor detection by nuclear magnetic resonances. Science 171, 1151-1153 (1971).

(2) P. Lauterbur, Image formation by induced local interactions : Examples employing NMR, Nature 242, 190-191 (1973).

(3) J.A. Koutcher, K.S. Zaner and R. Damadian, ^{31}P as a nuclear probe for the diagnosis and treatment of malignant tissue. In : NMR in Medicine, pp 101-119 (Ed. R. Damadian). Springer-Verlag, Heidelberg 1981.

(3a) J.R. Griffiths, A.N. Stevens, R.A. Iles, R.E. Gordon and D. Shaw; ^{31}P-NMR investigation of solid tumours in the living rats.Biosci. Rep. 1, 319-325 (1981).

(3b) J.R. griffiths and R.A. Iles; NMR studies of tumours. Biosci. Rep. 2, 719-725 (1982).

(4) P.T. Beall, D. Medina and C.F. Hazlewood, The "Systemic effect" of elevated tissue and serum relaxation times for water in animals and humans in cancers : In NMR in Medicine, pp 39-57 (1981) (Ed. R. Damadian), Springer-Verlag, Heidelberg 1981.

(5) L.A. Saryan, D.P. Hollis, J.S. Economou and J.C. Eggleston, Nuclear Magnetic Resonance Studies of Cancer. IV Correlation of water content with tissue relaxation times. J. Natl. Cancer Inst. 52, 599-602 (1974).

(6) A. Zipp, T.L. James, I.D. Kuntz and S.B. Shohet; Water proton magnetic resonance studies of normal and sickle erythrocytes. Temperature and volume dependence. Biochim. Biophys. Acta 428, 291-303 (1976).

(7) D.C. Chang, C.F. Hazlewood and D.E. Woessner, The Spin lattice relaxation times of water associated with early post mortem changes of skeletal muscle. Biochim. Biophys Acta 437, 253-258 (1976).

(8) J. Sinadinovic, S. Ratkovic and M. Kraincanié, Relationship of biochemical and morphological changes in rat thyroïd and proton spin -relaxation of the tissue water, Endokrinologie 69, 55-66 (1977).

(9) M. Schara, M. Sentjurc, M. Anersperg, and R. Golough, Characterization of malignant thyroïd gland tissue by magnetic resonance methods, Br. J. Cancer 29, 483-486 (1974).

./...

(10) G.N. Ling and M. Tucker, NMR relaxation and water contents in normal tissues and cancer cells : In NMR in Cancer, pp. 161-174 (Ed. R. Damadian), Springer-Verlag, Heidelberg (1981).

(11) P.L. Davies, L. Kaufman, L.E. Crooks and A.R. Margulis, NMR characteristics of normal and abnormal rat tissues : In Nuclear Magnetic Resonance Imaging in Medecine, pp. 71-100 (Eds. L. Kaufman, L.E. Crooks and A.R. Margulis, Igaku-Shoin, Tokyo (1982).

(12) F.W. Smith, Clinical applications of NMR tomographic Imaging, pp. 125-131. Proceedings of an International Symposium on Nuclear Magnetic Resonance Imaging. (Held at Wake Forest University, Winston Salem, N.C. October 1-3, 1981).

(13) J.C. Gore, The meaning and significance of relaxation in NMR imaging, pp. 15-23. Proceedings of an International Symposium on Nuclear Magnetic Resonance Imaging (Held at Wake Forest University, Winston Salem, N.C. October 1-3, 1981).

(14) C.F. Hazlewood, W.S. Yamanashi, R.A. Rangel and L.E. Todd; In vivo NMR imaging and T_1 measurements of water protons in the human brain. Magnetic Resonance imaging 1,3-10, (1982).

II. ULTRASONOGRAPHIE / ULTRASONOGRAPHY

Université Libre de Bruxelles
Hôpital Universitaire Brugmann
Dpt. d'Obst. et Gyn. (Prof. R. Vokaer)
Clinique d'Ultrasonologie
SALVATOR LEVI
Chargé de Cours ULB-ULg

LE SCANNER ULTRASONOGRAPHIQUE AUTOMATISE

RESUME.

Quelques avantages des différents systèmes d'exploration "Temps Réel", statique manuel à contact direct et statique automatisé sont comparés. Le système automatisé présente en particulier les avantages suivants: la qualité de l'image est indépendante du manipulateur, la reproductibilité est possible, le traitement de l'image peut être envisagé avec plus de rigueur, l'acquisition et la qualité de l'image sont d'un niveau supérieur, l'exposition est réduite.

I. INTRODUCTION

L'évolution de l'ultrasonographie depuis son introduction en clinique - au milieu des années 60 -fut marquée par quelques faits dominants.
L'imagerie bidimentionnelle, dérivée du mode B, a succédé au mode A sans l'éliminer toutefois. L'imagerie statique a été suivie très vite par l'image en temps réel dont la qualité s'est améliorée considérablement depuis l' apparition des barrettes à balayage électronique par transducteurs multiples.
Aux images en noir et blanc ont succédé les échogrammes à tonalités de gris et aux convertisseurs analogiques les convertisseurs digitaux. Leur intérêt est principalement dû aux innombrables possibilités liées à l'emploi de l'informatique, de la puce à l'ordinateur.
Les techniques Doppler à émission continue font place aux Dopplers pulsés: la voie est ouverte à de nouvelles informations: mesure sélective de vitesses, de débits, imagerie à destinée anatomique et fonctionnelle.

Les systèmes de balayage en temps réel ont fini par supplanter presque entièrement les équipements à image statique par contact, qui demandent une adresse et un apprentissage du manipulateur bien plus long qu'avec les barrettes et autres transducteurs sectoriels du "Temps Réel" qui se manipulent beaucoup plus facilement, plus rapidement.
Ces derniers forment l'image par eux-mêmes. Les équipements "Temps Réel" sont moins encombrants, souvent plus économiques, plus mobiles et même parfois très facilement transportables à bout de bras. La disparition des systèmes statiques, capables de visualiser en une fois de larges étendues anatomiques laisserait un vide inacceptable.

Pourcelot (1), dans son exposé de synthèse du même Symposium International de 1979, exprimait l'avis suivant: "Toute technique manuelle est en effet fortement tributaire de l'expérience et de l'adresse du manipulateur. Aussi voit-on de plus en plus se dessiner la tendance vers une automatisation plus grande des appareils mais cette automatisation n'est envisageable de maniière efficace que sur du matériel assez peu évolutif, ce qui n'est pas encore tout à fait le cas dans le domaine des ultrasons". L'automatisation dans le domaine de l'échographie a été réalisée et l'évolutivité du système démontrée dans la pratique. C'est le sujet de notre exposé.

II. ELEMENTS FAVORABLES A L'ULTRASONOGRAPHIE DIAGNOSTIQUE.

L'application de l'ultrasonographie au diagnostic médical est soumise à une série de conditions idéales que l'on ne peut évidemment qu'approcher.
Il est important que tous ceux qui sont concernés par l'ultrasonographie - utilisateurs et producteurs - aient toujours ces éléments présents à l'esprit et s'efforcent d'y obéir dans la mesure de leurs moyens.
1) La sécurité est la condition la plus importante quels que soient les résultats des expérimentations sur les effets biologiques des ultrasons. Ils sont rassurants mais parfois contradictoires.
Il nous semble évident que l'énergie reçue par le patient doit être limitée au minimum indispensable à l'obtention de l'information requise.
Par conséquent l'exploration ne doit demander que le minimum d'énergie nécessaire à l'obtention de bonnes images pendant le temps le plus court possible (tableau II).

2) Le confort du patient importe aussi pour la qualité des images, condition essentielle si l'exploration est un peu longue ou que l'on examine des enfants. La position du patient dépend souvent de la région à explorer; la conception du support, le mécanisme explorateur et la manière de s'en servir font partie des éléments du confort.

3) La qualité des images à examiner pour découvrir, décrire et identifier d'éventuelles anomalies ou lésions est l'élément de base pour l'efficacité de l'exploration. Sans pouvoir entrer dans les détails, rappelons les éléments qui contribuent à produire une image de qualité: le nombre de lignes qui forment l'image, les résolutions axiales et latérales, la dynamique de l'échelle des gris, la vitesse d'acquisition des images....
La perturbation ou le flou d'une partie de l'image par des mouvements physiologiques (pulsations vasculaires, respiration) sont évitables en augmentant la vitesse d'acquisition, que ce soit pour les systèmes statiques ou en "Temps Réel".

4) Le dessin anatomique produit par l'échogramme devrait

ressembler aux images de référence connues, celles publiées dans les livres d'anatomie par exemple (fig.6). Il devrait comporter beaucoup de détails morphologiques, couvrir la plus grande étendue posssible afin de mieux étudier les rapports entre les structures cibles et les structures ou organes voisins. La largeur ou la longueur de la coupe explorée dépend du système utilisé. Elle est maximale en surface et en profondeur pour les systèmes statiques. Elle est réduite aussi bien en surface et en profondeur pour les "temps réels" à transducteurs linéaires, très réduite même en surface mais plus large en profondeur pour les "temps réels" à balayage sectoriel (Fig.9).
La profondeur de l'image dépend de la vitesse d'acquisition, de l'énergie produite et de la fréquence des impulsions. La recherche de la qualité de l'image est à l'origine de difficiles compromis techniques.

5) L'accessibilité des organes dépend de la pénétration déjà évoquée, de la maniabilité et de la forme des transducteurs, de l'éloignement du transducteur et de la cible; la déformation due à la pression des transducteurs - particulièrement sensible au niveau des structures superficielles - peut aussi être évitée par l'éloignement du transducteurs (fig.3).

6) Les balayages simple et composé. Il peut être avantageux pour une exploration donnée de pouvoir utiliser aussi bien les balayages simples que les balayages composés pour en additionner les avantages et en soustraire les inconvénients respectifs. L'examen d'une région à partir de plusieurs points de vue (le balayage composé) montre des structures complètement dessinées (fig.3 et 4). Les échos qui auraient pû échapper aux transducteurs effectuant un balayage simple sont reçus ici. L'échogramme ressemble beaucoup à la coupe anatomique correspondante. Le balayage simple autorise une meilleure représentation des modifications de l'image dû au changement d'atténuation, comme les ombres et les renforcements.
Cette propriété est tantôt utile: pour mieux caractériser les tissus et certaines de leurs altérations; tantôt fâcheuse par l'ombre jetée qui masque la région d'intérêt. Le bayalage simple est aussi supérieur au balayage composé en présence de structures pulsatiles: les mouvements ne dégradent pas l'image. Passer d'un type de balayage à un autre, en fonction des nécessités, est un moyen élégant d'associer leurs avantages.
7) La reproductibilité des images intéressantes, en plus des qualités importantes que l'on est en droit d'exiger d'un système doit néanmoins permettre de suivre l'évolution des lésions (guérison ou aggravation).
Cette possibilité n'est retrouvée pratiquement dans aucun des systèmes connus.
En effet, s'il est nécessaire que l'acquisition des images soit indépendante du manipulateur - condition réalisée dans les systèmes "Temps Réel" et statiques automatisés - il faut encore que la position des transducteurs soit déterminée avec suffisamment de précision. Cette dernière condition n'est pas réalisée dans les "Temps Réels"; elle l'est avec

les scanners automatisés: des renseignements précis sur la position spatiale des transducteurs par rapport aux repères anatomiques choisis sont accessibles.

8) La technique d'exploration devrait s'adapter à l'information recherchée et être la plus polyvalente possible sans altérer les qualités principales du système. En effet, les informations demandées, qui peuvent être nombreuses et variées pour un patient ou pour une spécialité particulière, nécessiteraient un équipement spécifique pour chaque application particulière. Parmi elles citons les organes superficiels (thyroïde, testicules, seins) l'analyse du mouvement, la vitesse (le flux, le débit) du sang impliquant des conditions très particulières et des techniques comme le M-mode, le Doppler pulsé associé à l'image. De plus, le traitement de l'information par l'ordinateur aide à mesurer l'altération des tissus par l'analyse des effets de l'interaction entre sons et tissus. Ceci implique des conditions de reproductibilité rigoureuse avec un minimum d'intervention du manipulateur.

Nous nous attachons à montrer comment le scanneur automatisé répond aux conditions de la qualité de l'image, de vitesse d'acquisition, de reproductibilité, par la description qui suit.

III. DESCRIPTION.

Le scanneur ultrasonographique automatique dont il sera question est le système U.I. Octoson. Il a été concu et développé par l'équipe de l'Ultrasonic Institute dirigé par G. Kossoff et commercialisé par Ausonics, tous deux à Sydney Australie (2)(Fig.1). Le système d'acquisition des échos a été imaginé de telle sorte qu'il produise des échogrammes de haute qualité à grande vitesse, formés- au choix- par des balayages simples et composés. Le système est dessiné pour s'adapter à la plupart des régions du corps humain, pour explorer dans des conditions optimales tout l'abdomen, les seins, la glande thyroïde, le scrotum les membres, le cerveau des jeunes enfants (fig 6 et 7).
Le système est de type statique, il présente une double originalité comparé au système manuel à contact direct.
Il comporte 8 transducteurs situés à distance variable de la partie à examiner, le milieu de couplage est l'eau maintenue à 37°.

A. Choix de l'eau comme milieu couplant.

Le balayage par contact, sur la peau, présente quelques avantages: utilisation simple, localisation immédiate du plan de balayage, forte angulation du plan de coupe si nécessaire et si la dimension du transducteurs le permet, utilisation maximale des zones d'accès réduites par un balayage simple.
Le contact direct limite cependant l'ouverture du transducteur et, comme la résolution est proportionnelle à l'ouverture,

elle est forcément limitée.
Lorsque le couplage est réalisé par eau, l'ouverture peut être beaucoup plus grande. Plusieurs transducteurs peuvent être utilisés. Le temps d'acquisition de l'image sera plus court. L'examen d'organes déformables sera facilité (fig. 7, A et C).

B. Les transducteurs.

Chaque transducteur mesure 70 mm de diamètre, opère à 3 MHz, 1.5 MHz et en Doppler pulsé. La distance focale est de 340 mm. La sortie acoustique correspond à 4 microJoules par impulsion, la puissance acoustique moyenne est de 6 mW.
Placés sur un berceau en arc de cercle, les 8 transducteurs sont actionnés par des moteurs. Les mouvements suivants peuvent être commandés à distance: oscillation variable de chaque transducteur de 1 à 65° (balayage sectoriel) déplacement du berceau latéralement d'avant en arrière, de haut en bas, avec une angulation et une rotation autour de son axe central (fig. 2). L'ensemble est situé dans une citerne d'eau avec fenêtre sur le flanc pour observer les mouvements du berceau, une ouverture vers le haut où est placée la région à explorer, recouverte ou non d'une membrane souple (fig. 1).

L'image est obtenue par un balayage de un ou plusieurs transducteurs que l'on sélectionne préalablement; le déplacement est programmable, pas par incréments de 1, 2, 5, 10 et 20 mm dans les directions 2 et 3 de la figure 2 et de 1° dans les plans 4 et 5. Les transducteurs larges concaves permettent d'obtenir une focalisation sur longue distance; de pouvoir visualiser les structures superficielles en détail. L'écueil des échos de répétition est évité par le traitement des signaux.

C. Acquisition de l'image.

En résumé, le système recherche d'abord le premier transducteur sélectionné, le connecte au récepteur correspondant et au compteur de délai de propagation dans l'eau. Le transducteur est excité, le temps de réception du premier signal mesuré, la courbe de gain initialisée, les artefacts de répétition entre le transducteur et la peau effacés, les échos sur la première ligne visualisés. Le système recherche alors le deuxième transducteur sélectionné et ainsi de suite.
Quand tous les transducteurs ont été activés, le moteur les fait osciller de 1/10 de degré (0.0878°) et le cycle recommence jusqu'à ce que l'angle de balayage présélectionné soit atteint (une ligne par transducteur et par dixième de degré). La vitesse d'acquisition des images dépend de plusieurs facteurs (tableau I): du mouvement du transduteur, du secteur exploré et donc du nombre de lignes, de la distance transducteur-patient, du temps requis pour obtenir une ligne (temps variant selon la vitesse de propagation et la profondeur). L'expression suivante permet le calcul du temps d'acquisition (ti) de

l'image en fonction de la distance transducteur-peau (t T-P), du nombre de lignes (L) et du nombre de transducteurs activés (Nt). Prenons un exemple: une image de la zone située à 8 cm de profondeur dans le corps est acquise avec un transducteur formant un secteur de 60° en 0,27 sec. et avec 8 transducteurs en 2.16 sec.

$$t = \frac{2\,d1 + 2\,d2}{154.10\ 3\ cm/sec} \times L \times Nt + \left(Nt\ a + (Nt-1)b \right)$$

t = temps d'acquisition de l'image
d1 =distance Transducteur-Peau
d2 = distance Peau-profondeur (équivalent à d1)
154.10 3 cm/sec = vitesse moyenne des ultrasons dans l'eau et les tissus biologiques
L = nombre de degrés du secteur/valeur de l'incrément ou 0.0878°
Nt = Nombre de transducteurs sélectionnés
a & b = délais de commutations électroniques
a = 60.10 -6 sec
b = 11.10 -6 sec

IV. ENERGIE DELIVREE PAR LE SYSTEME.

Les paramètres acoustiques du système automatisé ont été mesurés et comparés à d'autres: statiques, TM-mode et temps réel, par Barnett et Kossoff (1982).
Les mesures ont porté sur l'intensité maximale instantanée (peak instantaneous intensity), la puissance moyenne de sortie (temporal average power output), le contenu énergétique des pulsations transmises, la quantité d'énergie utilisée pour produire une image et la quantité totale d'énergie utilisée pour la pratique d'un examen échographique. Enfin, sans doute plus significative que la dose moyenne sur toute une région explorée, l'exposition en un seul point du tissu.
Un résumé de ces constatations est porté dans le tableau II.
Admettons que la durée moyenne, assez courte pour un examen portant sur les organes génitaux (homme ou femme) ne dépasse pas 5 min. en "Temps réel" ou 20 coupes en "statique"; l'énergie reçue par le patient sera respectivement de 1,35 Joules, de 0.4 Joules pour 20 échogrammes composés par contact direct et de 0,16 Joules pour 20 échogrammes composés par système automatique.
Ce dernier entraîne donc une exposition 8 fois moindre qu'avec le temps réel et même plus souvent 16 à 32 fois moindre parce que l'usage de 8 transducteurs n'est pas nécessaire pour ce type d'exploration.

V. RESULTATS.

Des images de régions différentes sont montrées à titre documentaire (fig.3-8). Les explorations complètes peuvent être réalisées assez rapidement pour autant que les conditions

appliquées soient uniformes. La procédure systématique peut être interrompue a tout moment pour faire place à des variantes dont le choix est nécessité par la nature du cas examiné.
La position en décubitus ventral utilisée pour la majorité des examens présente l'avantage - au niveau de l'abdomen - de repousser les gaz intestinaux plutôt vers la profondeur permettant au moins l'examen des couches les plus superficielles de la cavité abdominale; certains artifices, comme l'absorption de boissons pour remplir l'estomac, produit une fenêtre à l'instar de ce qui est fait depuis longtemps pour la vessie quand il s'agit d'examiner le pelvis (fig.6 et 8).

VI. CONCLUSION.

Complété par un "temps réel" destiné à sélectionner les cas où son utilisation est justifiée, le scanneur automatique donne d'excellents résultats. Ils sont intéressants en particulier pour les structures superficielles, pour les examens où la reproductibilité est importante, pour les explorations de régions très étendues, chez les enfants. Le contact direct est évité et une bonne visualisation globale réalisée; il est indispensable pour les petites parties comme le sein, le scrotum.
Le Doppler pulsé et le TM-mode apportent le complément jugé souvent indispensable aux explorations ultrasonographiques.
Citons encore Pourcelot (1979): "L'association des trois techniques (Bidim.TM.Doppler) leur donne un potentiel remarquable qui va marquer l'évolution des ultrasons dans les années prochaines. En particulier, l'exploration Doppler des flux intracardiaques ou au niveau des vaisseaux abdominaux fournit avec élégance des diagnostics qui nécessitent souvent de nombreuses investigations lourdes ou dangereuses par les méthodes traditionnelles. Cependant, l'utilisation en routine de cette association à un bon niveau de perfectionnement nécessite une combinaison complète des techniques ce qui correspond à un appareillage utilisant simultanément le balayage électronique, l'orientation de faisceaux, la focalisation dynamique, la détection Doppler multiporte, ... L'intérêt d'une association de ce genre est très grand car de nombreuses études nouvelles en découlent." Le flou cinétique qui altère quelque peu la netteté de l'imagerie statique est compensé ici par la vitesse d'acquisition que l'on peut augmenter en fonction des besoins en supprimant les transducteurs non indispensables à la qualité de l'image et en réduisant l'angle du secteur exploré.
L'automatisme autorise aussi, en connectant l'appareil à l'ordinateur, un meilleur traitement de l'information par une plus grande rigueur dans la captation des signaux.

REFERENCES

1. POURCELOT L. Exposé de synthèse sur l'échographie.
In : Compte-rendus du Symposium International Fondements des Nouveautés Techniques en Echographie, Planning Dosimétrique, Traitement des Informa tions.
J. Garsou, W. Gordenne. G. Merchie ed. Presses Universitaires de Liège.
Vol.4 pp 73-80 1979.

2. CARPENTER D., KOSSOFF G., GARRETT W.J., DANIEL K. and BOELE P.
The U.I. Octoson - A new class of ultrasonix echoscope.
Australian radiology, 23 : 85-89, 1977.

3. BARNETT S.B. and KOSSOFF G.
Ultrasonic exposure in static and real time echography.
Ultrasound in Med. & Biol. 8 : 273-276, 1982.

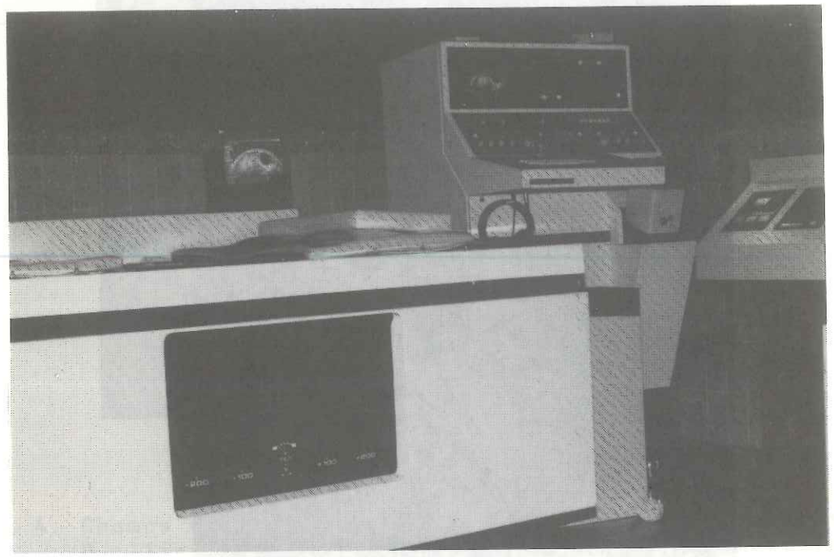

Fig. 1. Scanneur automatisé U.I. Octoson montrant le plan d'examen, la cuve dans laquelle se trouvent les transducteurs et le pupitre de commande.

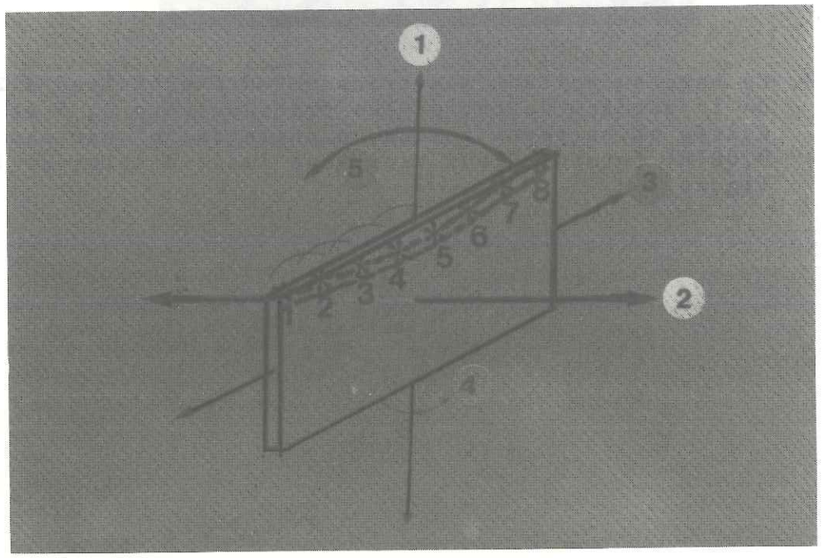

Fig. 2. Berceau portant les 8 transducteurs et les différents sens dans lesquels il se meut. 1 = Haut-bas; 2 = des pieds à la tête; 3 = de la gauche vers la droite; 4 = rotation autour de 1'axe 1; 5 = inclinaison autour de 1'axe 3.

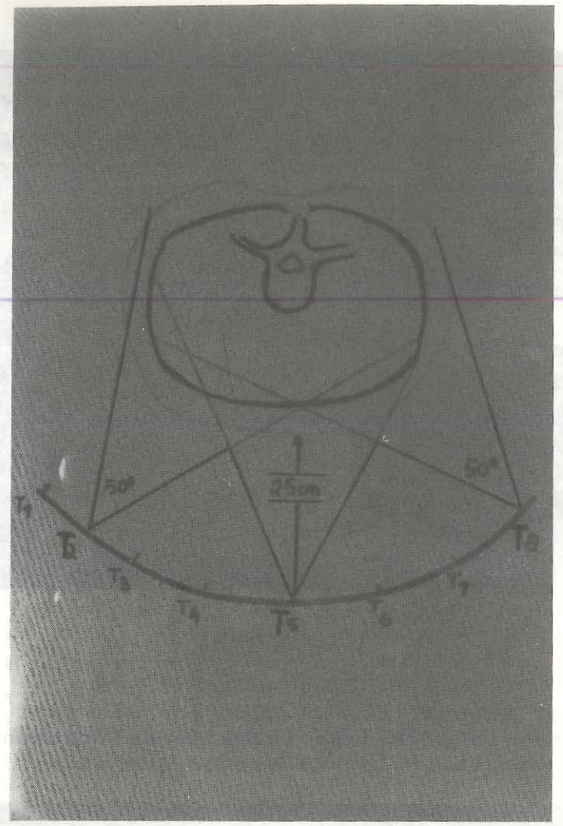

Fig. 3. Le berceau portant les transducteurs est situé à 25 cm de la surface du corps; les transducteurs 2, 5 et 8 sont exités et balayent chacun un angle de 50° par pas de 0,0878° formant à eux trois une image de plus de 1700 lignes.

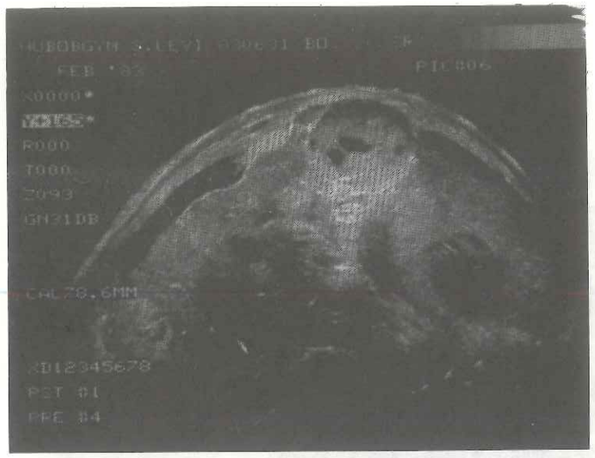

Fig. 4. Champs explorés par les "Temps Réels"; A : sectoriels; B : linéaires. Il s'agit d'images d'un même rein atteint d'hydronéphrose en section transversale. Le champ du sectoriel est réduit en surface, large en profondeur; l'image est de qualité inférieure à celle du linéaire.

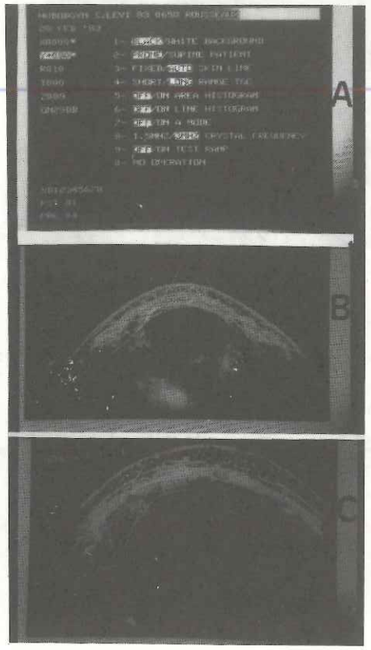

Fig. 5. Quelques unes des possibilités offertes par le scanneur : choix de différentes fréquences, profondeurs, position, etc., positionnement des points focaux, mesure de diamètres et d'aires.

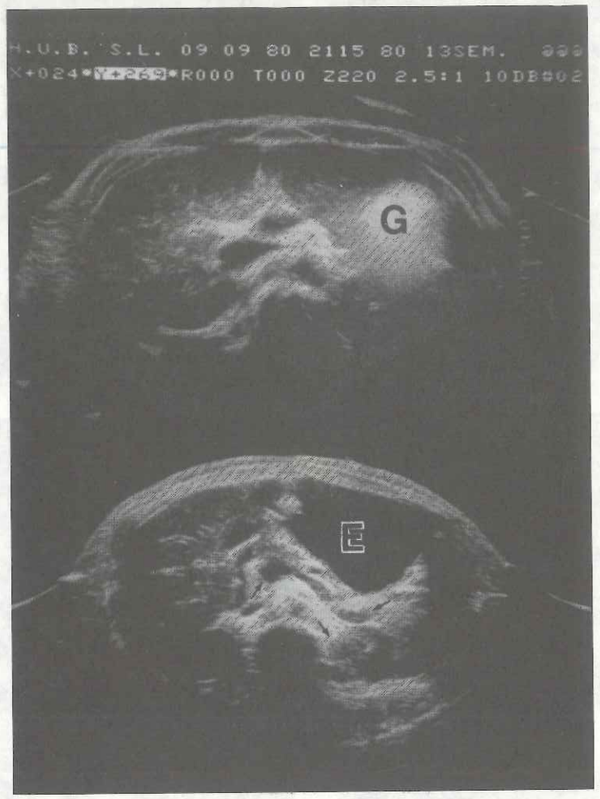

Fig. 6. Scanneur automatisé, patient en décubitus ventral. A gauche, l'estomac est vide et des gaz (G) localisés dans l'hypochondre gauche masquent le corps à la queue du pancréas ainsi que le rein gauche. A droite, l'estomac contient du liquide de boisson (thé) et joue le rôle de fenêtre pour visualiser pancréas et rein gauche (flèche).

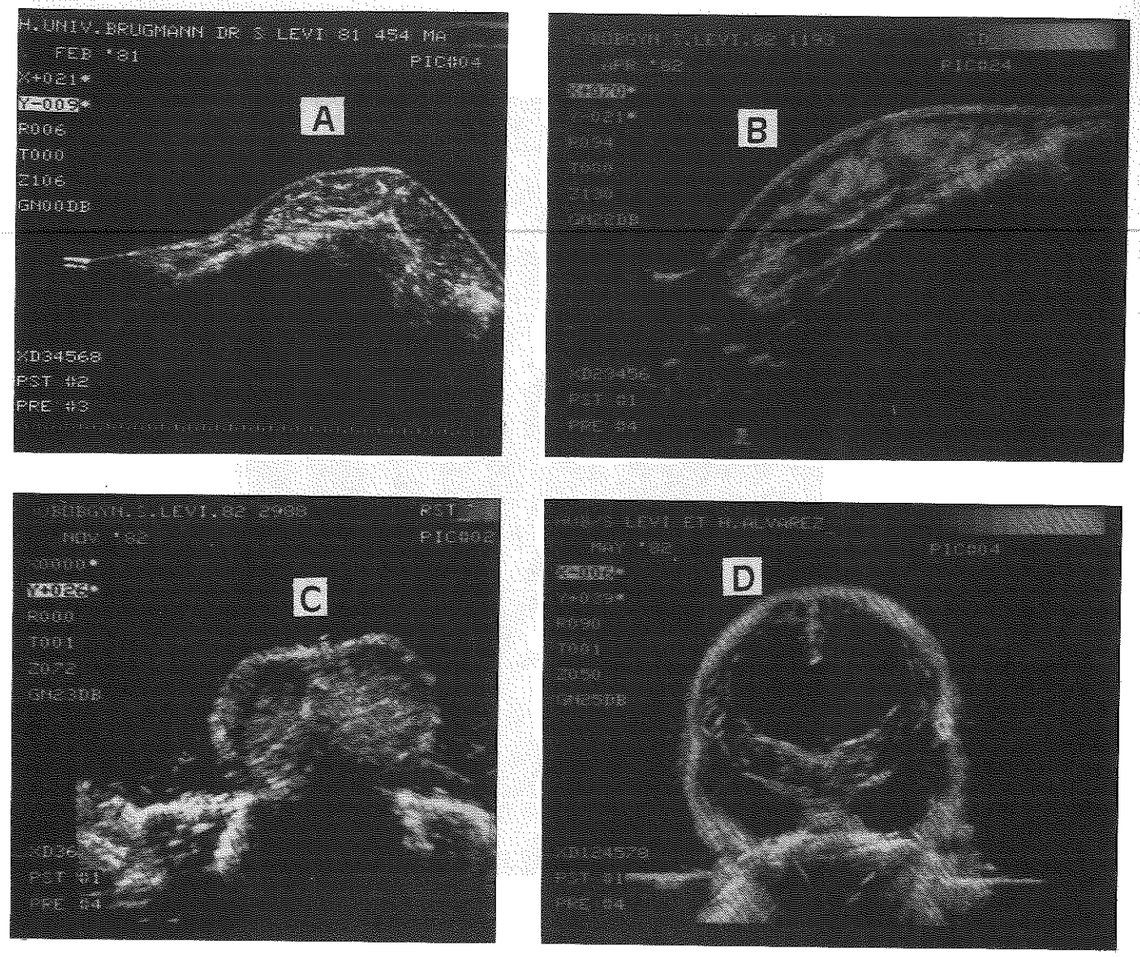

Fig. 7. Application du scanneur automatisé à l'examen d'une petite partie. A : sein comprimé par la membrance; B : seins libres dans l'eau du réservoir; C : scrotum; D : crâne et cerveau de nouveau-né hydrocéphale.

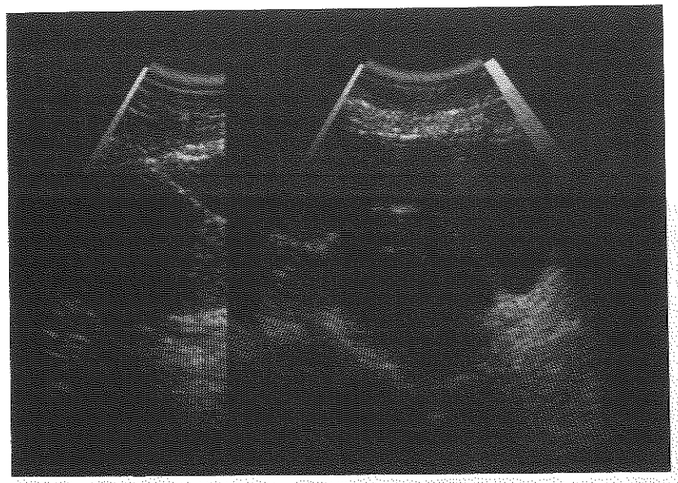

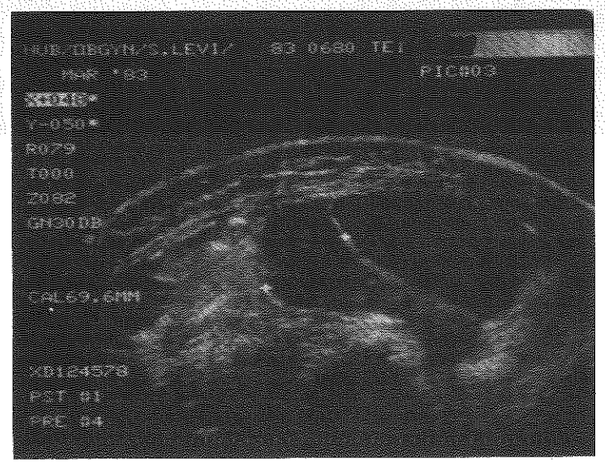

Fig. 8. Comparaison entre le champ réduit du balayage sectoriel nécessitant deux images juxtaposées pour voir une partie du pelvis par opposition à l'aire d'exploration du scanneur automatique (1,5 MHz).

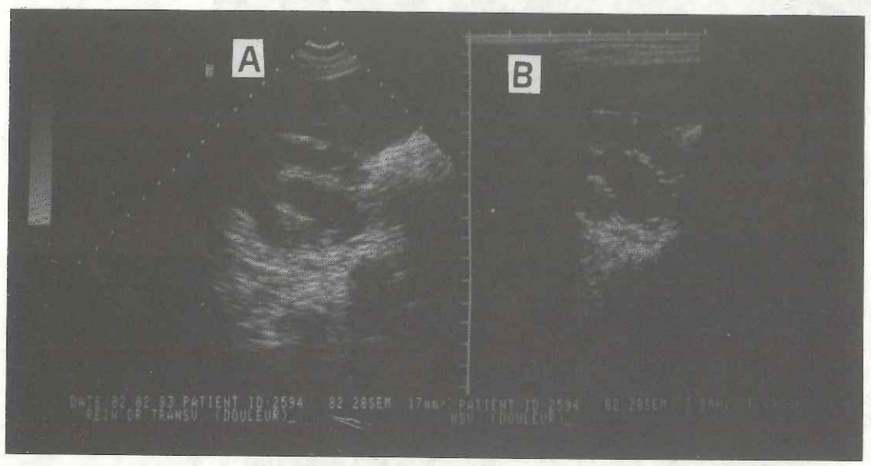

Fig. 9. Etendue de l'aire visualisée par le scanneur automatisé qui permet l'étude de rapports entre les organes.

Tableau I

Vitesse d'acquisition des images : Fonction

du nombre de transducteurs sélectionnés : 1 à 8

du secteur exploré : 0 à 65°

de la distance Transducteur-Patient : max. 32 cm

du nombre de ligne de l'image : 11 par degré de secteur

du temps requis pour une ligne : $\frac{\text{distance transducteur-organe} \times 2}{\text{vitesse propagation du son}}$

Tableau II

ENERGIE FOURNIE : COMPARAISON ENTRE SYSTEMES.

	CONTACT Simple	CONTACT Composé	M - MODE	T. REEL	AUTOM. Simple 1	OCTO Composé 8
1. Energie par impulsion (µJ/i)	2	2	2	1.8	2	2
2. Nbre impulsion par échogramme	10^3	10^4	-	10^2	5.10^2	4.10^3
3. Nbre d'échogramme par examen	20	10	-	25/sec	20	20
4. Nbre d'impulsions par examen (2.x3.)	2.10^4	10^5	10^3/sec	25.10^2/sec	10^4	8.10^4
5. Energie par examen (µJ) (1x2x3 ou 1x4)	4.10^4	2.10^5	2.10^3/sec $1,2.10^5$/mn	45.10^2/sec $2,7.10^5$/mn	2.10^4	$1,6.10^5$
6. Energie par examen en 1 point (mJ)	0.12	1.15	120/mn	27/mn	0.01	0.08

(d'après BARNETT et KOSSOFF 1982 (3))

II.0.18.

II.1.1.

Fourier Transform Applications in Medical Ultrasonography

R. Vaknine and W.J. Lorenz

Institute of Nuclear Medicine, DKFZ, Heidelberg, FRG.

Abstract

The discrete Fourier transformation enables the frequency-based digital processing of A- and B-scan data. Using a computerized echographic data acquisition system and an interactive color display interfaced to a VAX 11/780 computer, the Fourier transform is applied to analyse local patterns in B-scan images, to improve the image resolution through the use of filtering and deconvolution processing in frequency domain and to extract textural properties from B-scan image regions.
A segmental pre-image filtering technique which improves the lateral resolution and the application of the Fourier transform to a series of clinically confirmed liver B-scans are presented.

Introduction

The detail in a B-scan image depends on the resolution achieved by the scanning instrument. Whereas axial resolution is determined by the ultrasonic pulse length, lateral resolution is relatively poor and depends on the effective beamwidth.
Due to the interaction of ultrasound with biological tissue, the parameters which determine the quality of images obtained by to-day's ultrasonic instruments have physical

limits and cannot be optimized independently of each other. The application of digital processing techniques provides, however, an improvement in the image quality [1,2,3] and can lead to an objective tissue characterization.
The Fourier transformation makes it possible to process echographic data in frequency domain. The techniques described are applied to clinical liver B-scan image data to improve the lateral resolution in the far field and to enhance features for picture recognition purposes.

System description

Figure 1 shows a block diagram of the hardware configuration used to acquire, process and display ultrasonic B-scan image data. The x and y coordinate signals supplied by the ultrasonic instrument [4] are digitized by two 12-bit analog-to-digital converters, while a transient recorder is used to digitize the echo-amplitude signal with an amplitude resolution of 8 bits. In this way, each A-line may contain up to 1024 digital values between 0 and 255. The penetration depth in tissue may reach 30 cm. To produce a B-scan image, the echo-amplitudes along 1024 A-lines are acquired and stored on a magnetic tape controlled by a PDP 11/34 computer. Using the VAX 11/780 computer, B-scan picture matrices of 256x256 data points are then generated and displayed on a RAMTEK 9000 interactive color display system [5] . The display image buffer is controlled by a PDP 11/34 which is itself interfaced to the central computer. Peripheral devices of the display system include a graphical tablet, a function box and a set of three potentiometers coupled to an analog-to-digital converter, all operating in real time.

Processing of the beamwidth effect

The degradation caused by the beamwidth effect is oriented perpendicularly to the A-lines acquired during B-scanning. Since the ultrasound intensity in the beam falls off gradually as we move further from the beam axis and since the degradation is approximately symmetrical, the point spread function (PSF) is assumed to be a normal distribution function whose variance varies with the effective beamwidth.
Consider the data matrix formed by the 1024 A-lines acquired during B-scanning and the amplitude values along these lines. The set formed by the first value of each one of the A-lines is denoted by the sequence $g_1(x)$, the set of the second values by $g_2(x)$, etc. If for simple scanning action in the far field the degradation along $g_i(x)$ (i=1,2,...) is assumed to be shift invariant, one writes the following convolution relation:

$$g_i(x) = \int h_i(x-x')\, f_i(x')\, dx' + n_i(x) \qquad (1)$$

where $f_i(x)$ is the ideal sequence corresponding to $g_i(x)$, $h_i(x)$ the PSF for $g_i(x)$ and $n_i(x)$ the measurement noise. Using the Wiener filtering technique [6], one gets for the transfer function:

$$W_i(u) = \frac{1}{H_i(u)} \frac{|H_i(u)|^2}{|H_i(u)|^2 - N_i(u) / S_i(u)} \qquad (2)$$

where $H_i(u)$ is the Fourier transform of $h_i(x)$, $N_i(u)$ the noise spectral density and $S_i(u)$ the spectral density of the random field to which $f_i(x)$ is considered to belong. N and S are assumed to be white [1]. The noise-to-signal spectral density ratio in Eq.(2) is therefore a constant which is empirically adjusted to design the filter in the far field.
Figure 2 shows the processing steps performed on the VAX computer for simple scanning action. The sequences are fast Fourier transformed [7] and Wiener filtered before B-scan image formation. For the present computation the beamwidth variation with distance from the transducer as measured in water on wire phantoms has been applied. The program reads the beamwidths as an array and adjusts the PSF width for each sequence, accordingly.
The algorithm has been applied to liver B-scan data of various clinical cases. The resulting B-scan images show a marked contrast enhancement. The overall image blurring is reduced and fine detail is restored.

Power spectrum

The two-dimensional discrete Fourier transform is displayed to analyse local patterns in B-scan image regions. For the normal liver, the Fourier transform appears to be squeezed towards the zero frequencies. However, a fatty liver structure or the presence of distinct space-occupying lesions which break the uniform reflexion pattern of the liver tissue, demonstrates high power at higher spatial frequencies. The non-uniform structure of a cirrhotic liver shows spectral components over a larger range of frequencies. Spectral energy along the axes is particularly noticeable for cystic liver patterns which usually present sharp edges. Useful textural properties are derived from the Fourier transform $F(u,v)$. If (r,θ) are the polar coordinates in the (u,v) plane, one computes:

$$F_1(r) = \int_0^{2\Pi} |F(u,v)|^2 d\theta \quad \text{and} \quad F_2(\theta) = \int_0^{\infty} |F(u,v)|^2 \, dr \qquad (3)$$

These integrals are approximated by summing over a set of thin rings centered at the origin, and over a set of narrow angular sectors emanating from the origin, respectively.The values of $F_1(r)$ and $F_2(\theta)$, for specific r and θ, characterize the texture of the region.
For a series of 67 patient livers including 16 normals, 21 cirrhotic, 17 metastatic and 13 fatty livers, the total number of points in the (u,v) plane, F , gives the results shown in Figure 3. The diagram shows the mean value and twice the standard deviation for each group. This parameter discriminates well normal echo-patterns from patterns modified by disease. The groups of cirrhotic and fatty livers present a slight overlapping. F does not differentiate metastatic from fatty liver structures. However, a combinaison of the variables extracted from the (u,v) plane leads to a better discrimination between these two groups.

Discussion

The application of frequency-based analysis to medical ultrasonic image data shows that these processing techniques improve the B-scan image quality and provide additional information about tissue properties.
The one-dimensional segmental filtering method used, leads

to a marked contrast enhancement in the B-scan images obtained from long A-scans that are returned from organs. This approach can be applied for the recognition of relevant clinical fine details whose size is smaller than the effective beamwidth size. The speedy algorithm of the fast Fourier transformation used, contributes to the acceleration of the numerical procedure.
The textural properties derived from the Fourier transform can serve as features in the categorization of ultrasonic images by pattern recognition techniques.

References

1 Fatemi, M. and Kak, A. C., Ultrasonic B-scan imaging: Theory of image formation and a technique for restoration, Ultrasonic Imaging, 2, 1-47 (1980).

2 Papoulis, A. and Beretsky, I., Improvement of range resolution of a pulse-echo system, Ultrasound in Medicine, White, D. and Brown, R. E., ed., 3B, Engineering Aspects, pp. 1613-1627, (Plenum Press, New York, 1977)

3 Farrell, E. J., Processing limitations of ultrasonic image reconstruction, in 1978 IEEE Conf on Pattern recognition and Image Processing, pp. 8-15, (IEEE Cat. No. 78CH 1318-5C).

4 Picker Corp. 595 Miner Rd. Cleveland, OH 44143.

5 Ramtek Corp. 585 North Navy Avenue, Sunnyvale, CA 94086.

6 Rosenfeld, A., and Kak, A. C., Digital Picture Processing, Chapt. 7, (Academic Press, New York,1976).

7 Bergland, G. D., A guided tour of the fast Fourier transform, IEEE Spectrum, 6, 41-52 (1969).

8 Wells, P. N. T., Biomedical Ultrasonics, (Academic Press, London, 1977).

9 Andrews, H. C., Hunt, B. R., Image Restoration, (Prentice Hall, Inc., New Jersey 1977).

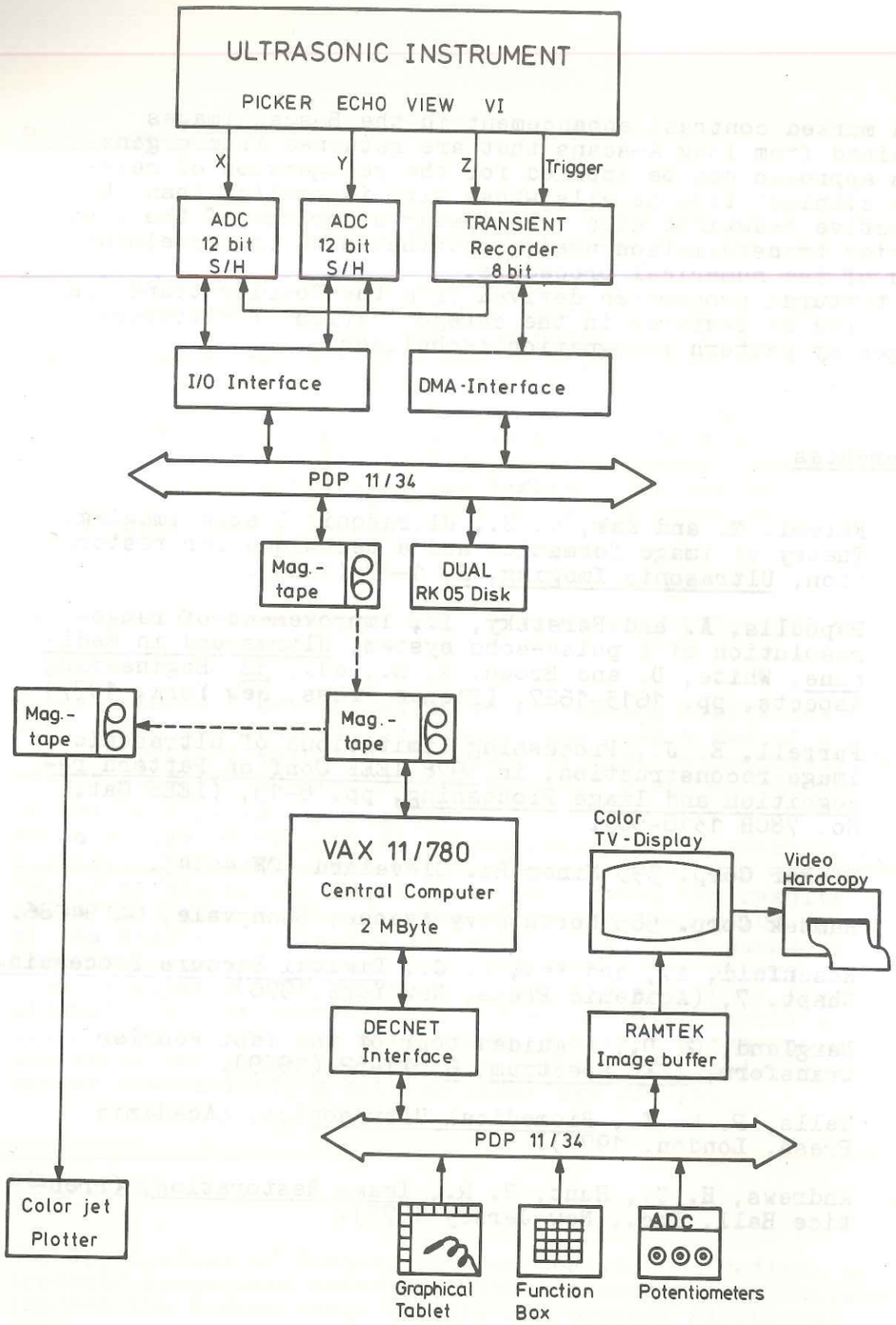

Fig. 1 Acquisition and processing hardware configuration.

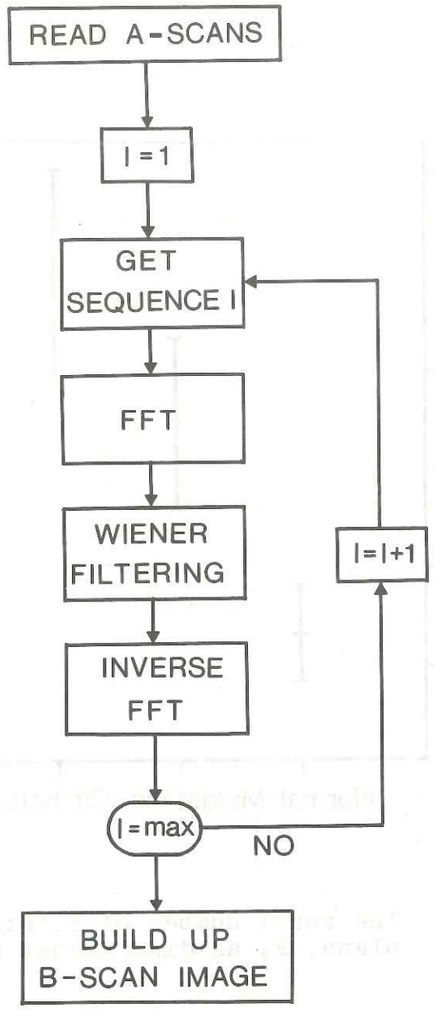

Fig. 2 Processing steps

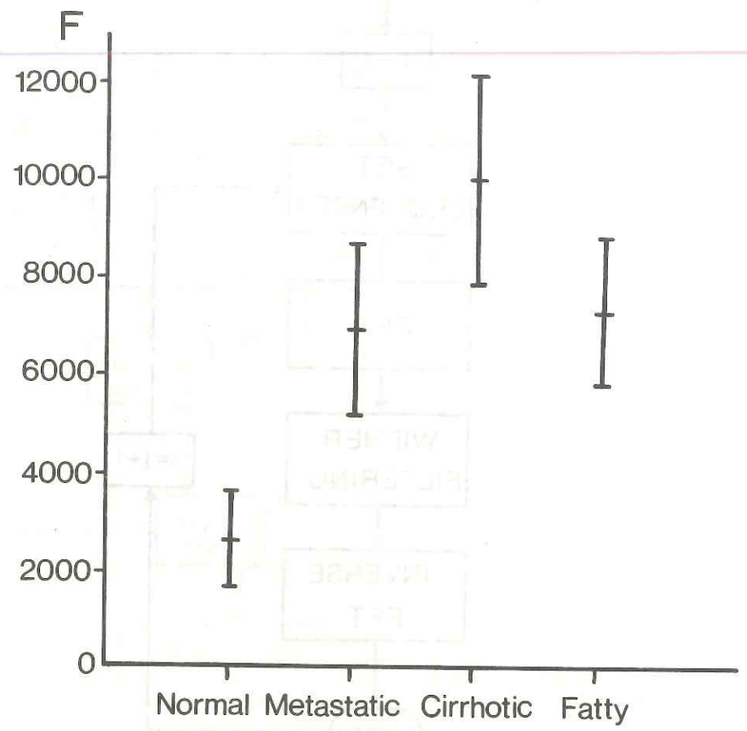

Fig. 3 The total number of points in the (u,v) plane, F, as discriminating parameter.

LA MICROSCOPIE ACOUSTIQUE : FONDEMENTS ET APPLICATIONS A LA BIOLOGIE ET A LA MEDECINE

J. ATTAL, J.L. LAMARQUE *, J.M. DANDONNEAU, J.R. VELLAS

Laboratoire d'Automatique et de Microélectronique
U.S.T.L., Place E. Bataillon
34060 MONTPELLIER

---

* Service Central de Radiodiagnostic
Hôpital St. Eloi 34059 MONTPELLIER

RESUME :

Nous disposons depuis quelques années d'un microscope acoustique haute résolution pouvant donner des images de coupes de tissu frais ou fixé avec définition meilleure que le micron. Il est ainsi possible d'observer sans coloration un prélèvement et d'y apporter un diagostic rapide. Cette dernière étape ne peut naturellement être franchie sans une connaissance préalable des échostructures caractéristiques des tissus à examiner et nous portons actuellement nos efforts dans ce sens où les premiers résultats sont déjà très prometteurs.

I - LE MICROSCOPE ET SON IMPACT SUR LES SCIENCES

De tout temps, le microscope a prouvé qu'il comptait parmi les instruments les plus puissants de recherche scientifique. Ceci a été surtout le cas au fil des siècles dans le domaine des sciences biologiques et médicales où les grands progrés ont été réalisés à partir d'observations microscopiques. L'avènement, il y a une vingtaine d'année, du microscope électronique a apporté une contribution décisive à la science et il y a tout lieu de penser que chaque fois qu'un microscope basé sur tel ou tel type de radiation est développé notre connaissance des structures microscopiques de la matière s'en est trouvé grandement améliorée. L'introduction des ultrasons en microscopie devrait donc avoir un impact similaire. C'est une des motivations qui a poussé les chercheurs vers le développement du microscope acoustique.

II - PLACE DE LA MICROSCOPIE ACOUSTIQUE PARMI LES AUTRES MICROSCOPIES

Elle est liée à la nature même de la radiation utilisée, c'est-à-dire que l'on retrouvera le dénominateur commun des ultrasons : rayonnement non ionisant donc sans danger pour le patient ou non destructif s'il s'agit d'une structure à imager, et possibilité de faire des observations in vivo.

- de par sa résolution le microscope acoustique se situe près des meilleurs microscopes optiques (résolution approchant

actuellement 0,3 micron),

- de par la nature de la radiation, les informations contenues dans les images se différencient nettement des autres microscopies car elles sont le reflet des variations d'impédance (densité et vitesse de propagation) et d'absorption acoustique. Par exemple, un morceau de plastique transparent est optiquement comparable à un morceau de verre c'est-à-dire ne produira qu'un faible contraste tandis qu'en microscopie acoustique le verre est beaucoup plus réfléchissant aux ultrasons que le plastique et le contraste sera plus fort. Ces mêmes particularités se retrouvent au niveau de la biologie où par exemple le collagène apparait très opaque acoustiquement.

En plus des différences fondamentales au niveau des images, le microscope acoustique se différencie totalement des autres microscopies par ses possibilités de faire des images plan par plan en profondeur. Il existe dans la nature plus de corps "transparents" aux ultrasons qu'à la lumière car les constantes d'absorption acoustique sont généralement un bon millier de fois inférieures aux absorptions optiques. De cette propriété de physique fondamentale nait la possibilité d'imager des structures enterrées à l'intérieur de corps optiquement opaques.

III- DESCRIPTION DU MICROSCOPE ACOUSTIQUE (Voir schéma de principe et références de 1 à 4)

De tous les microscopes acoustiques réalisés à ce jour c'est le modèle à balayage, qui de par sa simplicité et ses possibilités a été retenu dans le présent exposé. Le principe utilisé s'inspire beaucoup de l'optique puisqu'il comprend essentiellement un générateur d'ultrasons constitué par un matériau piezoélectrique d'épaisseur de l'ordre du micron (oxyde de zinc par exemple), ce matériau transforme avec un rendement de l'ordre de 50% environ un signal électrique à 1 Gigahertz en signal acoustique de même fréquence. Cette onde ainsi créée se propagera dans un matériau sélectionné par ses qualités acoustiques (barreau de saphir synthétique de formule chimique Al_2O_3 avant d'être focalisée sur l'objet à analyser. En optique la focalisation se fait à l'aide d'une lentille qui n'est autre qu'un dioptre sphérique constitué de deux milieux dont les indices, c'est-à-dire les vitesses de propagation électromagnétiques sont différente, en acoustique il en va de même excepté que les matériaux choisis pour constituer le dioptre auront des vitesses acoustiques différentes. Concrètement le barreau de saphir comportera à son extrémité une cavité creusée et polie d'un diamètre pouvant aller de 30 microns à quelques millimètres suivant la distance focale choisie. Le second milieu sera liquide afin d'assurer le contact acoustique de l'objet et permettre son balayage, les ultrasons ne se propageant pas dans l'air. Le faisceau d'ultrasons ainsi produit est focalisé par la lentille acoustique en une très petite tâche située dans le plan de l'objet. On explore l'image en déplaçant mécaniquement l'objet suivant deux directions perpendiculaires dans le plan focal de la lentille. A ce stade, il est possible de visualiser l'objet par réflexion ou transmission par récupération du faisceau réfléchi

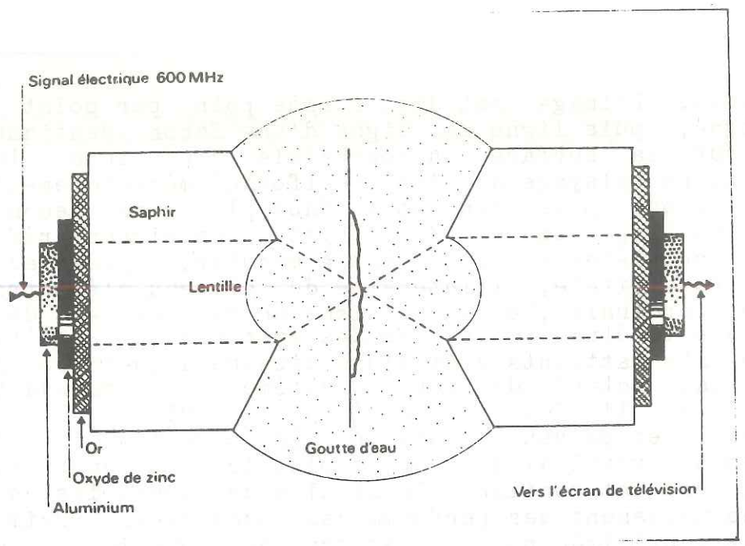

Figure 1. Schéma de principe du microscope acoustique

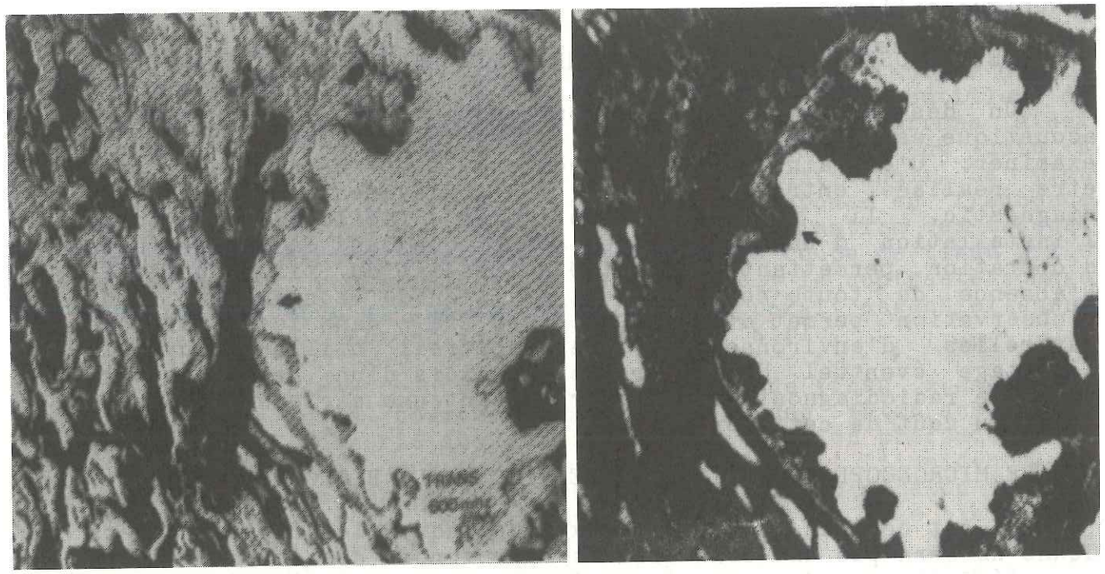

Figure 2. Comparaison des images acoustiques prises à 600 MHz (gauche) et 1GHz (droite) sur tissu mammaire

ou transmis. L'image est donc formée point par point le long d'une ligne, puis ligne par ligne d'une façon identique à celle formée sur la surface photosensible d'un tube image de télévision. Le balayage de l'objet effectué mécaniquement est par contre beaucoup plus lent et il faut plusieurs secondes pour acquérir une image complète de l'objet. Les signaux réfléchis ou transmis sont détectés et servent à moduler, après acquisition sur mémoire digitale, l'intensité du faisceau d'électrons d'un téléviseur ordinaire,le synchronisme entre mouvement de l'objet et balayage TV étant assuré par des capteurs de position. Les grandissements atteints vont d'une dizaine à quelques milliers. Dans l'état actuel de notre système, le balayage rapide horizontal de l'objet est assuré par un vibreur fonctionnant jusqu'à 50 Hz et pouvant assurer un déplacement de 5 millimètres. Le mouvement vertical de l'objet plus lent est entraîné par un moteur à courant continu. Le liquide de transmission utilisé dépend actuellement des performances escomptées. Primitivement l'eau était utilisée pour son absorption acoustique plus faible que bien d'autres liquides et sa compatibilité avec les objets biologiques. Il n'en reste pas moins qu'elle présente une absorption considérable (200 db par millimètre traversé à 1 GHz) et limite les performances du microscope autour d'une fraction de micron de résolution. La dimension des lentilles permettant d'obtenir cette résolution se situe autour d'une trentaine à une centaine de microns de rayon de courbure et sont usinées dans le saphir à l'aide de microbilles, ou d'outils diamantés à bout sphérique calibré.

IV - LE MICROSCOPE ACOUSTIQUE COMME OUTIL DE DIAGNOSTIC RAPIDE

Un des aspects les plus fondamentaux de la microscopie acoustique est l'absence de toute coloration préalable du tissu à examiner. C'est ainsi qu'une économie de temps considérable peut être réalisée entre le moment du prélèvement et celle du diagnostic. Il pourrait être très facilement envisagé l'installation d'un microscope acoustique dans la salle même d'opération permettant le contrôle immédiat du tissu prélevé. L'absence de toute coloration et de liquide contaminant pour l'observation permet d'imager du tissu frais dans les conditions naturelles d'environnement. Cet appareil utilisé pour le dépistage éventuel de tumeurs serait alors d'un grand secours pour le radiodiagnosticien, en réalisant une sérieuse économie quant au coût de cette opération.

V - LE MICROSCOPE ACOUSTIQUE AU SERVICE DE LA BIOLOGIE

Il est certain que le sérieux avec lequel le diagnostic sera donné ne sera pas une connaissance approfondie des échostructures caractéristiques du tissu à examiner. Cette première étape que nous sommes en train de franchir en travaillant notamment sur le sein, est donc fondamentale et nous avons déjà des premiers résultats concernant par exemple le contraste donné par le tissu collagène, les cellules épithéliales ou la membrane enveloppant le tissu épithélial. Cette dernière est d'ailleurs particulièrement visible en microscopie acoustique car composée

plus ou moins de collagène générateur de fort contraste. D'autres exemples concernant l'hémoglobine ainsi que le changement de viscosité du cytoplasme durant la mitose sont également générateurs de contraste acoustique. Notre étude s'est limitée sur le sein mais peut très bien concerner n'importe quel domaine de la biologie où tout reste à faire. Le but poursuivi est de mener le microscope jusqu'à une utilisation clinique, et dans ce sens là, nos recherches sont particulièrement prometteuses.

VI- PROGRAMME DE RECHERCHE ACTUEL

Afin de passer à ce stade d'utilisation par un personnel hospitalier, nous poursuivons un double but :

- Améliorer encore la connaissance acoustique au niveau histologique en adjoignant à la microscopie optique et historadiologique existant déjà, la microscopie acoustique par transmission, réflexion et absorption. Nous obtiendrons ainsi 5 images superposables ce qui permettrait de comprendre très précisément le comportement acoustique de chacune des structures tissulaires. Une analyse quantitative est également prévue couplée avec un traitement par mini ordinateur de ces 3 images acoustiques pour en retirer des informations spécifiques au niveau microscopique telles que l'effet de l'hydratation des tissus ou une dosimétrie acoustique de telle ou telle composante.

- Le second but consiste à faire le lien entre microscopie et échographie acoustique. Pour ce faire, nous sommes en train de fabriquer un certain nombre de jeux de lentilles (autour de 5) pouvant s'interchanger un peu à la manière des lentilles de microscopes optiques montées sur tourette. Nous pourrons ainsi "descendre la fréquence" en augmentant l'épaisseur du tissu à analyser jusqu'à arriver à l'échographe traditionnel. La plus grande prudence toutefois s'impose car la réponse en fréquence est aussi l'une des composantes de la caractérisation des tissus. Ainsi que le montre la figure 2,sur une même coupe de tissu prise en microscopie acoustique à 600 MHz et 1GHz, le contraste change avec la fréquence et une différenciation apparait essentiellement entre zones où l'absorption à 600 MHz est faible.

A plus basse fréquence les épaisseurs de tissu augmentant, nous allons nous heurter aux problèmes des interfaces à 3 dimensions. L'imagerie acoustique de structures en profondeur est conditionnée par deux paramètres essentiels : L'incidence du faisceau et la longueur d'onde comparée à la dimension de la structure à imager. Les figures 3 et 4 montrent très clairement ces deux effets et les erreurs d'interprétation qui peuvent en découler quant à la caractérisation tissulaire. D'autres effets peuvent également être observés tels que échos multiples déviations de faisceau pouvant provoquer sur une interface courbe un phénomène de focalisation ou de déconcentration.

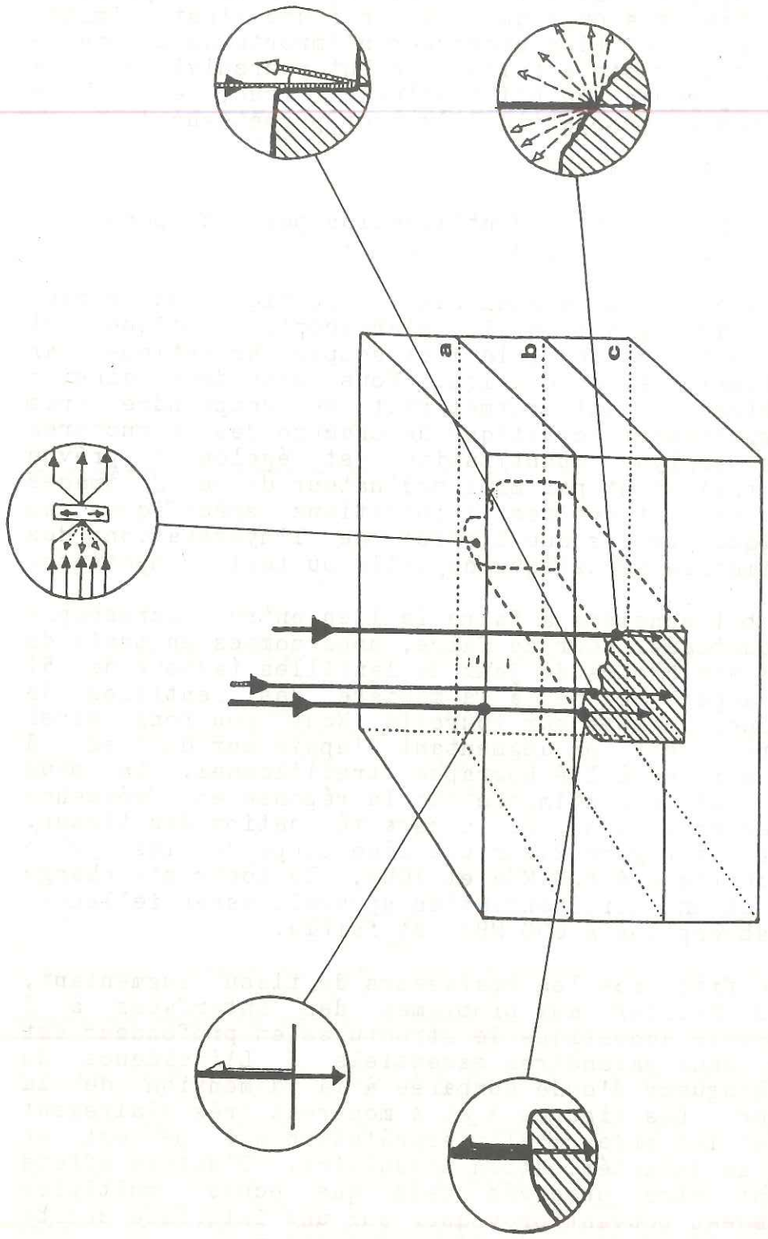

Figure 3. Effets de l'incidence du faisceau sur une structure interne montrant la dispension de l'énergie acoustique.

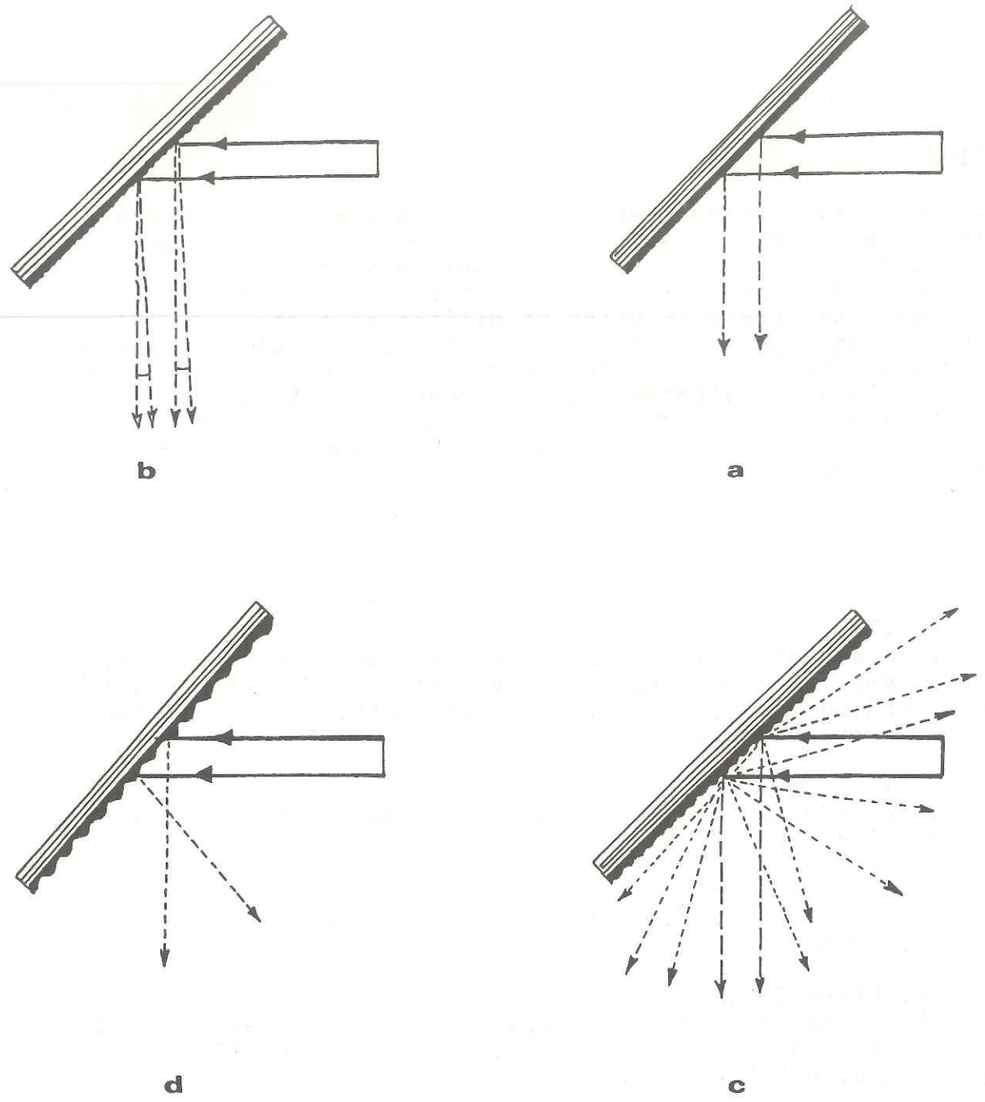

a → reflex on a perfect surface

b → defects are smaller than the wave lenght (l)
(diffusion appears)

c → defects = (l) → maximum of diffusion

d → defects are bigger than (l) → each point will react separately like a, b, or c

Figure 4. Effets de la longueur d'onde par rapport à la dimension des structures observées.

CONCLUSION

Les résultats obtenus depuis quelques années en microscopie acoustique montrent très nettement ses possibilités de développement dans la recherche et l'instrumentation biomédicale. Son intérêt, dans ce domaine, se situe essentiellement dans l'examen de tissu frais in vitro et bientôt peut être in vivo, avec une rapidité de diagnostic et donc d'intervention chirurgicale. Une étude toutefois sérieuse est nécessaire visant la mise en évidence d'échostructures caractéristiques du tissu examiné normal et pathologique et dans ce domaine la collaboration entre physiciens, biologistes et radiodiagnosticiens est un gage de bonne réussite.

BIBLIOGRAPHIE

1) J. ATTAL
"The acoustic microscope : a tool for non destructive testing" dans "Non destructive evaluation of semiconductor materials and devices, chap.12, p.631-676, 1979, (plenum publishing coorporation).

2) J. ATTAL
"L'age adulte du microscope acoustique" dans la Recherche n°121, Avril 1981, p.477-482

3) L. BROOMHEAD
"Les microscopes acoustiques" dans Sciences et Avenir n°375, p.70, 1978

4) J.L. LAMARQUE and J.ATTAL
"The research characteristic echostructures of the different component of mammary tissue. Congrés on "Acoustical Imaging" Cannes, Octobre 1980, p.309-314

5) J. ATTAL
"Imaging microelectronic circuits with liquid metals" dans "Scanned Image Microscopy",p.97-118,(Academic Press), 1980.

INTERET DE LA MICROSCOPIE ACOUSTIQUE DANS L'ETUDE DES STRUCTURES MAMMAIRES

J.L. LAMARQUE, A. DJOUKHADAR, J. ATTAL

service central de radiodiagnostic
Hôpital SAINT-ELOI
MONTPELLIER

Les ultrasons ont connu un développement considérable durant les dernières années et occupent actuellement une place de choix dans l'exploration des difrérents organes. Néanmoins leur rôle dans l'exploration de la glande mammaire est très contreversé et il est difficile actuellement de situer objectivement la place de l'échographie mammaire parmi les différentes méthodes d'exploration du sein.

Nous avons recherché à un niveau microscopique les échostructures caractéristiques des différentes composantes du tissu mammaire grace à la microscopie acoustique dans le but de mieux comprendre les images obtenues en échographie mammaire dans la pratique médicale courante et donc d'améliorer la fiabilité diagnostique de cette méthode.

METHODE

Nous étudions au microscope acoustique des coupes histologiques de tissu mammaire fraichement prélevées de 5 Microns d'épaisseur. Ce fragment tissulaire est étudié successivement en transmission, réflexion à deux fréquences différentes 600 MHZ et 1 GHZ. Ce même fragment est ensuite fixé, coloré suivant les méthodes conventionnelles bien connues d'anatomopathologie et étudié au même agrandissement en microscopie optique (schéma 1).

Des corrélations et comparaison des 2 méthodes (microscopie acoustique - microscopie optique) peuvent être aisément réalisées avec une certitude d'identification formelle et absolue des différentes structures du fait que c'est la même coupe tissulaire qui est étudiée par ces 2 méthodes.

... / ...

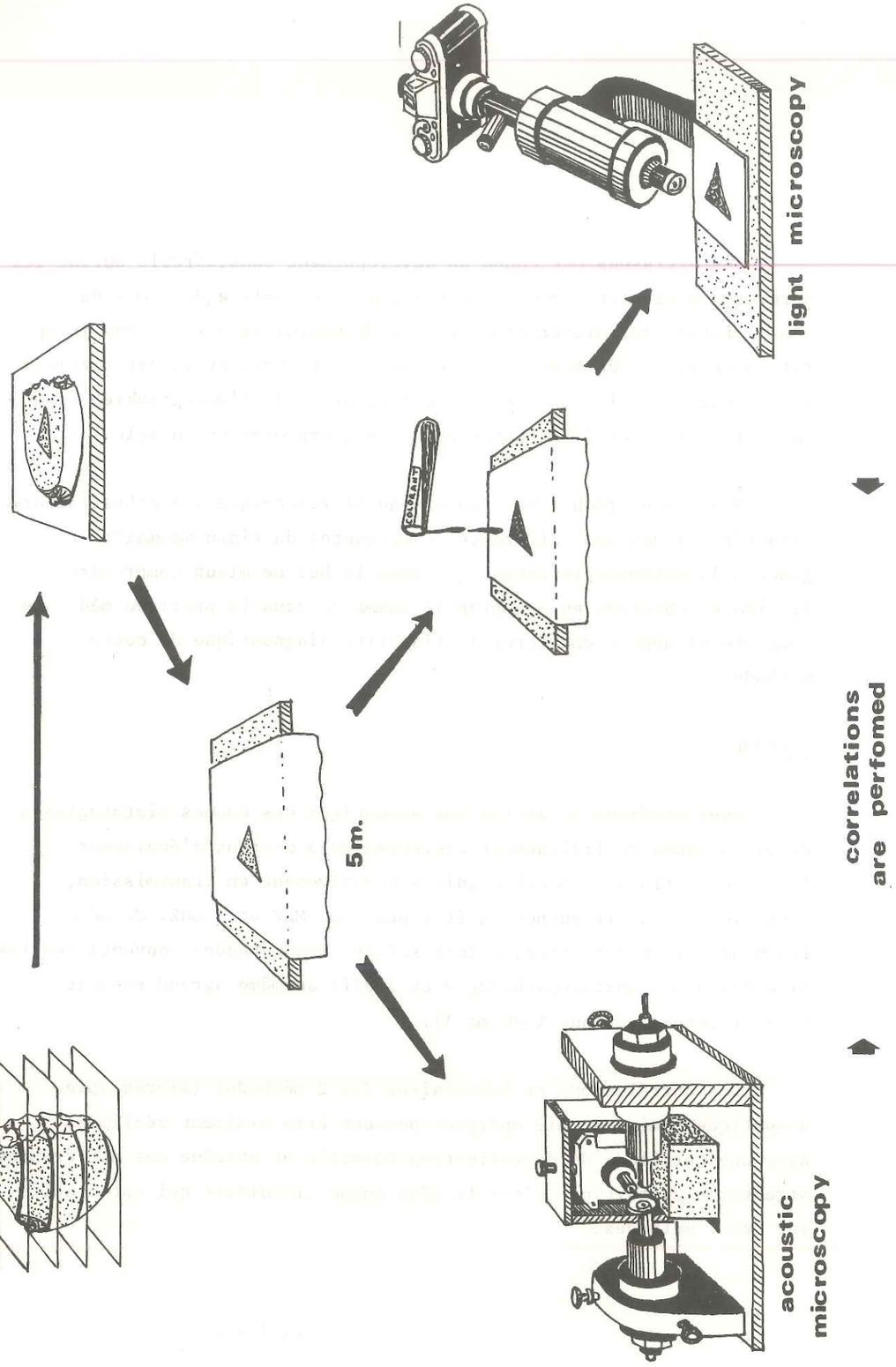

RESULTATS

La microscopie acoustique identifie bien les différentes composantes tissulaires de la glande mammaire. L'épithélium galactophorique est bien individualisé ainsi que les composantes conjonctives. La microscopie acoustique est une méthode de choix pour l'identification des différents types de tissu conjonctif et de la fibrose (fig. 1)

En effet, c'est avec une étonnante facilité que l'on distingue le collagène jeune du collagène mature dit de soutien ; la fibrose étant quant à elle caractérisée par une importante réflexion des ultrasons qui est pathognomonique car ce tissu réfléchit 30 fois plus que n'importe quel autre tissu dans le sein (fig. 2).

La raison de cette facilité de séparation des différents type de conjonctif est fondée sur le principe même de la microscopie acoustique qui dépend de l'élasticité mécanique tissulaire : le tissu conjonctif jeune étant hormonodépendant et subissant des modifications d'hydratation considérable a donc une élasticité totalement différente du collagène mature qui n'est qu'un squelette fibreux de soutien.

DISCUSSION

Même si les images obtenues en microscopie acoustique sont d'une qualité comparable a la microscopie optique notamment les images obtenues à 1 GHZ. Ces mêmes images sont malheureusement inconstantes.

... / ...

En effet, pour percevoir une structure tissulaire, cela dépend non seulement de son échostructure caractéristique mais aussi de son environnement. C'est pour cette raison essentielle qu'une structure sera tour à tour bien perçue et ultérieurement mal individualisée - un exemple est donné par l'épithélium mammaire qui est très bien perçu lorsqu'il borde des galactophores à lumière vide mais qui l'est moins lorsqu'il s'agit d'épithélium lobulaire entouré de conjonctif jeune dont les caractéristiques échographiques sont assez proches de l'épithélium.

Nous percevons très bien les microcalcifications et les monocytes en microscopie acoustique car ces structures sont différentes de leur environnement.

CONCLUSION :

La microscopie acoustique permet une compréhension quasi totale des phénomènes d'interaction (ultra-sons - tissu). A un niveau microscopique. La compréhension de ces phénomènes est fondamentale pour l'interprétation de l'échographie de pratique courante car elle met bien en évidence les différents facteurs qui doivent être pris en compte lors de l'interprétation échographique. On se doit d'être très prudent quant à la caractérisation tissulaire car tout dépend de l'environnement. Il est prudent, sinon illusoire, d'essayer de rattacher les images obtenues en pratique courante à des modifications tissulaires pathognomoniques d'un tissu ou de sa pathologie.

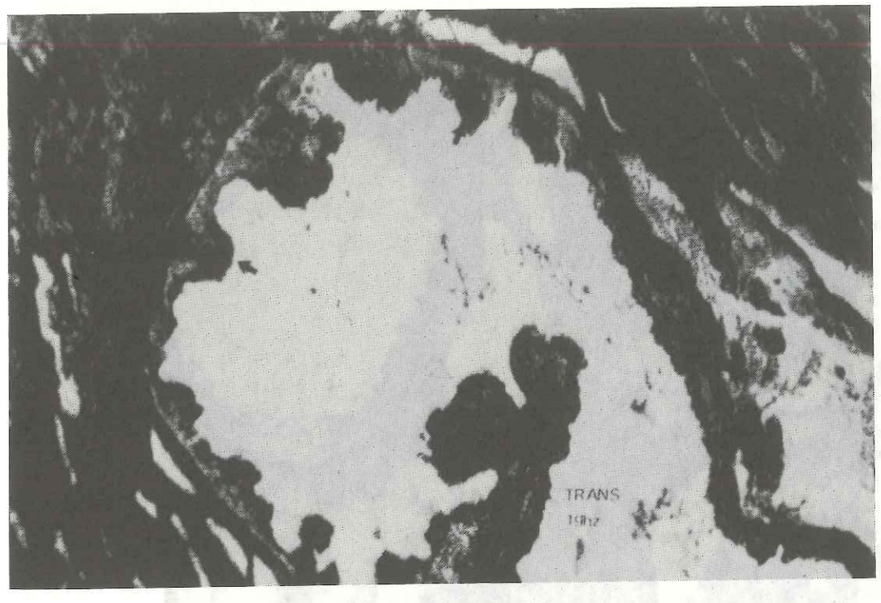

FIGURE 1 - Microscopie acoustique par transmission
Galactophore vue en coupe avec une hyperplasie épithéliale et vététation endo-canalaire.

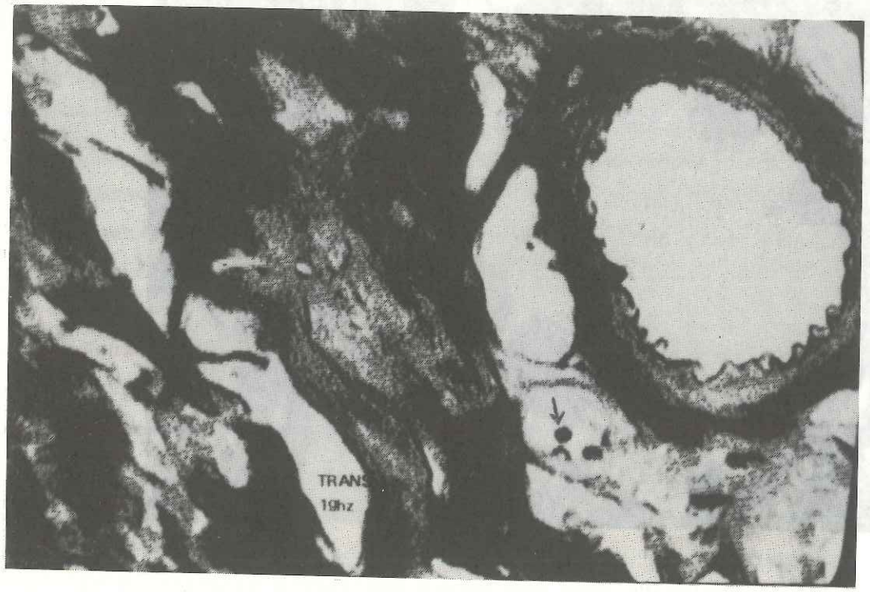

FIGURE 2 - Microscopie acoustique
- bonne perception des monocytes (flèche)
- différenciation des différents types de collagène; le collagène mature se présentant comme zone hyper-réflectives noirâtres.

CIRCULATION DANS LES VAISSEAUX DIGESTIFS ET RENAUX

L. POURCELOT (Tours, France)

E C H O E N D O S C O P Y

J. SOUQUET

CGR ULTRASONIC

PARIS, (FRANCE)

ABSTRACT

The advent of real time imaging, the miniaturisation of array transducer and the increase of scanning ultrasound frequency has led to the development of endoscopic ultrasound imaging.

This paper describes the design and realization of two kinds of systems and presents some clinical results obtained on patients.

INTRODUCTION

Since 1972 (1) some attempts have been made to record important parameters of the heart through the esophagus using an endoscope. In 1972 (2) a linear array has been fitted at the tip of an ACMI gastroscope to ultrasonically image the pancreas.

More recently (3) a phased array has been placed on an OLYMPUS gastroscope to observe the heart through the esophagus for monitoring purposes during surgery.

This paper will describe the two kinds of ultrasound endoscopes previously mentioned : a phased array endoscope for cardiac applications and a linear array endoscope for abdominal applications.

.../...

PHASED ARRAY ENDOSCOPE :

1. DESCRIPTION OF THE PHASED ARRAY TRANSDUCER :

The transducer array is composed of 32 elements of PZT 5A material with a center frequency of 3.5 MHz. The spacing between adjacent elements is 0.28 mm, resulting in a total aperture of approximately 9 mm. The elevation dimension was also chosen to be 9 mm. Thirty two flexible phono wires are soldered on each individual element of the array,a bigger wire is used for the returning ground.

While the main emphasis in the design of the esophageal array was to reduce its size for comfortable insertion, it remained necessary to provide high efficiency along with good bandwidth in order to achieve good signal-to-noise ratios as well as adequate depth resolution.
Detailed consideration of the above factors, along with the desire of low spurious response, led us to a design employing a front matching layer and a mismatched backing.
The impulse response for an element of this array is shown in Fig. 1, demonstrating only a small amount of ringing.

In a phased array system the acceptance angle is an important factor, ± 45° was achieved at 5 dB. Finally for the contacting surface of the transducer , a spherical lens made of a low velocity material was chosen. The optics were designed to give a depth of field from 2cm to 10 cm in front of the array with such a lens, the - 6dB beamwidth measured at 50 mm in front of the array was equal to 3 mm in azimuth and elevation.
the - 6 dB pulse width indicates an axial resolution of about 1 mm.

The completed array was fitted on the distal end of a gastroscope. The outside diameter of the gastroscope is about 9 mm and the outer dimensions of the array are 35 mm long, 15 mm wide and 16 mm thick. This is the only rigid portion of this new echoendoscope. For this first gastroscope, the fiber optics components for viewing and illumination have been removed.
With such a system the scanning plane is perpendicular to the longitudinal axis of the esophagus, in some cases it is important to image two perpendicular scanning planes. It has been achieved by mounting 2 phased array at 90° at the tip of a 9 mm gastroscope.

2. RESULTS

After insertion of the gastroscope to about 35 to 40 cm, the root of the ascending aorta with all three cusps is identified as an echocardiographic landmark (fig. 2). By a slight counter clockwise rotation of the gastroscope, the left venticular outflow tract with the anterior mitral leaflet and the interventicular septum is clearly visualised (Fig.3).

As can be seen from these few images, the major advantages of phased array transesophageal imaging are :

1. There is no discomfort to the patient
2. There is no need for an oil bag as a sound complying system.
3. Both the right and the left ventricule could be identified within one sector image.

.../...

LINEAR ARRAY ENDOSCOPE :

Using a similar approach to the phased array, a high frequency linear array (10MHz) has been developped and fitted on the semi rigid portion of a 10 mm gastroscope. This 10MHz linear array is 3 cm long and 0.7 cm wide, the field of view with such an image is 3 x 5 cm. For such a system since the gastroscope can be guided in the duodenum the optics have been kept intact.
The suction part has been preserved too because it enables the operator to collapse the organ (stomach or intestin) around the linear array thus providing a good contact.

This device has mainly been developped for imaging the pancreas, but important informations coming from the mucosa of the stomach can also be gathered with this device, as will be seen during the conference.

CONCLUSION:

Although the transesophageal technique implies some discomfort to the patient, and some skill is required to introduce the gastroscope into the esophagus, the high imaging quality due to the close anatomical relationship between the esophagus and the heart or the stomach compensate for the disadvantages.

REFERENCES
==========

1. R.M. OLSON, D.K. SHELTON " A non destructive technique to measure wall displacement in the thoracic aorta"
J.AppL. Physiol . vol 32, N° 1, 1972

2. B. ROJOPOLAN, E.D. DI MAGNO, P.S. GREEN " Transesophageal imaging of the heart"
Proc. 9th Int. Acoustic Imaging 1979

3. J. SOUQUET and al. "Transesophageal phased Array for imaging the Heart" BME Oct. 1982.

FIGURE CAPTION

FIGURE 1 : Impulse response for one element of the phased array.

FIGURE 2 : Root of the ascending aorta with its three cusps.

FIGURE 3 : Left ventricular outflow tract with the anterior mitral leaflet and the interventricular septum.

FIGURE 1

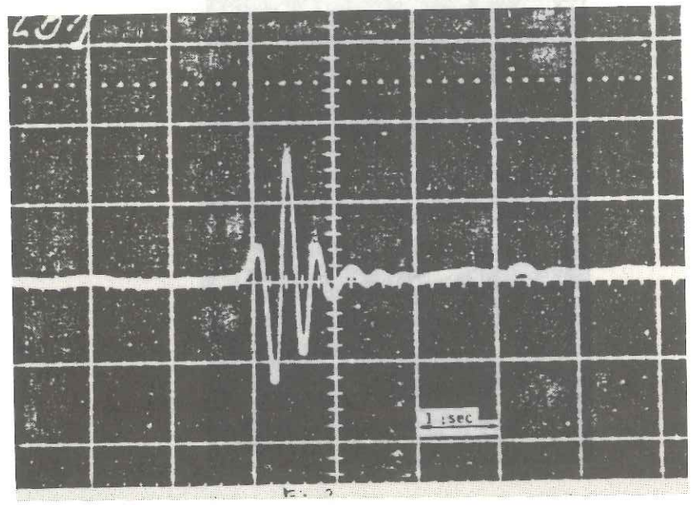

FIGURE 2

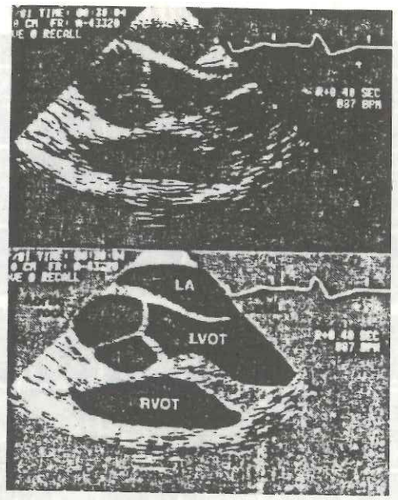

FIGURE 3

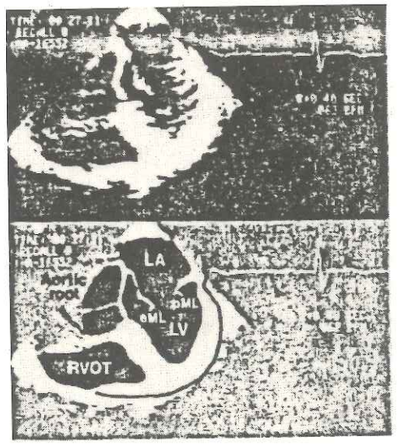

L'ECHOGRAPHIE DE CONTACT PER-COELIOSCOPIQUE

J.P. SCHAAPS

Service de Gynécologie et d'Obstétrique
(Professeur R. LAMBOTTE)
Université de Liège
81, Boulevard de la Constitution
B- 4020 LIEGE

L'utilisation des ultrasons en diagnostic a pris son essor comme méthode d'investigation sans effraction cutanée et sans produire de modification moléculaire due à un phénomène d'ionisation. Cette technique a permis d'obtenir des images bidimensionnelles des structures internes du corps humain bien avant l'arrivée des Tomographes à RX. Il s'agissait donc essentiellement d'une technique non sanglante.

Très rapidement cependant, en urologie et en obstétrique, on s'est attaché à utiliser cette représentation dans l'espace des tissus explorés pour s'en servir comme guide d'une aiguille à ponction. Cette ponction était soit évacuatrice (abcès, collections kystiques du sein)soit biopsique, surtout en sénologie et en urologie.

Il ne s'agissait pas d'un changement d'indications mais plutôt d'un prolongement de celles-ci . La localisation topographique des cibles internes étant tellement aisée et fiable, il était logique d'utiliser la technique comme d'un contrôle pour supprimer les aléas d'une ponction à l'aveugle. Dès l'avènement de ce couplage entre une méthode d'observation et l'acte agressif, on a pu constater rapidement un effondrement du nombre d'accidents de ponctions.

Dans la même optique on voit actuellement se développer une tendance à pratiquer, sous contrôle échographique, une série d'actes permettant de placer des drains ou de dériver des collections pour empêcher la destruction de tissus nobles du foetus au cours de la grossesse.

La nécessité pour l'échographie d'explorer des organes profonds a rendu obligatoire l'utilisation d'une gamme de fréquences relativement basses (2 à 3,5 MHz). La longueur d'onde du son utilisé limitait la définition longitudinale et la taille des émetteurs (monocristaux ou multiéléments) réduisait la définition latérale moyenne malgré tous les systèmes de focalisation à l'émission comme à la réception.

Vu leur faible pouvoir de pénétration, les sons de plus haute fréquence furent ainsi confinés à l'exploration des tissus superficiels d'atténuation faible (sein, thyroïde, cerveau du nouveau-né).

Après des applications concernant l'exploration prostatique en utilisant une sonde rotative, le développement des systèmes d'endoscopie a stimulé les bureaux d'études pour mettre au point des appareils d'échographie applicables aux endoscopes. L'avantage de cette échographie de contact est l'utilisation de sons de très haute fréquence (7 MHz) dans l'exploration de régions inaccessibles auparavant.

On assiste donc actuellement à la naissance d'une nouvelle génération d'appareils permettant de pratiquer une échographie des structures que l'on voit au travers des systèmes d'endoscopie (gastroscopie, cystoscopie, laparoscopie).

LAPAROSCOPIE PAR ULTRA-SONS

Matériel

Il s'agit d'un laparoscope contenant, outre les fibres optiques classiques, le cablage d'une barrette située au devant du tube et contenant 64 cristaux. La largeur de la barrette est inférieure à celle du laparoscope (1cm) et sa longueur 3cm. La profondeur d'exploration dépend des tissus explorés et du contact entre la sonde et l'organe. La suppression du canal de fibres optiques permet l'utilisation d'un trocart de 7mm de diamètre.

Méthode d'examen

L'exploration gynécologique par laparoscopie exige un grand champ de vision et une intensité lumineuse importante. En outre, même pour des laparoscopies exploratrices il est souvent nécessaire d'utiliser une double voie pour manipuler les organes au moyen d'un palpateur.

C'est pour cette raison qu'il nous semble préférable d'employer la double voie pour positionner exactement la barrette sur l'endroit à explorer.

Aucun produit de contact n'est nécessaire, tous les organes internes sont recouverts d'une pellicule liquide permettant le passage du son (Fig. 1).

Description échographique des organes génitaux par voie interne

L'accès direct et la fréquence utilisée modifient sensiblement l'aspect échographique des organes explorés.

L'utérus est d'une échogenéïcité faible, fait de petits échos d'une tonalité uniforme (Fig. 2).

La cavité utérine,très étroite et anéchogène, est bordée par un renforcement muqueux très finement vacuolisé et plus échogène (Fig. 3).

L'injection de bleu de méthylène, SANS pression, la dilate très aisément et permet d'en apprécier le recouvrement muqueux (Fig.4).

Les trompes sont, dans cette étude préliminaire, difficilement visibles dans leur portion isthmique. Elles sont le siège d'échos plus denses que l'utérus.

La cavité tubaire, pratiquement invisible dans l'isthme devient accessible au niveau de l'ampoule et du pavillon (Fig. 5,6).

Les ovaires sont peu échogènes, ils montrent une vascularisation intense grossièrement parallèle au grand axe de l'organe. On y voit parfois des petites zones étoilées correspondant vraisemblablement à des cicatrices de corps jaune en atrésie (Fig. 7).

Les vaisseaux lombo-ovariens et utérins apparaissent comme étant des amas de coupes circulaires bien limitées, pulsatiles et pauvres en échos (Fig. 8, 9).

Pouvoir discriminatif

Nous avons eu l'occasion de pratiquer une échographie de contact chez une patiente porteuse de kystes bilatéraux dont l'examen conventionnel ne montrait pas de distinction structurelle. Le premier apparaissait comme étant vide d'écho et le second était peuplé de fins échos. Il s'agissait d'un kyste séreux et d'un kyste d'endométriose (Fig. 10, 11,12).

Discussion et possibilités

Ce nouveau créneau de l'échographie doit trouver ses indications , prouver ses capacités et définir ses limites.

Il semble que la haute définition et la suppression des artefacts dus aux tissus superficiels permettent d'affiner le diagnostic échographique.

Il s'agit plutôt de savoir si cette technique endocavitaire améliorera le diagnostic laparoscopique au point de vue anatomique et lors d'épreuves dynamiques.

a) L'anatomie laparoscopique

Aussi exercé soit-il, le laparoscopiste ne peut toujours mobiliser les organes de telle sorte qu'il puisse voir l'entièreté des cibles. Elles peuvent être peu mobilisables par suite d'adhérences ou bien leur aspect extérieur peut très bien cacher une pathologie interne (ovaires micropolykystiques ou fibromes intramuraux).

La visualisation aisée des systèmes vasculaires peut amener à poser objectivement le diagnostic de varices pelviennes alors qu'en position de Trendelenbourg, elles sont peu visibles.

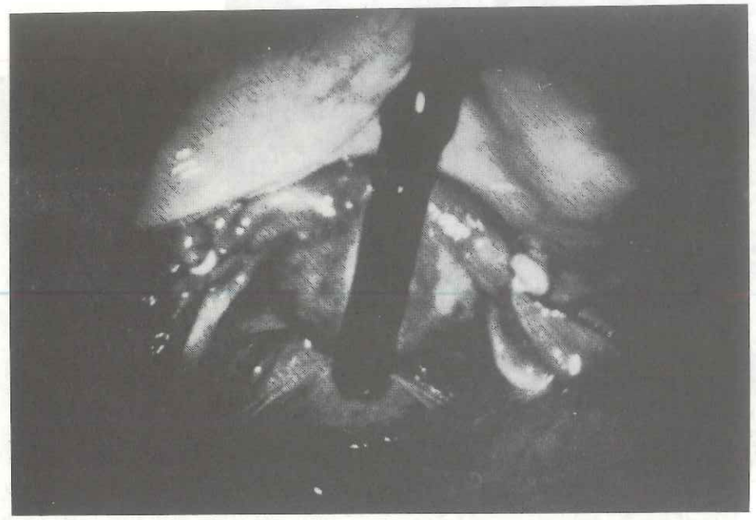

Fig. 1. Ultrasonic probe in contact of the uterus.

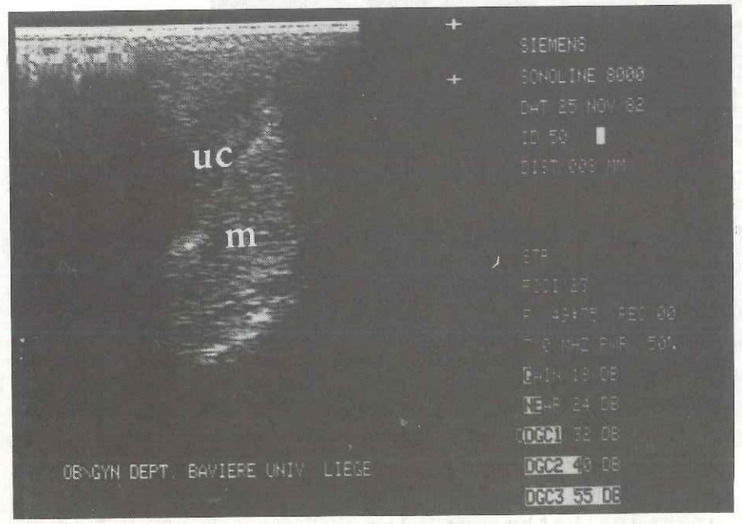

Fig. 2. Endometrium in luteal phase.

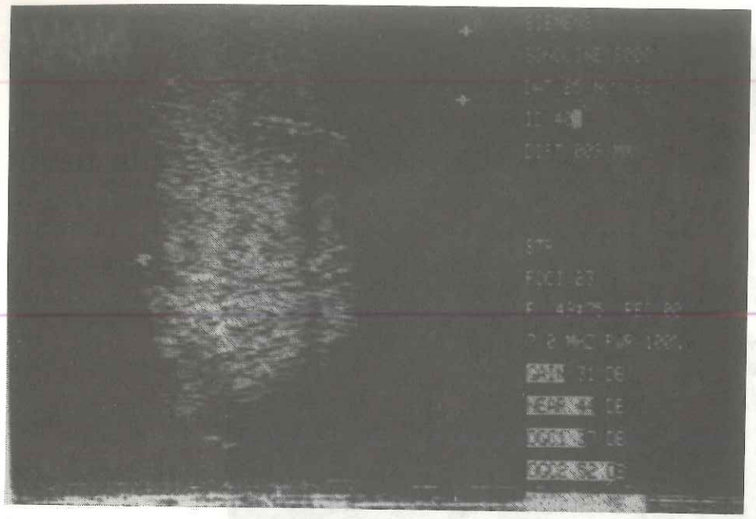

Fig. 3. Endometrium in follicular phase.

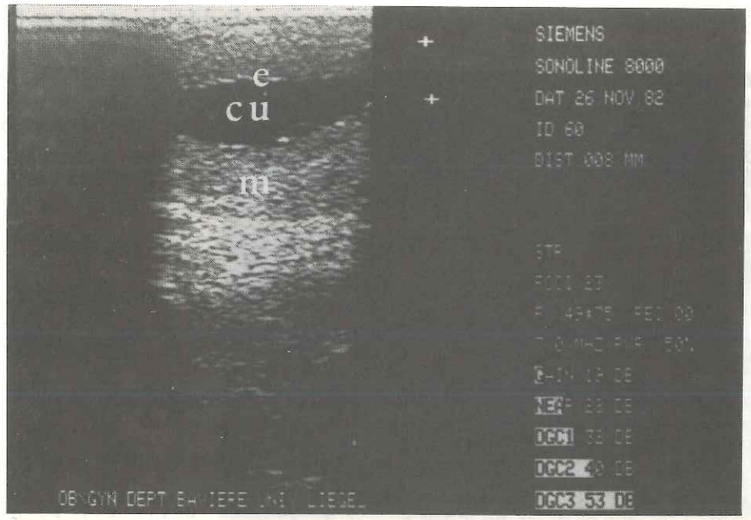

Fig. 4. Low pressure Methylene blue injection of the uterus. Dilatation of the cavity.

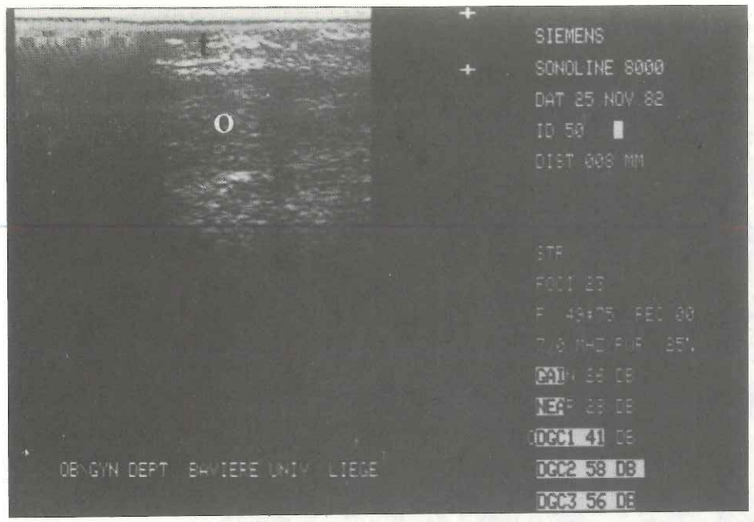

Fig. 5. Isthmic part of the tube.

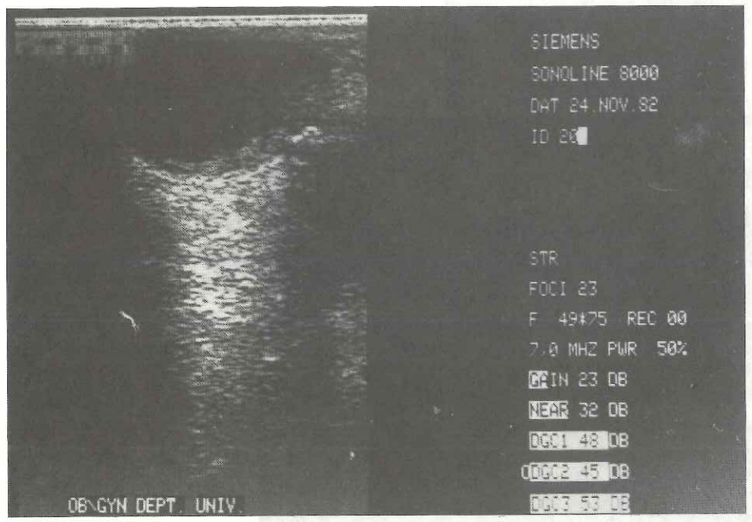

Fig. 6. Hydrosalpinx.

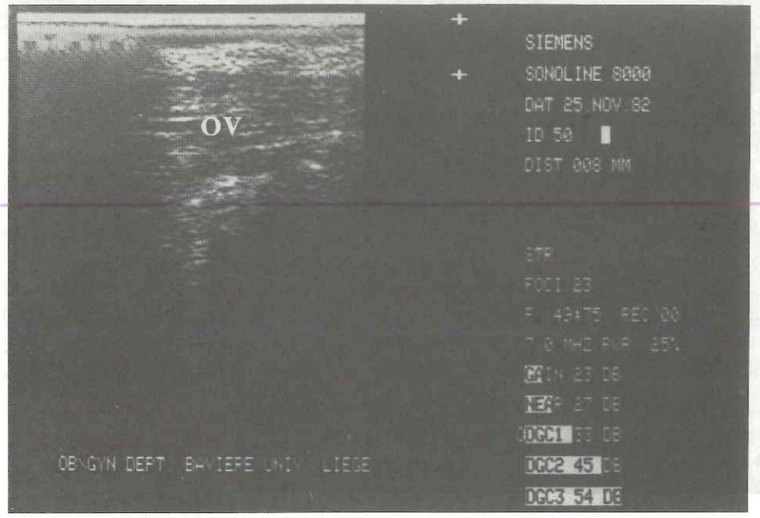

Fig. 7. Intra ovarian vessels.

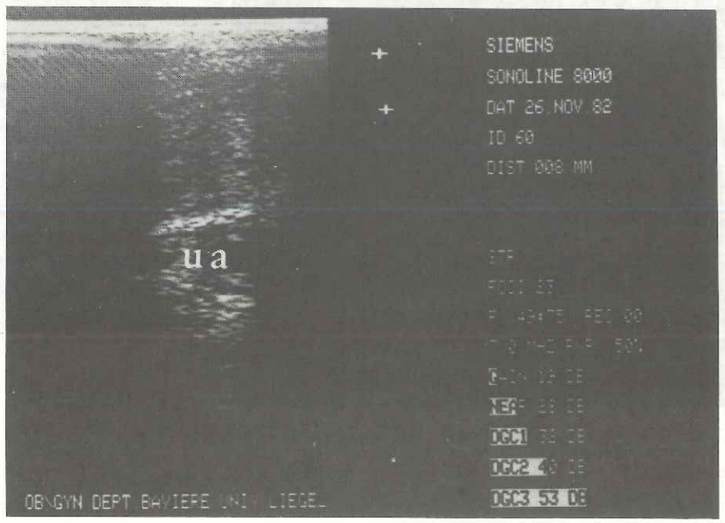

Fig. 8. Uterus (oblical section across the artery).

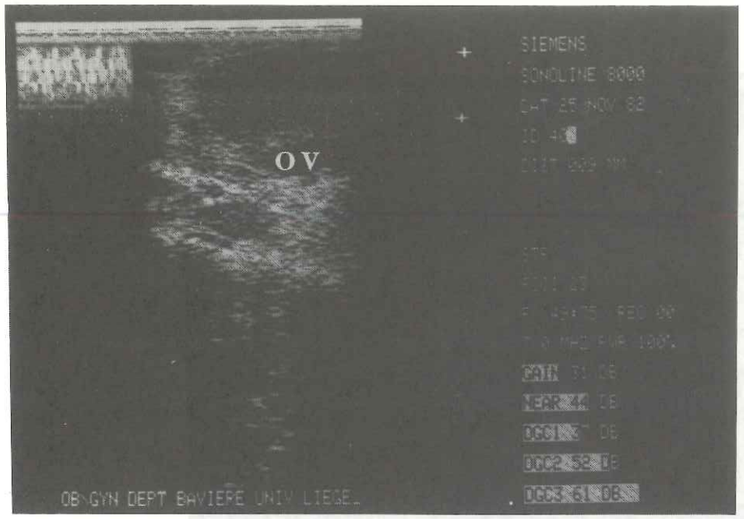

Fig. 9. Ovarian vein.

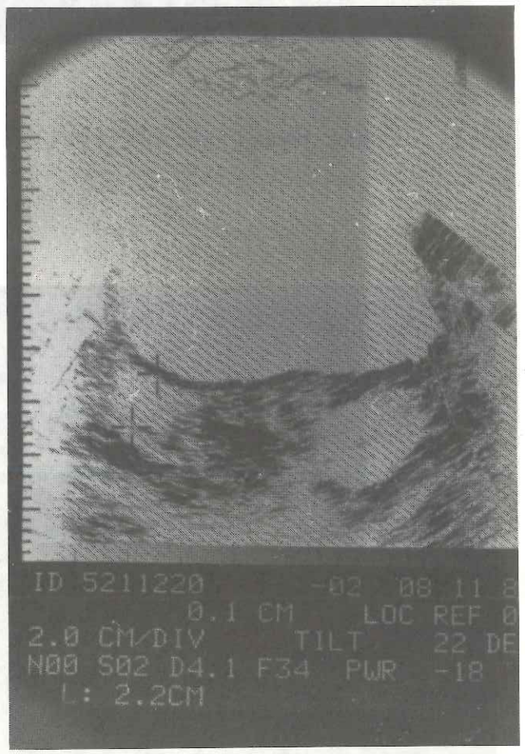

Fig. 10. Normal ultrasonography : bilateral ovarian cysts.

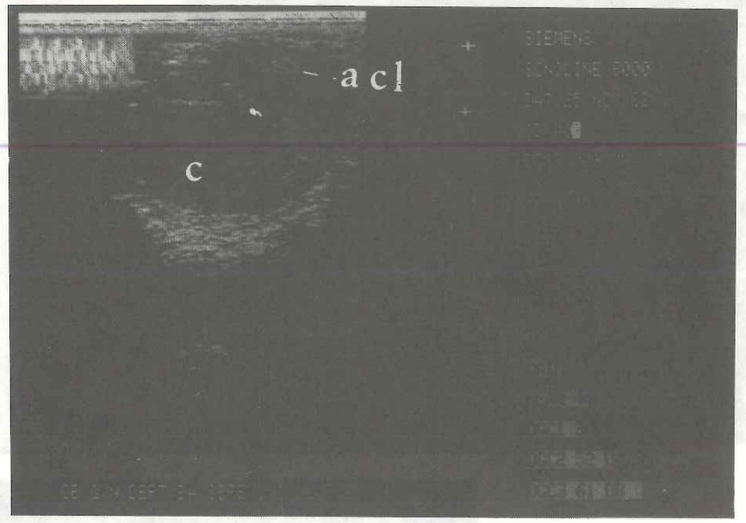

Fig. 11. Right ovari serous cyst with atretic corpus luteum.

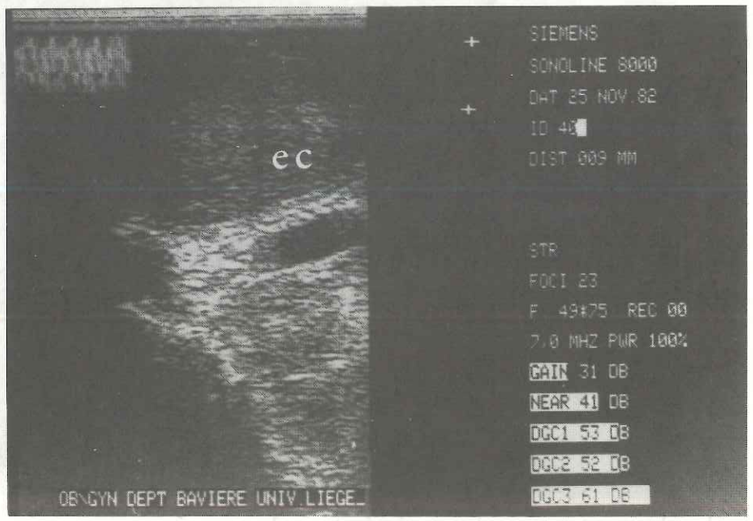

Fig. 12. Endometriotic cyst of the left ovary.

RESISTANCE CIRCULATOIRE PLACENTAIRE ET PATHOLOGIE FOETALE

L. POURCELOT (Tours, France)

Ultrasonography of Superficial Organs - Focussing on Scrotal Contents.

D.Beyer,Lorenz,R.,Heuser,L.

Radiologisches Institut der Universität Köln
(Direktor:Prof.Dr.G.Friedmann)

High resolution ultrasonography has been shown to be an effective and clinically acceptable technique for the evaluation of superficially located organs ("small parts") such as the breast,the thyroid and parathyroid gland, peripheral soft tissue masses,peripheral vessels and -last not least- the scrotum.
Because of the limited time we would like to focus our interest on high-resolution ultrasonography of the scrotal contents showing all the merits of this relatively new diagnostic technique.Our report - based on more than 3oo cases - concerns our experience with high-resolution real-time ultrasonography, which produces detailed anatomic images of the scrotal contents, especially of the testes.

1.Materials and Methods

3o9 consecutive patients were scanned with a 5MHz high-resolution real-time paralell scanner(PICKER LS 3ooo).Additionally we were able to use a dedicated "small-parts" real-time scanner with a built-in water bath and a 1o MHz transducer (PICKER MICRO-VIEW) showing a superb resolution (o.5mm axial,1 - 2mm lateral resolution.
Several parameters of examination were noted:

1. The testis itself was characterized as echogenically normal or abnormal.For size comparison anteroposterior and longitudinal measurements were made on both testes.
2. For evaluation of the epididymis,the diameter was measured on every section on which the epididymis was clearly defined as a separate structure.Extratesticular masses were characterized as solid,cystic,or complex.
3. The amount of peritesticular fluid was classified as normal or as minimally,moderately,or excessively increased.

Proof of diagnosis was based on histological examination after surgery and/or clinical and ultrasonographical follow-up.

2.Anatomy

Ultrasonographically the testis has an even,highly echogenic, fine-granular echo texture.The rete testis cannot be visualized. A small amount of fluid may be present around the normal testis

presumably between the two layers of the tunica vaginalis.
The scrotum (skin and dartos tunic)and other tissue layers surrounding the testis cannot be individually identified and appear as an echogenic stripe 2 - 3 mm thick.
The epididymis has a much coarser,more echogenic texture than the testis.Usually the epididymal head and body can be visualized,whereas the tail is only seen when a hydrocele is present. Other appendages of the testis and epididymis are not seen under normal conditions,although peritesticular fluid collections enhance the visibility of these appendages.

3.Indications

The problems presented in scrotal diagnosis are well known to every urologist.On the basis of physical examination alone,it is often difficult or impossible to decide whether a palpable abnormalityarises from the testicle itself or from extratesticular elements.
In addition,the normal examination may overlook significant pathology.Therefore the indications for scrotal ultrasonography are:

- Scrotal swelling or palpable masses(acute or chronic, with or without associated pain),
- scrotal trauma,
- non-resolving epididymo-orchitis,
- orchalgia,and
- detection of a nonpalpable testicular neoplasm(in patients presenting with metastatic adenopathy or lung nodules suspected to be of testicular origin).

Undescended testes in the inguinal canal may be seen as well with ultrasonography.

4.Pathology

Based on sonographic localisation of scrotal pathology,an anatomic classification can be devised,which places abnormalities into one of three categories: extratesticular,testicular,or combined extratesticular and testicular.
In general,a purely extratesticular abnormality with a normal testis is usually benign and may be treated conservatively.On the other hand,if the testis is ultrasonographically abnormal,surgery may be required to exclude tumor.

In our series small-parts real-time ultrasonography was able to distinguish testicular from extratesticular pathology in over 9o% of the cases,additionally subclassifying the lesions as solid, cystic,or complex.

5.Extratesticular Lesions

5.1.Hydrocele

Hydrocele,one of the most common causes of chronic,painless scrotal swelling,represents a peritesticular collection of serous fluid. It may be primary-idiopathic or secondary to almost any disease in the scrotum,including epididymo-orchitis,torsion,trauma and tumor.Ultrasonography reveals anechoic fluid surrounding the testis except posterolaterally at the attachment of the epididymis (Fig.1).With chronicity of following infections or hemorrhage septations may develop in the hydrocele.

5.2.Spermatocele

A spermatocele is a cystic collection of seminal fluid in an affferant duct near the epididymal head and may occur secondary to previous epididymitis or trauma.Sonographically,it is seen as a simple cyst near the epididymal head which usually does not deform the testicle.It cannot be differentiated from epididymal cysts.

5.3.Epididymal Cyst

An epididymal cyst or a cystic degeneration of the epididymis may occur as a result of previous epididymitis and appear ultrasonographically as cystic fluid collections,sometimes containing debris along the course of epididymitis (Fig.2).It may occur together with a spermatocele.

5.4.Trauma - Hematocele

In trauma to the scrotum ultrasonography may yield important information regarding the integrity of the testicle in addition to demonstrating a usually clinically apparent hematocele.Since hematomas change in consistency over time,the ultrasound appearance of a hematocele is variable.Appearances ranging from almost purely cystic to complex,bizarre extratesticular masses may be seen. Ultrasound can also be used to localize the position of scrotal

foreign bodies.Epididymitis or epididymal hematoma occuring secondary to trauma may be demonstrated simultaneously.

5.5.Varicocele

A varicocele represents dilatation and tortuosity of pampiniform plexus veins and appears ultrasonographically as a complex extratesticular mass with serpinginous,grape-like cystic areas representing dilated veins with predilection for the left side. Most varicoceles are not seen on ultrasound because they drain when the patient is scanned in supine position.Therefore scanning in upright position to fill the veins is recommended.

5.6.Acute and Chronic Epididymitis

Acute epididymitis - by far the most common intrascrotal inflammation - most often presents with an acutely swollen and tender scrotum.Causes include gonococcal,nonspecific pyogenic or tuberculosis infection,and trauma.It may accompany mumps or syphilitic orchitis,too.Ultrasonography showes a diffusely or focally thickened epididymis which is more sonolucent than normal,and concomitant scrotal thickening and most often a reactive haydrocele(Fig.3)Ultrasound can also demonstrate other abnormalities associated with epididymitis such as focal or generalized orchitis,testicular tumor (occasionally causing epididymitis),abscess or hydrocele formation.Since testicular tumors and orchitis may appear ultrasonographically as identical lesions, they cannot be reliably distinguished except with follow-up scans after antibiotic treatment,which show resolution of orchitis but persistence of tumor.
If paraepididymal or testicular abscess develops,ultrasound usually demonstrates a complex mass combined with a fluid collection.

5.7.Epididymal Tumor

Although very rarely encountered,the most common epididymal tumor is the benign,slowly growing adenomatoid tumor,ultrasonographically presenting as a solid extratesticular mass.

6.Testicular Tumors

6.1.Torsion

The first imaging study to be ordered in suspected testicular torsion in still the radionuclide scan.Ultrasonography has only limited use in certain circumstances,for instance,when the radionuclide scan is equivocal or if there is an additional palpable scrotal mass.
The ultrasoundappearance of torsion seems to be time-related. In the early stage the involved testis appears normal,but gradually it becomes swollen and abnormally echopoor.Additionally a thickening of the scrotal skin and the epididymis may be observed.Chronically torsed testes become atrophic and appear echopoor as well.

6.2.Orchitis

Orchitis often develops as a complication of epididymitis.It is most commonly seen on ultrasound as a focal or diffuse echo-poor alteration of the testicular echopattern.Follow-up scans are necessary to differentiate this appearance from tumor.An abcess may develop,appearing as a complex testicular and/or peritesticular mass.(Fig.4)

6.3.Testicular Neoplasms

Approximately 95% of testicular tumors are of germ cell origin, imcluding seminoma,embryonal carcinoma,teratoma and teratocarcinoma,chorioncarcinoma and mixed patterns.Most of the remainder arise from the interstitial cells of Leydig or the Sertoli cells and are often hormonally active.Rarely,tumors originate from testicular vascular or connective tissue.Leukemia,Hodgkin's or Non-Hodgkin's lymphoma may involve the testes as well.
Testicular tumors usually present as painless scrotal masses, although pain may occur if there is associated hemorrhage or necrosis.
Sonographically testicular tumors appear as focal or diffuse alteration of the normally homogeneous testicular echo texture. Most frequently focal,relatively echo-poor regions are seen;concomitant necroses or hemorrhage cause a complex appearance with

cystic and solid areas(Fig.5 and 6).
Occasionally a tumor may replace a testis totally and produce diffuse and sometimes only subtle alteration of testicular echo texture.The ultrasound appearance of testicular neoplasms is non-specific although teratocarcinoma has the propensity to contain cystic areas.Therefore there is no reliable correlation between tumor histology and echotexture.There is a wide differential diagnosis in echopoor or complex testicular masses including abscess,orchitis or torsion.Purely hyperechoic or echogenic testicular lesions are likely to be benign often representing scars or calcifications.

7.Combined Testicular and Extratesticular Lesions

This group consists primarily of the various combinations of the previously described testicular and extratesticular abnormalities.The combined category carries the same significance as testicular pathology alone in terms of the possibility of tumor.

8.Conclusions

By evaluating the various parameters of scrotal ultrasonography, a distinction can be made in the majority of cases between those requiring immediate surgery and those in which carefull clinical follow-up appears adequate.
In the case of intratesticular tumor,torsion or solid extra-testicular tumor,surgery is indicated,while for the other entities not.
The two "key findings" in ultrasonography which indicate a surgical lesion are decreased echogenicity of the mostly enlarged testis and a solid extratesticular mass.However,neoplasms and hematomas are not the only abnormalities causing decreased intratesticular echogenicity.Torsion and severe epididymo-orchitis may give the same ultrasonographic picture.
But our experiences suggest some distinguishing features between tumor and the other two conditions.Epididymal enlargement,marked increase in peritesticular fluid,and skin thickening strongly suggest a nontumerous condition even in the presence of decreased testicular echogenicity.

Controversely,tumor is likely when an intratesticular area of decreased echogenicity is present without any of these peri-testicular findings.
According to our present experience,high-resolution real-time ultrasonography of the scrotum with a 5 MHz transducer proves to be an effective method in disclosing the site,delineating the extent and characterizing the nature of extra- and intra-testicular disease.
It is clearly the best method for detecting occult testicular neoplasms.

Figures

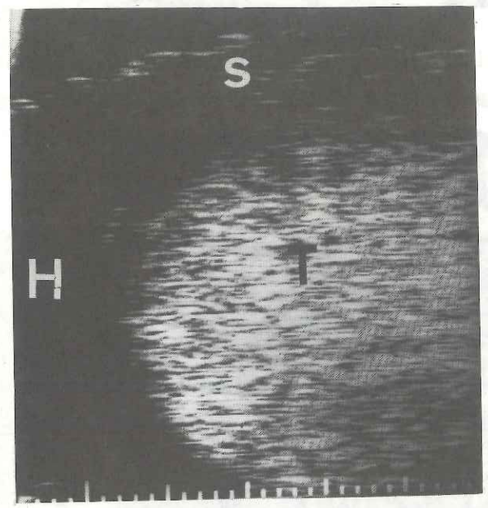

Fig.1 Normal testicle with concomitant hydrocele.
Sagittal section demonstrates homogeneous echogenicity of the testicle (T) and anechoic fluid surrounding it(H).
Moderately increased thickness of the scrotal skin.
(1o MHz transducer).

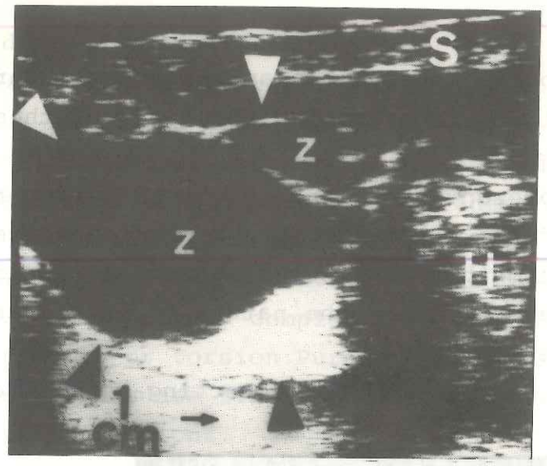

Fig.2 Normal testicle(H).Cystic degeration of the head of the epididymis (▶).(s = scrotal skin)(1o MHz transducer)

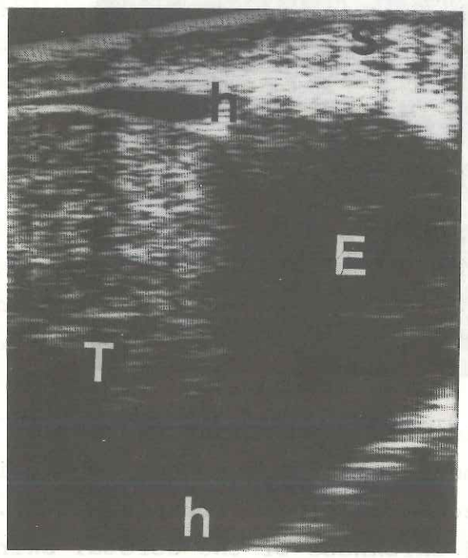

Fig.3 Severe epididymitis(E) with concomitant minimal hydrocele (h) and scrotal skin thickening(s).The epididymal tail is echo-poor and excessively enlarged.
(1o MHz transducer)

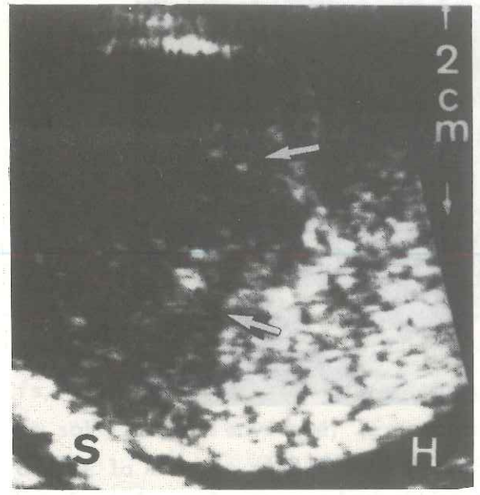

Fig.4 Focal orchitis.
Enlarged testicle with lobulated echopoor mass (⟶) and concomitant hydrocele (H) and scrotal skin thickening(s).

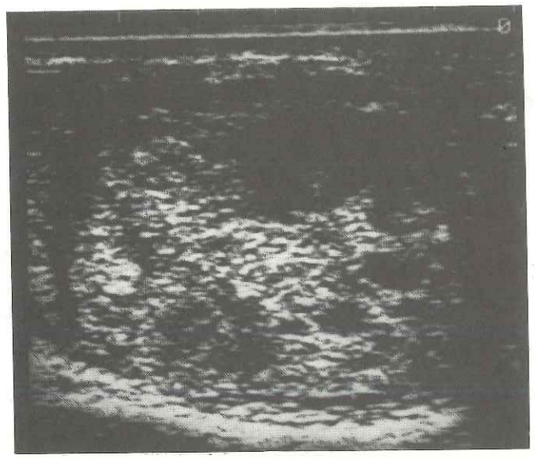

Fig.5 Mixed seminoma and embryonal carcinoma of the testis.
Grossly enlarged testicle with large echogenic mass and echo-poor halo and multiple echo-poor regions of necrosis.
(5 MHz transducer)

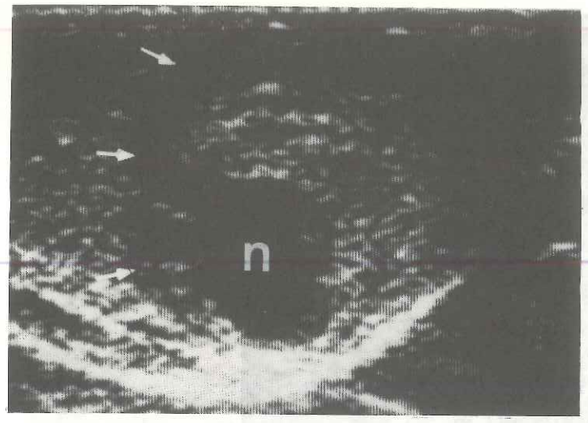

Fig.6 Teratocarcinoma of the testis
Relative echogenic mass with halo sign (➡) and echo-free cyst (necrosis = n).

For bibliography please contact:

Priv.Doz.Dr.med.Dieter Beyer
Radiologisches Institut der Universität zu Köln
Joseph-Stelzmann-Str.9,Zentralklinikum
5ooo Köln - 41
W.Germany

ULTRASONOGRAPHIE D'INTERVENTION - DONNEES TECHNIQUES

P.M. BRET, Unité de Radiologie Digestive
Hôpital Edouard Herriot - 69374 - LYON CEDEX 8 - FRANCE

L'échographie interventionnelle représente l'ensemble des gestes invasifs, à visée diagnostique ou thérapeutique, guidés par l'échographie. Quel que soit le geste envisagé, le premier stade est la ponction guidée, c'est à dire la mise en place, sous guidage échographique d'une aiguille dans une cible. Aprés la ponction, trois types de geste peuvent être pratiqués :

- prélèvements (anatomopathologiques (cytologique ou histologique), bactériologiques ou chimiques) ;
- injections de produits de contraste pour opacification radiologique,
- gestes thérapeutiques : injections médicamenteuses, drainages d'une collection circonscrite ou de cavités excrétrices en rétention.

LA PONCTION GUIDEE PAR ECHOGRAPHIE :

En fonction du matériel dont on dispose, plusieurs méthodes peuvent être utilisées pour le repérage ou le guidage d'une ponction :

1) Le repérage de la ponction par l'échographie :
La méthode la plus simple pour repérer une cible grace à l'échographie consiste à marquer sur la peau du patient un point situé à l'aplomb de la lésion. La profondeur de celle-ci est ensuite mesurée sur l'image échographique. La ponction est alors pratiquée à "l'aveugle" à partir des renseignements fournis par le repérage échographique. Cette technique est utile pour la ponction de cibles de grande taille, dans un plan perpendiculaire à la lésion ; elle ne permet pas une approche oblique de la cible et ne tient pas compte des modifications des repères qui peuvent intervenir entre l'échographie de repérage et la ponction.

2) Le guidage échographique

- avec un apparail de balayage manuel, on peut adapter une sonde spécialement conçue pour la ponction sur le bras articulé. Le centre de la sonde est muni d'un trou, ou d'une fente, pour le passage de l'aiguille. Celle-ci suivra toujours l'axe du faisceau ultra-sonore. La sonde de ponction préalablement stérilisée , est montée sur le bras articulé de l'échographe et l'image de la lésion est construite. Sur l'écran, en surimpression sur l'image échographique, s'inscrit l'axe du faisceau ultrasonore (et de la ponction). Lorsque l'obliquité de la sonde est telle que le plan de coupe passe par la cible, l'aiguille de ponction est introduite jusqu'à la profondeur souhaitée. Cette méthode permet une approche oblique des lésions mais ne permet pas de tenir compte des mouvements éventuels de la cible, notamment au cours de la respiration.

- les appareils en temps réel sont mieux adaptés à la réalisation de ponctions guidées, car ils permettent de suivre en permanence sur l'écran de contrôle, l'image de la lésion cible et celle de l'aiguille de ponction au cours de sa progression jusqu'à celle-ci. Certaines barrettes multi-sondes sont percées d'un orifice central, destiné au passage de l'aiguille. La ponction est pratiquée dans l'axe du faisceau ultrasonore et il est généralement possible de repérer l'écho de l'extrémité distale de l'aiguille au fur et à mesure de sa progression. Avec les appareils à balayage secto-riel mécanique, et sur certaines barrettes multisondes, le guidage peut être effectué grâce à un accessoire fixé sur la partie latérale du transducteur. L'approche de la lésion est oblique et on peut contrôler sur l'écran l'image de la cible et de l'aiguille de ponction au cours de sa progression. L'uti-lisation d'une sonde dite de ponction comporte certains inconvénients : l'achat d'un transducteur qui ne sera utilisé que pour la ponction, néces-sité d'utiliser des aiguilles longues de 15 à 20 cm, trop souples pour être facilement dirigées qui sont généralement introduites au travers d'une aiguille guide de plus gros calibre, nécessité de réaliser la ponction à 2 opérateurs, l'un tenant le transducteur de ponction, l'autre réalisant véritablement la ponction.

- avec la méthode que nous utilisons, la ponction est pratiquée sous guidage échoscopique avec une sonde d'échographie standard, placée dans un sac en plastique stérile afin de respecter l'asepsie du geste ; de l'huile de vaseline stérile assure le couplage entre la peau du patient et le transducteur; la sonde est placée de telle sorte que la lésion se projette au centre de l'image observée sur l'écran. L'aiguille est alors introduite au ras du milieu de la sonde dans un plan discrétement oblique par rapport à l'axe du transducteur, de façon à ce que son extrémité recoupe le plan du faisceau ultrasonore à la profondeur approximative de la lésion. Dès les premiers centimètres sous la peau, l'extrémité distale est repérée sous la forme d'un écho de haute amplitude. Cet écho est visible à la fois dans les lésions liquides et solides. L'aiguille est amenée progressivement dans la cible à ponctionner. La précision du geste permet la ponction de cibles dont le diamètre est inférieur à 5mm. Deux critéres permettent d'affirmer que l'aiguille est en place dans la lésion : visibilité de l'écho de son extrémité distale, sensation tactile de pénétration dans une tumeur solide.

LES GESTES PRATIQUES APRES LA PONCTION :

La ponction sous échographie est indiquée pour la réalisation de trois types de gestes : les deux premiers sont diagnostiques : prélève-ment guidé (surtout anatomo-pathologique) dans le diagnostic des lésions circonscrites abdominales, opacification sélective de canaux, de vaisseaux ou de certaines collections liquidiennes ; la troisième indication concerne les gestes thérapeutiques : évacuation d'une collection liquidienne, drainage des cavités abcédées, des voies biliaires, des cavités excrétrices du rein ; injection de substances médicamenteuses diverses.

Certains de ces gestes sont pratiqués entièrement sous contrôle échoscopique ; d'autres nécessitent un guidage mixte échoscopique et radioscopique télévisé ; ils utilisent à la fois les principes de la ponction guidée et ceux du cathétérisme en radiologie vasculaire.

- les prélèvements :

Les prélèvements sont habituellement pratiqués à l'aide d'une aiguille fine capable de traverser sans les léser la plupart des organes intra-abdominaux. Une aiguille de calibre 22 G (0,7mm de diamètre externe) est le plus souvent utilisée ; elle doit être la plus courte possible pour être maniable. Elle permet d'obtenir des prélèvements cytologiques ou histologiques si l'on utilise des aiguilles à extrémité cylindrique, sans biseau, qui sont vissées dans la lésion. Lorsque la lésion est superficielle, des ponctions biospies conventionnelles peuvent être pratiquées à l'aide d'aiguilles de plus gros calibre (Tru-cut, Menghini). Lorsque l'aiguille est en place dans la cible, l'aspiration peut débuter : elle est pratiquée par l'intermédiaire d'une seringue en plastique reliée à un "pistolet-aspirateur". L'aspiration est maintenue pendant quelques secondes au cours desquelles des mouvements de va-et-vient sont appliqués à l'aiguille afin d'enrichir les prélèvements. L'aspiration est relâchée avant de retirer l'ensemble aiguille-seringue.

- l'opacification sélective

En pathologie abdominale, l'échoscopie couplée à la radioscopie télévisée peut guider l'opacification percutanée des voies biliaires ou pancréatiques, des vaisseaux portes et de toutes les collections circonscrites liquidiennes. L'aiguille est mise en place sous guidage échoscopique dans la cible puis une aspiration douce de quelques ml est pratiquée pour diminuer la pression intra-canalaire (ou intrakystique). L'aiguille est ensuite reliée à un raccord souple et le produit de contraste injecté sous contrôle radioscopique télévisé. En fin d'examen, le produit de contraste est retiré par aspiration.

- les ponctions à but thérapeutique.

Le drainage percutané s'applique aux obstructions des voies biliaires et des cavités excrétrices rénales et aux collections liquidiennes intra-abdominales stériles ou abcédées. L'évacuation d'une collection peut être

obtenue par aspiration simple à l'aiguille fine ou à l'aiguille cathéter Le drainage biliaire, les néphrostomies et les drainages d'abcès nécessitent la mise en place d'un cathéter selon la technique de Seldinger. L'introduction de l'aiguille cathéter, la manipulation des guides et des cathéters de drainage peut être pratiquée sous guidage purement échoscopique ou sous contrôle radiotélévisé.

Central Institute of Roentgenology, University-Clinics
Zürich

Experience with ultrasound guided fine needle punctures (2100 patients)

R. Ch. Otto

Using modern tomographique techniques like sonography or computertomography, the yield of macromorphological diagnoses has become tremendously enlarged. The parenchymal organs in the body and the chest can be differentiated and, moreover, smaller and larger lesions can be recognized up to a minimal seize of o.5 to 1.0 mm in diameter. Radiologists of today do not depend any more from indirect images being offered by vascular patterns (angiography) or duct systems (endoscopic pancreatography), but may see the lesion of an organ or the region of interest directly.

Nevertheless, the different tomographic techniques often are not able to give the definitive information concerning the dignity of a mass or a more generalized change of an organ (hepatoma!) and it is of utmost importance to know about it's microscopical structure. Many attempts were made during the last years to obtain additional information about alterations of the tissues. Therefore, sonography and computertomography have been combined with puncture techniques to get definite cytological material from the tissues in the depth or to obtain some fluid suspicious for an abscess from a collection in the body.

Method:

In our institute a hollow-core focused linear array transducer of a realtime ultrasound machine has been modified for the purpose of fine-needle punctures (1). Through the removal of three crystals in the center of the transducer head an aperture is created which allows the passage of Chiba fine-needles or other special biopsy sets and drainage systems.*

---

*Angiomed, D 7505 Ettlingen, Western-Germany

A regular transducer head of the above mentioned real-time unit is used first to examine the patient and then to select the most convenient place for the biopsy if ever necessary. The abdomen or thethorax has be prepped and draped around this area. In order to guarantee strictly aseptic criteria Merfen solution is used as the coupling agent between the transducer and abdominal skin.

With the steril aspiration transducer the ultrasound findings are verified. Due to the central perforation of the transducer a linear echofree line of sight is displayed indicating the passage which the needle will follow through the tissues.(Fig 1). The site selected for biopsy can be anesthetized with 1 % Procaine. The needle is guided through the central aperture in the transducer and after penetration of the skin it is carefully advanced. Due to the perpendicular penetration of the tissues the tip of the needle will appear as a bright echo-spot on the ultrasound picture. Lateral bending or angulation of the needle is carefully avoided because the echo of the needle tip may be lost from the tomographic plane displayed on the ultrasound screen. Once the needle tip has been placed into the lesion or fluid collection aspiration is performed with a 10 cc syringe (Fig. 2). Any change of the lesion or the organ by respiration ist immediately noticed due to the constant visual surveillance of the procedure on realtime B-scan.

Complications

Serious complications due to fine needle punctures under sonographic control have been observed in rare cases (n=14 patients). These were pain attaques up to three hours in 9 patients, probably due to localized discrete hemorrhage or peritonitis (extravasation of bile!). No patient had to be operated upon, but a 76 year old man suffered from a perforated stress ulcer of the duodenum one day after the puncture procedere.

Results

The new biopsy method under sonographic control was used to study lesions of different organs in the abdomen, chest, cervical region and extremities. Most of the punctures were performed for evaluation of abdominal lesions mainly in the liver. The first punctures have been performed in 1977.

During the last two years more and more drainage procedures have been performed using a new set under ultrasound control and permanent view as well.

Table I shows the different organs punctured in the abdomen, thorax, neck and extremities during the last four years. The total amount of patients with sonographically guided interventions surpasses today the number of 2100.

Tab. I
Fine needle aspiration biopsy
(n=1299 patients/ 1. 1979 - 1. 1983)

Liver	379
Pancreas	123
Kidney	118
Retroperit. Tumors	279
Cysts, Abscesses, Pseudocysts	211
Others	189
	1299

In many instances fluid aspiration was necessary. Our procedure proved to be safer than "blind" punctures, especially when fluid collections were localised (Tab. II, III).

Tab. II
Fluid collections punctured during the last 2 years
(n=211)

Ascites	79
Pleural effusion	51
Amniocentesis	42
Others (hematoma etc.)	39

Tab. III
Cyst of the breast = 89

Drainages may help as definitive or intermediate therapy. Since two years we have to perform more and more of these therapeutical interventions (Tab. IV).

Tab. IV
Drainages under ultrasound control
(n=116 patients/failures 24= kindney disorders without hydronephrosis)

Hydronephrosis	39
Abscess	21
Bile system	9
Ascites(Gynecology)	32
Pleural effusion	15

In 1981 we controlled the percentage of malignant lesions suspected by ultrasound alone and verified by cytology (Tab. V), (2).

Tab. V
Results of fine needle biopsies under ultrasound control and permanent view 1980/81
n=480
Dignity of focal tissue alterations
(no abscess, no cyst)

Evaluation by biopsy	sonography alone
70,8% malignant	92,1%
29,2% benign	7,9%

The average is fairly the same even today but there are fewer benign lesions (-5%).

The fine needle puncture under real-time guidance which was started 5 years ago in addition to tomographic techniques especially for sonography could be developed in the course of time. It has simplified the exploration of focal lesions and has made the procedure more comfortable and economic for the patient. Cell material, specific for a tumor, is obtained in 80 to 90% of the cases. Using this method it is possible to come up with a very high percentage of definite diagnoses in comparison to other diagnostic methods in medicine.

There are no false positive results. But false negative results may be observed due to inevitable aspiration of blood, aspiration of necrotic material, in superinfected malignancies or hightly fibrotic tumors (sclerotic form of Hodgkin's disease) and very small tumors less than 1 cm in diameter.

A new skill still to be developed is the drainage of kidneys, fluid collections and abscesses. These methods will certainly become important in the near future, as surgical intervention can be avoided very often.

Literatur

1. Otto R. und Deyhle P.
Ultraschallgezielte Feinnadelpunktion unter permanenter Sichtkontrolle. Dtsch med. Wschr. 104: 1665-1669, (1979)

2. Otto R.
Results of 1000 fine needle punctures guided under real-time sonographic control. J. belge Radiol. 65: 193-199 (1982)

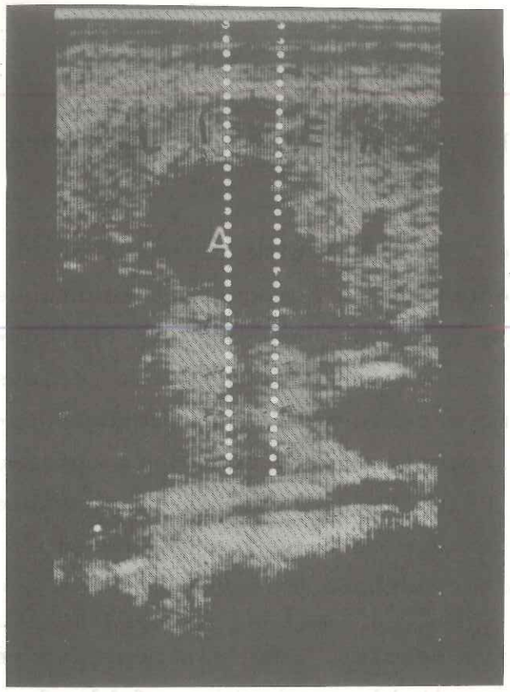

Fig. 1. Liver abscess (A), Dotted line = Line of sight.

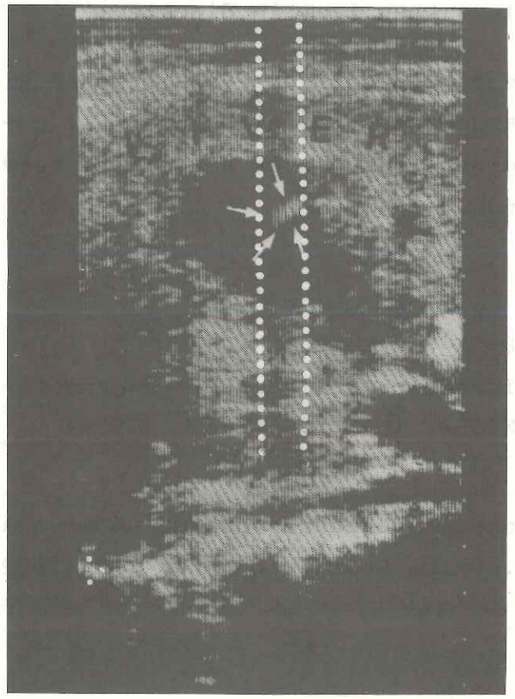

Fig. 2. Tip of fine needle (white arrows) in the abscess.

L'ULTRASONOGRAPHIE PER OPERATOIRE

LIEGE

M.C. PLAINFOSSE, A. HERNIGOU, S. MERRAN.

Les ultrasons permettent une excellente palpation des tissus mous, complètant ainsi les sensations recueillies par la main et trouvant des informations que celle-ci n'avait pas perçues. C'est là tout l'interêt de l'ultrasonographie transcutanée.

Les ultrasons vont apporter une aide identique au chirurgien dont la main, par l'incision per-cutanée, cherche la lésion, sa localisation, sa consistance et son extension. Car si capable que soit cette main, elle a aussi ses limites dont nous allons donner quelques exemples. Elle ne pourra percevoir : l'extension d'un cancer de la tête du pancréas, l'existence d'une métastase hépatique petite et profonde, le siège d'un petit calcul caliciel, la persistance d'un calcul dans le bas cholédoque.

Nous voyons donc poindre une nouvelle application de l'ultrasonographie qui prend, après les rayons X, le chemin des salles d'opération. Ceci suppose une adaptation du matériel existant et la création de machines en fonction de ce nouveau besoin.

TECHNOLOGIE DES ULTRASONS EN SALLE D'OPERATION (5. 6)

Les appareils utilisés doivent répondre à quatre exigences que nous envisagerons successivement :

- l'examen doit être de brève durée
- Les sondes doivent pouvoir pénétrer dans toutes les incisions, avoir une haute fréquence et s'adapter sur des appareils peu encombrants.
- Les sondes et les cables doivent être parfaitement aseptiques
- Celui qui assure l'examen doit être compétent
- le recueil des informations doit être immédiat.

L'examen doit être de brève durée :

Seul un appareil en temps réel peut répondre à cette exigence. Il aura de plus l'avantage d'être beaucoup plus maniable, car il n'y a pas à l'heure actuelle en France d'appareil qui reste à demeure dans une salle d'opération. Ces machines peuvent servir à plusieurs services de chirurgie et être utilisée dans les intervalles libres par le Service central d'ultrasonographie pour les examens des parties molles. La facilité du transport et le faible encombrement sont des qualités importantes.

Les sondes :

La sonde est certainement la partie de l'appareillage qui doit le plus évoluer pour atteindre le but recherché : s'adapter à toutes les incisions chirurgicales, aller rechercher par ces incisions toutes les informations.

Une bonne solution est d'utiliser un sector scan ayant une petite porte d'entrée.

La sonde que nous avons utilisée (*) a un diamètre de 20 mm et mesure 95 mm de long. Le balayage sectoriel a un angle de 40 à 60°, cet appareil permet d'obtenir 20 images par seconde. L'inscription se fait sur une mémoire de 256 x 256 avec 16 niveaux de gris. Il existe trois fréquences (5, 7 et 10 MHz). A 7 MHz, la résolution axiale est de 0,3 mm et la résolution latérale est de 1 mm à 6 dB. La focalisation est assurée par une lentille

L'agrandissement de l'image est de 2. La sonde pèse 200 g, l'appareil 20 kg (fig. 1).

Les barettes ont été modifiées en vue du per opératoire (5.) Un premier modèle est une barette de 96 mm de long comportant 400 éléments, très peu épaisse car le boitier de relai est à distance. (* *)

Un deuxième modèle de barette extra plate possède un certain degré d'angulation qui permet un abord plus facile des viscères profonds. (* * *). La fréquence de la sonde sera d'autant plus élevée que l'organe à étudier est plus superficiel. C'est ainsi qu'une sonde de 10 MHz sera adaptée à tous les vaisseaux, une sonde de 7 MHz conviendra au rein, mais pour la face profonde du foie, il faudra descendre à 5 MHz.

Le prix de l'appareil étant de beaucoup supérieur à celui d'une sonde, tous les constructeurs essaient de fabriquer des sondes spécialisées branchables sur des coffrets de coût raisonnable. Ainsi on voit apparaitre des "modules échographiques pour les chirurgiens". A l'appareil de base, on ajoute une sonde per-opératoire, un sector scan utilisable par voie externe et des

* EDAP ** ALOKA *** SIEMENS

sondes endorectales, endovésicales.

Couplage et asepsie

Le couplage se fait par de la xylocaïne visqueuse. Il n'est pas toujours nécessaire, les organes ayant une humidité naturelle suffisante.

L'asepsie doit être rigoureuse pour le cable, la sonde et le doigtier. Quant au coffret électronique, il est hors du champ opératoire car le cable qui le relie au boitier est toujours long. La stérilisation ne peut être faite à chaud car elle détruirait les propriétés piezo-électrique des céramiques :

. on peut utiliser un champ opsite pour envelopper sonde et câble, mais ce procédé est jugé insuffisant par beaucoup de chirurgiens.

. on peut tremper la sonde 6 heures dans de l'aldylène qui libère des vapeurs d'aldehyde formique, puis rincer ensuite l'extrémité de la sonde qui sera en contact avec les organes.

. la poche à eau doit être remplie en salle d'opération avec du sérum stérile et recouvert d'un doigtier stérile qui aura été rincé au sérum physiologique.

Opérateur

L'opérateur de l'examen ultrasonore devrait être l'échographiste. Il doit donc s'habiller stérilement pour rentrer au bloc. Sa disponibilité doit être très grande pour s'adapter à tous les horaires des chirurgiens demandeurs. Cette disponibilité pouvant avoir des limites, il semble parfois nécessaire que le chirurgien lui-même puisse manipuler avec compétence.

Fixation des documents

La fixation de documents nécessite un gel d'image et une deuxième personne, qui n'a pas besoin d'être habillée stérilement, pour prendre les photos. C'est cette personne qui branchera l'extrémité du cable sur la machine. Le recueil de l'image doit être le plus simple possible et le résultat immédiat. Ceci impose pratiquement l'usage de films à développement instantané qui est très pratique. On pourra ainsi doubler les documents ou en refaire très rapidement s'ils sont insuffisants.

LES APPLICATIONS DE L'ULTRASONOGRAPHIE PER OPERATOIRE

Elles sont, dans l'état actuel de nos travaux, au nombre de cinq :

- la détection des lithiases, surtout rénales.
  Cette pathologie a été la première application de cette méthode.
- la localisation des petites tumeurs (par exemple tumeurs endocrines, pancréas, métastases hépatiques)
- l'appréciation de l'extension des cancers donc de leur opérabilité.
- le diagnostic de nature d'une masse (liquide, solide)
- la visualisation des plaques d'athérome et des thrombus sur les vaisseaux, puis ensuite leur morphologie pour opération chirurgicale.

Il faut auparavant connaitre les images des structures normales (fig. 2, 3, 4, 5)

I - LA LITHIASE

a) Nous aurons essentiellement en vue la lithiase rénale (1. 2. 4.)

L'image typique de calcul est bien connue. C'est un écho très dense suivi d'une ombre acoustique (fig. 6)
Avec une sonde de 7,5 MHz les calculs de 1 mm sont visibles, mais pour repérer des lithiases si petites, il est indispensable d'avoir une idée de leur localisation par une urographie intra veineuse pré opératoire et/ ou par les films sans écran en per opératoire, car le balayage d'un rein avec une sonde sectorielle de 2 cm de diamètre à la recherche d'une image aussi petite est longue. Lorsque le calcul est visualisé à l'échographie, on le place au centre de la sonde et on imprime avec celle-ci une marque sur le rein ; une aiguille est introduite en son centre jusqu'à obtenir un contact avec la lithiase. Puis une courte néphrotomie permettra son extraction la plus atraumatique possible.

L'interêt de l'échographie en dehors de ce repérage est de choisir le lieu idéal de cette néphrotomie. Il faut, dans ce but, minutieusement rechercher une zone dépourvue de vaisseaux et la partie du cortex la plus amincie.

Trois pièges sont à connaitre : les bulles d'air, les cicatrices fibreuses et les papilles calcifiées.

Pour éviter le premier, il est préférable de ne pas commencer l'intervention par une pyélotomie. Ceci peut être difficile si la lithiase est coralliforme. En effet, la pyélotomie s'accompagne d'une introduction d'air dans les cavités pyélocalicielles dont il sera difficile ensuite de se débarrasser. L'artefact réalisé est important à connaitre car la bulle d'air donne aussi une raie d'absorption acoustique. Cependant sa mobilité est plus importante que celle d'un calcul et des mouvements imprimés au rein vont toujours déplacer la bulle vers la partie la plus haute, tandis que la lithiase reste en position déclive.

Les cicatrices fibreuses ou les amas graisseux peuvent être parfaitement absorbants aux ultrasons et donner aussi une raie anéchogène derrière eux. Cependant lors de l'introduction de l'aiguille, il n'existe dans ce cas aucune sensation tactile de lithiase.

Les papilles calcifiées donnent une image identique à la lithiase, mais adhérente au parenchyme rénal. On ne peut donc en faire l'exérèse et de toute façon celle-ci est parfaitement inutile.

Nos échecs sont survenus essentiellement pendant notre temps d'apprentissage : matériel inadapté, ouverture première du bassinet, méconnaissance d'une bulle d'air.

Nos succès ont été l'exérèse de 200 lithiases sur 30 malades, les indications de cette technique étant les lithiases calicielles multiples, les lithiases coralliformes, les lithiases radiotransparentes parfois (1 cas de calcul bloquant la jonction pyélourétérale) et les lithiases difficiles sur rein opéré, sur rein malformé ou sur rein infecté.

Le bénéfice de cet examen est le raccourcissement important de l'acte chirurgical et du temps de clampage de l'artère rénale.

b) La lithiase biliaire arrive en second plan de nos indications. La chirurgie vésiculaire étant toujours une exérèse, il faut être sûr du diagnostic. S'il y a une micro-lithiase, la palpation est inopérante et l'échographie utile.

Les problèmes de la chirurgie cholédocienne sont généralement résolus par la cholangiographie per opératoire. Ce ne sont donc que les lithiases très petites ou excentriques (canaux hépatiques, bas cholédoque) qui ont nécessité un examen échotomographique. (fig. 7)

II - LA LOCALISATION DES PETITES TUMEURS (6.)

Lorsque l'on a une certitude biologique d'une tumeur endocrine, sa localisation est très difficile en raison de sa taille habituellement réduite (apudome , adénome de Conn, tumeur à rénine, adénome parathyroïdien).
Tous les examens d'imagerie médicale pré opératoire sont assez souvent inopérents, seuls les dosages veineux étagés peuvent préciser la région interessée.

Certains auteurs ont eu des succès sur des syndrôme de Zollinger Ellisson. Pour notre part, nous avons eu seulement l'occasion d'échographier une tumeur à rénine qui était suffisamment grosse (2 cm) pour avoir pu être repérée en pré opératoire.

La recherche des masses hépatiques est maintenant indispensable dans le traitement chirurgical des cancers digestifs.(fig.8) De petites masses échappent à la palpation surtout si la métastase est profonde ou si le foie est induré. De plus, toute masse hépatique chez un cancéreux n'est pas forcément une métastase et la découverte d'une structure franchement liquidienne amènera à faire une ponction per opératoire et une cytologie.

L'échographie des métastases apporte deux renseignements : leur siège exact dans un segment déterminé, leur nombre. La métastase est d'autant plus chirurgicale qu'elle est unique et qu'elle permet une hépatectomie réglée. C'est en repérant les veines sus hépatiques que l'on aide au pronostic d'opérabilité.

III - APPRECIATION DE L'EXTENSION D'UNE MASSE

Dans un cancer profond, et surtout un cancer du pancréas, il est toujours difficile en pré opératoire de connaitre l'opérabilité. Nous avons dans les cancers de la tête et du corps du

pancréas, toujours vu la veine mésentérique supérieure, la veine porte, le cholédoque. On sait que l'envahissement de ces structures complique ou contre indique une chirurgie d'exérèse, par contre leur refoulement est compatible avec une exérèse. Il est plus aisé de le voir en échographie que de le découvrir par la palpation ou la dissection (fig. 9 et 10)

Des renseignements importants ont pu être apportés dans un cancer rénal sur rein unique ; la tumeur étant bien limitée et la veine rénale libre, une tumeurectomie a été possible. (Pr Le Duc).
L'extension de masses bénignes est aussi importante à connaitre, surtout pour les hépatectomies réglées. Nous avons échographié ainsi un angiome (Pr H. Bismuth), un kyste hydatique (fig.11) (Pr Alexandre) dans lesquels nous avons vu les limites de la masse, la place des veines sus hépatiques et où nous avons exploré le reste du foie.

Tous ces renseignements ont été des arguments importants pour l'exérèse.

IV - NATURE D'UNE MASSE

Une masse de nature insuffisamment identifiée est aussi une indication à l'échotomographie per opératoire. Ainsi au cours d'une affection étiquetée kyste du pancréas, nous avons pu montrer l'aspect irrégulier de cette collection qui était à l'anatomopathologie, un cancer nécrosé.
Par contre, dans le difficile diagnostic entre nodule de pancréatite chronique ou petit cancer, l'anatomopathologie est indispensable. (7.)

V - LA CHIRURGIE VASCULAIRE (8. 9.)

La chirurgie vasculaire est de plus en plus développée et nous donne un excellent champ d'application de notre méthode.

Avant le geste réparateur, nous repérons les thrombus, les sténoses, l'étendue en hauteur et en largeur des plaques d'athérome, les zones de bas débit circulatoire à cause de la visibilité très marquée des hématies. (3.) (fig. 12, 13,14)

Après intervention, on peut apprécier la qualité de la réparation, cependant il faut connaitre les images crées par les fils de suture et par les petits décollements de l'intima.

VI - PERSPECTIVES

Bien d'autres applications existent, notamment en neuro chirurgie et en cardiologie. Mais l'expérience nous manque pour parler longuement de nos résultats.

En neurologie, tout l'interêt est le repérage exact de la masse et de ses limites pour éventuellement pratiquer une biopsie et toujours pour décider d'une exérèse limitée.

En cardiologie, les points importants sont l'appréciation de la contractilité au cours de l'intervention, l'étude des vaisseaux coronaires (comme dans la chirurgie vasculaire périphérique), la localisation des tumeurs et surtout la certitude d'un bon dégazage du ventricule après fermeture du coeur en cas de circulation extra corporelle. Des sondes nouvelles doivent être mises au point pour cette application.

B I B L I O G R A P H I E

1. COOK J.H., LYTTON B.
The practical use of ultrasound as an adjunct to renal calculous surgery.
Urol. Clin. N. Amer., 1981, 8, 319.

2. LYTTON B., COOK J.H.
Intra operative ultrasound.
Ultrasound in Urology. The Williams & Wilkins Company. Baltimore. 1979.

3. MACHI J., SIGEL B., BEITLER J.C., COELHO J.C.U. JUSTIN J.R.
Relation of In Vivo Blood Flow to Ultrasound Echogenicity
J. Clin. Ultrasound 11 : 3-10 January 1983

4. MERRAN S., PLAINFOSSE M.C., CARIOU G., HERNIGOU A.
Localisation per opératoire des lithiases rénales par échotomographie temps réel.
Ann. Radiol. 1982, 25, 8, 543-546.

5. PLAINFOSSE M.C.
L'ultrasonographie per opératoire.
Ann. Radiol. 1982, 25, 8, 538-542.

6. SIGEL B.
Operative Ultrasonography.
Philadelphia. Lea & Febiger. 1982

7. SIGEL B., MACHI J., BEITLER J.C., COELHO J.C.U., DONAHUE Ph.E., DUARTE B.
Operative ultrasonography of pancreatic and biliary pathology.
Ann. Radiol. 1982, 25, 8, 547-550

8. SIGEL., MACHI J., BEITLER J.C., PRESTON FLANIGAN D., SCHULER J.J., COELHO C.U.
Imaging ultrasound during vascular surgery.
Ann. Radiol. 1982, 25, 8, 551-554

9. SIGEL B., COELHO J.C.U., FLANIGAN P., SCHULER J.J., SPIGOS D.G., MACHI J.
Comparison of B-Mode Real-Time Ultrasound Scanning with arteriography in Detecting Vascular defects during Surgery.
Radiology 145 : 777-780. December 1982.

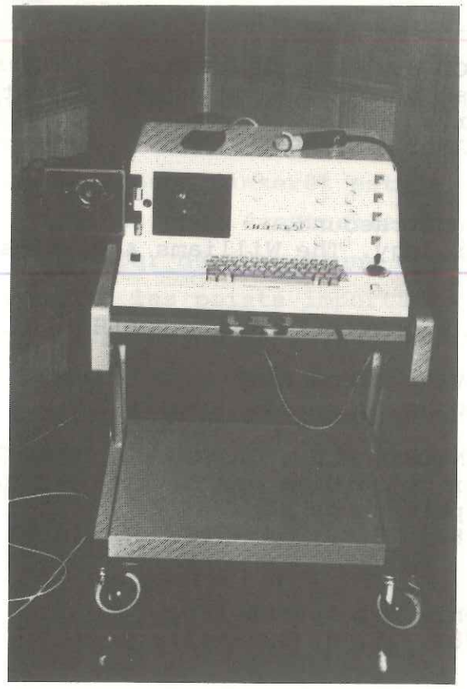

Fig. 1. Appareil mis au point par EDAP pour l'échographie per opératoire. On remarque le faible encombrement de la machine et la petite taille de cette sonde sectorielle recouverte de sa poche d'eau.

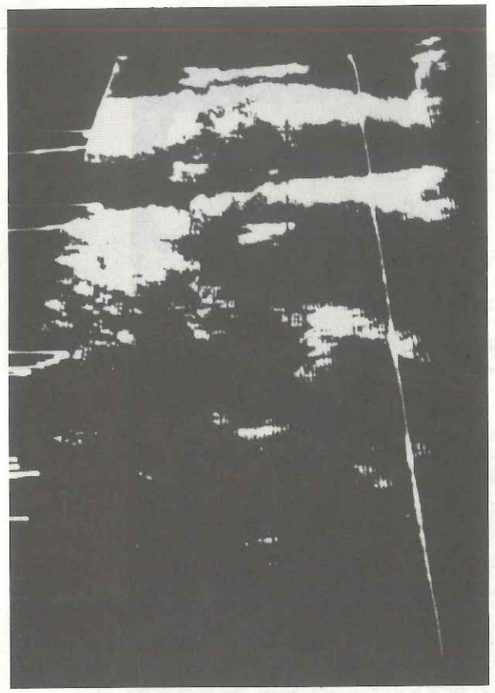

Fig. 2. Image d'un cholédoque normal. La sonde est appliquée sur le pédicule hépatique; compte tenu de l'agrandissement cette structure mesure environ 4 mm de diamètre. En arrière du cholédoque, on remarque une structure tubulaire correspondant à la veine porte.

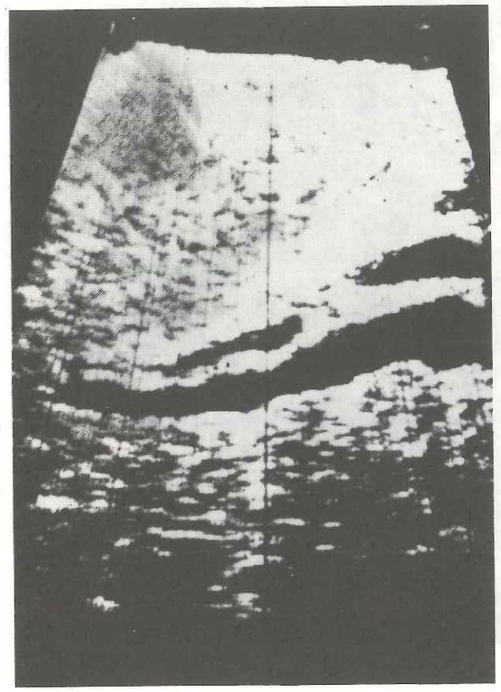

Fig. 3. La sonde est posée transversalement sur la partie antérieure du segment IV. A travers le foie on distingue l'image de la bifurcation de la veine porte en arrière et en avant d'elle les structures tubulaires correspondent à la réunion des canaux hépatiques qui vont former dans une région sous jacente le canal cholédoque.

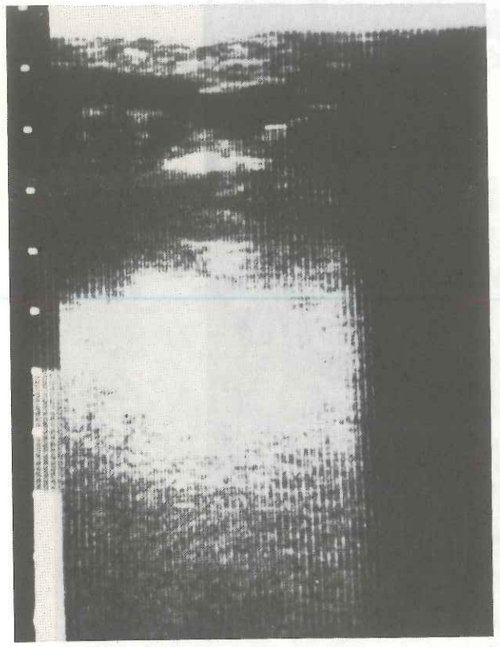

Fig. 4. La sonde est appliquée sur la face antérieure du pancréas. On peut voir à l'intérieur de celui-ci le canal de Wirsung dont le diamètre est d'environ 0,5 cm. Cette image a été obtenue avec une barette ADR.

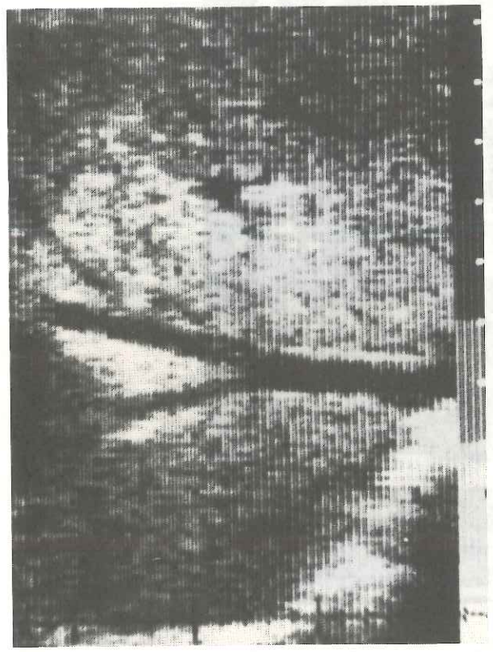

Fig. 5. Avec la même barette, vue à travers le foie de la veine sus hépatique droite normale.

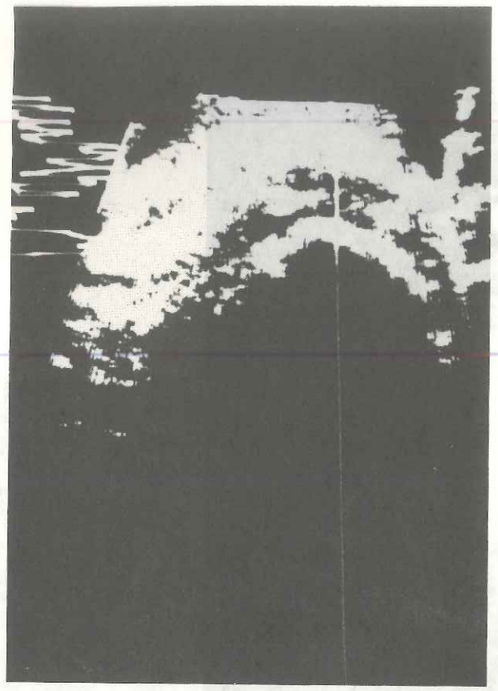

Fig. 6. Image typique d'un calcul : écho dense suivi d'une raie d'ombre acoustique.

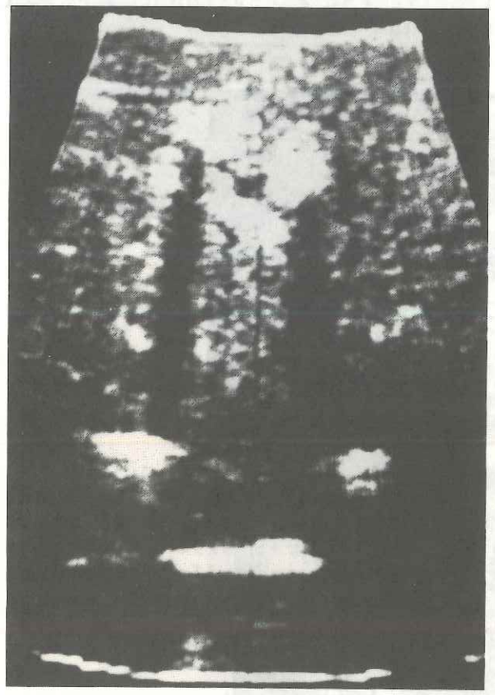

Fig. 7. Présence de plusieurs calculs dans un canal biliaire gauche. Ces lithiases sont petites, environ 3 mm de diamètre.

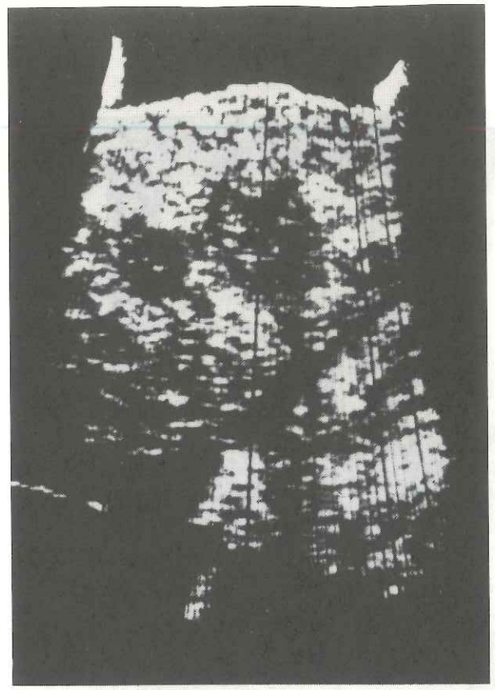

Fig. 8. Présence de deux petites métastases hépatiques non perçues à la palpation.

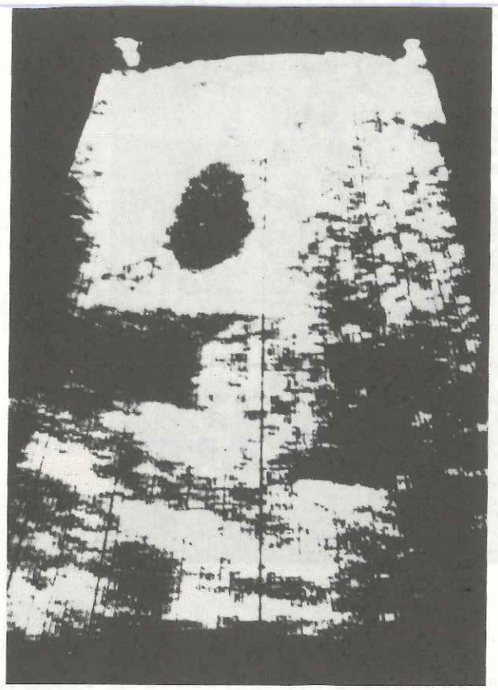

Fig. 9. Coupe du pédicule hépatique selon l'axe de la veine porte. On remarque dans celle-ci une thrombose d'environ 1 cm de diamètre; en avant de la veine porte, l'image lacunaire correspond à une circulation collatérale veineuse coupée transversalement.

Fig. 10. Sur un autre patient, coupe suivant l'axe veine porte-veine mésentérique supérieure. On remarque un rétrécissement de la veine mésentérique supérieure en regard d'une tumeur pancréatique maligne.

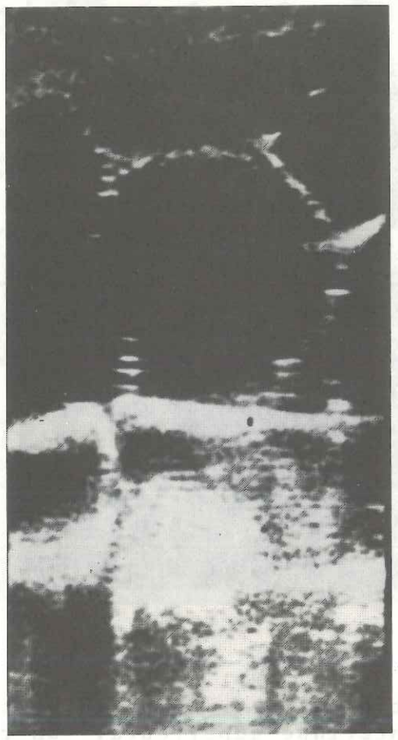

Fig. 11. Image multicloisonnée ayant toutes les caractéristiques d'un kyste hydatique. L'examen échographie en définissant les limites de cette masse par rapport aux veines sus hépatiques et aux voies biliaires a mieux défini son opérabilité.

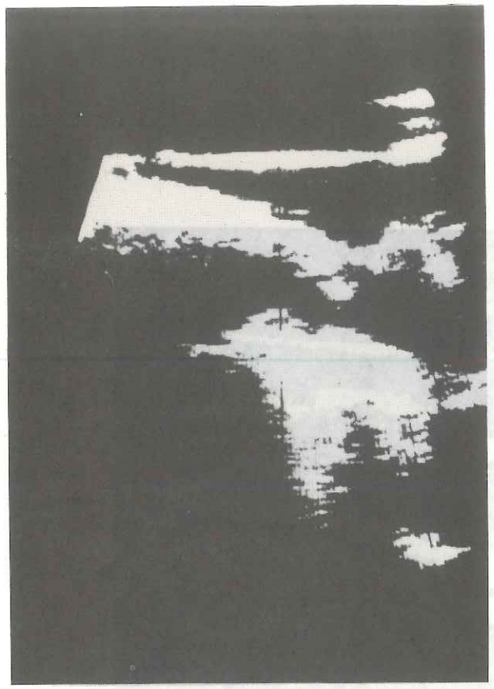

Fig. 12. Coupe suivant le grand axe d'une carotide primitive carotide interne. On voit juste au-dessus de la bifurcation l'existence d'une sténose très serrée.

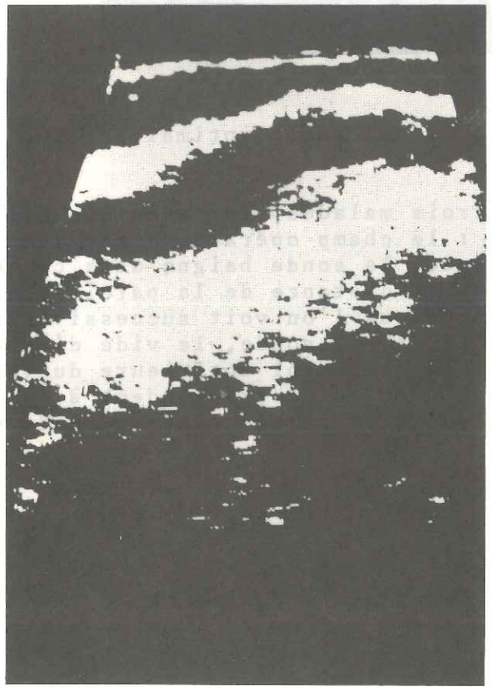

Fig. 13. Sur un autre malade, la coupe suivant l'axe de la carotide interne montre une plaque d'athérome sur la paroi postérieure de ce vaisseau.

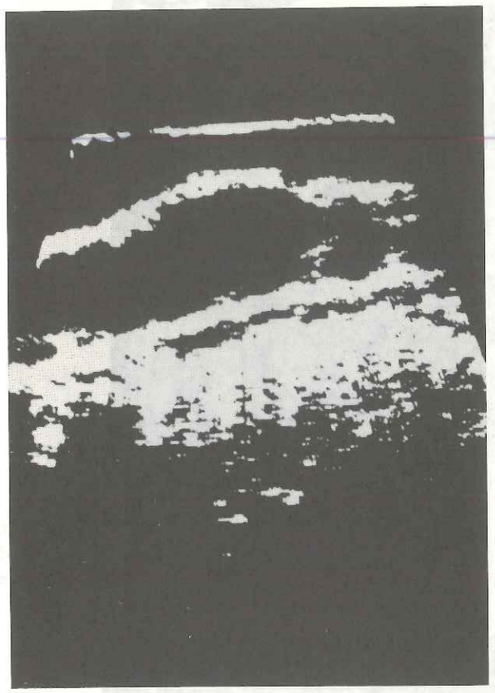

Fig. 14. Présence de décollement intimal sur une carotide interne.

Pour ces trois malades, la technique utilisée est semblable : le champ opératoire est rempli de sérum physiologique, la sonde baigne dans ce sérum et elle est à une relative distance de la paroi antérieure du vaisseau. Ceci explique que l'on voit successivement d'avant en arrière : le pic de sonde, le vide d'écho qui correspond au sérum salé, la paroi antérieure du vaisseau, une autre zone vide d'écho qui correspondent à la lumière de la carotide, enfin la paroi postérieure de celle-ci.

III. RADIOGRAPHIE DIGITALISEE / DIGITIZED RADIOGRAPHY

Design and Physical Performance of Digital Fluorography Systems

B M Moores

Regional Department of Medical Physics, Christie Hospital, Withington
Manchester M20 9BX

Abstract

The design and physical performance of digital fluorographic systems is discussed mainly from the point of view of image quality. Factors affecting resolution, noise, signal-to-noise and contrast are outlined and the interplay between them highlighted. The resolution is directly affected by the number of TV lines employed in both reading and displaying the final image and a great deal of development has been applied to these.

Besides the physical aspects which limit system performance some of the important biological factors are discussed. Also factors which affect radiographic performance, ie framing rates, gated studies, and image processing capabilities are mentioned.

1. Introduction

Medical imaging is one of the most widely used diagnostic modalities in modern medical practise. In the United Kingdom alone over 22 million examinations are undertaken annually (1). The techniques employed consist of conventional radiography, fluoroscopy, CT, ultrasound and radioisotope examinations. Over 75 per cent of these examinations involve conventional radiography, approximately 10-15 per cent fluoroscopy and a relatively small percentage the remaining modalities. CT, ultrasound and isotopic examinations have produced images in digital format for some time but the application of digital techniques to fluoroscopy, or photo-electronic imaging, means that the major imaging market is now being addressed by this technology. In fact the possibility of employing photo-electronic systems as a general radiographic transducer is already being considered (2). This would lead to totally digital departments of medical imaging with a corresponding enormous impact on both medical imaging and health care in general.

Digital fluorographic systems were developed initially for angiographic examinations (3,4). They offered the immediate potential to more clearly visualize vascular structres as well as the possibility of employing intravenous contrast injection in certain examinations. Although these systems have only been employed in the clinical environment for a relatively short period of time there has been an enormous amount of technical development in this field.

An important requirement of physical assessments of medical imaging systems should be to ensure that system design criteria necessary to undertake particular clinical examinations have been well chosen. Consequently some

understanding of the relationships between system design and physical performance is necessary, where the overall performance of any imaging system depends upon the performance of individual components within the system. In the case of digital fluorographic systems it is useful to consider physical performance in two main areas:-

a) Image quality measured in terms of resolution, noise, signal-to-noise and threshold contrast.

b) Radiographic capability provided by framing rates, ability to undertake gated studies and the need for and capability of image processing packages.

In this paper the design factors which affect physical performance of digital fluorographic systems will be discussed. Also, because photo-electronic systems are being considered as possible radiographic transducers special attention is given to those design aspects which have a major bearing on performance in this area.

2. Spatial Resolution

Spatial resolution is an important component in any assessment of image quality. In radiology images are interpreted by trained observers and ideally data should be presented optimally to the visual system. Consequently matching image resolution to that of the eye is desirable. Methods of describing spatial resolution and the way in which component resolutions combine to form the overall system performance may be found in any standard imaging text.

The resolution of any imaging system can be no better than that of the component with the poorest resolution. It is important, therefore, to ensure that efforts at improving resolution are undertaken cost-effectively. Improvements in any single component may produce little overall improvement due to limitations elsewhere. It is useful to consider the resolution associated with four different aspects of digital fluorographic systems. These are:-

a) Display mapping which relates the input image field size to the display matrix size. This is obviously governed by many inter-related factors but does provide a first indication of the smallest resolvable element. The largest possible display matrix for given field size is desirable for optimum displayed resolution and there has been a steady increase from 256 x 256 to 512 x 512 and more recently 1024 x 1024 formats. Increased display matrix size requires fundamental improvements in the system design which can only usally be obtained at increased cost. It is pointless, however, to increase matrix sizes if other more basic factors limit the resolution.

b) Geometric unsharpness governed by the focal spot size and the distances from the focus to patient and patient to imaging device. Digital fluorography employs high repetition, high X-ray output, exposures so that tube loading is important. Hence focal spot size which is an important aspect of tube loading and therefore, geometric unsharpness, needs to be considered.

c) Movement unsharpness due to involuntary movement of the patient or individual organs within. The amount of movement unsharpness

in any single X-ray image or frame will depend upon the speed of the anatomical motion and the length of the exposure time per frame. A wide variation of anatomical speeds are encountered clinically with motions of up to 400 mm/sec.encountered within the heart. Time interval studies can employ several seconds of imaging data and movement unsharpness between single frames may be relevant.

d) The combination of unsharpnesses from individual components in the total system. In digital fluorography these components are the image intensifier, optical coupling, TV camera, data collection, display system and finally the observer's visual process. This aspect of system sharpness contains all the factors which control the display mapping outlined in (a).

In order to highlight the relative importance of these inter-related factors it is worthwhile considering in more detail their physical basis. One of the more important aspectsis associated with the video or TV nature of image production and display. In fluoroscopic systems the image is read off the image intensifier by a TV camera which employs a line scan reading process. Similarly the image is displayed on a TV monitor by means of a line scan process. Intuitively one associates a single line TV with the fundamental element of resolution. There are, however, other factors which determine the element of resolution in line scan systems. The psycho-physical requirement that a certain number of TV lines must occupy the smallest dimension of an object if it is to be (a) detected, (b) recognised and (c) indentified (5). For detection approximately 2 lines are required per minimum object dimension, for recognition approximately 8 lines and for identification 13 lines. Hence, if a radiologist is to predict with a degree of confidence the state, healthy or otherwise of a contrast filled vessel lying in the direction of the scan lines, approximately 4 TV lines per vessel thickness are required. The minimum diagnostically recognizable object, where diagnostically recognizable implies something more than pure detection, depends upon the display mapping. That is the number of TV lines which are employed to image the total input field size. Ideally for maximum resolution one should keep the input field size as small as possible and employ the largest possible number of scan lines and/or matrix size. One cannot continue to increase the number of TV scan lines or display matrix size without encountering important design contraints.

In line scan imaging systems one does not normally get one TV lines worth of resolution for every scan line. The vertical resolution or number of effective TV lines produced is given by:-

$$V_R = K N_s \qquad (1)$$

Where N_s is the number of scan lines and K is the Kell factor (6). A Kell factor of approximately 0.7 is usually employed so that 100 scan lines are required to achieve 70 TV lines worth of resolution. For a 525 line system V_R is approximately 350 and for a 945 system V_R is 618. (Unless the matrix sizes employed correspond to approximately 40% more scan lines then the minimum object sizes will be somewhat larger.)

In any imaging system it is desirable to have both vertical and horizontal resolution the same and digital fluorographic systems are no exception. The number of TV lines determines the vertical resolution. The horizontal resolution H_R corresponding to the number of effective resolution elements

along a single line is given by:-

$$H_R = \frac{\text{BANDWIDTH}}{\text{FRAMES/SEC x LINES/FRAME}} \qquad (2)$$

For a 525 line system with 343 effective TV lines a bandwidth of 3.3 MHz is required whereas for a 945 line system 10.5 MHz is necessary. Attempts to increase both horizontal and vertical resolution require large increases in the bandwidth of the TV system if the number of frames/sec remains constant.

The number of scan lines employed in both the TV camera and display monitor are fundamental components in the resolving capability of digital fluorographic systems. It is important to consider how this aspect of resolution compares to other components. Figure 1 presents the MTF's of the important imaging components. A 1 mm focal spot with 100 cms FFD and 10 cms OFD will resolve 8 lp/mm which is significantly higher than the capability of the other components. Larger spots or poorer geometry would, however, produce a noticeable effect. Modern image intensifiers have resolving capabilities in the region of 4 lp/mm. Since a line pair is equivalent to 2 TV lines, 9" (22.5 cms) intensifiers can accommodate 1800 TV lines and 14" (35 cms) intensifiers nearly 3000 TV lines.

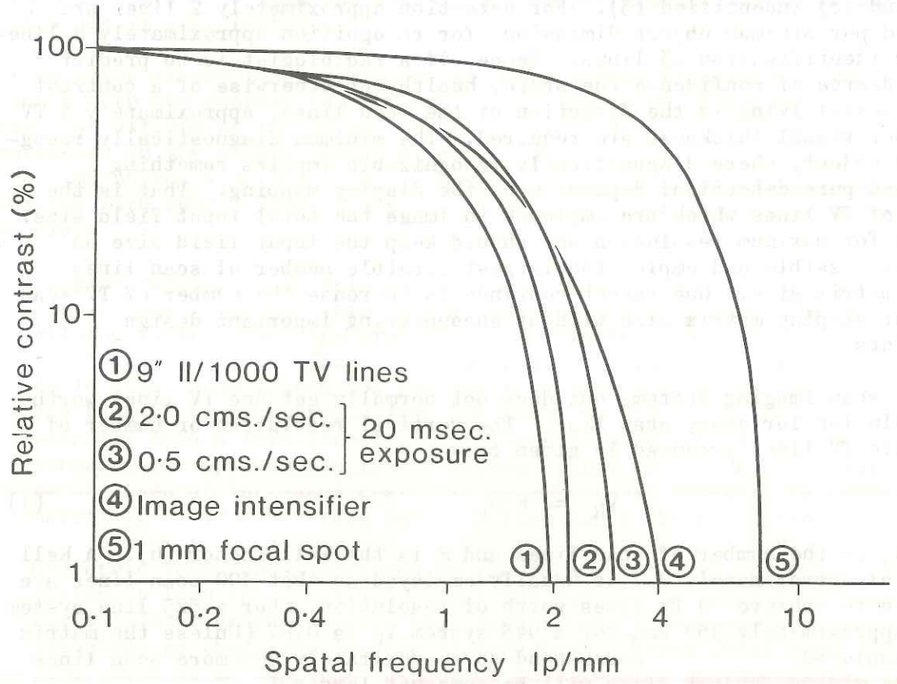

Figure 1 Modulation transfer functions of a 1 mm focal spot under standard geometry conditions, a modern image intensifier, and intensifier/TV system and movement unsharpness

The resolving capability of image intensifier/TV system is mainly dictated by the TV camera. Conventional vidicons with a 1" input face can employ up to 800 - 1000 scan lines. Employed with a 9" intensifier this is equivalent to approximately 2 lp/mm resolution. In order to utilize the full resolving capability of image intensifiers, TV cameras with many more scan lines must be employed. Vidicons with over 2000 scan lines are available (5) but these have larger input faces. Employing TV cameras with larger input faces and higher number of scan lines must affect the light intensity coupled from the intensifier onto each TV camera resolution element. If large format intensifiers are employed in digital radiographic systems then high scan live TV systems will be needed. These may well require multiple stage intensification systems to ensure adequate light intensity for each resolution element (5).

Figure 1 shows the MTF's for movement unsharpness arising from both 0.5 and 2 cms/sec. velocities when a 20msec exposure time with standard radiological geometry. Based upon these curves it is not surprising that many digital fluorographic systems employ repetitive pulsed X-ray exposures of short duration. This ensures that movement unsharpness is kept to a minimum in each individual frame. Motion unsharpness may lead to misregistration errors in subtraction studies employing many frames. Alternatively systems which employ continuous X-ray exposure and use frame integration to reduce noise (see next section) produce subtraction images in which motion blurring has been integrated.

3. Noise

Whereas spatial resolution determines the smallest size of object which can be resolved, noise sets the limit on the smallest contrast difference which can be detected. Every stage in a multi stage process introduces some noise or statistical uncertainty into the data transfer process. In fact the accuracy or quality of data transfer in imaging systems can be measured in terms of the comparative noise level or detective quantum efficiency DQE (7), where:-

$$DQE = \frac{\left(\text{NOISE IN}\right)^2}{\left(\text{NOISE OUT}\right)^2} \qquad (3)$$

The main noise processes in digital fluorographic imaging systems are:-

a) Quantum noise due to the finite number of X-ray photons employed to produce an image.

b) Beam shot or electron beam reading noise due to the finite number of electrons employed in reading the image from the TV camera input face or target.

c) General electronic noise due to thermal effects in circuit components.

One of the main design criterion of any radiological imaging system is to ensure that the quantum X-ray input forms the main noise process. The system is then X-ray quantum limited and ensures that, at least with respect to noise, optimum use is being made of the level of X-ray exposure employed. In fact most of the early development in fluoroscopic systems was concerned with producing an image which was bright enough to employ photopic vision and, therefore, maximum acuity (8), whilst maintaining an X-ray quantum

noise limit. Digital fluorographic systems employ high X-ray exposures in order to reduce quantum noise. The magnitude of system noise components relative to the quantum noise level is then important.

Figure 2 outlines the quantum transfer of information through an image intensifier for both fluoroscopic (100 μR/s) and fluorographic (1 mR/s) input exposure rates. At the intensifier input there is a decrease in X-ray quanta due to fractional absorpiton in the input phosphor. In the case of the fluoroscopic process the integration period of the eye must also be considered since one image is only available for approximately 0.1 secs. A large quantum gain results from conversion of X-rays to light followed by a decrease as the light is converted to electrons. Finally there is a large quantum increase at the output of the intensifier due to the acceleration of electrons within the device. Only a relatively small fraction of the light emitted from the back face of the intensifier can be coupled onto the TV camera and there is also some losses at the input face of the TV camera. These are more than overcome by the large electronic gain provided by the photoconductive process which occurs within the camera

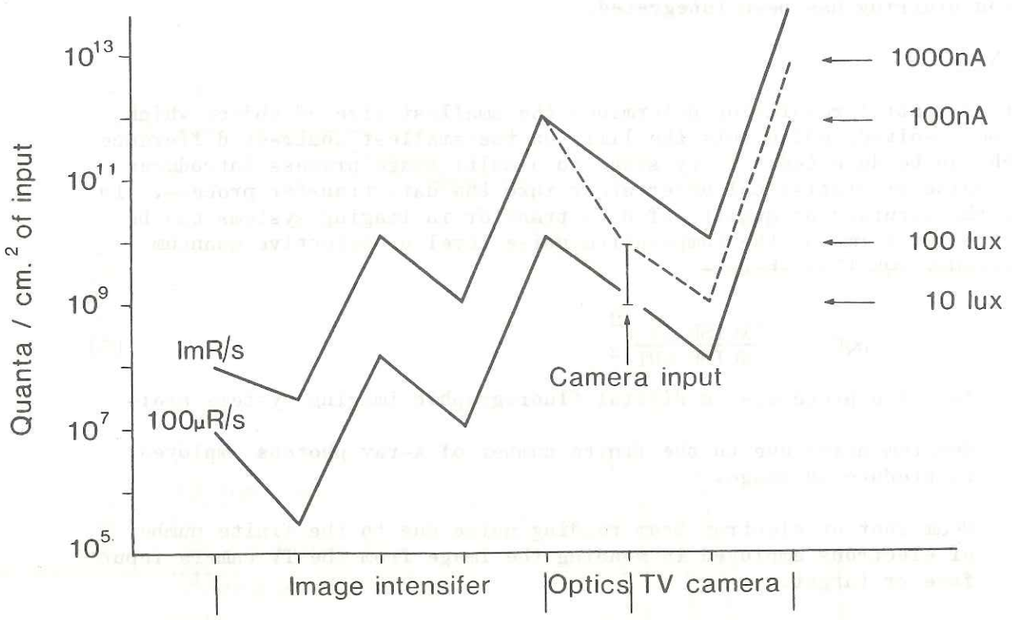

Figure 2 The quantum transfer of information through an image intensifier/TV system for fluoroscopic and fluorographic dose rates.

A key stage in this whole process occurs at the intensifier/TV camera coupling stage. TV cameras can only operate over a given range of light input intensities. The lower limit must be sufficient to overcome any dark

current in the device and the upper limit is set by saturation constraints. The upper and lower values indicated in Figure 2 are those applicable to a plumbicon camera (9) and give rise to the indicated operating range for TV camera currents. The lower limit of TV camera current is also dependent upon temporal modulation effects (10) and the value of 100 nA shown in Figure 2 is merely an indication of its magnitude. As the input X-ray exposure rate is increased the overall illumination of the camera face also increases. To ensure that saturation and possible damage to the camera does not occur the optical coupling from intensifier to camera is decreased by means of an iris diaphragm. To deduce the upper and lower limits of X-ray exposure we need to consider the camera illumination E, where (11):-

$$E = \pi \dot{D} G \frac{V}{4f^2} \qquad (4)$$

$\dot{D}$ = intensifier X-ray exposure rate (mR/s), G = the conversion factor (Cd/m^2 per mR/s), V = optical coupling transmittance and f = lens number. With these units E is given in lux. The light intensity incident upon the TV camera face gives rise to a signal current i_s, where:-

$$i_s \approx 10^{-7} \dot{D} G \frac{V}{f^2} \quad \text{(amps)} \qquad (5)$$

The upper limit of this current is set by the overload conditions and the lower limit by the system noise. Assuming that to prevent overload $i_s < 5 \times 10^{-7}$ amps and to exceed system noise $i_s > 10^{-8}$ amps then:-

$$10^{-1} < \dot{D} G \frac{V}{f^2} < 5 \qquad (6)$$

These numbers are only approximate but serve to indicate the design constraints imposed at this stage of the system. As the input dose rate is increased, since G and f are normally fixed, V must be altered to maintain satisfactory operating conditions. Changes in dose rates in the range 10 - 20 can probably be accommodated in individual intensifier/TV systems. This is, however, an important consideration if one attempts to employ a single photo electronic system to undertake both fluoroscopy with dose rates at the imaging device as low as 10 - 50 μR/sec and radiography with dose rates as high as 1 - 10 mR/sec.

The total system noise per pixel σ_s including both beam shot and general electronic components is given by (5):-

$$\sigma_s = \left[\Delta f(K_1 i_s + K_2 + K_3 \Delta f^2) \right]^{\frac{1}{2}} \qquad (7)$$

Where K_1, K_2 and K_3 are constants, i_s the TV camera signal current and Δf the electronic bandwidth which is inversely related to the time taken to read one picture element or pixel. Obviously in an area containing N pixels the noise will be reduced by a factor of $\sqrt{N}$.

The bandwidth plays a major role in defining system noise and as we will see in the next section by reducing the bandwidth it is possible to increase the signal-to-noise capability of the TV camera.

4. Contrast and Signal-to-noise ratio

The primary X-ray contrast in the transmitted X-ray beam is given by (12):-

$$C_p = \frac{N_1 - N_2}{\frac{1}{2}(N_1 + N_2)} = \frac{N_1 - N_2}{N_a} \qquad (8)$$

The signal to noise ratio (S/N) at the input to the intensifier is given by:-

$$(S/N)_{in} = C_p \sqrt{N_a A} \qquad (9)$$

Where A is the area of a region with contrast C_p relative to the background The smallest detectable or threshold contrast $C_{p\tau}$ is, therefore:-

$$C_{p\tau} = \frac{K}{\sqrt{N_a A}} = \frac{K}{(S/N)_{max}} \qquad (10)$$

Where K is the threshold signal-to-noise ratio normally in the region 3 - 5 (13) and $(S/N)_{max}$ is the maximum achievable signal-to-noise ratio. For quantum limited systems $(S/N)_{max}$ is determined by the number of photons employed, then

$$N_1 \gg N_2 \text{ and } (S/N)_{max} = N_a A/\sqrt{N_a A}$$

In digital fluorography high exposure rates can be employed to reduce quantum noise and hence minimise threshold contrast. Under these circumstances system noise and maximum achievable system signal-to-noise ratio is important. It can be shown that for a linear subtraction (14):-

$$(S/N)_{lin} = \left[\frac{1}{(S/N)_p^2} + \frac{1}{(S/N)_{TV}^2} \right]^{-\frac{1}{2}} \qquad (11)$$

Where $(S/N)_p$ is the photon signal-to-noise ratio and $(S/N)_{TV}$ that of the TV system. To ensure an X-ray quantum limited digital image then $(S/N)_{TV}$ should be as high as possible. As indicated in the previous section the electronic bandwidth plays an important role in defining system noise. By employing much narrower bandwidths it is possible to increase the signal-to-noise ratio of the TV camera compared to normal frame rates (5). This approach to noise reduction is termed slow scan and may be used to read short high intensity X-ray exposures with minimum quantum noise per frame. High camera signal-to-noise ratios require adequate discrimination in the A/D converter. Most units employ 10 bit A/D conversion.

Another approach to noise reduction involves frame integration. Several video frames are integrated which reduces both quantum and system noise in the final image. This places less stringent requirements on the TV camera signal-to-noise ratio. It does mean, however, that the final image is an average with respect to movement unsharpness.

The signal-to- noise ratio given in equation (11) may be written in terms of the number of X-ray photons (14), where:-

$$(S/N)_{lin} = \left[\frac{1}{N_a A} + \frac{T}{(N_a A)^2} \right]^{-\frac{1}{2}} \qquad (12)$$

T is a constant involving intensifier and TV camera factors. For a quantum limited exposure regime $(S/N)_{lin} \propto \sqrt{N_a A}$ whereas for a system noise limit $(S/N)_{lin} \propto N_a A$.

Measurements undertaken on one particular unit (14) indicate that the transition from quantum to video noise dominant regimes occurs at an exposure per frame of approximately 340 μR.

4. Contrast-Detail

An extremely useful measure of imaging system performance is provided by the contrast detail diagram where threshold contrast is plotted against the diameter of a circular target area (15). Contrast detail measurements have been undertaken on a digital fluorographic system for different exposure and field sizes (16). These results showed clearly that for small detail or resolution limited imaging the design characteristics of the digital system ie input field size and numbers of scan lines, played a major role in defining contrast detail behaviour. For larger detail (> 2mm diameter) where quantum efficiency is important, the digital system performed significantly better than a film subtraction technique requiring higher exposures. One reason for the potential improvement in contrast detail behaviour of digital fluorographic units over film/screen systems even at lower exposure lies in the ability to display the image optimally. Subtracted images possess a limited range of data since relevant information is superimposed on a uniform background. The relevant detail can be displayed at maximum gain or gamma. The effect of display gain or gamma on TV images has been investigated (17) and is known to have a marked effect on threshold contrast, particularly for gammas less than unity.

Threshold contrast behaviour in clinical digital fluorographic practise will be affected by certain biological factors. Not the least of these concerns the actual concentration of contrast agent which can be made to flow in vessels of particular diameters. High concentration boluses with 150 - 300 mg/cc of iodine will normally only exist in close proximity to the site of injection. The contrast of a 1 mm vessel with an iodine concentration of 150 mg/cc will then exceed 10 per cent, well above threshold.

Intra venous injection will lead to substantial dilution and concentrations in the region of 15 - 30 mg/cc can then be expected in the arterial vasculature. A 1 mm vessel with 15 mg/cc concentration will have a contrast in the region of 2.5 per cent for diagnostic beam energies. This level of contrast is close to threshold for digital fluorographic exposure rates. Besides the biological aspect associated with contrast injection scatter, patient movement etc will also affect threshold contrast capability.

5. Radiographic Performance and Image Processing

Image quality is important but so too are the radiographic and image processing facilities provided by digital fluorographic units. As indicated previously framing rates are in part governed by noise requirements in each frame. Normal video frame rates are in the region of 30 full images per second and A/D conversion with 10 bit wordlength and 10 MHz frequency are employed routinely to digitize them. Tube loading will not allow extremely high exposures at this frequency. Consequently frame integration or pulsed exposures with slow scan TV operation can be employed to reduce noise. Whichever approach is employed a key element in the process is the real time memory. The size of this memory dictates both the

image matrix size and frame frequency which can be handled in real time. For instance time interval difference studies involving subtraction of sequential frame can be undertaken in real time at a rate dictated by the size of the memory. One major area of development has been the increase in this memory size with 3 megabytes now standard and larger sizes being introduced.

Gated studies require a generator which can be triggered from an external control. The central processing unit can provide the necessary pulse sequence or alternatively this may be produced from physiological monitoring equipment.

A wide variety of image processing or software packages are now available. Straight forward subtraction with the facility to "remask" in order to overcome flow studies are now available as well as heart volume analyses. In fact digital fluorograph now combines cardio-angiography and video densitometry into a single facility.

Movement blurring is an extremely important phenomenon which it is impossible to eliminate from every examination. Software packages enable parts of an individual frame to be re-registered by shifting horizontally or vertically or even rotating an appropriate number of pixels. Frequency filtering an image in order to eliminate undesirable structures eg the heart in coronary angiography, are also under development.

All of these facilities enhance the ability to interrogate the original data. However, it must not be forgotten that a trained observer is an extremely powerful data handling entity. Nonetheless with the current trends in both hard and software developments in information technology, more sophisticated automatic image analysis packages are likely in the not too distant future. It is important that the radiological community is able to adequately assess their performance in order to ensure cost-effective implementation.

References

1. Kendall G M, Darby S C, Harris S V, and Rae S. 1980 A frequency survey of radiological examinations carried out in National Health Service Hospitals in Great Britain in 1977 for Diagnostic Purposes. NRPB Report 104. Harwell, Didcot, Oxon

2. Capp M P, Nudelman S, Fisher D, Ovitt T W, Pond G D, Frost M M, Roehrig H, Seeger J, and Oimette D. 1981 Photoelectronic radiology department. Proc SPIE, Digital Radiography, 314, 2-8

3. Mistretta C A, Crummy A B and Strother C M. 1981 Digital angiography: a perspective. Radiology, 139, 273-276

4. Hillman B J, Ovitt T W, Nudelman S, Fisher H D, Frost M M, Capp M P, Roehrig H, and Seeley G 1981 Digital video subtraction angiography of renal vascular abnormalities. Radiology 139, 277-280

5. Roehrig H, Nudelman S, Capp M P, and Frost M M 1977 X-ray image intensifier video system for diagnostic radiology: part I, design characteristics. Proc SPIE 127 216-225

6. Kell R D, Bedford A V and Trainer M A. 1934 An experimental TV system Proc IRE 22 1247-1252

7. Dainty J C and Shaw R 1974 Princples, Analysis and Evaluation of Photographic-Type Imaging Processes. Academic Press, London

8. Ter-Pogossian M M 1967 The Physical Aspects of Diagnostic Radiology. Harper and Row, New York.

9. Haan E F, Drift A. van der and Schampers P P M. 1964 The plumbicon, a new television camera tube, Philips Technical Review. 25, 133-180

10. Franken A A J, and Scheren W J L 1972 The influence of the camera tube on the temporal modulation transfer function in diagnostic X-ray television. Medicamundi, 17, 121-123

11. Kuhl W 1969 X-ray image intensifiers today and tomorrow. Medicamundi 14, 57-61

12. Moores B M 1983. Screen/Film Combination for Radiography Research Techniques in Non destructive Testing. Volume 6 Academic Press, London 289-308.

13. Rose A, 1948 The sensitivity performance of the human eye on a absolute scale. Journal of Optical Society of America. 38, 196-208

14. Cohen G, Wagner L K, and Rauschkolb E N, 1982, Evaluation of a digital subtraction angiography unit. Radiology 144, 613-617

15. Hay G, Chester M S 1976 Threshold Mechanisms in the presence of visible noise. 7th L H Gray Conference 'Medical Images' John Wiley and Sons, Chichester.

16. Macintyre W J, Pavlicek W, Gallagher J H, Meaney T F, Buonocore E, and Weinstein M A 1981 Imaging capability of an experimental digital subtraction angiography unit. Radiology, 139, 307-313

17. Oosterkamp W J, 1974 New concepts and progress in instrumentation for cine and video radiology. Medicamundi, 19 79-84

Silicon µstrip-Detectors for Linear X-Ray Sensing

R. NOWOTNY and J. KEMMER

Institut für Radiumforschung und Kernphysik, A-1090 Wien,
Boltzmanngasse 3, Austria,
L. Boltzmann-Institut für radiol.-physik. Tumordiagnostik,
A-1090 Wien, Austria
and
Fachbereich Physik der Techn. Universität München,
Garching, Germany.

1. Introduction

In various radiographic methods, as digital radiography and CT, linear arrays of radiation detectors are employed. Beside multiwire chambers such arrays consist of discrete radiation detectors, e.g. scintillators combined with photodiodes or photomultipliers. These structures limit the spatial resolution by their size but it becomes difficult to achieve pixel dimensions of much below 1 mm. Obviously, if solid state detectors, in particular silicon diodes, could be used as the detecting device techniques for the production of integrated circuits would make achievable a higher resolution as many diodes can be made on one silicon chip. Such detector arrays (µstrip-detector) have been already in use for some time for the detection of charged particles in the pulse counting mode /1,2/. We have investigated the feasibility for an application of µstrip-detectors in the detection of X-rays in the diagnostic energy range measuring diode ionisation current.

In general, the properties of solid state detectors with respect to an application in radiographic apparatus, as linearity, time response, uniformity and ruggedness, are expected to be good. It remains if silicon as a detector material yields a response over the diagnostic energy range which makes it suitable as a radiation sensor. The use of large surface barrier diodes for CT has already been reported /3,4/.

2. µstrip-detector characteristics

2.1. Material

The µstrip-detectors are fabricated by the planar process on n-Si wafers /1/ giving pn-junction diodes which exhibit low leakage currents at room temperature. Chip size of the detector under investigation was 10x10 mm² with a thickness of 300 µm. A common back electrode is applied by metallization with aluminium. The front side is structured with p^+ implanted diode strips and aluminized electrodes. This chip carried 27 strip diodes, 180µm x 6.7mm in size, at a pitch of 215µm. At the end of the electrodes contact pads are available for bonding (fig. 1). Many other electrode patterns and chip geometries are feasible.

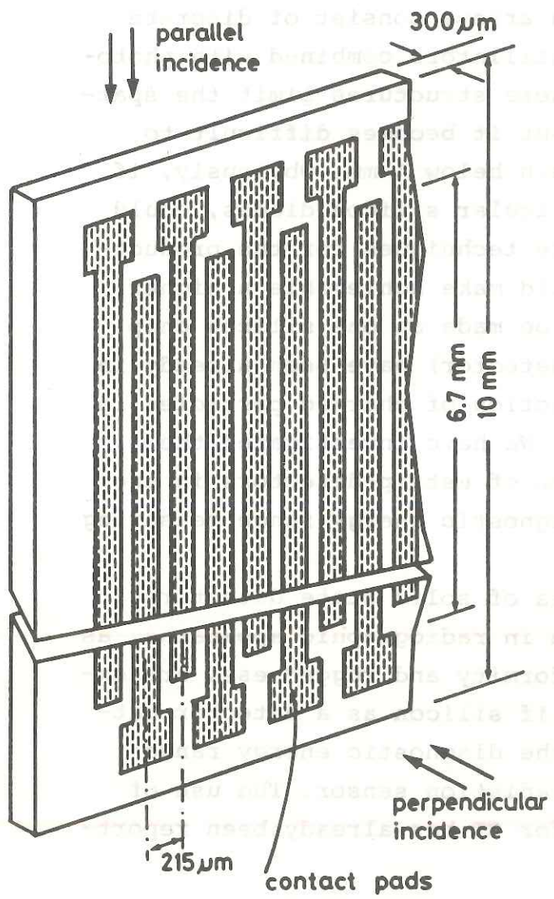

Fig. 1: Schematic outline of the µstrip-detector. Parallel incidence of radiation exposes a pixel area of 215x300µm², perpendicular incidence approx. 215µm x 6.7mm, resp.

The common electrode of the µstrip-detector was fixed with silver epoxy on a pc-board and contacts were made by ultrasonic bonding of 25 µm Al wire. The mounting of the chip with epoxy adhesive results in material flowing out at the edges of the chip. Due to the high absorbtion of radiation by the silver it was thus not possible to use the µstrip-detector with X-rays impinging in parallel with the electrodes where the cross section of the diodes determines pixel size (300 x 215 µm²). Other mounting methods should be used for this purpose.

The ionization current from each diode was measured with identical I/V-converter circuits as shown in fig. 2. The output signals were multiplexed and sequentially analysed. Time response is practically determined by the time constant of the I/V-converter feedback network /3/.

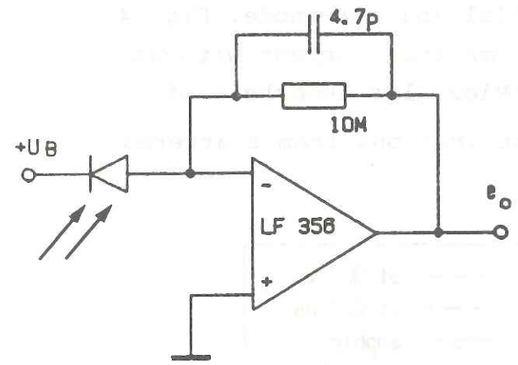

Fig. 2: Circuit of a single detector ionization current-to-voltage converter unit.

2.2. Theoretical analysis

The current signal I_s for one pixel in an X-ray field can be estimated according to

$$I_s = \frac{q}{\varepsilon_{Si}} \cdot F \cdot \int_0^{kVp} S(E) \cdot \varepsilon_a(E) \cdot dE$$

where q denotes electronic charge, ε_{Si} energy required in Si for the generation of charge carrier pairs, F pixel entrance area, kVp tube voltage, S spectral intensity and ε_a absorbed

energy for a Si detector of thickness L.

Absorbed energy ε_a is given by

$$\varepsilon_a = \left(1 - \exp\left(-\left(\frac{\mu}{\rho}\right).L.\rho_{Si}\right)\right).\frac{\eta}{\mu} \cdot E$$

where μ/ρ is the mass attenuation coefficient, η/ρ mass energy transfer coefficient and L the thickness of the Silicon detector.
This conforms to locally absorbed energy in intensifying screens /5/ with no escape of K-X rays. The spectral response for Si-detector thickness of 0.3 mm and 6.7 mm is shown in fig. 3. This data are relevant for perpendicular and parallel direction of X-rays. Also shown is locally absorbed energy in commercial screens (Lanex regular and Saphir, /5/).

Diode signal current was then calculated using the experimental data for the spectral distribution of X-ray photons for constant tube potential and a W-anode. Fig. 4 shows the diode response per 100 mA tube current without absorber and after aborption by Plexiglas absorbers of various thickness (excluding contributions from scattered radiation).

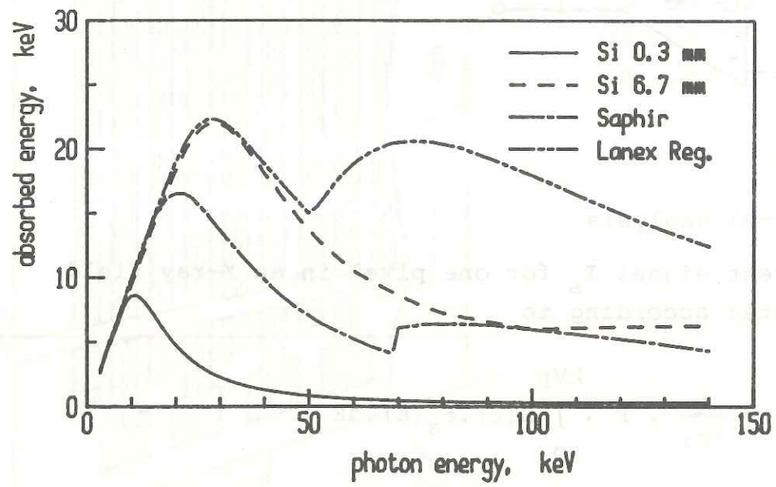

Fig. 3: Absorbed energy vs. primary photon energy for Si-detectors, and Saphir (43.8 mg/cm² $CaWO_2$) and Lanex Regular (130.8 mg/cm² Gd_2/La_2O_2S) screens.

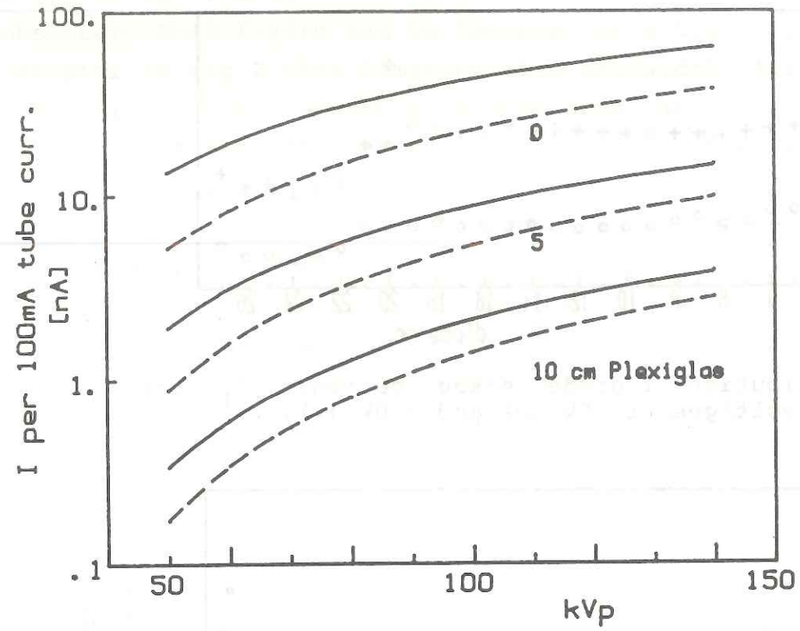

Fig. 4: Diode signal curren, I, referred to 100 mA tube current vs. tube voltage (calculated for W-anode 2.5mm Al, const.Pot. with data from /5/).

2.3. Detector characteristics

Biasing the diodes improves speed, detector homogeneity and reduces temperature effects on efficiency but gives rise to leakage current. Fig. 5 shows the distribution of leakage currents for bias voltages of 10 and 100 V, resp. The diodes at the edges (nr. 1 and 27) exhibit larger leakage currents than the neighbouring diodes due to an increased volume contribution. On that µstrip-detector diodes nr. 22 through 27 were aditionally provided with guard electrodes resulting in reduced leakage. High leakage of diode 20 indicates a surface defect.

The variation of diode geometry and of the effective carrier collection width along the chip leads to a variing diode response. Fig. 6 gives the distribution of diode signal currents referred to 100 mA tube current. The diodes at the edge of the array collect ioni ation current from a larger volume which is reflected in an increased signal.

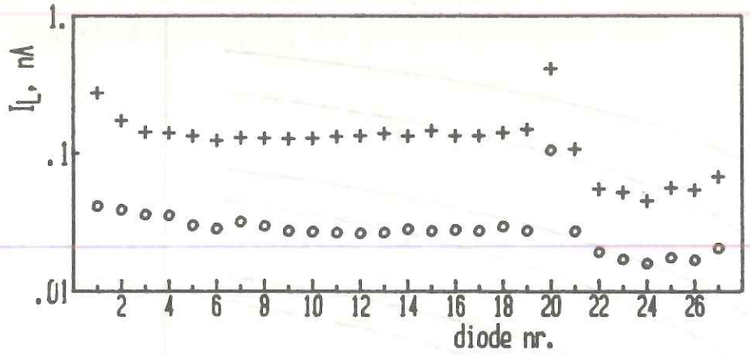

Fig. 5: Distribution of diode leakage currents, I_L, for bias voltages of 10V (o) and 100V (+).

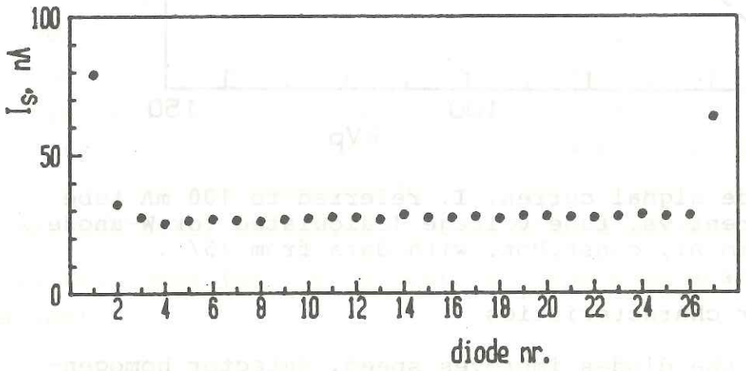

Fig. 6: Distribution of diode signal current, I_S, normalized for 100mA tube current measured at a tube voltage of 80 kV (6pulse, 2.5mm Al, W-anode) and at a distance of 75 cm with perpendicular incidence of radiation. Diodes were non-biased.

The remaining diodes (nr. 3 through 26) show excellent homogeneity of response ($\pm$ 2.7% s.d. from the mean value). Linearity of the ionization current ranges to dose rates of greater 25 R/sec. Higher dose rates could not be achieved with our generator.

3. Applications and conclusions

Signal-to-noise ratio and detectability of differences in absorbtion depends on detector properties and experimental conditions. For the circuit shown in fig 2. the noise referred to input signal current is about 15 pA. This yields

a S/N-ratio of about 400 for 80kV/100mA and 5cm Plexiglas-absorber. This figure can be improved by a higher feedback resistor in fig.2 thus limiting also bandwidth. Also higher tube currents seem possible in most applications than 100mA. Fig. 7 shows the difference in signal for 4 cm Plexiglas absorber containing in one half a sheet of 2mm water. The edge of the water sheet was aligned with the diode strips. The radiation beam was collimated with two slits 6mm wide in front of the absorber and close to the µstrip-detector assembly to reduce **the** intensity of scattered radiation. The detector was positioned perpendicular to the radiation beam. The edge is clearly resolved in the measurement.

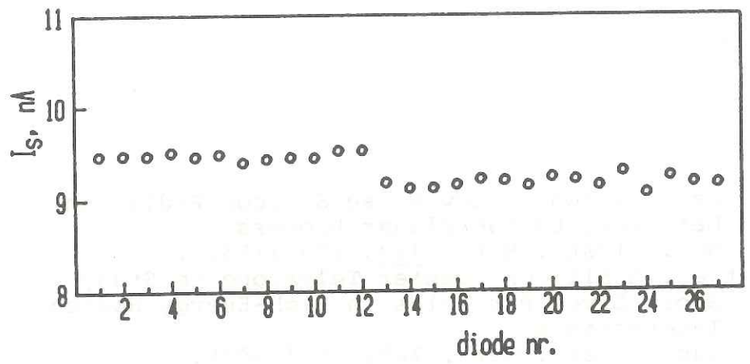

Fig. 7: Signal contrast in response to 4cm Plexiglas (diode nr. 1 to 12) and 3.8cm Plexiglas plus 2mm water (diodes 13 to 27) at 80kV/100mA and zero bias voltage. The data are normalized to diode response.

The situation with regard to other recording media will be analysed in more detail elsewhere /6/. So far, it can be said that µstrip-detectors show suitable characteristics particular at lower energies for an application as an X-ray detecting device. The low Z of silicon brings about lower current output than could be obtained with other semiconductor materials but silicon diodes can be operated at room temperature and need not be cooled. Absorbed energy in the µstrip-detector we were using is similar to that of common intensifying screens but the efficiency is much higher as no losses in signal transfer

occur.

The shapes of the electrodes can be made according to the requirements, e.g. fan beam geometry, simply by design of appropriate photomasks. For an incidence of radiation parallel to the chip (geometry for digital radiography) the pixel size is limited by chip thickness, i.e. effective carrier collection width, in one and by strip diode pitch in the other direction. Strip diode pitch can be made as narrow as 20µm /2/ but the collection width is about 250-300µm which therefore determines minimum pixel size. For CT applications (perpendicular incidence) strip diode pitch only is of imortance. Applications in the lower energy range as digital mammography or CT seem to be interesting.

References:

/1/ J. KEMMER. Fabrication of Low-Noise Silicon Radiation Detectors by the Planar Process. Nucl. Instr. Meth. 169, 499 (1980).

/2/ B. HYAMS et al. A Silicon Counter Telescope to Study Short-Lived Particles in High-Energy Hadronic Interactions. Nucl. Instr. Meth. 205, 99 (1983).

/3/ Y. NARUSE et al. Multichannel Semiconductor Detectors for X-Ray Transmission Computed Tomography. IEEE Trans. Nucl. Sci. NS-27,1,252 (1980).

/4/ Y. NARUSE et al. 200 Channel Semiconductor Detectors for X-Ray Computed Tomography. IEEE Trans. Nucl. Sci. NS-28, 1, 47 (1981).

/5/ R. BIRCH, M. MARSHALL and G.M. ARDRAN. Catalogue of Spectral Data for Diagnostic X-Rays. HPA Scient. Rep. Ser. 30, Hospital Physic. Assoc., London, 1979.

/6/ R. NOWOTNY and J. KEMMER. To be published.

DIGITAL SUBSTRACTION IN ANGIOGRAPHY

G. HAENDLE (Erlangen, FRG)

Text not received.

ETAT ACTUEL DE LA DIGITALISATION

R. KLAUSZ (Paris, France)

Texte non parvenu.

THE IMPACT OF DIGITAL ELECTRONICS ON THE RADIOGRAPHIC DEPARTMENTS

D. BLAKESLEY (Wembley, U.K.)

Text not received.

D.I.V.S.A. APPLICATIONS TO THE INTRACRANIAL VASCULAR SYSTEM

G. WILMS , J. SMITS , F. DE SOMER

With D.I.V.S.A. evaluation is possible of the large intracranial arterial branches and of the intracranial veins.
Concerning atherosclerotic disease, it is possible to visualize occlusion of the large vessels. In case of internal carotid artery occlusion the permeability of the cerebri media area can be stated before a bypass procedure. The patency of such a bypass can be controlled by D.I.V.S.A.

In case of vascular anomalies, such as aneurysm or A.V. malformations, D.I.V.S.A. can be used to evaluate therapeutic result, as a follow-up study of non treated lesions or as a first step in the diagnosis of hypercaptating lesions on CT.

By the perfect visualization of the dural venous sinuses, D.I.V.S.A. is the method of choice for the evaluation of intrinsic or extrinsic lesions of the dural venous sinuses.

As for tumor diagnosis, D.I.V.S.A. can be sufficient in the preoperative work-up of hypophyseal adenoma and in the evaluation of subdural hematoma. It can be used to confirm a CT diagnosis or to control lesions after embolization.

D.S.A. after intraarterial injection is useful in patients with renal failure and in children or if multiple injections are necessary. Moreover it is an elegant imaging method during embolization or dilatation.

Department of Radiology
Head : Prof.Dr.A.L.Baert
University Hospitals
K.U.LEUVEN

ANGIOPNEUMOGRAPHIE : TECHNIQUE OPTIMALE D'EXAMEN EN ANGIOGRAPHIE NUMERISEE.

G. TROTTEUR - P. MAGOTTEAUX - C. SAIVE - G.F. LEROUX

A condition d'être fiable, l'angiographie intraveineuse numérisée - digital subtraction angiography (DSA) - devrait remplacer l'angiopneumographie sélective (AP), technique invasive.

MATERIEL

Nombre total de patients : 99

60 patients suspects d'embolies pulmonaires subissent les deux examens avant toute thérapeutique. 15 patients sont contrôlés par DSA 48 heures après fibrinolyse, 12 patients 8 jours après héparinisation. 12 patients subissent une angiocardiographie par DSA pour raisons diverses : troubles respiratoires, condensation parenchymateuse inexpliquée, masse médiastinale.

METHODES

L'AP conventionnelle comprend le cathétérisme sélectif (cathéter NIH, 8F) de l'artère pulmonaire commune via la veine fémorale ou brachiale, injection de 50 cc de sodium méglumine ioxitalamate (76%) en 2 sec; sériographie en incidence de face (3 clichés par sec. pendant 2 sec., suivis de 2 clichés par sec. pendant 3 sec. et de 1 cliché par sec. pendant 3 sec.).
La DSA est réalisée à l'aide d'un appareil Technicare DR 960, matrice 512 X 512 ou 256 X 256, 8 bits, séquence respective de 1,25 ou de 6 images/ sec., 256 niveaux de gris, amplificateur de brillance 6 ou 9 pouces, tube Rx foyer 0,6 mm.

Conduite de l'examen

- Injection en 4 sec. de 40 cc de sodium méglumine ioxitalamate 76% suivis de 20 cc de glucosé à 5%.

Deux voies d'abord sont couramment utilisées : veineuse périphérique (abbocath 16 G), veineuse centrale (cathéter à trous

multiples en situation proximale juxtaauriculaire); quelques examens sont réalisés par injection sélective dans l'artère pulmonaire commune (injection en 2 sec. de 30 cc de sodium méglumine ioxitalamate (76%) dilués au I/3).

- Les 3 sites d'injection sont évalués et comparés.

- Deux modes d'acquisition sont évalués : 1,25 images/sec. avec matrice 512 X 512 X 8 bits et 6 images/ sec. avec matrice 256 X 256 X 8 bits.

Le patient est invité à maintenir une apnée d'environ IO sec. en phase expiratoire. Le temps de pose est court (maximum 13 m sec.) L'homogénisation densitométrique du champ exposé (poumon-médiastin) est obtenue par l'apposition d'un filtre en laiton (0,4 mm d'épaisseur) sur la partie pulmonaire.
Les incidences sont : oblique antérieure gauche et oblique antérieure droite de IO° respectivement pour le poumon droit et gauche.

Evaluation de l'examen :

I. 3 lecteurs estiment séparément la résolution comparée de la DSA et de l'AP dans 6 secteurs prédéterminés :

1. artères pulmonaires principales
2. lobaires
3. segmentaires
4. périphériques
5. parenchymographie
6. retour veineux.

La résolution de la DSA est qualifiée : supérieure, équivalente, inférieure.
En référence aux résultats obtenus par l'AP, la valeur de l'examen par DSA pour le diagnostic d'embolie pulmonaire est jugée excellente, bonne, suffisante ou insuffisante.

II. Les contrôles d'évolution après traitement sont corrélés aux données cliniques, hémodynamiques et scintigraphiques.

III. La valeur diagnostique de la DSA pour les 12 angiocardiographiques pratiquées est référée au diagnostic final obtenu dans tous les cas.

RESULTATS

I. A. DSA versus AP (60 cas)

RESOLUTION DSA	SUPERIEURE	EQUIVALENTE	INFERIEURE
A. PRINCIPALES	-	55 (92%)	5 (8%)
A. LOBAIRES	7 (12%)	42 (70%)	11 (18%)
A. SEGMENTAIRES	14 (23%)	33 (55%)	13 (22%)
A. PERIPHERIQUES	7 (12%)	39 (65%)	14 (23%)
PARENCHYMOGRAPHIE	8 (13%)	44 (73%)	8 (13%)
RETOUR VEINEUX	9 (15%)	40 (67%)	11 (18%)

Parmi les examens de résolution inférieure on répertorie 3 cas d'insuffisance cardiaque droite sévère (pression télédiastolique ventriculaire droite supérieure à 40 mm de Hg) ; tous les patients de ce groupe présentent une dyspnée sévère.

DIAGNOSTIC D'EMBOLIES PULMONAIRES		
Nb = 60	AP	DSA
NEGATIF	10	8 **
POSITIF FORMEL	34	36 ***
POSITIF PROBABLE	16	13
	60	57 *

*	3 examens soit 5% s'avèrent techniquement insuffisants que pour poser un diagnostic.
**	2 faux positifs par DSA, diagnostic erroné d'embolie probable
***	dans 5 cas soit 8%, la DSA permet de poser un diagnostic formel d'embolie alors que l'AP permet un diagnostic positif probable.

Le diagnostic positif formel est posé sur la reconnaissance de l'embol ou de l'obstruction vasculaire abrupte proximale, le diagnostic positif probable sur la reconnaissance d'obstructions vasculaires périphériques associées à des zones parenchymateuses hypoperfusées.

VALEUR DIAGNOSTIQUE DE LA DSA	Nb : 60	
EXCELLENTE	5	(8%)
BONNE	37	(62%)
SUFFISANTE	13	(22%)
INSUFFISANTE	5	(8%)

B. La résolution spatiale obtenue avec matrice 512 X 512 est supérieure à celle obtenue par l'AP, la limite étant la mise en évidence de l'occlusion d'un vaisseau de 2mm de diamètre.
L'utilisation de la matrice 512 X 512 implique une séquence d'acquisition de 1,25 images/ sec.
Parmi les 60 patients suspects d'embolie, la dyspnée a nécessité 45 fois (75%) une séquence rapide de 6 images/ sec. avec matrice 256 X 256

C. La résolution de contraste est équivalente quel que soit le site d'injection : veineux périphérique ou veineux central (comparaison intéressant 21 cas)
Paradoxalement les injections pratiquées dans l'artère pulmonaire

sont grevées d'artéfacts par dilution rapide du bolus.

II. Utilité de la DSA dans le contrôle du traitement médical : en référence à l'évolution clinique, hémodynamique et scintigraphique les examens de contrôle par DSA (N : 23) se sont avérés fiables.

III. La DSA a permis de poser le diagnostic de séquestration pulmonaire (1 cas), de retour veineux pulmonaire aberrant (4 cas, d'artère pulmonaire gauche aberrante (1 cas).
La vascularisation pulmonaire était normale dans 6 cas.

DISCUSSION

L'étude de la vascularisation pulmonaire (phases artérielle-capillaire - veineuse) par DSA est fiable. La résolution spatiale obtenue avec matrice 512 X 512 est supérieure à l'AP, la limite de résolution étant la mise en évidence des vaisseaux de troisième division segmentaire (1 à 2 mm).
Les malformations vasculaires pulmonaires sont parfaitement mises en évidence (6 cas), en particulier les anomalies de retour veineux.
La résolution de contraste est équivalente quel que soit le site d'injection : veineux périphérique ou central.Elle est globalement diminuée en cas d'insuffisance cardiaque droite sévère (pression télédiastolique ventriculaire droite supérieure à 40 mm Hg.
L'injection dans l'artère pulmonaire est grevée d'artéfacts par dilution du bolus et nécessite toujours une séquence d'acquisition très rapide.
Des problèmes techniques se posent chez les patients suspects d'embolie pulmonaire, présentant une insuffisance cardiorespiratoire sévère. L'état de dyspnée et de tachycardie a nécessité un rythme d'acquisition de 6 images/ sec. dans 75% des cas, avec utilisation obligée de la matrice 256 X 256 au prix d'une perte de résolution spatiale.

La valeur diagnostique dela DSA, dans la recherche des embolies pulmonaires est excellente, bonne ou suffisante dans 92% des cas. L'examen est insuffisant dans 8%.
Parmi les examens insuffisants, il y a eu 2 faux positifs d'embolie, déterminés à postériori par effet " mash" au niveau des artères segmentaires.
Ces erreurs doivent être particulièrement soulignées vu la gravité de l'incidence thérapeutique.
Dans 8% des cas, la DSA a permis de poser un diagnostic formel d'embolie par visualisation directe de l'embol endoluminal au niveau artériel segmentaire, alors que l'AP ne permettait de poser qu'un diagnostic probable d'embolie.
Dans tous les cas, la DSA est à même de juger de l'évolution de la maladie après traitement médical.
En dépit des insuffisances signalées, si l'on sait que l'AP de par son caractère invasif connaît un taux de morbidité de $\pm$ 3% et de mortalité de $\pm$ 0,2% selon les auteurs, l'examen de première intention dans le diagnostic d'embolie pulmonaire devrait être la DSA.
En cas de diagnostic positif, l'investigation est terminée, dans le cas contraire en présence d'arguments cliniques et scintigraphiques formels,il faut recourir au cathétérisme sélectif voire suprasélectif.

CONCLUSION

La DSA est une méthode fiable dans l'évaluation de la vascularisation pulmonaire, plus rapide et moins invasive que l'AP et de résolution spatiale supérieure avec matrice 512 X 512.
Le rapport coût-performance est favorable.
En ce qui concerne le diagnostic de la maladie embolique, des problèmes techniques sont rencontrés :

1. artéfacts de mouvements (dyspnée et tachycardie)
2. rythme d'acquisition rapide nécessaire
3. diminution significative de la résolution spatiale avec matrice 256 X 256

L'évolution technologique devrait permettre :

1. un rythme d'acquisition rapide avec maintien de la matrice 512 X 512
2. une acquisition des clichés couplée au rythme cardiaque (cardiac gated study) permettant de supprimer des artéfacts de mouvement
3. possibilité d'un système biplan permettant de multiplier le nombre de projections.

ADVANCES IN DIGITAL FLUOROSCOPY WITH SPECIAL EMPHASIS ON CARDIOLOGIC APPLICATIONS

by C. GILATH, Ph. D.

ELSCINT Ltd.

RAMAT GAN, ISRAEL

Digital fluoroscopy is on the way to become a well accepted diagnostic technique. Its advantages in angiography, are mainly in eliminating overlaying structures, improved contrast resolution and reduced invasiveness. Furthermore, the ability to perform some image processing in real time and further processing very shortly after the injection of contrast material and acquisition of pictures are of great value in clinical practice.

The majority of applications of digital fluoroscopy were in the field of non-cardiac angiography with examinations of the carotid arteries being probably the most popular. These applications involved the use of pulsed X-ray at a very low rate, e.g. one to two pulses per second and accordingly also one to two frames per second. This low rate is compatible with the needs of non-cardiac angiography, although in some situations a higher pulse rate could be beneficial.

The dynamics of cardiac systems requires a much higher frame rate (25 or 30 frames per second and sometimes even more). This involves either using a continuous X-ray exposure (such as in the "fluoro" mode) or pulsing the X-ray at a high rate (such as in the "cine" mode). The latter alternative is more attractive because of the following reasons :

- motion freeze during a short pulse (images are not "smeared");
- ease of synchronization with ECG and/or other physiological parameters;
- improved signal to noise ratio.

.../...

.../...

While the advantages of pulsing the X-ray for cardiac angiography were known for a long time, technical difficulties hindered the development of high rate pulsed systems.

The research and development efforts of ELSCINT in the field of digital fluoroscopy were concentrated from the beginning in the cardiac as well as non-cardiac applications. As a result of these efforts, a very advanced system capable of operation in both continuous and pulsed mode was developed. In the pulsed mode a rate of 30 (and in some circumstances 60) pulses and frames per second can be achieved, thus offering an excellent time resolution. In addition powerful processing tools for both on line and off line image processing enable the system to be successfully used in the cardiac angiography environment.

Ventriculographies can be performed by injecting the contrast agent in the superior vena cava or the pulmonary artery. A study consists of three consecutive phases :

1.- Collection of images ("masks") in the high rate pulse mode.

2.- Injection of contrast agent at the beginning of the phase, low rate pulse mode and display of subtracted images in order to enable the physician to observe the arrival of the contrast agent and start the next phase.

3.- Acquisition at high frame rate with the contrast material in the ventricule.

All these phases are synchronized with the ECG thus enabling an easy correlation of images acquired in phase 3 with their corresponding masks.

.../...

.../...

At the end of phase 3, subtracted images are computed and displayed in a cine mode (at a rate to be chosen by the operator). The images corresponding to end diastoly and end sistoly are selected. Time interval difference (TID) images are also generated. Volumes of the ventricule can also be computed at various phases and ejection fraction is readily available (using automatic edge detection procedures). Regional wall motions are computed based on the end diastoly and end sistoly contours. Further functional imaging such as maximum expansion rate, maximum contraction rate, maximum wall motion amplitudes, contraction phase, etc ..., can be done as part of the post-processing.

Imaging of the coronary arteries and grafts can be done non-selectively, by injection of the contrast agent at the aortic root or selectively. In either case, synchronization with ECG is of a great importance, for obtaining the best possible match of images with contrast material with the corresponding masks. Further improvement is possible by acquiring the images over a certain "slice" of the heart cycle, during which there is less motion. Even so, reregistration is sometimes important in order to visualize small arterial branches. Spatial resolution is of the order of 0,3 mm (for a 7 inch diameter image intensifier and 512^2 matrix). Images of coronary arteries can be used for the quantification of stenosis (if any). A sequence of images of coronary arteries taken at different times can be used for flow measurements.

The oral presentation will be accompanied by representative images emphasizing mainly cardiologic but also non-cardiologic applications of digital fluoroscopy.

CURRENT DEVELOPMENTS IN DIGITAL SUBTRACTION ANGIOGRAPHY - TEMPORAL, DUAL ENERGY.

DISCUSSION OF CLINICAL DATA AND FUTURE TRENDS

Peter Z. Wasowski.

1. INTRODUCTION

Good morning ladies and gentlemen. I am honored to be here with you today to discuss work by General Electric Company Medical Systems in the exciting new imaging field of Digital Subtraction Angiography (DSA). I wish to present to you several aspects of research topics in DSA that General Electric is presently studying. As an introduction, however, I wish to review with you some basic principles of DSA and show some clinical results.

2. PRINCIPLES OF DSA

A. Example

Consider this slide (Slide 1) which shows the lateral view of the knees of an elderly woman. She is suspected of having atherosclerotic disease. Several seconds after this image was made, another exposure was taken and is shown here (Slide 2). There is no visible difference between this image and the previous one. However, after doing a subtraction, the resultant difference image is shown here (Slide 3). The popliteal arteries in both legs are clearly shown as white vessels against a gray, uniform background. Small narrowings are evident in the trifurcations on the left and right sides (bottom of image). Atherosclerotic disease is readily demonstrated. This example illustrates the usefulness of DSA. The subtraction step cancels out many of the brightness signals that one is not interested in. For example, signals from the bone and soft tissue are removed. Only the brightness from the iodine-filled vessels remain.

./.

B. Schematic of DSA

The next slide (Slide 4) is a diagram of DAS. The top curve shows the brightness or pixel value plotted across an arbitrary horizontal line of the image. At the left of the line the signal is small and appears dark while in the centre the signal is larger and appears white. This curve corresponds to the signal in the "mask" image, taken before arrival of contrast agent. The second curve shows the brightness for the same line but for a short time later. Here the presence of small amounts of contrast agent in the blood causes small decreases in the signal level as shown. The difference between the top two curves is presented in the third curve. The result is very flat with several small changes corresponding to the iodine-filled vessels. The bottom curve shows the final result which is viewed on the TV monitor. Note that this is an enlarged or amplified version of the third curve. This is obtained the same way as using a smaller "window" setting in CT. In the final result the vessels appear very white against a flat gray background as seen in the clinical example. Note also the presence of noise.

C. Contrast Levels

The subtraction process is extremely sensitive to small changes in brightness. In fact this sensitivity allows intravenous rather than intra-arterial administration of contrast agents for most procedures studied thusfar. Generally, 30 milliliters (ml) of contrast agent are administered at 15-25 ml/sec. at sites ranging from an arm vein to the superior vena cavae. Typically the iodine concentration is diluted by a factor of 20 by the time the contrast agents arrives at the vessels under study. The difference in measured signal before and during the presence of the diluted contrast material can be 1% or

./.

less of the measured signal itself. In DSA, contrast levels are very small.

D. X-Ray Exposures in DSA

Let us next turn to the topic of noise. Its presence was noted in the bottom curve of this slide. Noise is probably the principle limitation of DSA and it can arise from several sources. The first and most important source is the noise from the X-Ray detection statistics. You are probably familiar with or have heard the expression "Poisson statistics". What this means is that as one detects more X-Rays, the statistical precision of the measurement gets better. An equivalent expression is that improved statistical precision in general demands higher patient exposure. Because the contrast levels in DSA are so small, somewhat higher X-Ray exposures are required than in, say, normal fluoroscopy.

Let us illustrate this concept with an example. The next slide (Slide 5) is a DSA image of a phantom. An X-Ray exposure equivalent to normal fluoroscopy was used and you can see that the image looks very noisy. It is difficult to see but in the image are several simulated arteries. These contain contrast levels very similar to those measured for DSA patients. Clearly this high noise level is unacceptable.

The next slide (Slide 6) is a DSA image of the same phantom but at a higher X-Ray exposure. The noise is much smaller in magnitude and many vessels can now be seen that were invisible in the previous image. The smallest vessel in the central group is 1 mm wide and has less than 0.75% contrast.

The X-Ray exposure used to form this image was about 400 times larger than that of normal fluoroscopy. However,

./.

these high exposure procedures are generally made at a rate of 1 per second. Normal fluoroscopy is done at 30 images/sec. in the U.S.A. or 50 images/sec. in Europe. Thus, total patient exposure per second for DSA exams is about 10 times higher than normal fluoroscopy.

3. SOME CLINICAL RESULTS

Next I wish to show you some examples of clinical images which were obtained with the General Electric Company DF 3000 digital fluorographic system.

A rather challenging area to image is the head. This first example (Slide 7) shows normal anatomy. Note the sharp detail of the small vessels. The next example (Slide 8) is the image of a large aneurysm, and the third case (Slide 9) shows an arteriovenous malformation.

Perhaps the largest application thusfar of DSA has been imaging the carotid arteries. This first example (Slide 10) shows normal anatomy. The darkness of the vessels indicates excellent blood flow. The second case (Slide 11) shows a stenosis at the origin of the right internal carotid artery. The third example (Slide 12) shows a small stenosis at the origin of the left internal carotid artery. The final carotid case (Slide 13) illustrates post-surgical follow-up.

Using a somewhat larger field of view one can image the aortic arch as in these examples (Slide 14, Slide 15). In the abdomen one is often interested in visualizing the renal arteries (Slide 16, Slide 17) and the aortic bifurcation (Slide 18).

Finally, peripheral vessels can also be studied such as the femoral arteries (Slide 19) and the popliteal arteries (Slide 20).

./.

These examples by no means should be considered as the limits of DSA. Many other procedures are yet to be devised, limited only by the ingenuity of the radiologist.

4. RESEARCH TOPICS

DSA has already been proven to be a useful imaging technique. One might question, however, into what new areas can DSA be applied. In the remainder of my talk I wish to discuss several of these research topics.

A. Cardiac Imaging

Perhaps the biggest goal of DSA is cardiac imaging. Some systems, such as the General Electric DF 3000, have the capability of imaging in "realtime", forming 30 difference images per second. This makes them particularly applicable to visualizing the heart chambers. Thus, one research area is in ventriculography. DSA could potentially replace many of the quantitative cardiac measurements presently done in nuclear medicine. To get an idea of the image quality consider this next image (Slide 21), taken at diastole, and another image (Slide 22) taken at systole. These images are individual frames from a 4-sec. long DSA procedure done at a 30 frame/sec. imaging rate. Using images such as these, one can potentially compute ejection fraction.

Another area within cardiac studies is the imaging of the coronary arteries. Ideally intravenous injections of contrast material would also be done in this case. However, there is a major problem with superposition. Contrast-filled cardiac chambers projected on top of the coronary arteries interfere with their perception. However, one can still use arterial injections, as in normal cineangiography, but with the advantage of seeing the results immediately. The next slide (Slide 23) is the result of

./.

such a selective injection. All three major coronary arteries are clearly visible along with many of their branches. Perhaps you prefer that the vessels be dark (Slide 24) rather than white. In either case the results compete very favourably with conventional cine.

B. Dual-Energy Subtraction

The final research topic I will present deals with a very exciting area of digital radiography. It is called energy subtraction, and a modification of this called hybrid subtraction. This work developed as a result of our close cooperation with Professors Brody and Macovski of Stanford University. Consider how different materials, such as bone and soft tissue, attenuate X-Rays. As the energy of the X-Ray beam changes, the relative attenuations of the two materials behave differently. Suppose one acquires X-Ray images with two different spectra, such as at 80 kVp and 130 kVp. From knowledge of the attenuation of the materials it is possible to cancel out selected materials and enhance others. Consider an example. Here is an image of a chest at 85 kVp (Slide 25) and an image of the same chest made at 135 kVp (Slide 26). By taking a weighted difference image one can form a bone subtraction image (Slide 27). Note that the contrast of all the bone shadows are eliminated and one can virtually see inside the chest. On the other hand an alternate difference image yields the tissue - cancellation (Slide 28) in which only the bones are visible.

Next consider how energy subtraction can be applied to DSA. Probably the major cause of unusable DSA procedures is patient motion. For example this slide (Slide 29) illustrates a motion artifact right at the carotid bifurcation. Often these artifacts are a result of soft tissue motion. Examples include the swallowing artifact shown

./.

here and the peristalsis motion during abdominal procedures. Suppose an energy subtraction image is made of a region before arrival of contrast material. The result would be an image of the bone structures. Next suppose the process is repeated some time later after contrast appears. In this case bone and iodine would be in the image. By subtracting these two resultant images from each other one is left with an image of the iodine above. This combination of energy and temporal subtraction is called "hybrid subtraction".

Consider an example. This is an image (Slide 30) of abdominal aorta using temporal subtraction,(Slide 31) of the same area using hybrid subtraction. Notice disappearance of the peristalsis motion artifacts. In the temporal subtraction (Slide 32) the white vessels are partly visible but obscured by the dark motion artifact. On the other hand here is the hybrid subtraction result (Slide 33). It is very impressive that the arteries are all visible and that the motion artifact has been completely eliminated.

General Electric Company is very excited about hybrid subtraction. We have presently completed building a system and are doing initial patient studies.

5. SUMMARY

Digital Subtraction Angiography is an exciting new field of imaging. General Electric is committed to providing quality DSA images now and searching for improvements in the future.

Thank you very much.

DIGITAL RADIOGRAPHY OF THE CHEST: CLINICAL EXPERIENCE WITH A PROTOTYPE MODEL

During 1982, a prototype digital apparatus dedicated to chest radiography was on clinical trial in this department. Over a six-month period, approximately 400 patients were examined, all patients having both conventional chest roentgenograms and digital studies. In this presentation, the results of a study designed to compare the capability of digital images and conventional chest roentgenograms to reveal normal anatomic structures and a variety of pathologic states will be reported.

From the approximately 400 patients examined, 50 were selected whose conventional roentgenograms displayed a variety of appearances, including no abnormality and a wide range of pathologic states. The images in both modes were randomized, arranged in groups of seven, and submitted for interpretation to seven board certified radiologists. A standardized questionnaire was completed for each study.

The results of the study can be summarized as follows: visibility of the seven anatomic structures in the mediastinum was consistently better on the digital images than on the conventional roentgenograms. In each case, the difference was statistically significant. The improvement was clearly attributable to an increase in exposure latitude and low contrast detectability. With minor exceptions, pathologic states were equally well seen in the two systems and in no case was the difference in detectability greater than would be anticipated from interobserver variability.

Eamann BREATNACH, M.D.
The University of Alabama
Department of Diagnostic Radiology
619 South 19th Street
BIRMINGHAM, Al. 35233

IV. TOMODENSITOMETRIE PAR RAYONS X / X RAY CT

TOMOGRAPHIE COMPUTEE, FACTEUR DE LUXE OU D'ECONOMIE ?

L. JEANMART (Bruxelles, Belgique)

Texte non parvenu.

CALCUL TC DE VOLUMES D'ORGANES. METHODOLOGIE, POSSIBILITES ET LIMITES

M. OSTEAUX, C. NICAISE, Ph. PEETRONS, L. COOLS, L. JEANMART
(Bruxelles, Belgique)

Texte non parvenu.

COMPUTED TOMOGRAPHY AND LUNG FUNCTION ANALYSIS IN DIFFUSE INTERSTITIAL LUNG FIBROSIS

B. Kurtz, G. Stöckle, K.-H. Hübener, U. Reinhard
Tübingen

X-ray diagnosis of lung fibrosis is based on conventional methods like chest radiograph and tomography of the mediastinum. There is a statistic correlation of predominant location and various radiographic patterns with certain pathologic entities, but in individual cases the chest roentgenogram is rarely diagnostic. In nearly 10 % of patients with such diseases the chest radiogram may even be normal (3). On the other hand an exact quantitative statement of the functional degree of lung fibrosis is not possible using these methods, because no exact quantitative relationship between radiographic morphology and lung function has been found (9).

Computed Tomography (CT) has become widely accepted in the study of mediastinal and pleural disease and in the staging of bronchial carcinoma. But there are few reports on the value of CT in diffuse infiltrative lung disease, mostly dealing with sarcoidosis (11). Because of the high resolution of modern CT, pattern recognition of diffuse pulmonary disease may be superior to that of conventional radiology. But even more interesting than the exact morphology in an axial plane is the possibility to quantify lung tissue density independent of overlying structures. The aim of study is (1) to compare the morphology of CT and conventional chest radiology in diffuse lung fibrosis and (2) to find correlations between lung density changes and alterations in lung function parameters in these patients.

Patients and Methods:

15 patients, 9 women and 6 men aged 22 to 73 years with pulmonary fibrosis were examined. In 12 cases the diagnosis was histologically proved by transbronchial lung biopsy or mini-thoracotomy: 6 Usual Interstitial Pneumonia (UIP), 4 Allergic alveolitis, 1 Histiocytois X, 1 Hard metal disease, 1 Sarcoidosis III, 1 Asbestosis and 1 fibrosis of unknown etiology. Laboratory data included immunologic tests for type III allergies of the lung, autoantibodies and rheumatic factors. Lung function tests were done by body plethysmography. Values are reported as percent of reference values (9). For CT studies we used a Somatom SF (Siemens, matrix 256 x 256 pixels). We examined all scans with a mediastinal and a lung parenchymal window and compared them to the chest radiographs and conventional tomograms of hilum and lung parenchyma. For density measurements we selected scans at three levels, according to the digital radiogram: At the lung apices, at the hilum and just above the diaphragm. All scans were taken at full inspiration (Total Lung Capacity). Regions of interest were selected by lightpin from both lung fields with at least 1 cm distance to the pleura and avoiding large vascular structures, especially at the level of the hilum. These density values were compared to the density values of a normal reference group. Statistical evaluation was done by means of unpaired T-test and linear correlation.

Results:

1) Lung morphology
While 3 patients had a normal chest roentgenogram and normal conventional tomograms, in 14 of the 15 patients parenchymal disease could be detected by computed tomography. Especially peripherally located and diffuse homogeneous disease was often better seen in CT. So was the distribution of lung changes in an axial plane; in many patients the parenchymal disease was predominantly peripheral. Small bullae, whether subpleural or central could easily be seen in CT and small pleural thickenings of few millimeters in diameter could be judged for calcifications. As for pattern recognition, most of the patterns seen on chest x-ray could be identified in CT as well. Honeycombing and diffuse nodular changes sometimes seemed to be better visible in CT, but Kerley B lines were regularly missed with the 256 x 256 matrix.

2) Lung function
As to be expected there was a reduction in vital capacity (VC) to 56 $\pm$ 11,6 % ($\bar{x}$ $\pm$ SD). Total lung capacity (TLC) was also reduced in 14 of 15 patients to 80 $\pm$ 17,2 % of the reference value. Thoracic gas volume (TGV) was 102 $\pm$ 21,5 %, residual volume (RV) 141 $\pm$ 49 %, forced expiratory volume was (FEV_1%) 82 $\pm$ 7,8 %.

3) Lung density (H)
Lung density increased significantly from apical (- 783 H) to basal (- 701 H; p 0.025). The density was -701 $\pm$ 154 H caudally and differed from a normal reference group significantly (- 836 $\pm$ 30,7 H; p 0.05). There was a close negative correlation between H and TGV (r = - 0, 8244, p 0.001), H and TLC (r = - 0, 8121; p 0.001), H and RV (r = - 0,7719; p 0.001) and H and VC (r = - 0,5227; p 0.05). There was no correlation with the dynamic lung volumes. (FEV_1, Airway Resistance (R_{aw})).

Discussion:

Spacial resolution in computed tomography is inferior to conventional techniques in small objects and high contrast. Because of the high contrast between air and lung parenchyma - that is lung vessels, connective tissue and bronchi- detail resolution in CT in a range of 0.3 to 0.4 mm object diameter is theoretically possible. Discrete alterations of lung parenchyma are visible in routine chest x-ray only from a size of 2 to 3 mm and small irregular lung pattern often is a summation of many different small changes. In computed tomography these small changes can be exactly localized on an axial plane. Small pleural and diffuse intraparenchymal lesions can be detected better than on a chest roentgenogram.

But by CT not only details of lung morphology can be shown, also exact measurements of lung densities are possible. Because lung density is made up out of the low density of air (0.001 g/cm^3) and relatively heavy lung tissue (1.06 g/cm^3), it is greatly dependent on the degree of inspiration. In maximal inspiration variations in lung density are smallest and there are also only small ventro-dorsal density gradients (12). Therefore we decided to obtain measurements at TLC. The intraindividual variations of measurements could be minimized by respiration feedback monitoring as suggested by Robinson and Jones (8). For density measurements we used the simple method of defining regions of interest (ROI) by lightpin, avoiding mediastinal structures and the thoracic wall by at least 1 cm and trying to avoid larger vessels at the level of the hilum. We used all CT numbers of those regions and not only a defined range of densities, because in lung fibrosis a variety of densities are to be expected in pathologic connective tissue changes. For the same reasons we neither did evaluate the patients with the isolated

lung field method proposed by Döhring and Linke (1,2); these authors pointed out that this method is not appropriate for evaluating lung density changes due to lung fibrosis.

In our study we found a greater sensitivity of CT than of chest radiograph for detecting lung parenchymal changes. Diffuse interstitial changes and the distribution of changes in an axial plane, especially of changes close to the pleura, are better recognized by CT. Using CT equipment with a 512 x 512 matrix, even recognition of specific lung patterns can be expected to be better than in conventional radiology, e.g. Kerley's B lines can be shown clearly.

On the other hand we found a significant negative correlation of lung density and static lung volumes. CT density of the lungs in lung fibrosis is influenced both by connective tissue raising and by surrounding emphysema lowering overall density. An increase of connective tissue results in a decreased compliance of the lung and a reduction of lung volumes. On the other hand vicarious emphysema often is predominant in advanced lung fibrosis. Because the two mechanisms predominantly influence TLC and TGV, a closer correlation of H to HLC and TGV than to VC can be explained. CT can help detect parenchymal and pleural changes in patients with suspected lung fibrosis and there may be a considerable help in evaluating disease pattern by CT with a 512 x 512 matrix. In addition, by measuring lung density with this method the severity of functional changes in interstitial lung fibrosis can be estimated and a more detailed evaluation of the course of disease will possibly be feasible.

% of reference value		y = mx + b	r	n	p
HU vs	TGV	y = - 0,116 x + 21,21	- 0,8244	15	<0,001
	TLC	y = - 0,0907 x + 16,54	- 0,8121	15	<0,001
	RV	y = - 0,2473 x - 31,92	- 0,7719	15	<0,001
	VC	y = - 0,0393 x + 28,60	- 0,5227	15	<0,05
	PaO_2	y = - 0,047 x + 36,28	- 0,4240	15	n.s.
	sRaw	y = - 0,266 x - 25,79	- 0,4060	15	n.s.
	FEV_1	y =. 0,0267 x + 101	0,3653	15	n.s.
	DL_{COSB}	y = - 0,2274 x - 111	- 0,3808	10	n.s.

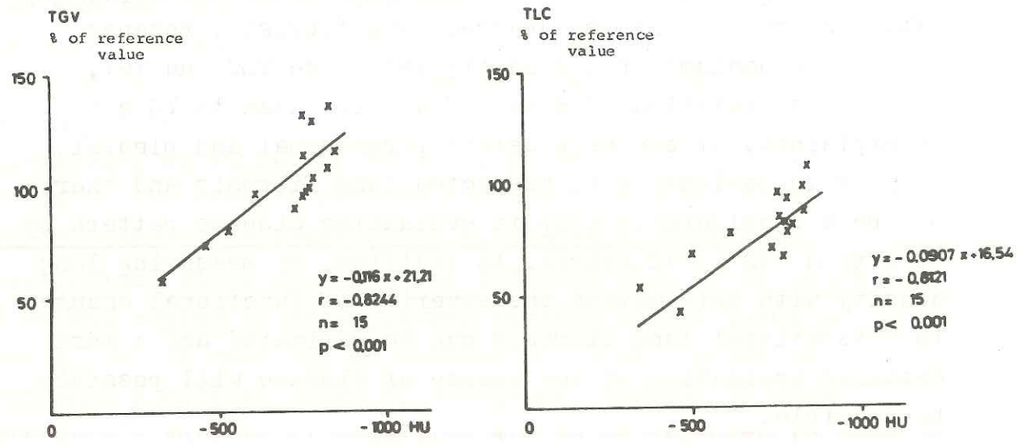

References

1) W. Döhring und G. Linke
Die Grundlagen der quantitativen pulmonalen Computer-tomographie
Fortschr. Röntgenstr. 130 (1979) 133

2) W. Döhring und G. Linke
Die Anwendung der Computertomographie zur quantitativen Belüftungsanalyse der Lunge
Atemwege und Lungenkrankheiten 5 (1979) 144

3) Epler G.R., McLoud T.C., Gänsler E.A. et al.
Normal chest roentgenograms in chronic diffuse infiltrative lung disease
N Engl J Med 298 (1978) 934

4) B. Felson
A New Look at Pattern Recognition of Diffuse Pulmonary Disease
American Journal of Roentgenology 133 (1979) 183

5) L.W. Hedlung and C.E. Putman
Analysis of Lung Density by Computed Tomography
in: Pulmonary Diagnosis, Imaging and Other Techniques,
Ed.: C.E. Putman, Appleton-Century-Crofts, New York, 1981

6) T.C. McLoud
Diffuse Infiltrative Lung Disease
in: Pulmonary Diagnosis, Imaging and Other Techniques,
Ed.: C.E. Putman, Appleton-Century-Crofts, New York, 1981

7) Liebow A.A.
New Concepts and Entities in Pulmonary Diseases.
In: Liebow A.A., Smith D.E. (eds.): The Lung
Baltimore, Williams and Wilkins 1967

8) Robinson P.J. and K.R. Jones
Improved Control of Respiration During Computed Tomography
by Feedback Monitoring
Journal of Computer Assisted Tomography 6 (1982) 802

9) Rühle, K.-H., Matthys, H.
Kritische Auswahl von Sollwerten für ein Computergrogramm
zur Routinelungenfunktionsdiagnostik.
Pneumologie 153, (1976) 223

10) Stender H.St. und A. Majewski
Feinfleckige Lungenverschattungen bei entzündlichen und
granulomatösen Prozessen
Radiologe 19 (1979) 461

11) Stiris M.G. and R. Bortwick
Computed Tomography (CT) Evaluation in Pulmonary
Sarcoidosis
Europ. J. Radiol 1 (1981) 16

12) Wegener O.H., P. Köppe und H. Öser
Measurement of Lung Density by Computed Tomography
Journal of Computer Assisted Tomography 2 (1978) 263

13) Wegener O.H. und R. Felix
Interstitielle Lungenerkrankungen
In: Ganzkörper-Computertomographie
Hrsg. G. Friedmann, E. Bücheler, P. Thurn
Georg Thieme Verlag Stuttgart/New York 1981

COMPUTERIZED TOMOGRAPHY OF THE HEART

K. Lackner

Radiologische Universitätsklinik Bonn
Dir.: Prof.Dr. P. Thurn

Computerized transmission tomography, ultrasonography and nuclear scintigraphy enhanced the role of radiology in the modern diagnostic methods. The role of cardio-CT in the diagnosis of cardiovascular diseases depends on regional conditions as the establishment of alternative non invasive methods for cardiac imaging like echocardiography, scintigraphy and digital subtraction angiography.

Technical considerations of cardio-CT

The density difference between the circulating blood and the myocardium is not sufficient for the distinction of the cardiac cavities in the plain scans. The intravenous contrast administration for the visualisation of the myocardium and the cardiac cavities can be done by different methods :

a) in the form of an angio-CT with injection of a bolus of contrast medium followed by a series of scans without movement of the table showing the flow of contrast medium through the various cardiac cavities, the myocardium and vessels (coronary bypass grafts).

b) with reference to the circulation time timing of the contrast injection and CT scanning in the way that a selective opacification of different cavities is achieved.

c) after an initial bolus injection of 90 ml 65% contrast medium and repeated intermittent injections of 5 to 10 ml during the interscan time to obtain an even, high density level of all cardiac cavities throughout the complete examination of all portions of the heart. This modality enables a wider range of findings. Depending on the indication and examination time a total quantity of 200 - 250 ml of contrast medium is required.

The CT scans are performed with the patient in full inspiration. Breathing is allowed between the scans. In ECG-gated

and ungated cardio-CT it is important, that the degree of inspiration is consistent for all scans, so that the heart is not shifted. Despite the motion artefacts caused by cardiac contraction and dilatation during the scan time, ungated cardio-CT provides a good assessment of cardiac morphology in cross sections, free from overlapping structures. To obtain ECG-gated scans, the measured data of 8 scans of a single sectional plane were collected and sorted. Only those measured data were employed for the image computation which coincide with a freely selectable ECG phase. The data for an ECG-gated image reconstruction may be obtained either prospectively by ECG control of the X-ray source, or retrospectively, by selecting data from a series of scans. The prospective gating modality has the potential for dose reduction, but involves modifications of the machine hardware. The time resolution of ECG-gated images is approximately 0.1 sec. and allows functional assessments (Fig. 1). The skin-dose is in ungated cardio-CT approximately 30 mGy and in ECG-gated cardio-CT (8 scans, 7 mm slice thickness) approximately 156 mGy. Ungated and ECG-gated cardio-CT has been tested under experimental and clinical aspects in several institutes (1-12).

Clinical considerations of cardio-CT

1. Pressure or volume overload

In pressure overload cardio-CT demonstrates the increased wall thickness of the ventricles (Fig.2). Precise measurements of wall thickness are possible. By ungated cardio-CT the thickness of the left ventricular myocardium as shown in normal hearts had a median value of 10-12 mm. By ECG-gated cardio-CT the median wall thickness was 10 mm in diastole and 14 mm in systole. In case of pressure overload the median left ventricular wall thickness increased to 16 mm (ungated) and 14 mm (diastolic) and 20 mm (systolic) in ECG-gated CT. ECG-gated cardio-CT in addition demonstrates the wall movement and the residual blood volume.

In volume overload the dilatation of the involved cardiac chambers are the leading diagnostic finding in cardio-CT (Fig.3).

Caused by this asymmetric dilatation of cardiac cavities the heart may rotate. This rotation can be measured as the angle between the sagittal body axis and the axis of the ventricular septum between trigonum fibrosum and interventricular sulcus. This angle increases if the heart rotates to the left side. We found a normal angle of 38°, in pressure overload of the left ventricle 42°, in volume overload of the left ventricle 48°, in pressure overload of the right ventricle 53° and in volume overload of the right ventricle 61°, indicating that dilatations of the right side cavities of the heart rotate the heart to the left side in a higher degree than dilatations of the left side cavities.

2. Cardiomyopathy

In congestive cardiomyopathy CT shows the dilatation and increased diastolic and systolic blood volume in the left ventricle. Ventricular thrombi may occur. In idiopathic hypertrophic subaortic stenosis cardio-CT demonstrates the circumscribed thickening of the ventricular septum obstructing the outflow tract of the left ventricle. The ratio of the myocardial thickness between the bulging ventricular septum and the left ventricular lateral wall corresponds well with echocardiographic findings. In restrictive cardiomyopathy positive CT findings can be expected only if the myocardium is thickened.

3. Intracavitary masses

Tumors or thrombi appear in cardio-CT as filling defects of different density or location. In general thrombi are combined with mitral valve stenosis, myocardial infarcts, cardiomyopathy or arrhythmia. Their density is lower than in tumors and they show no enhancement following contrast medium injection. The infiltration of the cardial wall or pericardium and the intracavitary part of malignant cardiac tumors can be schown by CT directly and precisely (Fig.4).

4. Coronary heart disease

Findings in ungated cardio-CT following myocardial infarcts are :

regional or generalized left ventricular dilatation
myocardial wall thinning
mural thrombi
myocardial calcifications (Fig.5)
ventricular false aneurysm
and in experimental studies decreased enhancement of the ischemic myocardium after contrast medium injection.
Findings in ECG-gated cardio-CT are :
regional or generalized reduction of the systolic movement of the ventricular wall (Fig.6)
decreased ejection fraction
reduction in the systolic thickening of the infarcted myocardium.
As the imaging conditions are most favorable for those structures of the heart that pass through the CT sectional plane nearly perpendicularly, the diagnostic results are better assessing the septum, lateral wall, apex, anterior and posterior wall near the ventricular apex. The sensitivity and specifity ranged between 80 and 90 % . Calculating the ejection fraction and comparing the results of ECG-gated cardio-CT and levocardiography showed a correlation coefficient of r = 0.8 .

5. Coronary bypass

Based on the increase in density within the graft following intravenous injection of contrast medium an assessment of the bypass perfusion is possible. The density measurement in cardio-CT is an objective parameter of the bypass function (Fig. 7). As the non demonstration of coronary bypass grafts in cardio-CT is suggesting bypass occlusion complete information concerning number and localisation of the grafts must be given before the examination. Assessing the bypass perfusion the sensitivity of cardio-CT was 90 % and the specifity was 70 - 80 % . In addition cardio-CT demonstrates the complications of cardiosurgery as hemorrhagic pericardial effusion, mediastinal hematoma or retrosternal abscess.

6. Pericardium

Pericardial effusions, encapsulated effusions, diverticula, lipoma, tumors and pericardial thickening and calcification in the course of constrictive pericarditis are readily detected by cardio-CT.

Conclusion

In conclusion cardio-CT has to be compared with the value of other alternative or complementary non invasive imaging methods in the diagnostic work up of the heart (Table 1) .
In coronary heart disease functional assessments of the left ventricle are similar using cardio-CT, echocardiography, gated blood pool scintigraphy, digital subtraction angiography. Only angiocardiography reveals stenoses of the coronary arteries. Under clinical conditions myocardial perfusion scintigraphy gives the best information concerning myocardial vitality.
The demonstration of cardiac valve movements and calculation of the area of valve opening are superior based on echocardiographic findings. In Cardiomyopathy findings of cardio-CT, echocardiography, digital subtraction angiography are similar. Thrombi are best demonstrated by cardio-CT. The localisation and size of cardiac tumors can be cleared completely using cardio-CT, echocardiography and digital subtraction angiography. Cardio-CT is superior in the localisation of cardiac calcifications and equal to digital subtraction angiography assessing coronary bypass graft perfusion. Pericardial diseases should be differentiated using cardio-CT.
In the demonstration of anomalies of the great vessels cerdio-CT and digital subtraction angiography show similar results. Except the demonstration of coronary artery stenoses konventional angiocardiography can be replaced by non invasive methods in the diagnostic work up of most of the different cardiac diseases.

THE VALUE OF THE DIFFERENT IMAGING METHODS IN THE DIAGNOSTIC WORK UP OF THE HEART

	COMPUTERIZED TOMOGRAPHY	ECHOKARDIO-GRAPHY	SCINTIGRAPHY BLOOD POOL	SCINTIGRAPHY PERFUSION	DIGITAL SUBTRACTION ANGIOGRAPHY	ANGIOCARDIO-GRAPHY
CORONARY HEART DISEASE	+	+	+	+	+	++
CARDIAC VALVES	−	++	−	−	+	+
CARDIOMYOPATHY	++	++	+	+	++	++
THROMBI	++	+	−	−	+	+
TUMORS	++	++	−	−	++	+
CALCIFICATIONS	++	−	−	−	−	−
CORONARY BYPASS	+	−	−	−	+	++
PERICARDIUM	++	+	−	−	−	−
GREAT VESSELS	++	−	−	−	++	++

References

1. Adams,D.F., S.J.Hessel, P.F.Judy, J.A.Stein, H.L.Abrams
   Computed Tomography of the Normal and Infarcted Myocardium
   American J. Roentgenol 126, 1976, 786

2. Brundage, B.H., M.J.Lipton, R.J.Herfkens, W.H.Berninger, R.W.Redington, K.Chatterjee, E.Carlsson
   Detection of Patent Coronary Bypass Grafts by Computed Tomography
   Circulation 61, 1980, 826

3. Godwin,J.D., L.Axel, J.R.Adams, N.B.Schiller, P.C.Simpson, E.W.Gertz
   Computed Tomography : A New Method for Diagnosing Tumor of the Heart
   Circulation, 63, 1981, 448

4. Harell,G.S., D.F.Guthaner, R.S.Breiman, C.C.Morehouse, E.J.Seppi, W.H.Marshall, L.Wexler
   Stop-Action Cardiac Computed Tomography
   Radiology 127, 1978, 413

5. Heuser,L., K.Lackner, H.Hauser
   Validität der Computertomographie bei der Darstellung offener und verschlossener aortokoronarer Venenbrücken
   Fortschr. Röntgenstr. 137, 1982, 619

6. Higgins,C.B., P.I.Siemers, J.D.Newell, W.Schmidt
   Role of Iodinated Contrast Material in the Evaluation of Myocardial Infarction by Computerized Transmission Tomography
   Invest. Radiol. 15, 1980, 176

7. Köster,O., K.Lackner, Th.Harder
   Computertomographische Diagnostik kardialer, perikardialer und parakardialer Raumforderungen
   Z. Kardiol. 70, 1981, 733

8. Lackner,K., P.Thurn
   EKG-gesteuerte Kardiocomputertomographie
   Fortschr. Röntgenstr. 132, 1980, 164

9. Lackner,K., P.Thurn
   Computed Tomography of the Heart : ECG-gated and Continous Scans
   Radiology 140, 1981, 413

10. Lipton,H.J., B.H.Brundage, P.W.Doherty, R.Herfkens, W.H.Berninger, R.W.Redington, K.Chatterjee, E.Carlsson
    Contrast medium-enhanced computed tomography for evaluating ischemic heart disease
    Cardiovascular Medicine 4, 1979, 1219

11. Morehouse,C.C., W.R.Brody, D.F.Guthaner, R.S.Breiman, G.S.Harell
Gated Cardiac Computed Tomography with a Motion Phantom
Radiology 134, 1980, 213

12. Newell,J.D., C.B.Higgins, J.L.Abraham, M.J.Kelley, W.S.Schmidt, F.Haiglar
Computerized Tomographic Appearance of Evolving Myocardial Infarctions
Invest. Radiol. 15, 1980, 207

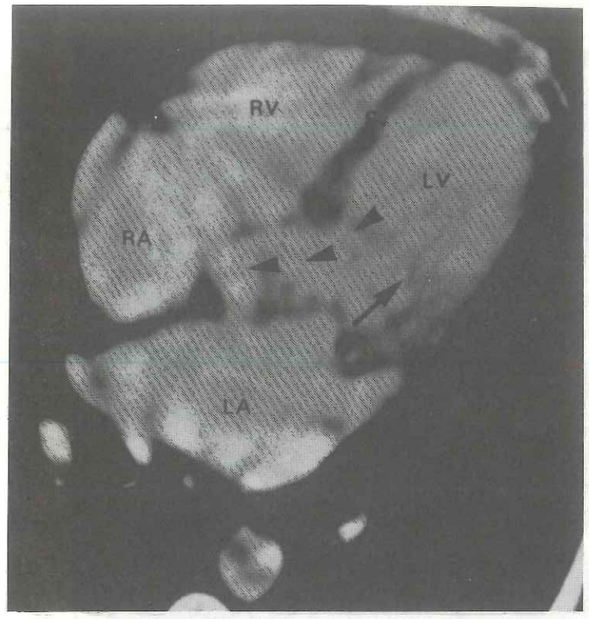

Fig. 1b.Ungated cardio-CT. Slice plane in the outflow tract of the left ventricle. RA = right atrium, RV = right ventricle, Sv = ventricular septum, LV = left ventricle, LA = left atrium, → = inflow tract, ◀ = outflow tract.

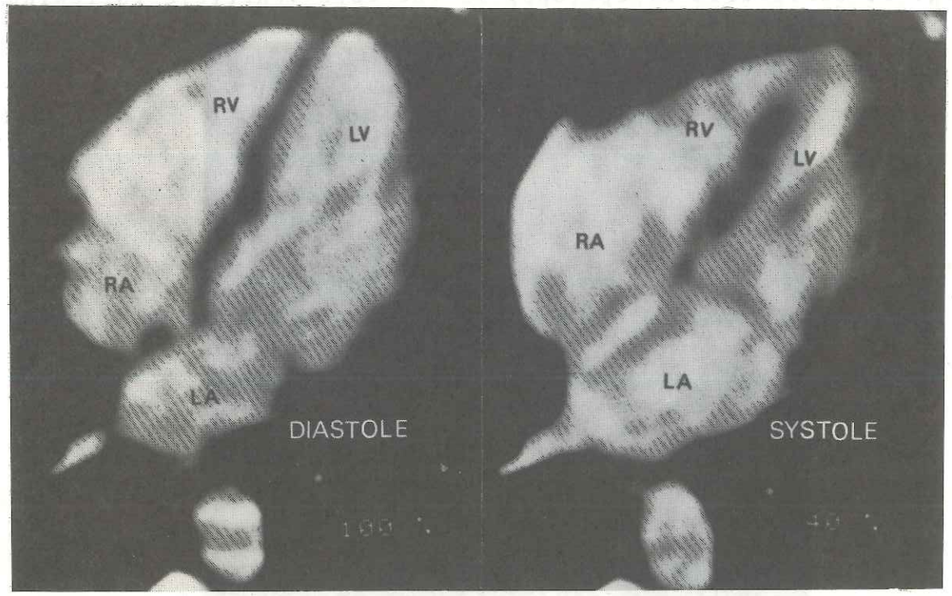

Fig. 1b.ECG-gated cardio-CT.

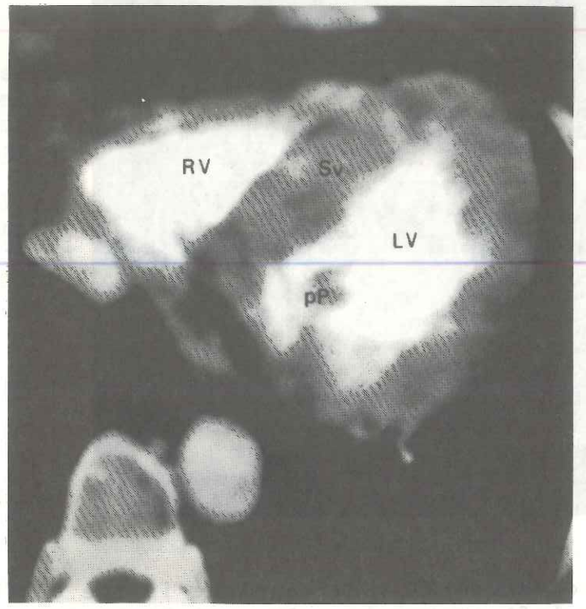

Fig. 2. Concentric hypertrophy of the left ventricle following aortic valve stenosis.

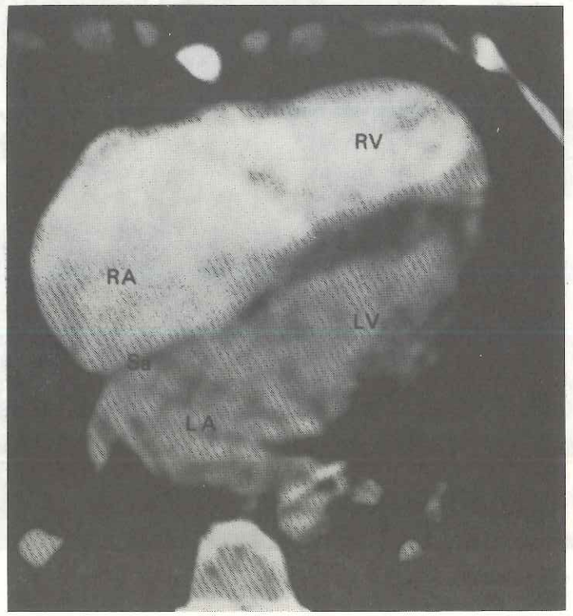

Fig. 3. Volume overload of the right atrium and right ventricle caused by atrial septal defect. Dilatation of the right atrium and ventricle. Rotation of the heart to the left side.

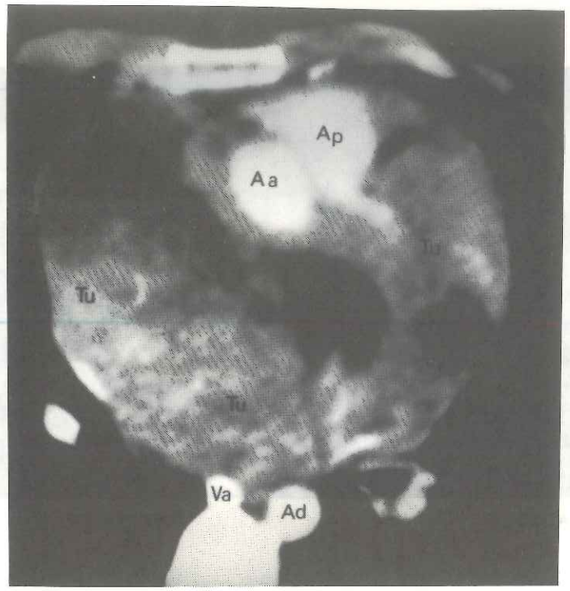

Fig. 4. Malignant tumor of the heart (mesothelioma including sarcomatous parts). Displacement of the ascending aorta and pulmonary artery by the tumor. Compression of the superior vena cava. Dilatation of the vena azygos (Va).

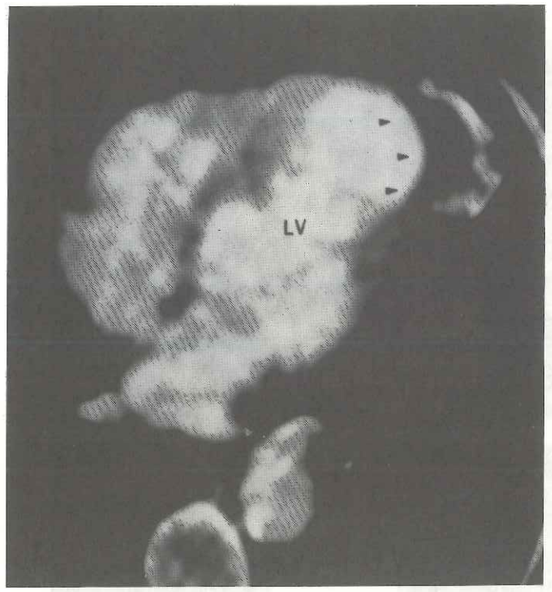

Fig. 5. Anterolateral aneurysm with parietal thrombus and wall calcification.

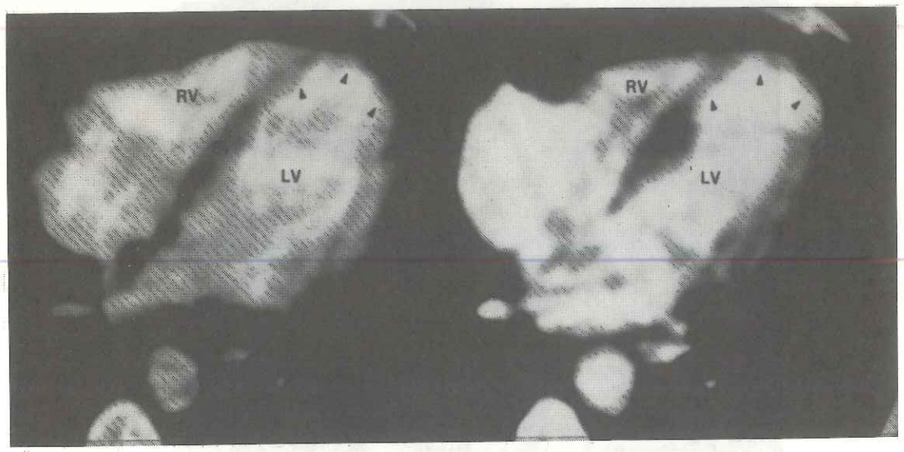

Fig. 6. Anterior wall aneurysm, ECG-gated scan. Thinning of the infarcted wall area, systolic thickening of the normal myocardium.

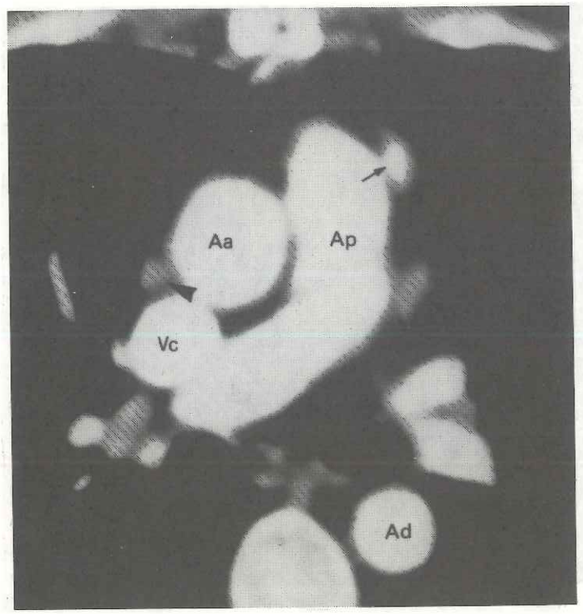

Fig. 7. Coronary bypass grafts to the right coronary artery (◀) and to the left anterior descending branch of the left coronary artery (⟵). Enhancement within the grafts following contrast medium injection.

HIGH RESOLUTION IN CT

G.P. VIJVERBERG (Eindhoven, the Netherlands)

Text not received.

TREATMENT PLANNING BASED ON AN ARRAY-PROCESSOR

by R. Trierweiler

- Introduction

Array-processors have already proven themselves to be powerful tools in the area of image processing. This paper will discuss the successful investigation into employing an array processor for therapy planning applications. Specific areas to be discussed will be as follows:

- Hardware and software design
- Results and comparisons
- Future applications

In this paper the array processor discussed is the BSP 11-TP, which was developped from the BSP 11 presently used in the SOMATOM DR for instant CT-image processing.

- Hardware design

The basic hardware configuration of a treatment planning system consists of two parts, first the CPU which is normally a micro- or minicomputer, second the peripherals which can consist of components such as disk-drives, digitizer, plotter, printer, alphanumeric terminal and graphic display and any other additions that may be desired.

To readily incorporate an array-processor in such a system with these many peripherals it is of great benefit to utilize the existing system software of the mini- or microcomputer and in turn,treat the array-processor as a peripheral.

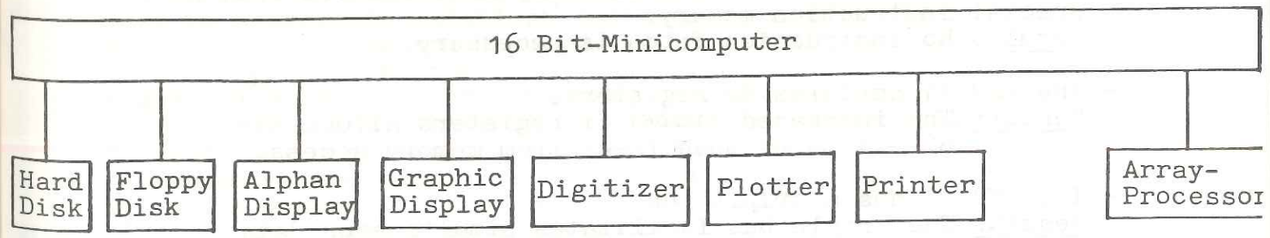

Because of this configuration an array-processor can easily be incorporated in an existing system or be treated as an option to a newly purchased system. The peripheral nature of this processor gives a therapy department the option of deferring the processor cost to a more opertune time.

- BSP 11 Interfacing

The BSP 11-TP can be connected to any PDP 11 with unibus and memory management. The data flow is from the PDP 11 through the UNIBUS, UNISYS and the systembus to the memory of the BSP 11.

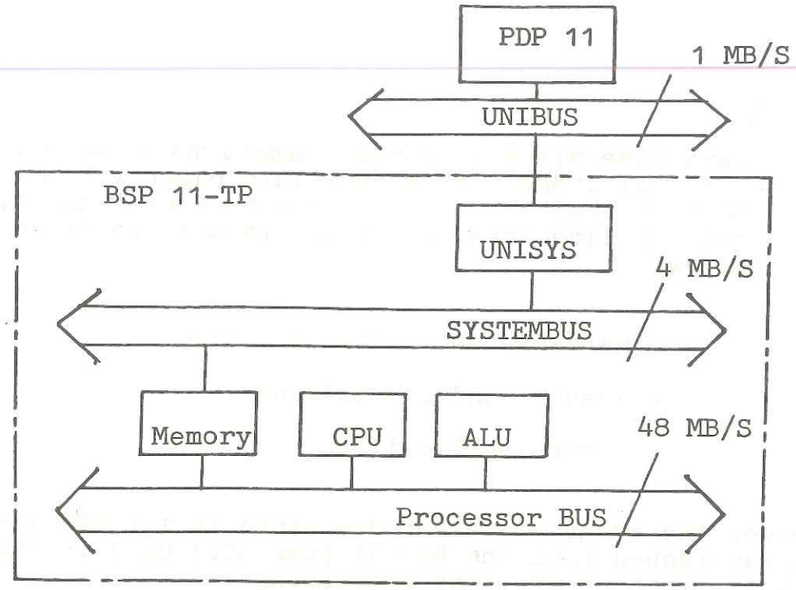

Once this is achieved, the BSP 11 takes over the data processing tasks and then passes the data back to the PDP 11 when processing is completed.

- BSP 11 design

The BSP 11 is designed to achieve calculation speeds much faster then conventional micro- or minicomputers. The main differences can be cited as:

- The instruction are loaded directly into the CPU from a special instruction memory.
  Result: No instruction fetch is necessary.

- The BSP 11 contains 32 registers.
  Result: The increased number of registers allows the BSP 11 to be much freer from memory access.

- The BSP 11 has a triple bus.
  Result: The triple bus facilitates simultaneous data loading of the calculation variables into the processor elements.

- The BSP 11 contains an independent memory control element.
  Result: The processor can execute any instruction independent of memory-cycle time.

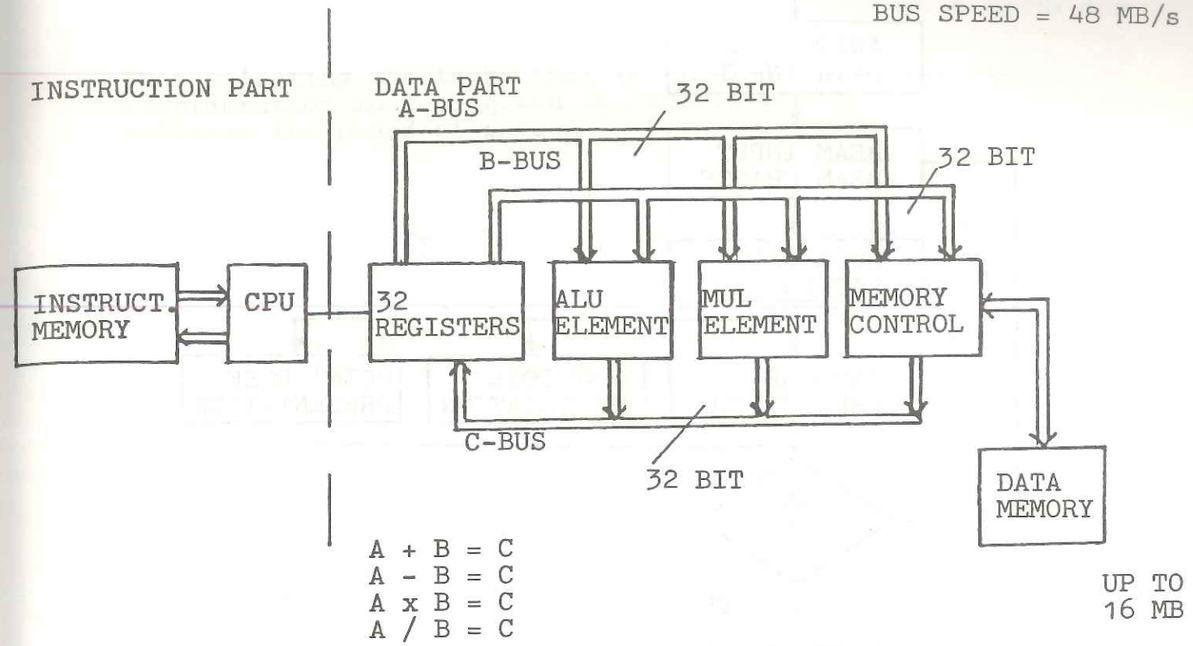

BSP 11 DESIGN

- Software design

The steps that must be taken in order to complete a doseplan can be summarized as follows. First, one must enter the administrative data of the patient, such as patient ID-number, patient name, site of planning, etc. Secondly, information concerning the anatomy of the patient in the treatment areas must be entered to establish the density matrix. This information may be obtained through the use of CT, radiographs, metal or plastic contours, etc. Thirdly, the set-up of the treatment must be established and inputted to the system. Once these three steps have been completed, the system will be able to calculate the dose matrix. The results of the dose-calculation can be presented in either an isodose presentation or a line dose presentation or a point dose presentation. At this time the user may alter the treatment set-up to achieve the desired dose distribution. If the plan is accepted a hard copy printout with a graphical presentation may be obtained.

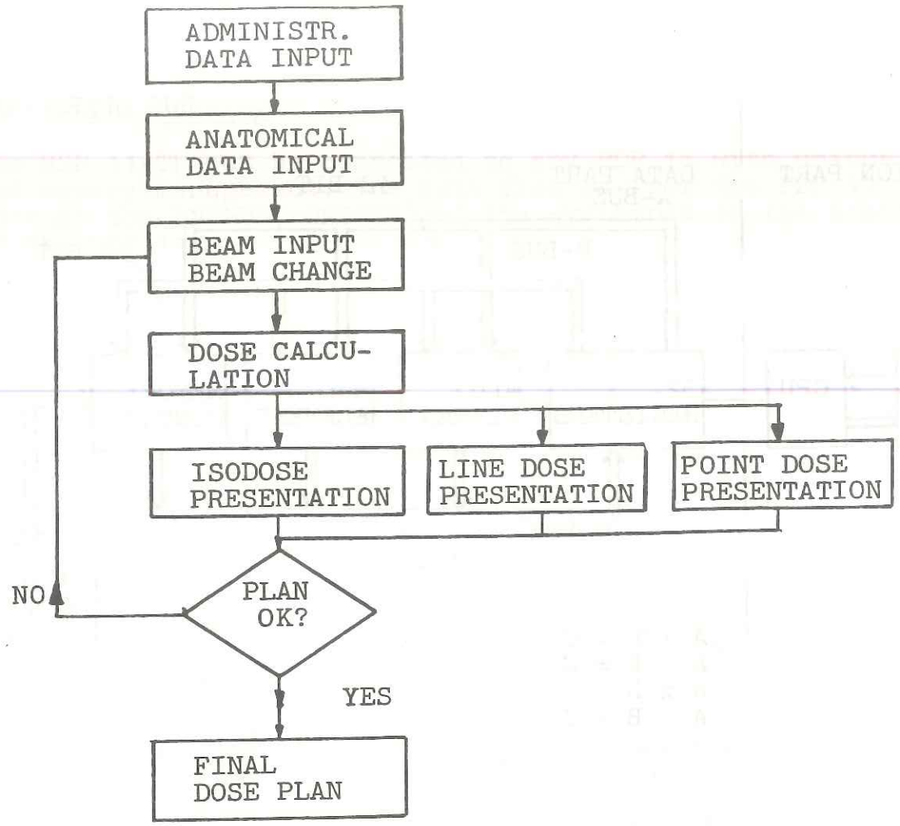

When considering the tasks involved in RTP-software, one must make the distinction between normal I/O tasks and computer intensive tasks. If the software is designed in a modular way, then the separation can be easily made. Normal I/O tasks are initialisation of the program, administrative data input, anatomical data input, beam input and beam change and contour and beam plotting. On the other hand, the computer intensive tasks are matrix calculation, point dose calculation, line dose calculation, density matrix generation and isodose generation.

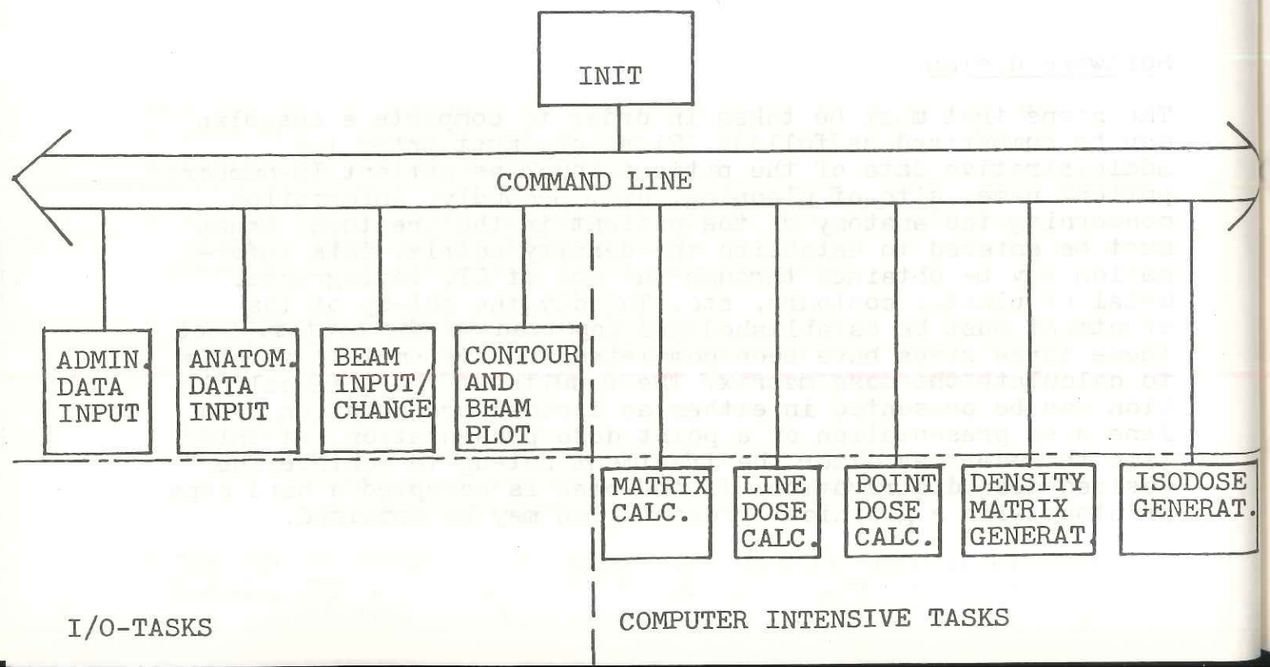

When selecting the tasks that the BSP 11 will take over, consideration must be given to certain points in order to optimize the speed of processing:

- The programs must be coded in 32 Bit BSP 11 assembly-language
- Specially designed software interfaces must be provided to avoid any data acquisition outside of the BSP 11 during processing.

To achieve the second point shown above for dose matrix computations the flow of information between the PDP 11 and the BSP 11 has been designed as follows:

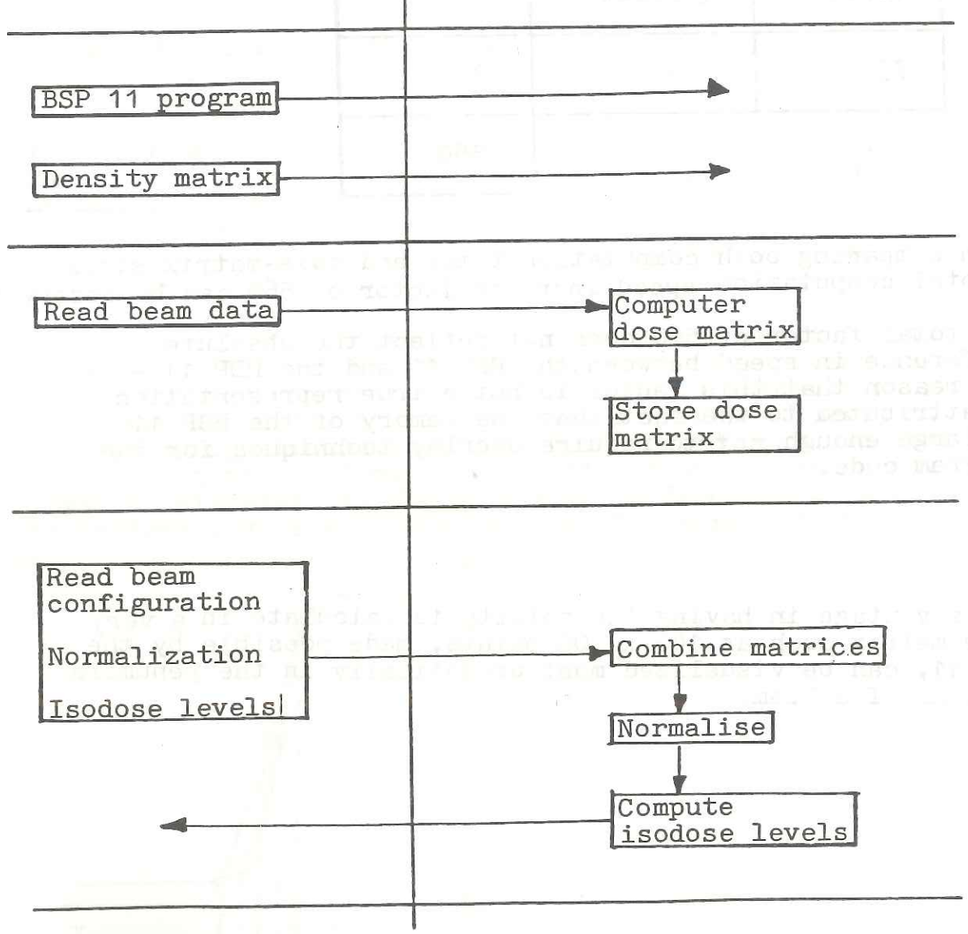

In the first step the PDP 11 loads the BSP 11 program into the array processor. The density matrix is then loaded into the array processor. When the beam parameters are sent to the array processor the dose computation is initiated and the dose matrix is stored. In order to present this dose information, parameters must be set that specify the type of presentation. These parameters are beam configuration, type of normalization and the desired isodose levels. After completion the array processor will send the isodose-plot-information back to the PDP 11.

- Results and comparisons

Using a PDP 11/34 A with floating point processor, calculation of a single fixed beam with pixel by pixel inhomogeneity correction and a dose matrix of 35 x 25 points requires approximately 7 seconds. When the BSP 11 is implemented into the system a calculation time of 0.2 seconds is achieved, using identical algorithms and a dose matrix of 140 x 100 points.

PDP 11	BSP 11	FACTOR
35 x 25 (875)	140 x 100 (14.000)	16
75	0.2	35
		560

When comparing both computation times and dose-matrix sizes, a total computation speed increase factor of 560 can be observed.

The total factor of 560 does not reflect the absolute difference in speed between the BSP 11 and the PDP 11 - the reason that this factor is not a true representation is attributed to the fact that the memory of the BSP 11 is large enough not to require overlay techniques for the program code.

The advantage in having the ability to calculate in a very fine matrix such as 140 x 100 points, made possible by the BSP 11, can be visualized most dramatically in the penumbra regions of a beam.

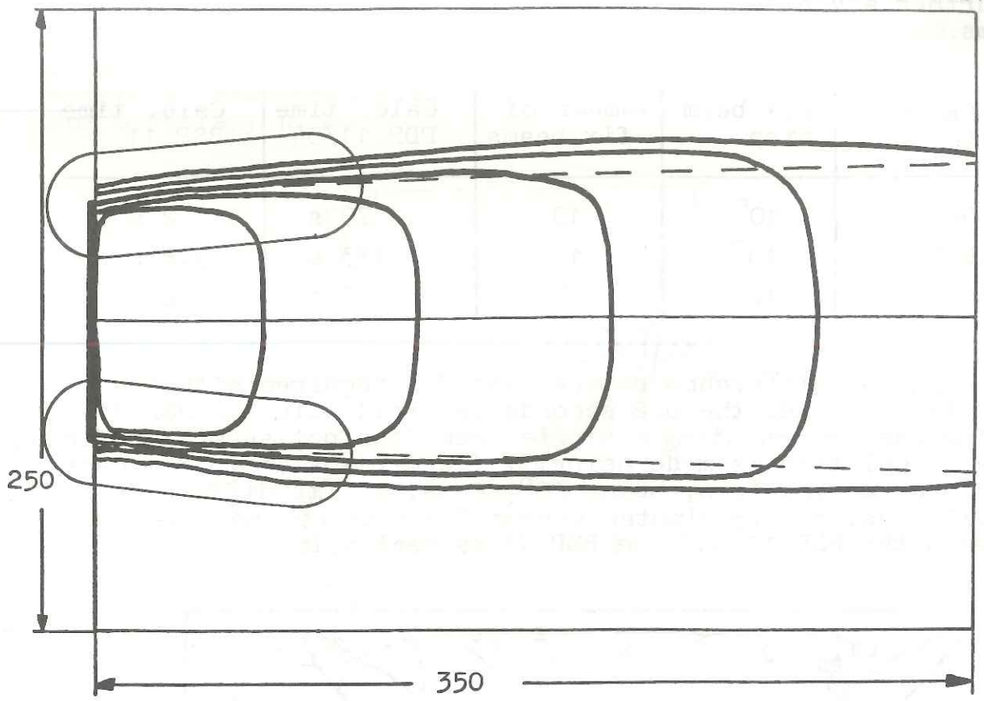

MATRIX 35 x 25 PTS GRID SIZE = 10 mm
MATRIX 140 x 100 PTS GRID SIZE = 2,5 mm

An intercomparison can be made by constructing a phantom measuring 350 by 250 millimeters. When a beam is calculated in this phantom using a 35 x 25 point matrix a grid size of 10 millimeters squared is achieved. If the same beam is calculated in the phantom using a 140 by 100 point matrix a grid size of 2,5 mm^2 is achieved.

The reason for the increased accuracy in the penumbra region can be seen when the comparison of the grid sizes is applied to the beam profiles. Due to the fact that the isodose levels are generated out of the dose matrix by linear interpolation, a significant error can be observed when applying a large grid size (10 mm) to a profile from a high energy linear accelarator. If the grid size is descreased to 2.5 mm the isodose levels will more accurately represent the stored data.

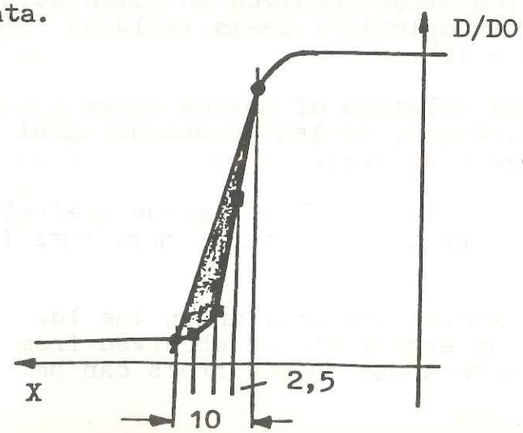

A further advantage can be cited in the application of moving beams.

Moving beam angle	Fix beam step	Number of fix beams	Calc. time PDP 11/34	Calc. time BSP 11
90°	10°	10	70 s	2 s
180°	10°	19	133 s	3.8 s
360°	10°	37	273 s	7.8 s

Although the difference between the 7 s required with the PDP 11-system and the 0.2 seconds required with the BSP 11-system when calculating a single beam does not seem significant, if a calculation is made using 37 fixed beams as in the case of a 360° moving beam, using 10° steps, a time difference of 273 secs. of 4.5 minutes versus 7.8 secs can be observed between the PDP 11 and the BSP 11 respectively.

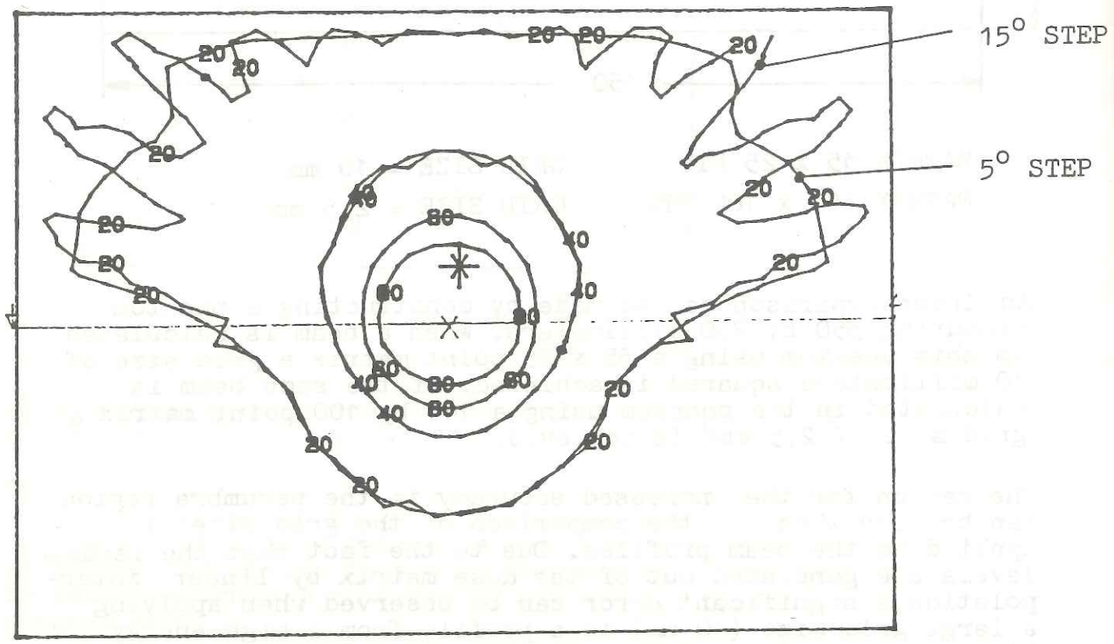

Because of the long computation times involved in calculating moving beams, users often calculate beams in large degree increments such as 10 - 15°.

Although this practice made calculation of moving beams feasable in the clinical invirоment, it led to unmeaningful isodose information in the low dose area.

With the introduction of the BSP 11 to RTP, it became realistic to calculate moving beams in very small angular increments in a reasonable amount of time.

Thus eliminating irrelevant isodose information in the low dose area. In the example shown errors can be observed from 30 % level down to 10 %. In some areas these errors can be seen to be as large as 8 %.

- Future applications

Future considerations can be shown in a theoretical model in which 40 CT-slices scanned at the recommanded 5 millimeters to represent a 20 centimeter body-section are used for a therapy plan.

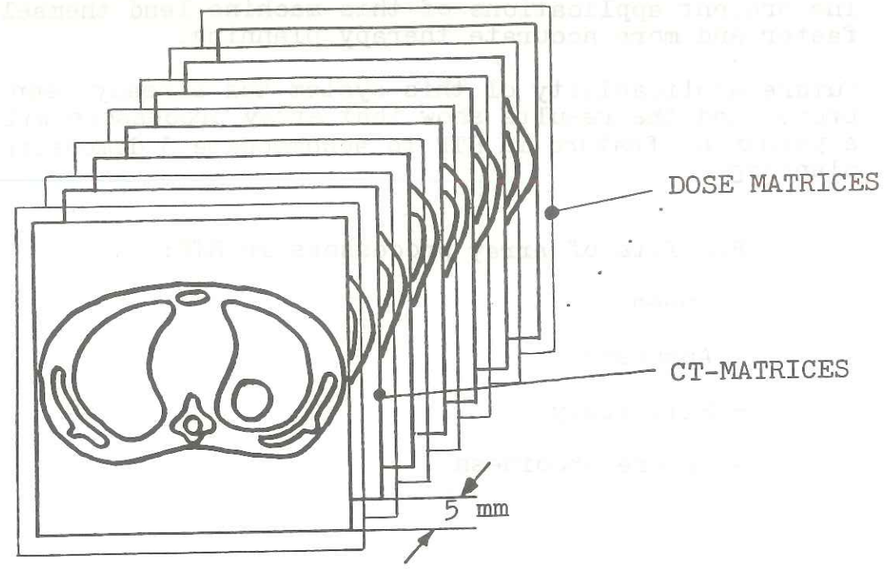

This body-section can be then cut into any desired plane and presented with the appropriate dose distribution. To make this possible, a dose matrix must be calculated for each CT-slice.

	PDP 11	BSP 11
Fix beam calculation (40 slices)	280 s (5 min)	8 s
Moving beam calculation 180° (40 slices)	5320 s (88 min)	151 s (2.5 min)

When calculated, utilizing present PDP 11 technology, the calculation time would be approximately 5 minutes for a single beam. In contrast the same beam calculated with the BSP 11 in the system, calculation time is approximately 8 seconds.

Perhaps a clearer illustration can be shown using a moving beam as an example. In this case the PDP 11 system requires 1 hour and 30 minutes to calculate a 180° pendulum beam. The BSP 11 based system requires only 2.5 minutes for the same 180° beam.

- Conclusion

In summary,all indications show that the BSP 11 is as valuable in radiation therapy planning as it is already proven in image processing.

The present applications of this machine lend themselves to faster and more accurate therapy planning.

Future applicability of this system has already been proven and the results show that array processors will become a permanent feature in RTP to accommodate 3 dimensional dose planning.

Benefits of array processors in RTP:

- Speed
- Accuracy
- Efficiency
- Future proofness

References

1) W. R. Delong, Programmieren mit einem schnellen Spezialrechner, Siemens Forsch. u. Entwickl.-Ber. Bd. 7 (1978) Nr. 4

2) Kenneth R. Hogstrom, Implementation of CT treatment planning AAPM 1982 Summer School

3) Imhof, Trierweiler, Verwendung der CT-Matrix im Bestrahlungsplanungssystem SIDOS-U Medizinische Physik 1980 Band 1

4) Edwin Mc Cullough, Using CT to achieve geometric accuracy AAPM 1982 Summer School

5) F. Nüsslin et al, A first approach to CT-assisted treatment planning using the SIDOS-U system Presented at the Workshop on computerized tomography scanners in radiotherapy in Europe, Geneva 28. - 30.03.1979

6) Schlegel, W. H. Scharfenberg and W. J. Lorenz, Calculation of dose distributions from CT-images in: Comptes rendus of fundamentals in technical progress in ultrasound, dose planning and nuclear medicine. Vol. II, II.41 - 4.32 (J. Garson, W. Gordenne, G. Merchie, eds) Presse Universitaire de Liege, Liege 1979

V. TOMOGRAPHIE D'EMISSION / EMISSION TOMOGRAPHY

EMISSION TOMOGRAPHY

M. M. TER POGOSSIAN (St Louis, U.S.A.)

Text not received.

PRINCIPES DE LA TOMOGRAPHIE POSITRONIQUE A TEMPS DE VOL

R. CAMPAGNOLO, P. GARDERET, J. VACHEZ (Grenoble, France),
F. SOUSSALINE (Orsay, France)

Texte non parvenu.

TIME-OF-FLIGHT POSITRON EMISSION TOMOGRAPHY : DESIGNS AND REALISATIONS

M.M. TER POGOSSIAN (St Louis, U.S.A.)

Text not received.

NOUVELLES PERSPECTIVES TECHNOLOGIQUES OFFERTES PAR LA TOMOGRAPHIE POSITRONIQUE A TEMPS DE VOL

R. ALLEMAND, E. TOURNIER, M. LAVAL, J.L. LECOMTE, A. BOUVIER, P. DARIER, R. GARIOD (Grenoble, France), D. COMAR (Orsay, France) M. BOURDOISEAU, M. BARDY (Saclay, France)

Texte non parvenu.

BIOMODELIZATION OF KINETIC STUDIES WITH POSITRON EMISSION TOMOGRAPHY

J.C. DEPRESSEUX - Cyclotron Research Center - University of Liege - Sart-Tilman B30 - B 4000 LIEGE.

Positron emission tomography (PET) is characterized by four advantages as compared with single gamma emission techniques :

- higher counting efficiency;
- utilization of a number of metabolic tracers without heteroatoms;
- possibility to detect different tracers in the same efficiency and resolution conditions;
- opportunity to quantify contents of reconstructed images in terms of radioactivity per unit volume.

It nevertheless appears that all of these potential advantages are often not optimally reached, especially with the methods using a PET detection performed at equilibrium of concentration of the tracer within the tissues.

The relatively unfavourable time resolution encountered with PET in comparison with single probe detection without image reconstruction, makes that the most commonly used approach is to design methods in which a constant radioactive concentration of the tracer is reached within tissues and blood in view of performing detection at equilibrium.

For example, with $^{15}O_2$ and $C^{15}O_2$, the steady state is obtained by continuous inhalation of the indicators; with ^{82}Rb, it is reached by continuous infusion; with ^{18}FDG, it is the result of a so called tissular trapping.

In spite of the fact that PET data are unavoidably time-integrated for longer periods than with single probes or cameras, it remains that it is possible to perform sequential scans and to analyse the kinetics of indicators with appropriate numerical procedures.

Research Associate - National Fund for Scientific Research.

The purpose of this presentation is to propose a systematic overview of respective advantages and drawbacks of "kinetic" and "equilibrium" methods, in the light of concrete examples and in view to try to found the design of new methods upon a more clear insight in the "figure of merit" of the possible approaches.

"Equilibrium" VS kinetic PET strategy.

	Kinetic mode	"Equilibrium" mode
Number of computed parameters	> 1	1
Good control of input function	Good	Sometimes difficult
Repeatability	Yes	No
Time of date processing	Longer	Generally shorter
Number of slices	Limited by the one- or multislice capability of the PET	Flexible
Spatial resolution	Generally limited	Flexible
Absorbed dose to the patient	Relatively low	Relatively high

The analysis of these points is illustrated by :
- comparison of the evaluation of cerebral blood flow and oxygen uptake rate by bolus (kinetic approach) (1-2) and continuous inhalation (equilibrium approach) (3) of $C^{15}O_2$ and $^{15}O_2$
- comparison of the evaluation of cerebral glucose uptake rate using ^{18}FDG (4) and utilizing ^{11}C-glucose (5-6).

It is generally concluded that :
- The methods at "equilibrium" are to be prefered in studies where semi-quantitatively or qualitatively analyzed patterns of distribution of the parameter of interest are sufficient, with high spatial resolution, without repeatability, with maximum flexibility in the number of possible studied slices with one slice devices.
- The kinetic methods allow a multiparametric approach, with maximum accuracy and they do justify the effort being made in designing of multislice and high count rate accepting devices.

(1) S.C. HUANG, R. CARSON, M.E. PHELPS.
J. Cereb. Blood Flow Metab., 1982, 2 : 99-108.

(2) J.C. DEPRESSEUX in "Positron Emission Tomography of the Brain", HEISS and Phelps, Eds. Springer Verlag, 1983.

(3) R.S.G. FRACKOWIACK, G.L. LENZI, T. JONES, J.D. HEATHER.
J. Comput. Assist. Tomogr., 1980, 4 : 727-731.

(4) M. REIVICH, D.E. KUHL et al.
Circ. Res., 1979, 44 : 127-137.

(5) M.E. RAICHLE, K.B. LARSON et al.
Am. J. Physiol., 1975, 228 : 1936-1948.

(6) J.C. DEPRESSEUX, A. FERON et al.
Eur. Neurol., 1981, 20 : 270-272.

CLINICAL APPLICATIONS OF TIME-OF-FLIGHT POSITRON EMISSION TOMOGRAPHY

M.M. TER POGOSSIAN (St Louis, U.S.A.)

Text not received.

METHODES DE RECONSTRUCTION ET FACTEURS INTERVENANT DANS L'EXPLOITATION QUANTITATIVE EN TOMOGRAPHIE D'EMISSION GAMMA

F. SOUSSALINE (Orsay, France)

Texte non parvenu.

SINGLE PHOTON EMISSION COMPUTED TOMOGRAPHY - current status, limitations and applications

Stig A. Larsson

Dept of Hospital Physics, Karolinska Hospital,
Box 60500, S-104 01 STOCKHOLM, Sweden

Current status

Introduction. Twenty years after the first approach by Kuhl and Edwards (1), 1963, Single Photon Emission Computed Tomography - SPECT - is now emerging as a most useful diagnostic tool. Its overall impact on nuclear medicine may not yet be possible to assess, but there are already two major fields of clinical applications where the usefulness of SPECT can clearly be identified.

I. In detection and localization of accumulation defects in various organs of the human body. In these applications, *qualitative* SPECT-imaging seems to have establishing itself in recent years; both as an alternative and as a complement to conventional imaging modalities.

II. In quantitative studies of biokinetics and physiological flow, where *quantitative* SPECT-imaging may be used for accurate determination of radionuclide concentration, total radioactivity and functional volume of organs. This field of application of SPECT has not yet been as widely spread as the former, presumably due to cumbersome techniques and lack of suitable radiopharmaceuticals.

The physical and instrumental requirements on SPECT are, in principle, the same for both these fields of applications, but qualitative SPECT-imaging may frequently afford larger errors and approximations without serious loss of diagnostic accuracy.

Instrumentation. Various specially designed devices, such as the MARK-scanners (2), the HARWARD (the earlier CLEON-scanner (3)) and the J & P-scanner (4), have been developed and used clinically with good results. The currently most frequent SPECT-devices, however, are those which are based on a gamma camera on a rotation gantry. This technique was introduced and tested by the inverse situation; that is by rotating a patient in front of a fixed positioned gamma camera (5). Later on, the development continued with the design of detector devices (6-9).

The reasons for the fast and wide-spread use of SPECT with gamma cameras are that the properties and limitations of the Anger camera as well as the mathematical reconstruction principles were already wellknown. The modifications from fixed to rotating devices were quite simple to design and even large organs were possible to cover in a single examination. A serious limitation of the technique is, however, that fast dynamic studies are not possible. In addition, the current design of gamma cameras does not permit examinations of the skull and the brain with optimal performance — the shoulders of the patient does not allow rotation of the camera close to the skull.

For these reasons, new and specially designed devices have been developed, mainly for examinations of the brain — for example the SPRINT (10), the combined PET- and SPECT-unit HEADTOME (11) and the DCAT (12). The two first units have been designed for high spatial resolution, about 10 mm (FWHM) or less, while the DCAT has been designed for high sensitivity (about 20 kcounts/μCi/cm^3 with ^{133}Xe).

Rotating gamma cameras with parallel hole collimators permit a spatial resolution, varying between about 15-25 mm (at 20 cm radius of rotation). The sensitivity/section varies from around 400 to 1400 counts/μCi/cm^3 (8). The resolution, however, is greatly dependent on the radius of rotation of the gamma camera (Fig 1). By supplying the camera with a specially designed parallel slant-hole collimator (Fig 2), the spatial resolution can be improved; in the example in Fig 2 from 19 mm (FWHM) to about 15 mm without any loss of sensitivity. The disadvantage of this technique is essentially that the spatial resolution will vary from section to section but the quality of images obtained is still better than that obtained with the conventional collimators available at present.

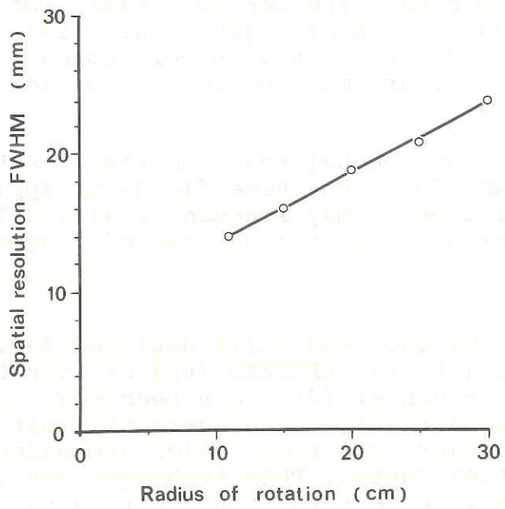

Fig 1: Spatial resolution (FWHM) as a function of the radius of rotation of the gamma camera (8).

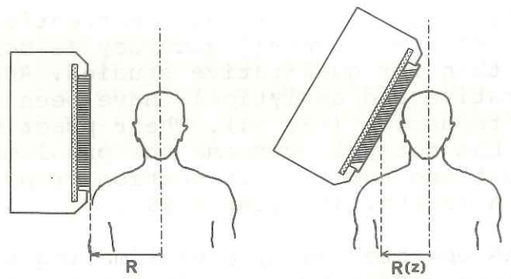

Fig 2: Examinations of the skull and the brain with rotating gamma camera. Left: With conventional parallel hole collimators. Right: With parallel slant-hole collimator (30° oblique holes).

Algorithms. Most present SPECT devices operate with algorithms which are based on back-projection of filtered projections. The filtering may be performed in the spatial or in the frequency domain as a matter of preference and the reconstruction time can be made short enough for most clinical demands. As an example (Fig 3) the reconstruction time per section of the SPECT-system (8) which we have developed at the Karolinska hospital has been decreased from about 60 to about 2.5 seconds during a 4-year period by optimizing the algorithm and by the introduction of an array-processor, MSP-3X (CDA, Boston, Mass. USA). It is therefore no need to hesitate for long initial computation times in the development of, for instance, more advanced techniques of correction for attenuated and scattered photons.

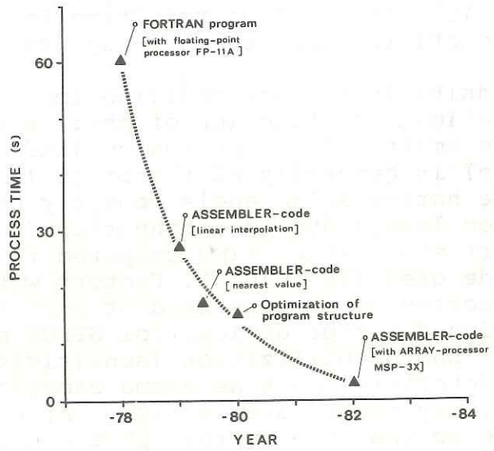

Fig 3: The reconstruction time per section during the time period from 1978-1983. Reconstruction are performed on a PDP 11/34 (Digital Eq. Corp.). Matrix size: 64 x 64 pixels.

All kinds of SPECT-applications require correction for attenuation and scatter but their overall accuracy is more critical for quantitative than for qualitative studies. Accurate algorithms, both iterative and analytical, have been developed for correction for attenuation (13, 14). Their practical implementation, however, has not yet overcome the problems of determining the body outline and the attenuation properties of the cross section in a general and simple way.

Most SPECT-systems operate now by approximating the body outline with an ellipse and assuming uniform attenuation and scatter in the section. Whether a combination of CT and SPECT images, an extra transmission scan or some predicted models of attenuation properties will be a practical solution for the future is still an open question.

Furthermore, a proper correction for attenuation can not be performed without taking into account the contribution from scattered photons. The use of semiexponential transmission curves for correction or subtraction of scatter with some approximate scatter distribution function, (in the actual plane, or in the projections) are tools which have been used and found to be convenient in combination with correction for attenuation (15, 16).

Limitations

Noise due to counting statistics remains the main limiting factor of SPECT like it is of other imaging methods in nuclear medicine. A conventional scintigram, for instance, is build up by a density of detected photons that is of the order of 10^3 per cm^2 while an x-ray image is created by a photon density of the order of 10^7- 10^8 per cm^2 thus resulting in about 100 times more noise in a scintigram than in an x-ray image.

The low photon density in nuclear medicine images is due to low photon utilization. The fraction of photons being detected out of those being emitted from the source (and contributing to the radiation dose) is generally of the order 10^{-5} to 10^{-7}. This is due to the narrow solid angle geometry of collimation (10^{-3}-10^{-4}), photon losses due to attenuation (0.3-0.5) and, in general, a short examination time compared to the life-time of the radionuclide used (10^{-1}-10^{-3}). Factors within paranthesis denote the fraction of photons used at each stage. Specially designed ring-detector devices for SPECT may have a 10-20 times higher photon utilization (sensitivity) *per section* than planar area-detectors (such as gamma cameras). The latter, on the other hand, may record events from many consecutive sections at a time so that the overall photon utilization may be of the same order for both devices in complete examinations of large organs, such as the liver/spleen, the lungs and the brain.

A rough estimate of the number of recorded events (N_T) per section in SPECT may be of the order of 10^5 to 10^7, giving a

count density (N_d) of the order of 200-5000 counts per cell (pixel). As has been shown by Budinger et al. (17) noise due to counting statistics in SPECT can not be assessed with the $N_d^{-\frac{1}{2}}$-rule as in conventional scintigrams. They therefore developed a semiemphirical, formula which takes the size of the source area n (number of resolution cells) into account:

$$\text{rms } (\%) = k \cdot 100 (n)^{3/4} (N_T)^{-\frac{1}{2}} \ldots\ldots\ldots \quad (1)$$

where k is a factor that depends on the convolution kernel used. (Budinger et al. obtained a factor k = 1.2 with their reconstruction method). Eq. (1) may be rewritten as a function of the count density N_d by dividing the total number of event N_T with the source area n (cells), which gives:

$$\text{rms } (\%) = k \cdot 100 (n)^{1/4} (N_d)^{-\frac{1}{2}} \ldots\ldots\ldots \quad (2)$$

By comparing eq. (2) with the conventional $(N_d)^{-\frac{1}{2}}$-formula, one obtains:

$$R = \frac{k\ 100\ n^{1/4}\ N_d^{-\frac{1}{2}}}{100\ N_d^{-\frac{1}{2}}} = k\ n^{1/4} \quad (3)$$

showing that the noise of SPECT dominates over that of conventional scintigraphy by a factor ($n^{1/4}$) that depends on the area of the radioactivity distribution in the section. The noise in a reconstructed section with 256 cells, for instance, will thus be about four times higher than the noise in a planar view at comparable count-density.

Despite these high noise levels which will seriously limit the ability of high spatial resolution in quantitative studies of large organs — especially in the thorax and the abdomen, their influence on image quality is reduced due to the amplification of image contrast in SPECT. The influence from noise may be further reduced in qualitative SPECT imaging — at the cost of spatial resolution — by chosing a reconstruction filter with some suitable smoothing characteristics. This is demonstrated in Fig 4, which shows the resulting noise (random uncertainty) in reconstructed sections of a 20 cm diameter circular phantom (with $^{99}Tc^m$), using different filtering (and interpolating) functions.

Other factors that may deteriorate image quality and limit the usefulness of SPECT are:

- a non-stationary target
- imperfections of the detector device
- image reconstruction from a finite number of projections and too coarse approximations in methods of correction for attenuation and scatter
- too low contrast resolution of the image display

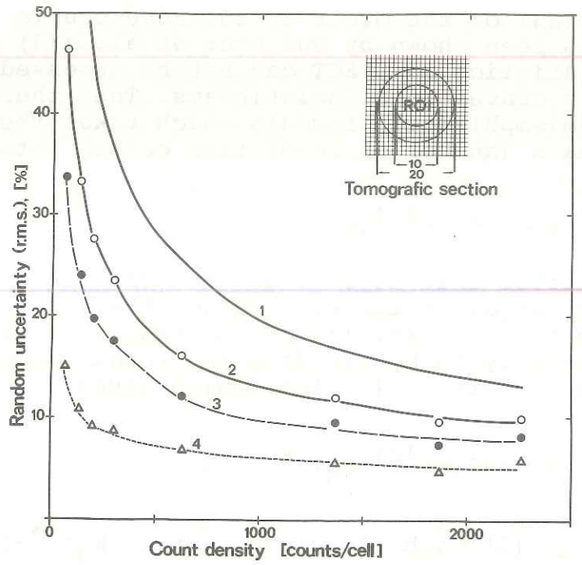

Fig 4: Noise, assessed by r.m.s. in transverse sections of a 20 cm diameter circular phantom. 1: Predicted noise from eq. (1) with k = 1.20. Curves no 2 and 3 are the results of using the Shepp-Logan filter with "nearest-value" (k = 0.70) and linear interpolation (k = 0.50), respectively. Curve no 4 was obtained using the modified version of the Shepp-Logan filter (k = 0.19).

Most of these factors must be carefully considered and whenever necessary being corrected for in order to avoid serious image artefacts. This may be illustrated by the following two examples beginning with the uniformity of the detector device, which is critical if "ring-artefacts" should be avoided (Fig 5). The effect of detector non-uniformity can be corrected for by a flood-field correction with a suitable radioactive source configuration (18) (Fig 6). The second example illustrates the importance of a correct body outline. An incorrect outline will seriously distort the images and result in erroneus quantitative values (Fig 7).

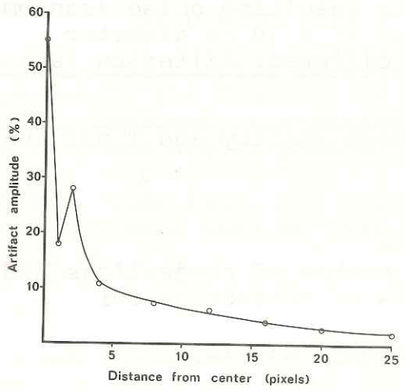

Fig 5: Positional dependence of a 2 per cent "bad ray in each view" of a simulated reconstruction.

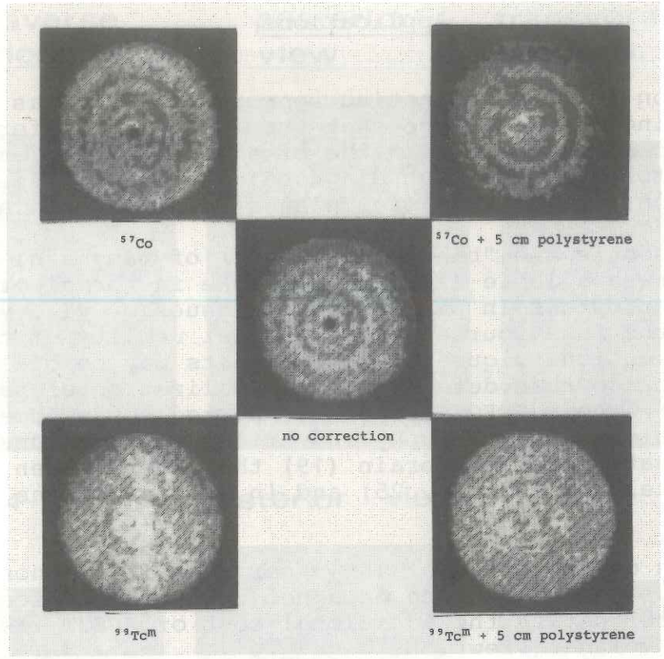

Fig 6: Reconstructed sections of a 30 cm diameter cylindrical phantom, using different flood-field source configurations for correction of the non-uniformity of a rotating gamma camera (Maxicamera II-400T, General Electric).

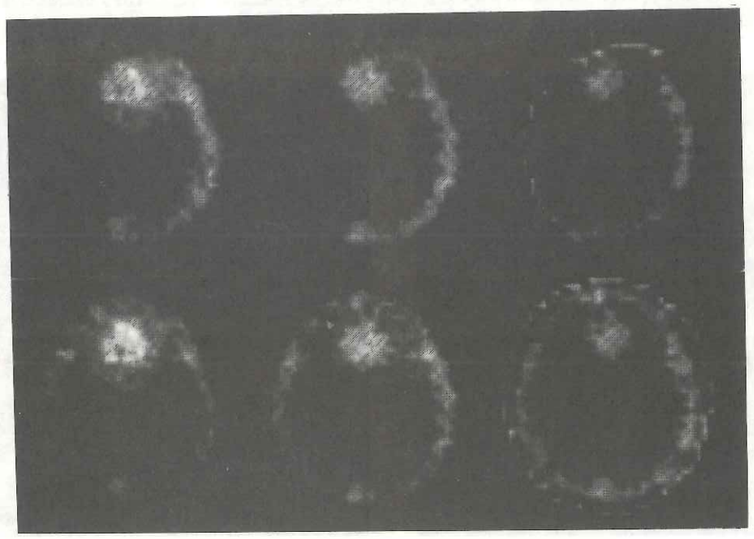

Fig 7: Transverse sections of the brain (with a frontally located meningioma) with $^{99}Tc^{m}O_4^-$. Above: Incorrect positioning of the skull outline. Below: Correct position of the elliptical outline.

Applications

A main reason for the dominating approach of SPECT as a qualitative imaging method may be that this technique offers a reasonable compromize between the often conflicting aspects on clinical simplicity and high diagnostic accuracy, especially in comparison with conventional planar imaging techniques.

Another reason is the "binary" behaviour of many radiopharmaceuticals now available (i.e. high uptake in normal organ tissue and no uptake in pathological tissues or vice versa). Because of the behaviour and the clinical utility of these radiopharmaceuticals, quantitative aspects may be of less clinical importance than detection and localization of pathological findings, where SPECT has been reported to be superior over conventional scintigraphy in various applications, such as in examinations of the brain (19) the liver/spleen (20, 21, 22) skull skeleton (23, 24, 25) and in studies of the myocardium (26).

Improvements of the order of 10-15 per cent in diagnostic accuracy have generally been obtained in these application and this may well justify the additional cost of SPECT instead of conventional planar views.

The growing field of qualitative SPECT imaging may be illustrated by two recent clinical applications when the SPECT technique has been optimized with respect to high resolution — in studies of liquor circulation and the liquor space of the brain (27), Fig 8, utilizing a slant-hole collimator (see previous text) and in studies of patients with ankylosing spondylitis of the spine (28) using a parallel hole high resolution collimator (Fig 9).

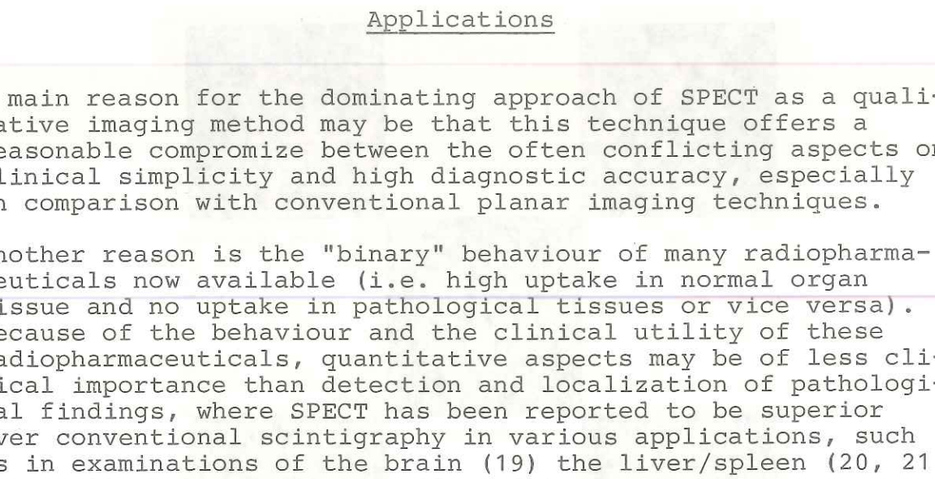

Fig 8: Cisternography with SPECT using 100 MBq $^{99}Tc^{m}$-DTPA. Left: 4 consecutive sections of a normal case. Right: Pathological case with intra-ventricular distribution of the radiopharmaceutical (arrows in section 17).

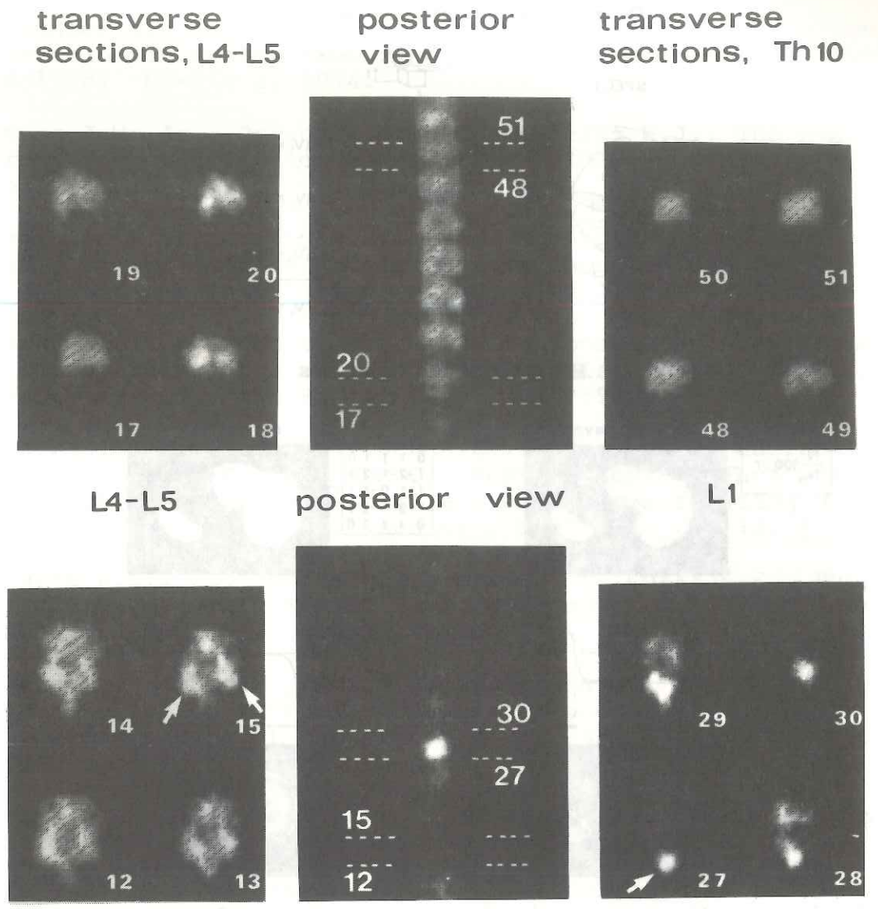

Fig 9: SPECT examinations of the spine with 350 MBq $^{99}Tc^{m}$-MDP. Above: Normal case. Below: High uptake of the interverebral joints in section 15 to the left (arrows) and of the spinous process at L1 (section 27 to the right). The latter uptake is also seen on the posterior view.

The second utility of SPECT, as a measuring device, has not been as widely spread as the former; one reason being a more cumbersome examination technique but another main reason being the lack of suitable radiopharmaceuticals. The potential of SPECT for quantitative measurements of the brain, however, has been documented in, for instance, quantitative assessments of regional brain blood-flow using ^{123}I-amphetamine (29). Quantitative studies has also been performed for determination of the functional organ volume (30, 31), (Fig 10).

However, with synthesis of new suitable radiopharmaceuticals and further development of instrumentation and algorithms, quantitative SPECT imaging is believed to be the most important field of application for the future.

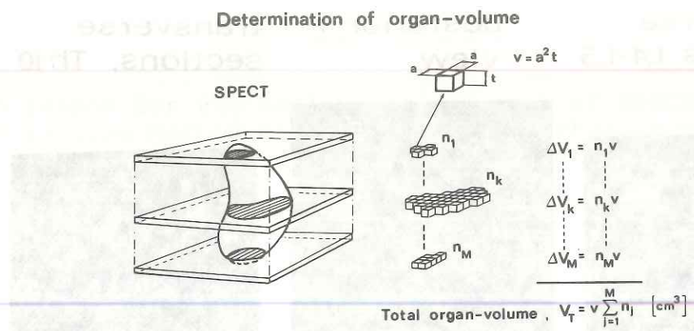

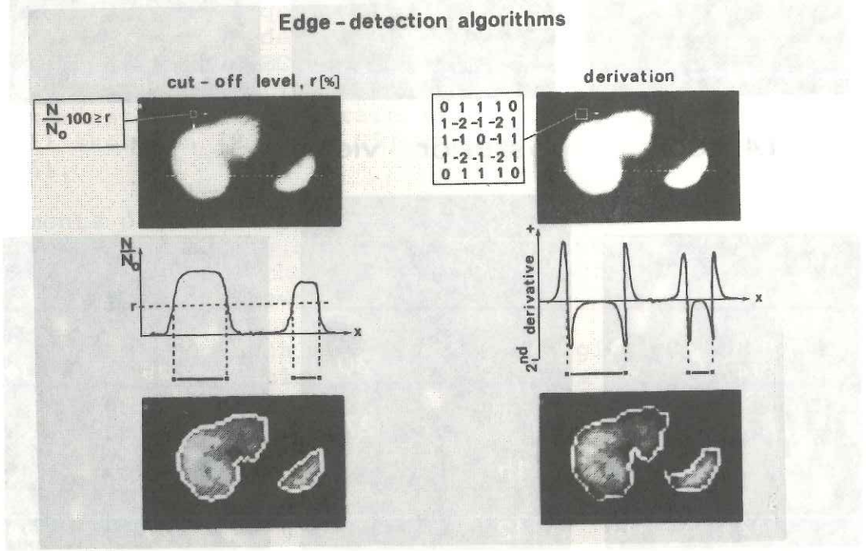

Fig 10: Above: The principle for quantitative determination of the functional volume of organs from a set of consecutive SPECT-sections. Below: Alternative algorithms for assessment of the sectional organ size by edge detection.

References

1. Kuhl D.E. and Edwards R.Q.: Image separation radioisotope scanning. Radiol 4: 653, 1963.

2. Kuhl D.E., Edwards R.Q., Ricci A.R., A.B., Yacob R.I., Mich T.I. and Alavi A.: The MARK IV system for radionuclide computed tomography of the brain. Radiol 121: 405, 1976.

3. Stoddart H.F. and Stoddart H.A.: A new development in single gamma transaxial tomography. Union Carbide focused collimator scanner. IEEE Trans Nucl Sci NS-26: 2710, 1979.

4. Bowley A.R., Taylor C.G. and Causer D.A.: A radioisotope scanner for rectilinear, arc, transverse section and longitudinal section scanning: (ASS - the Aberdeen Section Scanner). Br J Radiol 46: 262, 1973.

5. Budinger T.F. and Gullberg G.T.: Three-dimensional reconstruction in nuclear medicine emission imaging. IEEE Trans Nucl Sci NS-21: 2, 1974.

6. Keyes J.W. Jr., Orlandea N. and Heetderks W.J.: The Humongotron - a scintillation camera transaxial tomograph. J Nucl Med 18: 381, 1977.

7. Jaszczak R.J., Murphy P.H., Huard D. and Burdine I.A.: Radionuclide emission computed tomography of the head with $^{99}Tc^{m}$ and a scintillation camera. J Nucl Med 4: 373, 1977.

8. Larsson S.A.: Gamma camera emission tomography. Development and properties of a multi-sectional emission computed tomography system. Acta Radiol Suppl 363, 1980.

9. Soussaline F., Todd-Pokropek A.E., Zurowski S., Huffer E., Raynaud C. and Kellershohn C.: Physical performances of an emission computed tomography system using a rotating conventional gamma camera. (Abstr) J Nucl Med 21: 16, 1980.

10. Rogers W.L., Clinthorne N.H., Stamos J., Koral K.F., Knoll G. and Keyes J.W.: SPRINT: A single photon ring tomograph. (Abstr) J Nucl Med 5: 59, 1982.

11. Kanno I., Vemure K., Minra S. and Minra Y.: HEADTOME: A hybrid emission tomograph for single photon and positron emission imaging of the brain. J Comp Ass Tomogr 5: 216, 1981.

12. Stokely E.M., Sveinsdottir E., Lassen N.A. et al.: A single photon dynamic computer assisted tomograph (DCAT) for imaging brain function in multiple cross sections. Comp Assist Tomogr 4: 230, 1980.

13. Budinger T.F. and Gullberg G.T.: Transverse section reconstruction of gamma-ray emitting radionuclides in patients. In: Reconstruction Tomography in Diagnostic Radiology and Nuclear Medicine, p. 315. University Park Press, 1977.

14. Moore S.C., Brunelle J.A. and Kirsch C.-M.: Quantitative multi-detector emission computerized tomography using iterative attenuation compensation. J Nucl Med 23: 706, 1982.

15. Tsui B.W.T., Chen C.T., Yasillo N.J. et al.: A whole-body scanning system for collection of quantitative in vivo distribution data in humans: 3rd Int Radiopharmaceutic Dosimetry symp., Oak Ridg, Tenn. HHS-publ. FDA 81-8186, BRH, 1980.

16. Bergström M.: Performance evaluation and improvements of quantification accuracy in transmission and positron emission computer assisted tomography. Diss. Stockholm 1982, ISBN 91-7146-202-3.

17. Budinger T.F., Derenzo S.E., Greenberg W.L., Gullberg G.T. and Huesman R.H.: Quantitative potentials of dynamic emission computed tomography. J Nucl Med 3: 309, 1978.

18. Axelsson B., Israelsson A. and Larsson S.: A method for correction of gamma camera non-uniformity in singel-photon emission computed tomography. Radioactive Isotope in Klinik und Forschung 15: (teil 2), 519, 1982.

19. Carril J.M., Mac Donald A.F., Dendy P.P., Keyes W.I., Undrill P.E. and Mallard J.R.: Cranical scintigraphy: Value of adding emission computed tomographic sections to conventional pertechnetate images (512 cases). J Nucl Med 20: 1117, 1979.

20. Israelsson A., Lagergren C., Larsson S. and Lundell G.: Detection of space occupying lesions of the liver and spleen: A comparison of computed emission reconstructive tomography and conventional gamma camera scintigraphy. BRH-publ (FDA 81-8177), 171, 1981.

21. Raynaud C., Syrota A., Soussaline F., Todd-Pokropek A. and Kellershohn C.: Single photon emission tomography in diagnosis of liver metastases. J Nucl Med 22: 31, 1981.

22. Strauss L., Bostel F., Clorius J.H., Rapton E., Wellman H. and Georgi P.: Single photon emission computed tomography (SPECT) for assessment of hepatic lesions. J Nucl Med 23: 1059, 1982.

23. Brown L.B., Keyes J.W., Leonard P.F., Thrall I.H. and Kircos L.T.: Facial bone scanning by emission tomography. J Nucl Med 18: 1184, 1977.

24. Ell P.J. and Kahn O.: Emission computerized tomography: Clinical applications. Sem Nucl Med 11: 50, 1981.

25. Bergstedt H., Israelsson A., Larsson S. and Lind M.: Computerized emission tomography of the facial skeleton and skull base. BRH-publ (FDA 81-8177), 177, 1981.

26. Maublant J., Cassagnes J.J., Le Jenne D., Mestas D., Veyre A., Jallut H., Meyniel G.: A comparison between conventional scintigraphy and emission tomography with Thallium-201 in the detection of myocardial infarction: Concise communication. J Nucl Med 23: 204, 1982.

27. Bergstrand G., Larsson S., Bergström M., Eriksson L. and Edner G.: Single photon emission tomography and positron emission tomography in the evaluation of CSF-circulation. To appear in Am J Neurorad (May-June) 1983.

28. Jacobsson H., Larsson S., Vestersköld L. and Lindvall N.: Detection of ankylosing spondylitis in the spine by single photon emission computed tomography - SPECT. Submitted to Brit J Radiol (1983).

29. Kuhl D.E., Barrio J.R., Huang S.-C., Selin C., Ackerman R.F., Lear J.L., Wu L., Lin T.H. and Phelps M.E.; Quantifying local cerebral blood flow by N-isopropyl-P(^{123}I)--iodoamphetamine (IMP) tomography. J Nucl Med 23: 196, 1982.

30. Kan M.K. and Hopkins G.B.: Measurement of liver volume by emission computed tomography. J Nucl Med 20: 514, 1979.

31. Tauxe W.N., Soussaline F., Todd-Pokropek A., Cao A., Collard P., Richard S., Raynaud C. and Itti R.: Determination of organ volume by single-photon emission tomography. J Nucl Med 23: 984, 1982.

ETUDE DU BRUIT STATISTIQUE EN TOMOGRAPHIE D'EMISSION GAMMA

F. AUBRY, R. DI PAOLA (Villejuif, France)

Texte non parvenu.

NEW TECHNICAL DEVELOPMENTS IN ECT

G. VAN OORTMARSSEN (Uithoorn, the Netherlands)

Text not received.

AN IMPROVEMENT STOCHASTIC RECONSTRUCTION TECHNIQUE FOR TOMOGRAPHIC IMAGING

F. VERMEULEN (Ghent, Belgium)

Text not received.

COMPARISON OF SPECT RESULTS WITH ELLIPTIC ROTATING CAMERA AND ROTATING SLANT HOLE COLLIMATOR

P. BLOCKX, F. VAN DE VIJVER (Antwerpen, Belgium)

Text not received.

APPLICATIONS TOMOGRAPHIQUES DE L'ISOPROPYL IODO AMPHETAMINE I 123 (AMP I 123) EN PATHOLOGIE CEREBRO VASCULAIRE

J.L. MORETTI°, S. ASKIENAZY°°, C. RAYNAUD°°°, P. CESARO°,
J. RAPIN°°°°, A. BARDY*

Les investigations neuroradiologiques conventionnelles ne permettent pas de réaliser l'image du flux sanguin cérébral qui est pourtant le facteur pathogénique essentiel des affections cérébrovasculaires. La tomodensitométrie X (TDM) permet seulement devant un accident vasculaire cérébral constitué de mettre en évidence une hémorragie intraparenchymateuse spontanément hyperdense et de préciser après la 48ème heure la topographie du territoire infarci hypodense avec sa réaction oedemateuse. Les régions de bas débit critiques ne sont malheureusement pas décelables par le TDM.

Une autre approche tomographique utilisant une méthodologie différente présente un intérêt en pathologie ischémique cérébrale: l'application de traceurs positroniques (1, 2) se distribuant selon le flux régional cérébral tel le Co_2 marqué à l'oxygène 15. Cette technique relativement sophistiquée n'est en fait que du domaine de la pharmacologie clinique de recherche avancée et difficilement applicable au diagnostic en routine. Par contre la tomographie d'émission moins onéreuse réalisée avec des traceurs γ permet d'approcher le débit sanguin régional avec une résolution spatiale de 1.7 cm. Deux techniques et philosophies concurrentes sont applicables. La première utilise une machine spécifique pour la tête, elle est très sensible mais ne donne que 3 coupes axiales transverses du flux cérébral (3, 4), la deuxième utilise une gamma caméra rotative de moins bonne sensibilité, donne des coupes selon les 3 axes de l'espace au prix d'un examen beaucoup plus long. La première méthode utilise un système rotatif rapide de forme carré composé de 64 NaI permettant de suivre sur les 3 coupes tomographiques de 2 cm d'épaisseur les courbes locales de désaturation du Xenon 133 (4). La deuxième méthode utilise un traceur diffusible (5 - 8) non gazeux l'AMP I 123 dont l'extraction est voisine de 100% lors du premier passage dans le cerveau (5,9). L'étude autoradiographique effectuée chez le rat WISTAR démontra que la distribution

initiale représentant le débit sanguin avec des redistributions de faible amplitude durant la première heure (9) KUHL (10) démontra la corrélation de la fixation cérébrale de l'AMP I 123 au débit sanguin, il nota cependant un phénomène d'échappement aux flux élevés. LASSEN (11) démontra la concordance de la distribution de l'activité du Xenon 133 et de l'AMP I 123 immédiatement après l'injection chez des sujets atteints de neuropathies diverses, parmi lesquels les affections cérébrovasculaires étaient bien représentées.

L'objet de notre étude a été de vérifier en premier lieu la fiabilité diagnostique de l'AMP I 123 en pathologie ischémique cérébrale et dans un deuxième stade de déceler des zones ischémiques peu "parlantes" en tomodensitométrie.

PATIENTS

Une série de 23 patients, 16 hommes d'âge moyen de 62 ans, 7 femmes d'âge moyen de 53,5 ans a été incluse dans cette étude. Douze de ces patients ont été explorés au decours d'un accident cérébral constitué non regressif dont huit au niveau du territoire carotidien. Neuf autres patients ont subi l'examen au decours d'un accident arétiel cérébral régressant nettement entre 2 et 8 jours. Un patient était porteur d'une atrophie cérébrale avec un état multilacunaire et une autre présentait une c omitialité généralisée en rapport avec une occlusion carotidienne. Chacun de ces patients a subi un examen TDM avec un délai moyen de 20 jours après l'accident l'examen scintigraphique a été réalisé en moyenne à J 27.

METHODES

Préparation de l'AMP I 123

Le marquage de l'isopropyl iodo amphetamine fut effectué par échange entre de l'Iode 123 produit soit par irradiation de l'iode 127

(reaction p.5n) soit du Tellure 124 (reaction p. 2n) et l'iode stable placé en position para de la molécule. Le procédé de marquage (8) utilise un produit lyophylisé (10 mg AMPI + 1 mg $CuSO_4$) auquel est rajouté 5 mCi d'iode 123 en tampon Acetate de sodium (pH:3.6)*. L'échange est obtenu par chauffage à 130°C pendant 40 Minutes. Le résidu sec est repris par une solution saline permettant l'isotonicité de la préparation. Un contrôle chromatographique utilisant un gel de silice (60 F 254) et un solvant Methanol, Chloroforme, Acide acétique 85: 15: 1 a permis de constater un rendement de marquage égale à 98.13 $\pm$ 0.88%. (n = 12)

Exploration

Les deux gamma caméras tournantes utilisées furent des ACTICAMERAS 3400** informatisée l'une par un SIMIS 3*** et l'autre par un IMAC **. L'injection intraveineuse des patients fut effectuée sans contrôle d'ambiance particulier, avec une dose moyenne de 5 mCi pour 10 mg d'AMP. L'examen tomographique fut effectué après une attente de 20 Minutes, selon 64 projections, dura en moyenne 40 minutes pour accumuler 5 Millions d'impulsions. Les projections initiales en 64x64 furent soit simplement soustraite du bruit de fond° soit traitée par un filtre de WIENER°° avant d'être retroproje tées grâce à un filtre rampe. Une rotation du volume reconstruit fut effectué par interpolation pour rendre les coupes transverses parallèles à la ligne orbitomeatale dans les cas de deflexion antérieure insuffisante de la tête°. Dans l'un des centres° où cette étude coopérative fut menée, une compensation de l'attenuation fut appliquée sur les tomographies transverses, la méthode de CHANG (12) à μ constant. Chaque tomographie présentée possède une profondeur de mémoire égale à 2 éléments d'image élémentaires (pixels) soit 12 mm.

RESULTATS

Chez les 23 patients explorés fut remarquée une fixation pulmonaire et hépatique importante dont la cinétique est rapportée ailleurs (8). Les résultats sont résumés dans le tableau ci-après.

Les résultats sont résumés dans le tableau ci-après.

TYPE DE PATHOLOGIE	RESULTATS du T D M	RESULTATS de l'AMP I 123	DEFICITS NEURO-LOGIQUES	DIASCHISIS CEREBELLEUX
Accident artériel cérébral régressif à TDM Normal **3 cas**	N	1 normal	Aphasie transitoire	O
		1 foyer hypoactif parietal D	hemiparesie G sensitivo motrice	O
		1 foyer frontal gauche	Hemiparesie droite	O
Occulsion carotidienne unilatérale **1 cas**	N	1 hypoactivité fronto-parietal Gauche	Syncope	O
Accident artériel cérébral régressif avec TDM anormal **6 cas**	Lacune capsulaire interne gauche	hypoactivité parietale gauche	hemiplegie droite avec aphasie	O
	Foyer hypodense temporal gauche	hyperactivité temporo parietale gauche	paralysie faciale droite +aphasie	O
	lacune capsulaire G. foyer hypodense sylvien G.	hypoactivité parietal G	hemiplegie droite	O
	lacune capsulaire G.	hypoactivité frontale G.	hemiplegie droite + aphasie	O
	foyer hyperdense frontal G	hypoactivité rolandique G	Hemiplegie D + aphasie	+
	lacune capsulaire Gauche	hypoactivité parietale G	Hemiplegie D sensitivomotrice	+

TYPE DE PATHOLOGIE	RESULTATS du TDM	RESULTATS de l'AMP I 123	RESULTATS NEURO-LOGIQUE	DIASCHISIS CERE-BELLEUX
Accident artériel cérébral non regressif **13 cas** 9 carotides	hypodensité du territoire cérébrale AntG	hypoactivité fronto parietale G	hemiplegie D aphasie	+
	hypodensité fronto temporale G.	hypoactivité parieto temporale G	hemiplegie D Aphasie	+
	hypodensité du territoire sylvien G	hypoactivité fronto parietal G.	hemiplegie D Aphasie	+
	hypodensité sylvienne G	hypoactivité fronto parietal G = frontal D	hemiplegie D aphasie, occlusion carot G stenose Carot D	+
	hypodensité sylvienne G	hypoactivité fronto parietal G	hemiplegie D Aphasie	+
	hypodensité sylvienne D	hypoactivité frontale D	hemiplegie G+ Σ frontal	O
	hypodensité temporale G	Hypoactivité fronto parietale G	hemiplegie D + aphasie	O
	hypodensité temporoccipital G	hypoactivité parieto occipital G	aphasie	O
	hypodensité parietale D et frontal G	hypoactivité parietale D et frontal G	hemiplegie D + aphasie	O
3 vertebro basilaires	hyperdensité occipitale G	hypoactivité parieto occipitale G + Hemicervelet D	hemiparesie D + syndrome cerebelleux D	O
	hypodensité cerebelleuse G	hypoactivité cerebelleuseG	syndrome cerebelleux G	O
	Hypodensité cerebelleuse G	hypoactivité cerebelleuseG	syndrome cere-cerebelleux G	O
1 diffus	Atrophie cerebrale + lacunes multiples	dilatation ventriculaire hypoactivité frontal G temporal D occipital D protuberance	cecite corticale paralysie faciale D confusion	O

DISCUSSION

Dans cette étude toutes les images focales d'hypodensité ou d'hyperdensité avec accumulation du produit de contraste visibles en tomodensitométrie ont été clairement mises en évidence par la tomographie d'émission à l'AMP I 123 sous forme de zones d'hypoactivité suivant les 3 dimensions de l'espace. Dans la majorité des cas, l'étendue de l'hypoactivité était supérieure à celle de l'hypodensité.

Chez deux patients, ayant présenté un accident ischémique, l'un en rapport avec une artherosclerose, l'autre en rapport avec un mécanisme migraineux, l'examen TDM était strictement normal, la tomoscintigraphie décela des zones d'hypoactivité en relation avec leur déficit neurologique.

Chez un patient ayant présenté un accident ischémique intéressant le territoire sylvien gauche au TDM; l'examen tomoscintigraphique mit en évidence en plus de cette zone hyperactive, hypodense, d'autres dans le même hemisphère et dans l'hemisphere controlateral qui correspondaient à des foyers trouvés hyperactifs à la scintigraphie au pyrophosphate de Tc 99m.

Chez deux patients atteints l'un d'une occlusion carrotidienne gauche, l'autre d'une stenose serrrée carotidienne avec un ramollissement controlateral, l'examen TDM fut défaillant pour mettre en évidence les zones hypoactives montrées par la tomoscintigraphie au niveau du territoire carotidien gauche chez le premier malade et dans le territoire frontal situé en aval de la stenose carotidienne du second.

Chez 50 % de nos patients il fut mis en évidence une hypoactivité cérebelleuse controlaterale à l'accident ischémique hemispherique. Le diaschisis cerebelleux (13) était déja bien connu des explorations utilisant les émetteurs de positrons.

CONCLUSION

L'étude de cette série de patients atteints d'une pathologie cérébrale ischémique a montré que la tomoscintigraphie réalisée avec l'AMP I 123 possède une sensibilité égale à celle de la tomodensitométrie sur des foyers connus de celle ci malgrè une moins bonne résolution spatiale.

Par rapport à un examen tomodensitométrique normal la tomographie réalisée avec ce traceur hautement extractible qu'est l'AMP I 123 met en évidence :

- des anomalies fonctionnelles dont le diaschisis cerebelleux est le meilleur exemple.

- des anomales hemodynamiques en relation avec des stenoses arterielles.

Notre attention se porte actuellement sur l'étude des accidents ischémiques transitoires ou constitués et rapidement regressifs sans sequelles.

° Departement Neuro-Sciences Medicales Hôpital Henri Mondor 94000 CRETEIL
°° Departement d'imagerie Hôpital Sainte Anne 75674 PARIS
°°° Service Frédéric Joliot Centre Hospitalier d'Orsay 91406 ORSAY
°°°° Service de Neurophysiologice Centre Hospitalier St Antoine 75012 PARIS
* ORIS CEN 91191 SACLAY
** CGR Médecine Nucléaire 91 BUC
*** INFORMATEK Zone de Courtaboeuf 91190 GIF S/YVETTE

BIBLIOGRAPHIE

1. CELSIS P., GOLDMAN T., HENRIKSEN L., LASSEN N.A. - A method for calculation regional cerebral blood flow from emission computed tomography of inert gas concentrations. J. Comput. Assist. Tomogr. 1981,5, 641-645

2. JONES T., CHESLER D.A., TER POGOSSIAN M.M. - The continuous inhalation of oxygen 15 for assessing regional oxygen extraction in the brain of man. Brit. J. Radiol. 1976, 49, 339-343.

3. STOKELY E.M., SVEINSDOTTIR E., LASSEN N.A., ROMMER P. - A single photon dynamic computer assisted tomograph (DCAT) for imaging brain function in multiple cross sections. J. Comput. Assist. Tomogr. 1980, 4, 230-240.

4. LASSEN N.A., HENRIKSEN L., PAULSON O.B. - Regional cerebral blood flow in stroke by 133 xenon inhalation using emission tomography. Stroke, 1981, 12, 284-288.

5. WINCHELL H.S., BALDWIN R.M., LIN T.H. - Development of I 123 labeled amines for brain studies: localization of I 123 iodophenylalkyl amines in rat brain. J. NuclMed 1980, 21, 940-946.

6. WINCHELL H.S., HORST W.D., BRAUN L., OLDENDORF W.H., HATTNER R., PARKER H. - N-isopropyl (^{123}I) p-iodoamphetamine: single pass brain uptake and washout; binding to brain synaptosomes; and localization in dog and monkey brain. J. Nucl. Med. 1980, 21, 947-952.

7. HILL T.C., HOLMAN B.L., LOVETT R., O'LEARY D., FRONT D., MAGISTRETTI P., ZIMMERMAN R.E., MOORE S., CLOUSE M.E., WU J.L., LIN T.H., BALDWIN R.M. - Initial experience with SPECT (single photon computerized tomography) of the brain using N-Isopropyl I-123-p-iodoamphetamine: concise communication. J. Nucl. Med. 1982, 23, 191-195.

8. J.L. MORETTI, S. ASKIENAZY, C. RAYNAUD,N.A. LASSEN, E. SANABRIA, Cl. DESPLANCHES, J.R. RAPIN, P. CESARO, Cl. MARSAULT, J. BARBIZET, Y. KERAVEL, D. FREDY. - La N-Isopropyl P iodoamphetamine I 123 en tomoscintigraphie cérébrale. Annales de Radiologie VOl 26, 1983 n° 1,59-67.

9. J.R. RAPIN, D. DUTERTE, M. LE PONCIN LAFITTE, S. COORNAERT, G. DESPLANCHES, A. BARDY, S. ASKIENAZY, J.L. MORETTI, C. RAYNAUD.- Aspects chimique et pharmacologique des traceurs cellulaires cérébraux. Annales de radiologie 1983, Vol.26 n° 1, 48-52.

10. KUHL D.E., BARRIO J.R., HUANG S.C., SELIN C., ACKERMANN R.F., LEAR J.L., WU J.L., LIN T.H., PHELPS M.E. - Quantifying local cerebral blood flow by N-isopropyl p (123 I) iodoamphetamine (IMP) tomography. J. Nucl Med 1982, 23, 196-203.

11. LASSEN N.A., HENRIKSEN L., HOLM S., BARRY D.I., PAULSON O.B. VORSTRUP S., RAPIN J.R., LE PONCIN LAFITTE M., MORETTI J.L., ASKIENAZY S., RAYNAUD C. - Cerebral blood flow tomography Xenon 133 compared to isopropyl amphetamine iodine 123. J. Nucl Med 1983, 24,17-24

12. CHANG L.T. - A method for attenuation correction in radionucleide computed tomography IEEE Transaction on Nuclear Science NS 25:1978,638-643.

13. BARON J.C., BOUSSER M.G., COMAR D., CASTAIGNE P.- Crossed cerebellar diaschisis in human supratentorial brain infarction. Trans Am. Neurol. Ass. 1980, 105, 459-461.

Neurological Applications of Positron Emission Tomography

R.S.J. Frackowiak, MA, MD, MRCP

MRC Cyclotron Unit, Hammersmith Hospital,
National Hospital for Nervous Diseases, Queen Square

The investigation of cerebral function with positron tomography (PET) has expanded rapidly since the introduction of quantitative and commercially available, reliable tomographs. At present the fields of endeavour may be divided into:

(a) the study of normal cerebral function and its modification from the resting state by various physiological stimuli[9,29]

(b) the study of cerebral pathophysiology[9,29].

The second of these fields has been retarded by the slow development of appropriate physiological tracers and models to describe their distribution in the brain in disease. To some extent this has meant that considerable emphasis has been placed on the imaging characteristics of PET and the insights they provide in predominantly focal disease, at the expense of the quantitative potential of this technique. This pattern is being reversed as the technological advances occur. There is a considerable and continuing development in the capabilities of the hardware required for performing PET studies. Multislice tomographs with improved sensitivities and resolution and lower noise have been and continue to be produced. Furthermore as greater experience is obtained with the techniques and as the capabilities and limitations are becoming clearer, more complex problems are now coming under study.

Normal brain

The normal brain has been studied with the fluorodeoxyglucose technique[27,32] and the steady state oxygen inhalation method[13,21). A question of continuing interest is the metabolic state of the brain during normal ageing and whether this sheds any light on the process of senile dementia or the pathogenesis of cerebrovascular disease. Kuhl has recently reported and reviewed on studies of ageing[19]. Measurement of cerebral glucose and oxygen consumption have been compared. Oxygen consumption appears to decline little if at all in normal ageing whereas there may be a small, steady and significant decline in glucose

consumption. This would suggest that the ageing brain to some extent utilises other substrates than glucose for energy production. However, a more recent report (still in press) from NIH seems to confirm the NINCDS studies from the 1960's in which no decline in cerebral glucose metabolism was observed in "supernormal" aged subjects when compared with normal young volunteers[31]. Whether the decline observed by Kuhl et al is real needs further study, probably by measurement of $CMRO_2$ and CRMGlu concurrently in the same normal population. This is now a feasible venture using PET[6,30,34].

The work of Phelps and Mazziotta has attempted to investigate the metabolic substrate of neuropsychological and neurobehavioural functions in normal man[24]. Throughout these studies the Sokoloff deoxyglucose model has been used[27]. This would seem to be a valid approach in view of the biochemical integrity of the tissue under study and the ready applicability of the model assumptions to such brain. The cerebral metabolic responses to verbal and non verbal auditory[2], simple and complex visual stimuli[28] and to sensory deprivation[25] have been investigated and specific changes from the normal resting pattern of metabolism have been demonstrated. These studies have been quantified in relative terms thus far, usually by a left-right ratio or a ratio of a given region to the hemispheric mean. Though such analysis is highly indicative of relative alterations in metabolic function, similar studies with quantitation of cerebral metabolic rates in absolute units is awaited to unravel more complex inter-relations between higher cerebral functions. Of particular interest in this respect is the demonstration by Mazziotta et al of a progressive decrease in mean CMRGlu with progressive sensory deprivation[25]. A most striking example of the power of PET as an investigative tool, even in a semiquantitative mode, is provided by the experiments of Phelps et al[28] who demonstrated a progressive increase in CMRGlu of the occipital cortex from patients with homonymous hemianopsia to subjects with eyes closed, exposed to white light, checkerboard stimulation of one eye and two eyes and finally visualisation of a complex scene.

In the auditory system Reivich and Alavi and coworkers have demonstrated unilateral changes of metabolism of glucose of significant proportions in subjects given various aural stimuli[2]. The topography of increased CMRGlu altered depending on the nature, complexity and intelligibility of the stimulus. Similar correlations with musical

stimuli have been shown by Mazziotta[26] who demonstrated an apparent topographical difference in cerebral metabolic response dependent on the strategy of analysis of a given musical sequence adopted by the subject. Thus the use of the deoxyglucose model in normal man, and the investigation of alterations of cerebral metabolic patterns quantitatively, opens a new perspective to neuropsychology as it attempts to further analyse the mechanisms underlying complex higher cerebral function in man.

Pathology

In pathology, investigation is most hampered by the techniques available. Oxygen extraction, consumption and blood flow can be measured using the steady state oxygen-15 technique. This method uses water as the traced molecule[13]. The behaviour of this probe can be predicted with considerable confidence in normal and abnormal tissue, so the application of this technique to neurological conditions such as stroke, extracerebral vascular occlusion, gliomas and other cerebral tumours has been extensive[9,29]. Cerebral blood volume can readily be measured using ^{11}C labelled carbon monoxide[16] and has been used in the investigation of cerebral trauma, subarachnoid haemorrhage and carotid occlusions[15].

The deoxyglucose model runs into serious problems because it measures glucose metabolism with reference to the rate of the hexokinase reaction and so reflects glycolytic rather than oxidative rates. In situations of enhanced anaerobic glycolysis or diversion of glucose into catabolic pathways, the CMRGlu will not faithfully reflect energy metabolism in the way that oxygen consumption will. Of considerable interest in this respect would be combined measurements of cerebral oxygen and glucose consumption which would give the stoichiometric relationship between the two and potentially permit quantitation of aerobic and anaerobic energy production[6,30,34].

The second problem however resides in the applicability of the glucose model to pathological tissue in general. Certainly any process interfering with normal transport of glucose and ^{18}FDG across the blood brain barrier might so interfere with the basic assumptions underlying the model that results would have to be viewed with a great deal of circumspection.

Stroke

Stroke has been studied by a number of investigators with the ^{15}O technique and ^{18}FDG. Kuhl's group reported observations using $^{13}NH_3$ as a flow marker[18]. Subsequent studies have shown this to be an unsatisfactory way of looking at flow. However their observation of uncoupling of flow and metabolism in patients who have suffered stroke has also been the experience of the Massachussets General[1] Orsay[3] and Hammersmith groups using ^{15}O[23].

The natural history and pathophysiology of human cerebral infarction has now been elucidated in vivo. The work of Wise et al[33] demonstrates that increased oxygen extraction, characterising ischaemia or a grossly impaired perfusion reserve, is invariable in the first phase following the ictus. This lasts from a few to forty eight hours at most, in the vast majority of cases and is superceded within 24 to 48 hours by a low oxygen extraction indicating adequate perfusion of the infarcted region. The time course of ischaemia is thus short. Established infarction can be characterised in the early days after stroke as a tissue with low oxygen consumption indicating compromised metabolism and a depressed oxygen extraction. This indicates that despite the delivery of oxygen to the affected tissue it is not being extracted and is finding its way into the venous effluent. A decreased oxygen extraction can occur in the context of a low, normal or high cerebral perfusion in absolute terms and the absolute level does not matter as long as the oxygen consumption is depressed proportionally more. Ackerman[1] has shown that at or before day 5 and after day 10 high absolute flows can be seen in such tissue and suggested this might have prognostic significance, although it probably only reflects a greater or lesser degree of reflow and/or neovascularisation through the infarct. Lenzi[23] has demonstrated that certain levels of oxygen consumption appear to be invariably associated with lack of recovery of tissue. This appears to be the metabolic counterpart of the ischaemic threshold of CBF studies. Baron[4] has demonstrated that with time the oxygen extraction gradually normalises, especially if the infarct has been small. The time course of this recoupling between blood flow and metabolism is long, normalisation usually occurring after a month.

Larger infarcts can remain uncoupled but always with a low oxygen extraction. Studies of patients with infarcts have also shown remote effects of the acute ischaemic insult. Depression of metabolism globally correlates with conscious level. There are effects on the contralateral cerebral hemisphere and of possible prognostic significance in terms of rehabilitation, depression of metabolism in the contralateral cerebellar cortex has been demonstrated[4,23]. This latter effect may be due to interruption of cerebro cerebellar pathways or possibly a decline in afferent sensory traffic from a hemiparetic limb.

Some attempts at therapy in the earliest truely ischaemic phase in stroke have commenced. It is self evident that an objective and quantitative technique such as PET affords an ideal tool for monitoring the effects of therapy directly, thus obviating the need for large and costly therapeutic trials in the screening of new and rational forms of treatment[5,22].

More recently the consumption of glucose and oxygen, as well as blood flow and volume have been measured in stroke patients in the phase of established infarction[6,34]. The results suggest preferential metabolism of glucose to lactate with preserved or even elevated glucose extraction in regions of very low oxygen extraction. These results must however be regarded very warily as they may simply reflect a significant breakdown of the glucose model in pathological tissue.

The Hammersmith group has begun to study cerebral physiology in patients with severe extracranial artery stenoses or occlusions. A phase of diminished perfusion reserve anteceding any rise in oxygen extraction has been documented by Gibbs et al[15] with reference to blood flow and blood volume measurements combined. The cerebral blood volume measured regionally provides an excellent index of the state of vasodilation of the local vasculature and this combined with a flow measurement indicates how close the circulation is to haemodynamic decompensation, and in turn an elevation of oxygen extraction, ischaemia and possible infarction. This interesting approach also suggests a method applicable by non PET nuclear medicine centres to the objective selection of at risk patients for preventative revascularisation surgery.

Gliomas

Gliomas have been studied with ^{18}FDG despite the reservations of using this technique in such pathological tissue. The group of DiChiro[8] has claimed a correlation between degree of malignancy and CMRGlu. The in vivo typing of tumour malignancy would obviously be of considerable clinical importance. However the results are preliminary and require confirmation. Of equal use would be a method of differentiating postradiation necrosis from tumour recurrence and it seems that the ^{18}FDG method may make this possible.

The oxygen technique has shown that gliomas are not hypoxic at tissue level[17] at least not macroscopically. The demonstration of an invariably low oxygen extraction in such malignancies means that the draining venous blood must have a high P_{O_2} and the tissue cannot be hypoxic. This will have implications on the use of radiosensitisers and other adjuvant forms of cancer therapy.

Both techniques have demonstrated unequivocal remote effects of tumours on the uninvolved brain which cannot therefore be considered entirely normal. Crossed cerebellar diaschisis has been demonstrated as in stroke[8]. The oxygen studies of Ito et al[17] were interesting in that the depression of metabolism of the brain containing a sizeable malignancy did not have any obvious correlation with tumour size, degree of oedema or degree of midline shift.

Epilepsy

Epilepsy constitutes a condition where frequently the underlying cerebral tissue has normal or near normal structure. The glucose technique has been particularly successfully applied to the study of temporal lobe epilepsy by Engel and coworkers[10,11,12]. Discrete local areas of temporal lobe hypometabolism have been discerned and, it is claimed, correlate exceedingly well with the origin of epileptic discharge whether judged by EEG or by remission following surgical resection. Studies performed ictally, in contrast to the interictal phase have shown focal hypermetabolism. It is of interest that these areas of abnormality have been shown to correlate excellently with site of epileptogenic lesion but poorly with the degree or nature of electroencephalographic abnormality. These findings are being comfirmed prospectively on surgically treated patients and may constitute a very effective way of deciding which temporal lobe to resect in the treatment of refractory temporal lobe epilepsy.

Miscellaneous

Important studies in Huntington's disease are suggesting that the carrier or pre-clinical state may be discernable with PET and ^{18}FDG[20]. Studies testing hypotheses about the biochemical pathogenesis of this disease are also under way. Patients with Parkinson's disease are being studied to assess the basal ganglia and to follow the effects of therapy on the dysfunctioning areas[22].

The pathogenesis of dementia of both Alzheimer and multi-infarct types has been under intensive study. The theory of chronic cerebrovascular insufficiency has been effectively disposed of with studies using the oxygen technique[14]. Patterns of dysfunction have been observed which have been mirrored in terms of glucose metabolism and more recently methionine incorporation into tissue protein[7]. This latter technique, still in the stage of development, as is the leucine technique for measuring protein synthesis promise to be interesting tools in the study of cerebral degenerative diseases and metabolic encephalopathies.

As can be seen the explosion of investigative work in neurology with PET techniques is such that a short review of this nature is only capable of giving the briefest idea of what has already been demonstrated and what is presently being investigated. The future lies in the versatility of isotope tracer methods available for use with PET and the application of such methods to the objective study of the natural history, pathophysiology and effects of therapeutic intervention in human disease.

References

1. Ackerman RH., Correia JA., Alpert NM et al. Positron imaging in ischaemic stroke disease using compounds labelled with oxygen-15. Arch.Neurol:1981;38,537-543.
2. Alavi A., Reivich M., Greenberg J. et al. Mapping of functional activity in brain with ^{18}F fluordeoxyglucose. Semin.Nucl.Med: 1981;11,24-31.
3. Baron JC., Comar B., Bousser MG et al. Etude tomographique chez l'homme, du debit sanguin et de la consommation d'oxygene du cerveau par inhalation continue d'oxygene 15. Revue Neurol.(Paris):1978, 134;545-556.
4. Baron JC., Bousser MG., Comar D. et al. Non invasive tomographic study of cerebral blood flow and oxygen metabolism in vivo. Europ.Neurol:1981;20,273-284.
5. Baron JC., Bousser MG., Rey A. et al. Reversal of focal 'misery perfusion syndrome' by extra-intracranial arterial bypass in haemodynamic cerebral ischaemia. Stroke:1981;12,454-459.

6. Baron JC., Lebrun-Grandie P., Collard P. et al. Non invasive measurement of blood flow oxygen consumption and glucose utilisation in the same brain regions in man by positron tomography. J.Nucl.Med:1982;23,391-399.
7. Bustany P., Sargent T., Sandubray SM.et al. Regional human brain uptake and protein incorporation of ^{11}C-L-methionine studied in vivo with PET. J.Cereb.Blood Flow and Metabol:1981;1(suppl 1)517-518.
8. DiChiro G., DeLaPaz RL., Brooks RA. et al. Glucose utilisation of cerebral gliomas measured by ^{18}F fluorodeoxyglucose and positron emission tomography. Neurology:1982;32,1323-1329.
9. Ell PJ and Holman BL. Computerised emission tomography. Oxford University Press:1982.
10.Engel J., Kuhl DE., Phelps ME. et al. Interictal cerebral glucose metabolism in partial epilepsy and its relation to EEG changes. Ann.Neurol.1982;12,510.517.
11.Engel J., Brown WJ., Kuhl DE et al. Pathological findings underlying focal temporal lobe hypometabolism in partial epilepsy. Ann.Neurol:1982;12,518.528.
12.Engel J., Kuhl DE., Phelps et al. Comparative localisation of epileptic foci in partial epilepsy by PCT and EEG. Ann.Neurol:1982;12,529-537.
13.Frackowiak RSJ., Lezni GL., Jones T et al. Quantitative measurement of regional cerebral blood flow and oxygen metabolism in man using ^{15}o and positron emission tomography: theory, procedure and normal values. J.Comput.Assist.Tomogr:1980;4,727.736.
14.Frackowiak RSJ., Pozzilli C., Legg NJ et al. Regional cerebral oxygen supply and utilisation in dementia: a clinical and physiological study with oxygen-15 and positron tomography. Brain:1981;104,753-778.
15.Gibbs JM, Wise RJS., Leenders K et al. The relationship of regional cerebral blood flow, blood volume and oxygen metabolism in patients with carotid occlusion: evaluation of perfusion reserve. J.Cereb.Blood Flow & Metabol:1983;3 (suppl) in press.
16.Grubb RL., Raichle ME., Higgins CS et al. Measurement of regional cerebral blood volume by emission tomography. Ann.Neurol:1978;4,322-328.
17.Ito M., Lammertsma AA, Wise RJS et al. Measurement of regional cerebral blood flow and oxygen utilisation in patients with cerebral tumours using ^{15}O and positron emission tomography: analytical techniques and preliminary data. Neuroradiology:1982;23,63-74.
18.Kuhl DE, Phelps ME, Kowell AP et al. Effects of stroke on local cerebral metabolism and perfusion: mapping by emission computed tomography of ^{18}FDG and $^{13}NH_3$. Ann.Neurol:1980;8,47-60.
19.Kuhl DE, Metler JE, Riege WH et al. Effects of human ageing on patterns of local cerebral glucose utilisation determined by the [^{18}F] fluorodeoxyglucose method. J.Cereb.Blood Flow & Metabol:1982;2,163-171.
20.Kuhl DE, Phelps ME., Markham CH et al. Cerebral metabolism and atrophy in Huntingtons disease determined by ^{18}FDG and computed tomographic scan. Ann.Neurol:1982;12,425-434.
21.Lammertsma AA, Wise RJS., Heather JD et al. The correction for intravascular oxygen-15 in the steady state technique for measuring regional oxygen extraction ratio. J.Cereb.Blood Flow and Metabol:1983; 3(suppl.) in press.
22.Leenders K., Wolfson L., Gibbs JM et al. Regional cerebral blood flow and oxygen metabolism in Parkinson's disease and their response to L-DOPA. J.Cereb.Blood Flow and Metabol:1983;3(suppl.)in press.
23.Lenzi GL., Frackowiak RSJ., Jones T. Cerebral oxygen meabolism and blood flow in human cerebral ischaemic infarction. J.Cereb.Blood Flow and Metabol:1982;2,321-335.
24.Mazziotta JC., Phelps ME., Miller J. et al. Tomographic mapping of human cerebral metabolism: normal unstimulated state. Neurology:1981;31,503-516.

25.Mazziotta JC., Phelps ME., Carson RE et al. Tomographic mapping of human cerebral metabolism: sensory deprivation. Ann.Neurol:1982;12,435-444.
26.Mazziotta JC., Phelps ME., Carson RE et al. Tomographic mapping of human cerebral metabolism: auditory stimulation. Neurology:1982;32,921-937.
27.Phelps ME., Huang SC., Hoffman EJ et al. Tomographic measurement of local cerebral glucose metabolic rate in humans with [^{18}F]2-fluoro-2-deoxy-D-glucose: Validation of method. Ann.Neurol:1979;6,371-388.
28.Phelps ME., Mazziotta JC., Kuhl DE et al. Tomographic mapping of human cerebral metabolism: Visual stimulation and deprivation. Neurology:1981;31,517-529.
29.Phelps ME., Mazziotta JC., Huang SC. Study of cerebral function with positron computed tomography. J.Cereb.Blood Flow and Metabol:1982;2,113-162.
30.Rhodes CG., Wise RJS., Gibbs JM et al. In vivo disturbance of the oxidative metabolism of glucose in human cerebral gliomas. Ann.Neurol:1983 in press.
31.Sokoloff L. Cerebral circulatory and metabolic change associated with ageing. Res.Pub.Ass.Nerv.Ment.Dis:1966;41,237-251.
32.Sokoloff L. Localisation of functional activity in the central nervous system by measurement of glucose utilisation with radioactive deoxyglucose. J.Cereb.Blood Flow and Metabol:1981;1,7-36.
33.Wise RJS., Bernardi S., Frackowiak RSJ et al. Serial observations on the pathophysiology of acute stroke: the transition from ischaemia to infarction as reflected in regional oxygen extraction. Brain:183;106, 197-222.
34.Wise RJS., Rhodes CG., Gibbs JM et al. Disturbance of oxidative metabolism of glucose in recent human cerebral infarcts. Ann.Neurol:1983 in press.

CARDIOLOGICAL APPLICATIONS OF EMISSION COMPUTED TOMOGRAPHY

C. DE LANDSHEERE, D. RAETS, M.P. LAROCK, W. BURGUET, D. LAMOTTE, M. CHEVIGNE, P. RIGO (Liège, Belgium)

Text not received.

EVALUATION OF THE DIGITAL GAMMA CAMERA ELSCINT APEX 415 ECT IN EMISSION TOMOGRAPHY : FIRST CLINICAL RESULTS

by C. SCHEIBER and J. CHAMBRON
Institut de Physique Biologique
Faculté de Médecine
4 rue Kirschleger
67085 STRASBOURG CEDEX
FRANCE

Single Photon Emission Computerized Tomography (SPECT) has two distinct advantages when compared to conventional static imaging. It allows a 3-D representation of the activity distribution, as well as a better contrast of the images.

Stringent technical requirements are mandatory, though, to materialize these theoretical advantages, at all steps of the instrument design, by allowing full control of the detecting circuitry as well as optimal image representation hardware and software during the process. Since the tomographic system is a contrast amplifier, it will also enhance all underlying imperfections.

Taking into account the nature of in-vivo tracers and the basic principles of the gamma camera, scanning conditions will generally be unfavorable to the detecting system (source-detector distance, counting statistics, etc).

Thus, to investigate on phantoms or in clinical cases the potential of our Elscint APEX 415 ECT, we have deliberately used routine conditions, namely study time no longer than 20 min., with a maximum dose specific for each examination type.

In this paper, we will review the following headlines

1. The gamma camera
   - physical (thermal) environment
   - manoeuverability
   - rotation axis and its quality control

2. Collimated head
   - uniformity and spatial resolution response as a function of distance and of the rotation azimuth
   - cold nodule (2 cm) evaluation under clinical condition in an active 30 cm phantom
   - use of asymmetrical windows.
3. We shall briefly discuss the reconstruction software, then review a few clinical cases

4. Finally hoped developments and desired improvements to the present instrument will be explicited.

EXPERIENCES FROM THE FIRST YEAR OF POSITRON EMISSION TOMOGRAPHY WITH SHORT-LIVED RADIONUCLIDES IN UPPSALA

P Malmborg, H Lundqvist, C-G Stålnacke, Gustaf Werner Institute, University of Uppsala, and B Långström, G Antoni, C Halldin, K Någren, H Svärd, Department of Organic Chemistry, University of Uppsala, in collaboration with medical groups at Uppsala Academic Hospital.

ABSTRACT

L- and D-^{11}C-methionine and other ^{11}C-labelled compounds have been used in 40 experiments on rhesus monkey using the newly installed (april -82) positron emission tomograph (PET) at the University hospital. The main projects for the moment are

1. Pharmaco-kinetic studies of morfine, petidine and codein in the brain.
2. Kinetic studies of nicotine in the brain with and without nicotine receptor blockers.
3. Placenta transport of amino-acids in the pregnant rhesus monkey.

^{11}C-L-methionine has been used in a clinical study on 15 patients having glioma making use of the PET. The uptake of the amino acid in the tumour area compared with healthy tissue is in the order 2 - 4 times higher, revealing a higher protein synthesis in the tumour. Work comparing ^{11}C-methionine and ^{11}C-glucose for PET-diagnostics of brain tumours has been started as a collaboration between the positron camera groups in Uppsala and Stockholm.

During this first year of PET-work in Uppsala emphasis has been put on the research potential of the instrument and the development of auxilliary techniques to complement the dynamic picture studies made with the above-mentioned radiopharmaceuticals.

EXPERIENCES FROM THE FIRST YEAR OF POSITRON EMISSION TOMOGRAPHY WITH SHORT-LIVED RADIONUCLIDES IN UPPSALA

P Malmborg, H Lundqvist, C-G Stålnacke, Gustaf Werner Institute, University of Uppsala, and B Långström, G Antoni, C Halldin, K Någren, H Svärd, Department of Organic Chemistry, University of Uppsala, in collaboration with medical groups at Uppsala Academic Hospital.

During 1982 the tandem accelerator has been used on one or two 8-hour shifts each week for routine production of ^{11}C-carbon dioxide using the ^{14}N(p,alpha)^{11}C reaction in our rather reliable 'third generation' gas target. Batches containing ^{11}C-carbon dioxide in the order of 10 GBq are obtained in a 1-hour bombardment. The labelled carbon dioxide has either been trapped in a reaction solution or in 4Å molecular sieves at the Tandem Accelerator Laboratory followed by rapid transportation to the chemistry laboratories at the Gustaf Werner Institute.

When trapped directly in reaction solution the ^{11}C-carbon dioxide has been used for example in a 7-step chemical reaction route to give 3-^{11}C-labelled phenylalanine , tyrosine and DOPA. The L-phenylalanine is obtained in enantiomeric excess, the amount of which is determined by use of the tRNA-method[1].

The labelled carbon dioxide trapped in molecular sieves has been used in the preparation of ^{11}C-formaldehyde and ^{11}C-methyl iodide, the latter now being adopted for wholly automatic, micro-processor programmed production of methylated radiopharmaceuticals (work in progress). 1-^{11}C-ethyl iodide and 1-^{11}C-propyl iodide have also been prepared.

The ^{11}C-methyl iodide has been used in the synthesis of the following ^{11}C-labelled compounds given in Table 1:

morphine	9,10-dihydroergotamin	tamoxiphene
codeine	bromocriptine	antipyrine
pethidine	nicotine	analgetics
zimelidine	heroine	

Table 1. Some compounds labelled with ^{11}C via ^{11}C-methyl iodide.

Furthermore the ^{11}C-methyl iodide has been used in routine production of L- and D-methionine and by use of a similar reaction route the following ^{11}C-labelled peptides have been made: Met-enkephalin (tyr-gly-gly-phe-met), phe-met and gly-phe-met.

In preliminary experiments 1-^{11}C-ethyl iodide has been used in the labelling of a well-known analgetics - xylocain.

The L- and D-^{11}C-methionine and the ^{11}C-labelled compounds in Table 1 have been used in 40 experiments on rhesus monkey using the newly installed (april -82) positron emission tomograph (PET) at the University hospital. The main projects for the moment are

1. Pharmaco-kinetic studies of morfine, petidine and codein in the brain[2].
2. Kinetic studies of nicotine in the brain with and without nicotine receptor blockers[3].
3. Placenta transport of amino-acids in the pregnant rhesus monkey[4].

^{11}C-L-methionine has been used in a clinical study on 15 patients having glioma making use of the PET. The uptake of the amino acid in the tumour area compared with healthy tissue

is in the order 2 - 4 times higher, revealing a higher protein synthesis in the tumour. Work comparing ^{11}C-methionine and ^{11}C-glucose for PET-diagnostics of brain tumours has been started as a collaboration between the positron camera groups in Uppsala and Stockholm.

During this first year of PET-work in Uppsala emphasis has been put on the research potential of the instrument and the development of auxilliary techniques to complement the dynamic picture studies made with the above-mentioned radiopharmaceuticals. Sampling and measurement of expired $^{11}CO_2$, separation of blood samples into different fractions to follow the metabolic fate of the labelled substance and development of new autoradiographic techniques are some lines of research being explored, as exemplified in the following paragraphs.

The nutritional studies in pigs by means of ^{11}C-L-methionine have continued. Some promising efforts to study the kinetics of metabolic products in plasma with the use of LC-technique have been made.

^{11}C-L-methionine has been used in radiobiological work on cell cultures and on rat intestine in order to evaluate the biological damage caused by the positron decay.

^{11}C-labelled compounds have also been used in mice for autoradiographic studies. The technique has been optimized to make use of the short half-life of ^{11}C and can now be used in double labelling experiments where ^{14}C, ^{3}H or ^{35}S is used as the second radionuclide[5]. The technique has proved to be a valuable tool in the evaluation of ^{11}C-labelled compounds and for dosimetric purposes.

Some preliminary and promising experiments have also made use of ^{11}C-labelled compounds in "in vitro" autoradiography. Slices (10 - 30 microns) of spinal cord or brain from monkeys and humans have been investigated for opiate receptors.

References:

(1) H Lundqvist, M Malmqvist and B Långström
Determination of enantiomeric purity in biogenic ^{11}C-labelled amino acids by aminoacylation of tRNA
J. Radioanal. Chem. In press.

(2) P Hartvig, A Tamsen, K Bergström, A Lilja, U Moström, P-O Lundberg, H Lundqvist, P Malmborg, B Långström, H Svärd, A Rane, J-O Svensson
Fördelning av morfin, petidin och kodein till hjärna studerat med positron- emissionstomografi
Abstract LÄ22 Med.Riksst.-82. Acta Soc.Med.Suec.Hyg. 91.183(1982)

(3) A Nordberg, B Lindberg, U Moström, A Lilja, S-M Aquilonius, G Antoni, B Långström, H Lundqvist, P Malmborg, P Hartvig
Regional dynamisk studie av nikotin med positronemissionstomografi (PET) hos Rhesus-apa
Abstract NE37 Med.Riksst.-82. Acta Soc.Med.Suec.Hyg. 91.203(1982)

(4) B Lindberg, K Bergström, C Halldin, P Hartvig, A Lilja, P-O Lundberg, H Lundqvist, B Långström, P Malmborg, K-G Stålnacke
Feto-maternell kinetik av metionin studerat med positronemissionstomografi (PET) hos Rhesus-apa
Abstract OB25P Med.Riksst.-82. Acta Soc.Med.Suec.Hyg. 91.213(1982)

(5) R d'Argy, S Ullberg, C-G Stålnacke, and B Långström
Whole body autoradiography using ^{11}C with double tracer applications
Int J Appl Radiat Isotopes. Accepted for publication.

DETECTION DES PLAQUES D'ATHEROME CAROTIDIENNES ET FEMORALES

L. POURCELOT (Tours, France)

Texte non parvenu.

DATA CAPTURE AND DISPLAY OF MOVING HEART WALLS FROM GAMMA CAMERA IMAGES

R J Whitrow
Department of Computing
Brighton Polytechnic
UK

Abstract

The image of the moving heart as displayed by the gamma camera is input to the computer via a camera. Software for randomly accessing the image is described. Features of interest are thresholded and a method for reconstructing the features from the data on sequential scan lines is described. Because of the small volume of data captured, the computer is able to follow the motion of the heart and valves in real time. Images taken in parallel from different angles enable volume changes to be noted in time.

1. Introduction

This paper describes a method of detecting moving edges in a noisy background from a gamma camera display. Considerable literature exists in the detection of still edges (Marr and Hildreth, 1979; Mitchie and Davies, 1982) and more recently work concerning moving edges has been published (Ullman, 1979; Jain 1981).

Moving surfaces such as heartwalls raise geometric problems associated with connectivity, holes and concavities. The difficulty of not being able to sample the same image twice means that points must either be reliably captured or the sampling in the vertical (y) direction is sufficiently close so that some points can be ignored if not reliably found. The method described allows lines to be digitised along the horizontal (x) of the image frame. We scan lines a fixed y-distance apart in each frame and store the pixel values in memory.

2. Data Capture

Images from a gamma camera are stored on video tape. The images are taken from patients during normal monitoring of heart functions. The video tape is replayed and the moving images digitised from a camera input. A typical still image is shown in Figure 1.

The video camera in connected to a PDP11/40 minicomputer via a Direct Memory Access interface. The volume of data involved in digitising a complete frame makes it impossible to make real time measurements on a sequential machine. This problem has been overcome by writing a D.M.A. software interface with random access facilities to the video image. The lines of the image which delineate (along the vertical axis) the moving region of interest are specified together with a suitable increment between the lines to be digitised. The increment must be small enough so that no sharp gradient changes on surface are missed. With a smooth object such as a heart this is not a problem and a spacing of twenty lines has been found adequate for accurate reconstruction later.

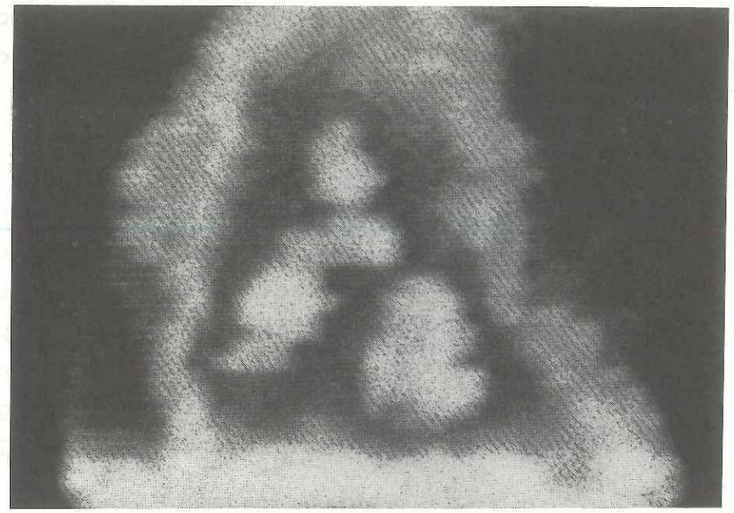

A Gamma Camera Image Showing the Heart Walls and Chambers

Figure 1

Typically, to digitise a frame, sixteen lines of 256 pixels are found sufficient. Since the data volume from each frame is small, repetitive scanning in real time is possible and data is stored in a memory buffer. Digitisation of a line requires about 64 micro seconds and at the above scanning rate a frame is digitised in about 16m seconds, the D.M.A. data transfer taking place while the camera is scanning down between specified lines.

The distortion from the beginning to end of each frame for the low frequency oscillation of the heart is small. The next frame can be scanned with a minimum delay of about 20m seconds or a variable delay can be specified before beginning the next frame capture. Thus each frame is scanned at 50Hz while a typical heart rate is of the order of 10Hz or less. This allows a complete picture of the volume motion of the heart to be built up during its cycle.

After a suitable number of frames have been digitised to give an accurate picture of the motion in question, the memory buffer is stored on disc. The same process is repeated for gamma scans at a number of different angles.

3. Extraction of Anatomical Features

Each pixel point exhibits up to 256 grey levels. Because of the nature of the sampling process, we have been unable to use edge operators determined from searching about a point other than along the current scan line. Averaging of pixel values is only possible if the sampling frequency is reduced. We have overcome this problem by thresholding above a given value provided a number of adjacent pixel values are also above the threshold.

Given a one dimensional image F(i), i = 1 ... n, then a region is assumed to exist if F(i) > the threshold (t) and the number of adjacent points that are less than the threshold is less than a noise value. The problem occurs at the boundaries of regions where it is found that the pixel values oscillate about the threshold for a short distance. The edge of an object is defined to be at the centre of the oscillatory region and the threshold value (t) is determined from the value of pixels in an optically uniform region of the image.

If a number of pixels have been found to be above the threshold value but there are less of them than the noise value, they are rejected as an artifact. This has been necessary because even in regions of approximately the same grey level, the statistical variation of the data is such that some pixels are outside the threshold value. This technique has proved useful in that it prevents the collection of spurious data inside continuous regions while not significantly distorting the edge point of a region.

4. Windowing of Data

Of necessity each video image contains information not relevant to the anatomical region of interest. There may even be spurious light reflections on the TV monitor from which the image is captured. This data is 'windowed' out before processing by specifying delimeters along the x-direction of each scan line and in the vertical direction.

5. Data Organisation for Display

The points obtained from threshold determination described in Section 3 are the edge points of each region of interest along each scan line. Although each scan line is stored sequentially, the connectivity of each point is not immediately apparent. The problem has received the attention of a number of authors (Arcelli and Levialdi, 1973; Mori and Doh, 1982).

The method described does not cater for all types of concavity but has proved robust for the variations in re-entrancy associated with moving heart walls and chambers. Many methods of searching involve eight-way searches for relating points for display purposes. This was found to be complex and unreliable since our scan lines are some distance apart and the data points along a scan line are usually obtained from more than one feature of interest. The problem is illustrated in Figure 2 where we show two possible ways of connecting the same thresholded edge points.

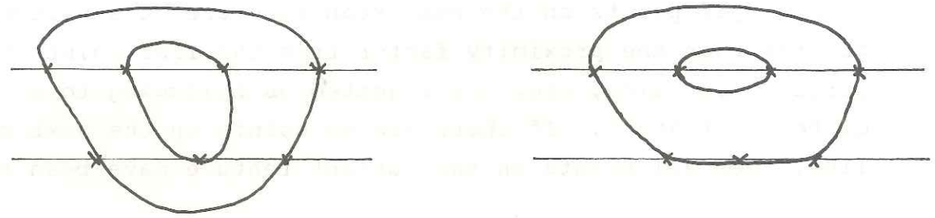

Ambiguity in connecting 4 image data points

Figure 2

Using the eight way search led to ambiguities when two points on subsequent scan lines were the same distance from a search point.

The approach taken was not to search from each point locally but rather to search globally from the outside in, until the outermost points on each scan line are found. As points are found they are stored and thus ordered in the correct form for a sequential plot. Within the method allowance is made for more than two points belonging to the same feature being found on the same scan line as illustrated in Figure 3.

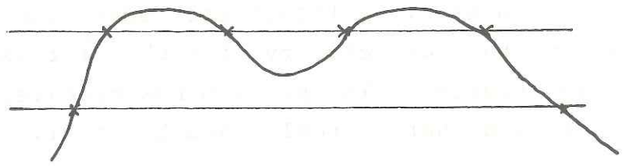

A scan line running near to object edge
Figure 3

This method has proved robust for the outline of single features such as heart walls. For obtaining the outlines of the atria and ventricles, the same procedure of searching inwards is used and a proximity factor is now introduced. The edge points of an object are found as before, but points are checked to see if they are greater than the proximity factor apart on the current and next scan line to be processed. If points on the next scan line are at a distance greater than the proximity factor from the last point on the current scan line, they are rejected as belonging to a different feature. If there are no points on the next scan line, then all points on the current feature have been found.

The proximity factor is governed by the nearest distance at which the heart chambers are likely to appear on the gamma camera images. It also depends to some extent on the

irregularity of the shape of the chambers. A typical image determination is shown in Figure 4.

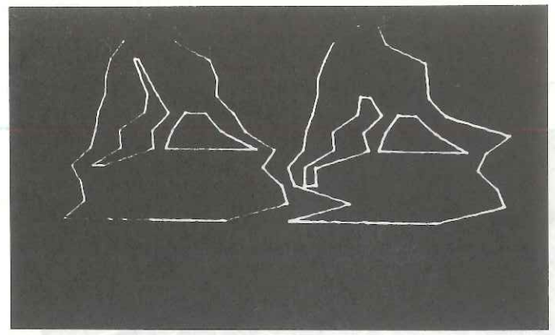

A typical image showing the heart wall and two chambers
Figure 4

6. Splined Reconstruction of Images

The description of the image shown in Figure 4 represents the outline determined from scan lines taken at some fixed distance apart. This is a somewhat unrealistic representation and would make for errors in blood volume measurements. The "tensioned spline" has been described by (Schweikert, 1966) and has been used (Whitrow, 1979) to describe the outline of complex anatomical structures.

If we have a set of knots x_i ($i = 1 \ldots n$) and corresponding function values y_i ($i = 1 \ldots n$) then we seek a function $F(x_i)$ to have continuous derivatives such that

$$F(x_i) = y_i \qquad i = 1 \ldots n$$

Also we seek the quantity $(F'' - \sigma^2 f)$ to vary linearly at the intervals $x_i - x_i$.

That is

$$F''(x) - \sigma^2 f(x) = [F''(x_i) - \sigma^2 y_i] \frac{x_{i+1} - x)}{} + [F''(x_{i+1}) - \sigma^2 y_{i+1}] \frac{x - x_i}{h_i}$$

where

$$h_i = x_{i+1} - x_i$$

A more detailed description and with solutions are given in (Ref 9). Choosing a suitable tension factor σ gives a more realistic outline of features by interpolation between the knots.

The outline from two frames is shown in Figure 5.

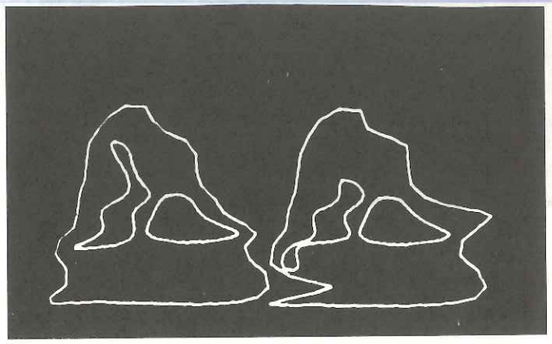

Two adjacent frames of the moving changes
Figure 5

The algorithm described is written in FORTRAN and runs on a PDP11/40 system using the GT40 refresh graphics facility for display purposes.

7. Conclusions

A real time image capture system has been described, which allows the capture and display of moving features in real time to be accomplished on a minicomputer. This is effected by a random access of the scan lines of the image and storage of only the edge points of features. Because of the small amount of data captured, a number of frames of a moving object may be captured in memory in real time. Data is reorganised for plotting purposes from each scan line to points relating to each feature of interest. The tensioned spline is used to give a realistic representation of the features.

Bibliography

1. D Marr and L Hildreth, Theory of edge detection. Proc Royal Society, London. 1979

2. A Mitchie and L Davis, Finding edges in natural texture. Signal Processing 4, 1982, pp 181-192

3. S Ullman, The interpretation of visual motion. MIT Press. 1979

4. R Jain, Dynamic scene analysis using pixel based processes. Computer, 14 (8), pp 12-18. 1981

5. C Arcelli and S Levialdi, On blob recognition. Computer Graphics and Image Processing 2, 1973, pp 22-38.

6. S Mori and M Doh. A sequential tracking extraction of shape features and in constructive description. Computer Graphics and Image Processing 19, 1982, pp 349-366

7. D Schweikert, An interpolation curve using a spline in tension. J Math and Physics 45, 1966, pp 312-317

8. R Whitrow. Computerised displays for radiotherapy treatment planning. International Symposium on Dose Planning, University of Liege. 1979